Doctoral Dissertation

博士論文

Functional Renormalization Group Study on Kitaev Quantum Spin Liquid

(Kitaev 量子スピン液体の汎関数繰り込み群による研究)

A Dissertation Submitted for the Degree of Doctor of Philosophy

December 2020

令和 2 年 12 月博士（理学）申請

Department of Physics, Graduate School of Science,
The University of Tokyo

東京大学大学院理学系研究科

物理学専攻

Kiyu Fukui

福井 毅勇

DOCTORAL DISSERTATION

Functional Renormalization Group Study on Kitaev Quantum Spin Liquid

Author:
Kiyu Fukui

Supervisor:
Prof. Dr. Yusuke Kato

A Dissertation Submitted for the Degree of Doctor of Philosophy

in the

Department of Physics, Graduate School of Science,
The University of Tokyo

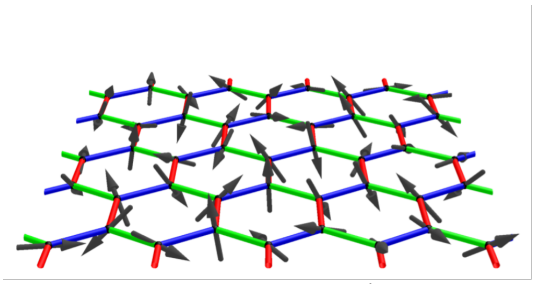

December, 2020

Abstract

In this doctoral dissertation, we study the feasibility of Kitaev quantum spin liquid in two types of systems: ultracold molecular systems and high-spin systems.

We adopt pseudo-fermion functional renormalization group (PFFRG) as a numerical method to address these studies. The method can handle systems with relatively large system sizes, and the computational cost is independent of the range of interactions. In addition, an extension to the general spin length S was proposed in 2017, and this extended method can be used to calculate spin susceptibilities in the model with arbitrary S without changing the computational cost from the case of $S = 1/2$. These features are suitable for the two studies mentioned above.

Our main results for the two studies mentioned above are presented in chapter 4 and 5. In chapter 4, we discuss the feasibility of the Kitaev quantum spin liquid in ultracold polar molecular systems trapped in the optical lattice. A microwave-based realization of Kitaev-type interactions in this system was proposed in 2013 [S. R. Manmana *et al*., Phys. Rev. B **87**, 081106 (2013), A. V. Gorshkov, K. R. Hazzard, and A. M. Rey, Mol. Phys. **111**, 1908 (2013)]. Based on these proposals, we define dipolar Kitaev model which has angle-dependent long-range spin interactions. We perform PFFRG calculation to reveal the phase diagram of this model. The results show that ferromagnetic (FM) order and zigzag antiferromagnetic (AFM) order are realized in the FM and AFM dipolar Kitaev model, respectively, for all anisotropy parameters. In order to investigate the reason why the quantum spin liquid state is not realized in the dipolar Kitaev model, we investigate the ordering behavior while increasing the range of the interaction from the nearest-neighbor case. As a result, the behavior of the susceptibility shows that the Kitaev quantum spin liquid collapses quickly as the range of the interaction increases. These results suggest that the Kitaev quantum spin liquid is fragile against long-range interactions and cannot be realized in the ultracold molecular systems at least based on the proposals above. This is the first time that the feasibility of the Kitaev quantum spin liquid has been calculated on the basis of the proposal mentioned above.

In chapter 5, we discuss the feasibility of the Kitaev quantum spin liquid in high-spin candidate materials. We regard the Kitaev-Heisenberg model as a minimal model of the candidate materials, and calculate the phase diagram of the spin-S Kitaev-Heisenberg model. We perform calculation of the susceptibility of the model with $S = 1/2$-$5/2$ and $S = 50$ in all parameter region. The obtained phase diagrams of the Kitaev- Heisenberg model for $S = 1/2$, $S = 1$, and $S = 50$ are in general good agreement with the previous studies on the $S = 1/2$, $S = 1$, and classical Kitaev-Heisenberg model by other numerical methods, respectively. From the results of these calculations, we have found that the upper limit of the spin length of the candidate material allowed for the realization of Kitaev quantum spin liquid is $S = 3/2$. The phase diagram calculation of the Kitaev-Heisenberg model with a systematic change of spin S, as we have done here, has not been performed before. Our results provide a guideline for the recent intensive search for candidate materials of $S > 1/2$ Kitaev quantum spin liquid.

Acknowledgements

I would like to thank all the people who supported me during my doctoral course. I would like to express my gratitude to those who have been especially helpful to me in the following.

First of all, I would like to express my sincere gratitude to my supervisor, Yusuke Kato for his thoughtful guidance and continuous support. He was always willing to discuss my questions about physics. I have learned a lot from the discussions with him. He also read the manuscript of this dissertation and pointed out typos and incorrect grammars.

Second, I would like to express my appreciation to my collaborators Yukitoshi Motome, Joji Nasu, and Yasuyuki Kato for their constructive suggestions and discussions. In my collaborative discussions with them, I learned a lot not only about the Kitaev quantum spin liquid, but also about numerical techniques. In particular, Yukitoshi Motome has consulted with me on my research as my assistant supervisor assigned in MERIT program. Joji Nasu provided me with the Mathematica files for the creation of the figure on the cover page of this dissertation.

Third, I would like to thank Takashi Miyake and members in his group, especially Taro Fukazawa, Nobuya Sato, and Shotaro Doi. During my internship at AIST, they taught me a lot about *ab initio* calculations and numerical computations.

I am also particularly grateful to Hiroaki Kusunose who let me read the manuscript of his textbook before it was published. I had a better understanding of localized electron systems, magnetism, and multipoles by his manuscript.

Special thanks to Tomonari Mizoguchi and Shinji Koshida for discussion about the Kitaev quantum spin liquid and related topics of it.

I am indebted to past and present members of Kato Yusuke group for beneficial seminars and discussions. Especially, I owe my deepest gratitude to Yusuke Masaki. From discussion and his advises, I have acquired a lot about physics and research spirit.

I am deeply grateful to Koji Hukushima and past and present members of his group, especially Makiko Hase, Yoshihiko Nishikawa, Jun Takahashi, Yasushi Nagano, and Kota Yoshiyama, for great coffee breaks and helpful discussions about Monte Carlo method, machine learning, and statistical physics.

I would particularly like to thank Chisa Hotta, Yuki Shiomi, and menbers of their group for including me in their journal club.

In addition, I want to thank my close friends.

Finally, I would like to express the deepest appreciation to my family for supporting me throughout my life.

I would like to acknowledge the financial support of MERIT (Material Education program for the future leaders in Research, Industry, and Technology), the Program for Leading Graduate Schools, the Ministry of Education, Culture, Sports, Science and Technology, Japan.

This research is partially supported by Initiative on Promotion of Supercomputing for Young or Women Researchers, Supercomputing Division, Information Technology Center, The University of Tokyo.

The computation in this dissertation has been done using following facilities:

- sekirei (system B) provided by the Supercomputer Center, the Institute for Solid State Physics, the University of Tokyo (Project No.H31-Cb-0012, 2020-Ca-0035, 2020-Cb-0010),

- Oakforest-PACS provided by Multidisciplinary Cooperative Research Program in Center for Computational Sciences, University of Tsukuba (Project Name:xg20i046) and Supercomputing Division, Information Technology Center, The University of Tokyo (Project No.po8022),
- Oakbridge-CX and Reedbush provided by Supercomputing Division, Information Technology Center, The University of Tokyo (Project No.po8012, po8013, po8023),
- MASAMUNE-IMR provided by Center for Computational Materials Science, Institute for Materials Research, Tohoku University (Project No.20S0022).

This dissertation was produced using Masters-Doctoral-Thesis-Template in Overleaf.

Contents

Chapter 1

Introduction

1.1 Quantum Spin Liquid

Magnetism has attracted people as well as physicists, like "lodestones", ever since the discovery of lodestones in ancient world. Magnetic materials have been used in various tools and techniques. In spite of its long history from the discovery, the origin of magnetism began to be clarified in early 20th century when quantum mechanics established. That is, magnetism is essentially a quantum mechanical phenomenon. Since the microscopic origin of magnetic moments has been revealed to be electron spins, we have been interested in what kind of magnetism they exhibit as a result of their interactions in materials. In the study of magnetism, theoretical and experimental researches have concerted, and they are still expanding its frontier.

In that long line of research, one of the topics that still have been studied intensively is quantum spin liquid. Quantum spin liquid [1–9] is a nontrivial ground state without symmetry breaking in which the transition to the magnetic ordered states is precluded by sizable quantum fluctuations and strong frustration in the quantum magnets. In quantum spin liquids, there are fractional excitations associated with topological order, and intensive research has been carried out not only purely scientifically, but also from the application side, because the robust topological quantum computing against disturbance can be performed by manipulating them. However, its existence had not been rigorously proved since it was proposed in the early 1970s [10, 11]. In 1973, P. W. Anderson suggested the RVB (resonating valence bond) states [10] and this state is one of the quantum spin liquid states. Since its proposal, an enormous amount of studies have been conducted to prove the existence of the quantum spin liquid ground states in materials with strong frustration. In general, exact results are not obtained theoretically in the presence of frustration, especially in 2 or 3 dimension. In numerical calculations, it is difficult to draw a clear conclusion because the results vary depending on the method and calculation conditions, as it is necessary to deal with small energy scales due to competing interactions. Quantum Monte Carlo methods, which provide reliable results, often suffer from the sign problem in the highly frustrated models. Even in experiments, to show the realization of the spin liquid state, we have to show that no order exists, which is the so-called "devil's proof," and it is impossible to investigate all possibilities.

Over the past decade the study of quantum spin liquids has developed rapidly, inspired by 2 revolutionary breakthroughs [12]. The first one is the proposal of the Kitaev model in 2006 [13]. This model is exactly solvable and we can show that its ground state is a quantum spin liquid. The other is a proposal in 2009 to realize the Kitaev model in real materials [14]. The magnetic interaction proposed in Kitaev model is expected to be realized in the Mott insulators with strong spin-orbit coupling, and many experiments have been carried out on iridium and ruthenium compounds. From these two proposals, theoretical and experimental studies have

collaborated to create a major boom in research related to Kitaev quantum spin liquids. In addition, by measuring the thermal Hall coefficient in 2018, we obtained evidence for the existence of Majorana fermions predicted by the Kitaev model in one of the candidate materials α-$RuCl_3$ [15, 16]. Kitaev quantum spin liquid is now one of major topics in condensed matter physics [12, 17–23] [1].

1.2 Kitaev Quantum Spin Liquid

In this section, we briefly review 2 proposals mentioned in the previous section: the Kitaev model [13] and the Jackeli-Khaliullin mechanism [14].

Kitaev Model

At first we introduce Kitaev model [13] [2]. It is the quantum spin model with $S = 1/2$ on the honeycomb lattice. Its Hamiltonian is

$$\begin{aligned}\mathcal{H} &= -\sum_{\mu=x,y,z}\sum_{\langle i,j\rangle_\mu} J_\mu S_i^\mu S_j^\mu \\ &= -J_x\sum_{\langle i,j\rangle_x} S_i^x S_j^x - J_y\sum_{\langle i,j\rangle_y} S_i^y S_j^y - J_z\sum_{\langle i,j\rangle_z} S_i^z S_j^z,\end{aligned} \tag{1.1}$$

where S_i^μ and J_μ ($\mu = x, y, z$) denotes respectively operators of the μ-component of $S = 1/2$ quantum spin at site i and the coupling constant of the exchange interaction on μ-bonds (see Fig. 1.1). The summation $\sum_{\langle i,j\rangle_\mu}$ runs over all pairs of sites on μ-bonds. This model is shown in Fig. 1.1. x, y, and z-bonds are colored blue, green and red, respectively. In the Kitaev model, the quantum spins of different components of each of the three types of bonds interact in the Ising-type interaction, which results in the model being highly frustrated. The sites belonging to the 2 sublattices of the honeycomb lattice are represented by black and white circles, respectively. Hereafter, we use the unit of $\hbar = k_B = a = 1$ in this paper. $\hbar$, k_B, and a represent the reduced Planck constant, the Boltzmann constant, and the lattice constant of the honeycomb lattice, respectively. In general, we cannot solve frustrated quantum many-body systems in two or higher dimensions. However, the Kitaev model can be solved exceptionally rigorously, because it has a macroscopic number of the conserved quantities. We prove it below. The Hamiltonian in Eq. [13] is rewritten by the Pauli matrices σ_i^μ as

$$\mathcal{H} = -\frac{J_x}{4}\sum_{\langle i,j\rangle_x}\sigma_i^x\sigma_j^x - \frac{J_y}{4}\sum_{\langle i,j\rangle_y}\sigma_i^y\sigma_j^y - \frac{J_z}{4}\sum_{\langle i,j\rangle_z}\sigma_i^z\sigma_j^z. \tag{1.2}$$

We define the flux on the plaquette p as

$$\begin{aligned}W_p &= \prod_{\langle i,j\rangle_\mu\in p}\sigma_i^\mu\sigma_j^\mu \\ &= \prod_{i\in p}\sigma_i^{\bar{\mu}},\end{aligned} \tag{1.3}$$

[1] In the published version [24] of Ref. [17], the chapter on the Kitaev model has been deleted.

[2] The name "Kitaev model" may refer to the 1 dimensional spinless fermion model for topological superconductivity [25] also called Kitaev chain and the model with macroscopically degenerate topologically protected ground states for quantum computation [26] also called toric code model, in addition to the model introduced here, depending on the context.

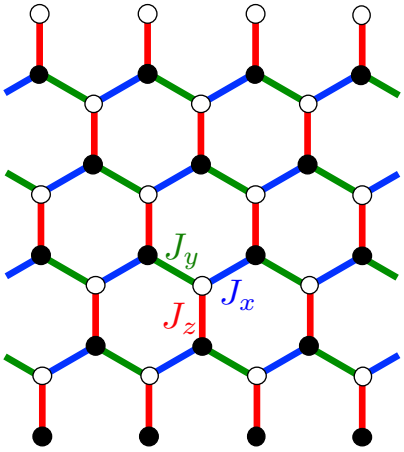

FIGURE 1.1: Kitaev model. The x, y, and z-bonds are colored blue, green and red, respectively. The black and write circles denote sites belonging to the two sublattices of the honeycomb lattice.

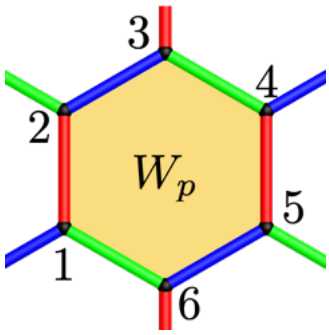

FIGURE 1.2: A plaquette of the honeycomb lattice and a $\mathbb{Z}_2$ flux defined on the plaquette.

where $\bar{\mu}$ denotes the label of the bond not included in the plaquette p among the three bonds connected to the site i. Here p denotes plaquette index. We use the relation of the Pauli matrices and we can rewrite the first line as the second line. As a example, we focus on the plaquette p shown in Fig. 1.2. This plaquette is composed of sites 1-6 and bonds connecting them. We define the flux on this plaquette as

$$\begin{aligned} W_p &= \sigma_1^z\sigma_2^z\sigma_2^x\sigma_3^x\sigma_3^y\sigma_4^y\sigma_4^z\sigma_5^z\sigma_5^x\sigma_6^x\sigma_6^y\sigma_1^y \\ &= \sigma_1^x\sigma_2^y\sigma_3^z\sigma_4^x\sigma_5^y\sigma_6^z. \end{aligned} \tag{1.4}$$

These W_p satisfy the relations:

$$(W_p)^2 = 1, \tag{1.5}$$
$$[\mathcal{H}, W_p] = 0, \tag{1.6}$$
$$[W_p, W_p] = 0 \ \ (p \neq p'), \tag{1.7}$$

for arbitrary plaquette p. Therefore, these fluxes are conserved quantities and $\mathbb{Z}_2$ fluxes which have the values $W_p = +1$ or -1. The Hamiltonian and aribitrary W_p can be diagonalized simultaneously. We can divide Hilbert space into subspaces

specified by a set of $\mathbb{Z}_2$ fluxes $\{W_p\}$. We introduce the Majorana fermion [3] operators to decompose the spin operators into flux degrees of freedom and others:

$$\sigma_i^\mu = \mathrm{i} b_i^\mu c_i, \tag{1.8}$$

where i denote the imaginary unit $\sqrt{-1}$. b_i^μ and c_i are Majorana fermion operators and these satisfy the anti-commutation relations

$$\{c_i, c_j\} = 2\delta_{ij}, \tag{1.9}$$
$$\{b_i^\mu, b_j^\nu\} = 2\delta_{ij}\delta^{\mu\nu}, \tag{1.10}$$
$$\{c_i, b_j^\nu\} = 0. \tag{1.11}$$

The Hamiltonian is rewritten using these operators as

$$\mathcal{H} = \frac{i}{4}\sum_{\langle i,j\rangle} J_{\mu_{ij}} u_{ij} c_i c_j, \tag{1.12}$$

with the operators defined on the bonds

$$u_{ij} = \mathrm{i} b_i^{\mu_{ij}} b_j^{\mu_{ij}}. \tag{1.13}$$

Here $\langle i,j\rangle$ and μ_{ij} represents the pairs of the nearest-neighbor sites and the spin component corresponding to the bond connecting $\langle i,j\rangle$. These bond operators u_{ij} also satisfy the relation

$$(u_{ij})^2 = 1, \tag{1.14}$$
$$[\mathcal{H}, u_{ij}] = 0, \tag{1.15}$$
$$[u_{ij}, u_{kl}] = 0 \ \ (\mu_{ij} \neq \mu_{kl}). \tag{1.16}$$

Thereby, $u_{ij} = \pm 1$ and these are $\mathbb{Z}_2$ gauge variables. The $\mathbb{Z}_2$ fluxes defined in Eq. (1.3) are rewritten by Eq. (1.8) as

$$W_p = \prod_{\langle i,j\rangle \in p} u_{ij}. \tag{1.17}$$

The $\mathbb{Z}_2$ fluxes are composed of the $\mathbb{Z}_2$ gauge variables u_{ij}. Thereby, b_i^μ Majorana fermions constitute the $\mathbb{Z}_2$ gauge field defined on the bond, on the other hand c_i represents itinerant Majorana fermions. Quantum spins are fractionalized into $\mathbb{Z}_2$ fluxes and itinerant Majorana fermions. If we fix the distribution of the gauge fields, the Hamiltonian Eq. (1.12) becomes quadratic in Majorana operators c_i.

Thus we need to find a flux configuration $\{W_p\}$ that minimizes energy to calculate the ground state energy. According to the Lieb's theorem [28], it is proved that the expectation value of the Hamiltonian is minimized in flux-free condition $W_p = +1$ (for all p), if at least two of J_x, J_y, and J_z are the same. In the original paper, A. Kitaev performed numerical calculation to obtain the energy in various flux distribution and found that. The extra degrees of freedom of the enlarged Hilbert space

[3] Majorana fermions are discovered originally as real solutions of the Dirac equation by E. Majorana in 1937 [27].

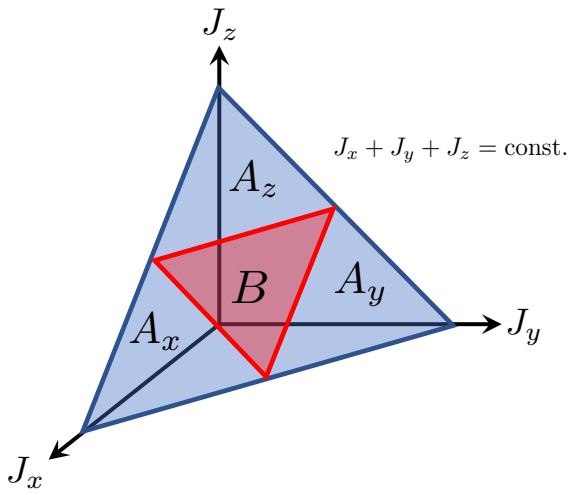

FIGURE 1.3: The ground state phase diagram in the plane $J_x + J_y + J_z = \text{const.}$ A phases (A_x, A_y, and A_z) are gapped and B phase is gapless.

by the introduction of the Majorana fermion operators correspond to $\mathbb{Z}_2$ gauge degrees of freedom. Different $\{u_{ij}\}$ distributions are transformed by the gauge transformations $D_i = b_i^x b_i^y b_i^z c_i$ which keep the Hamiltonian and the flux distributions invariant. The Hamiltonian and the gauge transformation operators are commutative in physical sectors of the enlarged Hilbert space. Hence, we can use a convenient set $\{u_{ij}\}$ for a given flux configuration $\{W_p\}$ when calculating the energy. Now we can set $u_{ij} = +1$ for all bonds and calculate ground state energy by diagonalization of the quadratic Hamiltonian. The resulting ground state phase diagram is shown in Fig. 1.3. We show the phase diagram in the plane with $J_x + J_y + J_z = \text{const.}$ There are 4 phases A_x, A_y, A_z, and B phases. Three A phases (A_x, A_y, and A_z) are essentially the same phase and in these phases Majorana fermions c_i have excitation gap. On the other hand, the itinerant Majorana fermions have continuous excitation spectrum in B phase. Note that in both phases spin excitations which flip $\mathbb{Z}_2$ fluxes are gapped. The spin-spin correlations in the ground state were explicitly calculated in Ref. [29], and it was proved that the spin correlations are only between the nearest-neighboring sites. In A phases, fractional excitations are Abelian anyons. In the limit where one of J_x, J_y, or J_z is large, the toric code model [26] is obtained as an effective Hamiltonian by fourth-order perturbation. In B phase, if a gap opens in the excitation spectrum of the fractional excitations, they become non-Abelian anyons. On of the way to open gap is to apply the magnetic field. We consider the magnetic field in $(1,1,1)$-direction and perturbation

$$\mathcal{H}' = -\sum_i (h_x S_i^x + h_y S_i^y + h_z S_i^z). \tag{1.18}$$

The additional term obtained by the third-order perturbation opens gap in the excitation spectrum of the Majorana fermions. As the result, the Chern number becomes ± 1 in B phase although the Chern number is zero in A phases. Therefore, these gapped Majorana fermions indicate thermal Hall effect and its quantized Hall coefficient should be half the value of normal fermions. Measurements of the thermal Hall coefficient were carried out in 2018 and this half coefficient was actually obtained [15, 16]. This is direct evidence of Majorana fermions in Kitaev magnets.

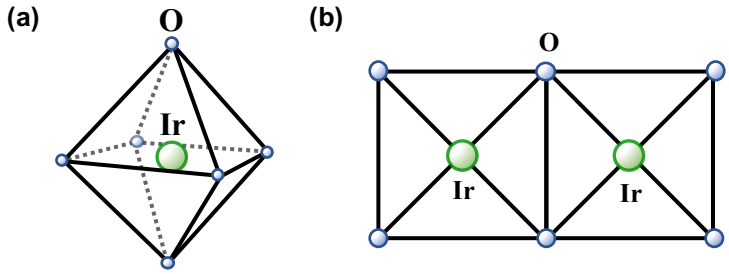

FIGURE 1.4: (a) IrO_6 octahedron constituting Na_2IrO_3 or Li_2IrO_3 and (b) edge sharing two octahedra. Iridium ions and oxygen ions are represented by light green circles and small light blue circles.

As we have discussed, the Kitaev model is exactly solvable, and its ground state is a quantum spin liquid in which quantum spins are fractionalized into fluxes and Majorana fermions. Numerical methods based on the Majorana fermion representation of the Kitaev model have been developed, and the physics of the Majorana fermions in the Kitaev model has been clarified, especially in the last decade [12].

Jackeli-Khaliullin Mechamism

Next, we review the Jackeli-Khaliullin mechanism briefly [14]. In 2009, G. Jackeli and G. Khaliullin consider an effective Hamiltonian for Mott-Hubbard systems with large crystalline electric field (CEF) and strong spin-orbit coupling (SOC). They assumed substances represented by the chemical formula A_2BO_3, where A denotes alkali and B is transition metal atoms such as Ir or Rh whose ion has a d^5-configuration. In particular, here we consider Na_2IrO_3 and Li_2IrO_3 [4] which are Kitaev magnets as mentioned in Chap. 5. Although Jackeli and Khaliullin considered strong correlation limit, A. Shitade and his collaborators discussed weak correlation limit and proposed the quantum spin Hall effects in Na_2IrO_3 [32].

In these materials, the oxygen ions coordinate around the iridium ions to form IrO_6 octahedra as shown in Fig. 1.4 (a). These octahedra share edges to form a honeycomb structure as shown in Fig. 1.4 (b). Due to the cubic CEF (crystalline electric field) caused by oxygen, the d-orbitals of Ir ions are split into t_{2g} and e_g orbitals, and the five d electrons constitute a low-spin state in which they occupy the t_{2g} orbitals because of large energy splitting. Due to SOC (spin-orbit coupling), the spin angular momentum and the effective orbital angular momentum of the t2g orbital $l_{\text{eff}} = -1$ are coupled and it cause further level splitting into the states with $j_{\text{eff}} = 3/2$ and $j_{\text{eff}} = 1/2$, where j_{eff} denotes the effective total angular momentum. The schematic diagram of these level splits are shown in Fig. 1.5. As shown in Fig. 1.5, four of the five electrons in d-orbitals occupy all of the low energy $j_{\text{eff}} = 3/2$ states that are quadruply degenerate, and the remaining one takes the $j_{\text{eff}} = 1/2$ state. The pair of two states with $j_{\text{eff}} = 1/2$ is a Kramers doublet and we can regard these states as pseudo-spins.

The strong Coulomb interaction acting on these states results in a spin-orbit Mott insulator and the effective Hamiltonian describes magnetic interactions between $j_{\text{eff}} = 1/2$ pseudo-spins. In the multi-orbital Hubbard model consisting of these

[4] More precisely, what we have in mind here is α-Li_2IrO_3 with a quasi-two-dimensional honeycomb structure, whereas β-Li_2IrO_3 and γ-Li_2IrO_3 have a three-dimensional hyper honeycomb [30] and stripy honeycomb structure [31], respectively.

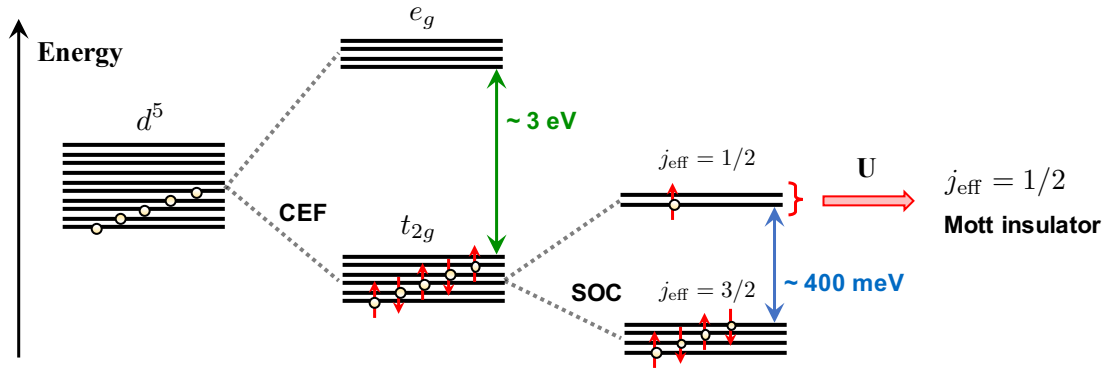

FIGURE 1.5: Relative energy levels and level splitting in Na_2IrO_3 or Li_2IrO_3. The horizontal thick black lines represent energy levels. The yellow circles and the red arrows denote electrons and its spins. The magnitude of the interactions was based on the values in Ref. [19].

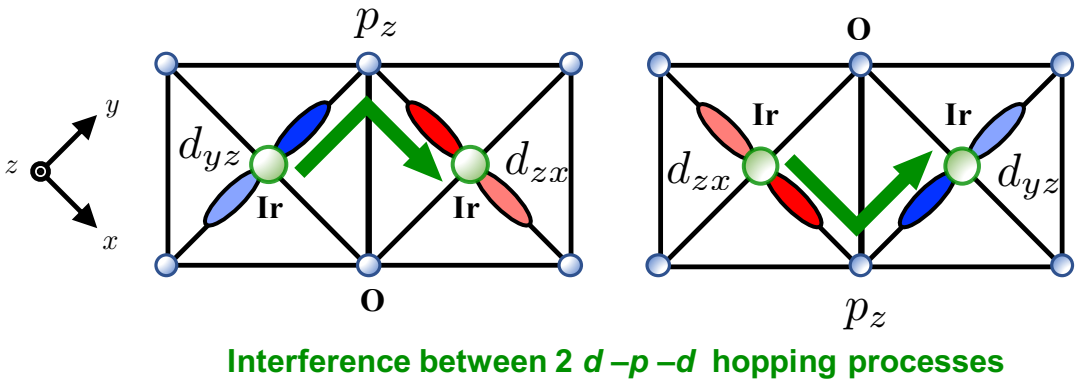

FIGURE 1.6: Schematic picuture representing two d-p-d hopping processes. The arrangement of the ions is the same as in Fig. 1.4 (b). d_{yz}- and d_{zx}-orbitals of Ir ions are colored in blue and red, respectively. These two processes interfere and realize Kitaev-type magnetic interaction as a result.

orbitals, the Kitaev-type interaction is obtained by considering the limit of strong Coulomb repulsion in Ir ions and deriving the effective model by incorporating the electron hoppings between Ir ions as perturbations. Here, we consider the hoppings of electrons in Ir ions in two IrO_6 octahedra that share an edge as shown in Fig. 1.4 (b) in the perturbation process. The important contributions are the hopping processes between electrons in the d-orbitals of neighboring Ir ions through the p-orbitals of oxygens at shared edges. As an example, consider the configuration shown in Fig. 1.6. In the figure, d_{yz}- and d_{zx}-orbitals are colored in blue and red, respectively. In this case, there are two different hopping processes as shown in (a) d_{yz}-p_z-d_{zx} and (b) d_{zx}-p_z-d_{yz} of Fig. 1.6, and these interfere quantum mechanically. As a result of this interference, the Heisenberg-type interaction, which is isotropic in spin space, is cancelled out, and the Kitaev-type interaction is realized.

This is the essence of the Jackeli-Khaliullin mechanism. Transition metal compounds in the 4d and 5d electron systems are thought to satisfy the conditions for this mechanism to be realized. Inspired by this point of view, a number of candidate

materials for the Kitaev model have been synthesized and their properties have been investigated intensively by various measurements [18–23].

1.3 Aim of This Dissertation

The observation of evidence of Majorana fermionic excitations in candidate materials, as predicted by Kitaev, does not mean the end of research on Kitaev quantum spin liquids. Through the study on it, many unanswered questions have emerged and connections with other fields have expanded. Kitaev himself aims to realize fault-tolerant quantum computation by anyons, and has proposed the Kitaev model as a model in which required anyons appear. This can be seen in the introduction of the original paper Ref. [13] in which the Kitaev model was proposed, and in the predecessor paper Ref. [26] in which the toric code was proposed. There is still a long way to go to realize the application of non-Abelian anyons in the Kitaev matters to fault-tolerant topological quantum computation.

As a stepping stone to such an application, it is first necessary to study (i) further exploration and understanding of the candidate materials and (ii) proposal of methods to control the Majorana fermions in Kitaev quantum spin liquid states. In addition, these issues are not independent, but closely related. In this doctoral dissertation, the research will focus on (i) above.

Due to the proposal of the Jackeli-Khaliullin mechanism, which was briefly reviewed in the previous section, many candidate materials have been proposed and experiments have been performed. However, in real materials, there are magnetic interactions that are not included in the Kitaev model, such as the Heisenberg interaction, which is isotropic in spin space, the spin-diagonal interaction, the spin-spin interaction beyond the nearest neighbor, and so on, due to effects and processes not considered in the above discussion, for example distortion of IrO_6 octahedra and direct hoppings between d-orbitals in transition metals. Phase transitions to magnetic orders have been observed at low temperatures in almost all candidates except $H_3LiIr_2O_6$ [33]. α-$RuCl_3$, a candidate material for which the thermal Hall effect was measured, also undergoes zigzag antiferromagnetic ordering at low temperatures. Therefore, the Hall coefficient was measured in the region where the ordering was suppressed by applying magnetic field. In addition, impurities and lattice defects inevitably appear in solids, and these induce spin-glass states.

Therefore, we investigate the feasibility of Kitaev spin liquids in ultracold atomic systems. In these systems, the strength and type of interaction can be controlled by irradiating a laser or other means, so that the desired interaction can be designed. In addition, there are no impurities or lattice defects that inevitably appear in solid materials. In particular, one of our goals is to elucidate whether Kitaev quantum spin liquids can be realized by focusing on the proposed in Refs. [34, 35] of designing Kitaev-type interactions in a cool polar molecular system in an optical lattice.

The other topic in this dissertation is related to the realization of quantum spin liquids in high-spin Kitaev materials. The Kitaev model is originally a quantum spin model with $S = 1/2$, but there has been a lot of research on the Kitaev model with $S > 1/2$ in recent years [36–44]. In particular, there has been much interest in the topological differences between the case where S is half odd integers and the case where S is integers, but no exact solution has been obtained as in the case of $S = 1/2$. It has been rigorously shown that the $\mathbb{Z}_2$ fluxes are conserved quantities even in the general case of S [45]. However, numerical calculations of specific heat and entropy indicate that there are contributions from degrees of freedom other than the

$\mathbb{Z}_2$ fluxes at low temperatures. It is considered that understanding these additional fractionalized degrees of freedom is important to elucidate the physics of the $S > 1/2$ Kitaev quantum spin liquid. The mechanisms for higher-spin Kitaev model are proposal and candidate materials for $S = 1$ Kitaev model [46] are proposed recently. In addition, the candidate materials for $S = 3/2$ Kitaev model are also discussed recently [47–50]. Experimental and theoretical studies on spin-S Kitaev materials are important for both elucidating the physics of spin-S Kitaev quantum spin liquid and exploring new spin liquid materials. In this dissertation, we consider the Kitaev-Heisenberg model [51, 52] as a minimal model for Kitaev materials and calculate phase diagram of spin-S Kitaev-Heisenberg model to estimate the upper bound of S for realization of Kitaev quantum spin liquid in higher-spin candidate materials.

In order to achieve these goals, we need methods that can handle the dipole interaction in ultracold polar molecular systems and the general spin length S. Therefore, we use pseudo-fermion functional renormalization group (PFFRG) method as our main numerical technique, which is an application of the functional renormalization group for interacting fermion systems to quantum spin systems. PFFRG is a new method developed in 2010 [53, 54], and its extension is still under active discussion. In this doctoral dissertation, we use this method to address the two topics mentioned above.

1.4 Structure of This Dissertation

We illustrate the structure of the dissertation in order.

In Chap. 2, we describe the 1-particle irreducble (1PI) scheme functional renormalization group (FRG) for fermion many-body systems, which is the basis of the PFFRG we use. First, we define the generating functionals of the Green's functions and the vertices, and then derive the exact flow equation. Finally, applications to electron systems are discussed.

In Chap. 3, we explain the formulation of PFFRG we use. We derive the renormalization group flow equations assuming that we are dealing with Kitaev-type interactions. First, we rewrite the spin Hamiltonians by introducing pseudo-fermions and apply the fermionic functional renormalization group to it. Next, we derive a formula to calculate the spin susceptibilities, which are observables, from the vertices obtained by PFFRG. Finally, we review the extensions of PFFRG, including the extension to general length of spin S.

In Chap. 4, we discuss the feasibility of the Kitaev quantum spin liquid in ultracold polar molecular systems using PFFRG. First, we discuss the application of ultracold polar molecular systems as a quantum simulator of the Heisenberg model,and review previous studies using numerical methods including PFFRG. Then, we will give a short description of previous studies that proposed the realization of Kitaev-type interactions in ultracold polar molecular systems trapped in optical lattice, set up the dipolar Kitaev model from the previous studies, and investigate the feasibility of Kitaev quantum spin liquid by PFFRG.

In Chap. 5, we discuss up to how long S it is possible to realize Kitaev quantum spin liquid in high-spin candidate materials. We regard the Kitaev-Heisenberg model as a minimal model of Kitaev materials and explain its properties, first. Then, we review some earlier studies on it. Finally, we conduct spin-S PFFRG calculation for spin-S Kitaev model and spin-S Kitaev-Heisenberg model.

In Chap. 6, we summarize the our main results described in Chap. 4 and Chap. 5. Then we mention our future perspective.

Chapter 2

The General Framework of the Functional Renormalization Group

In this chapter, we present the general framework of the functional renormalization group (FRG) approach. Then we review its implementation for spin systems in the next chapter. In the first section, we review the problems of the conventional field theoretical Wilsonian renormalization group (RG) methods and the key concept of FRG. Subsequently, we outline the fermionic FRG scheme based on the generating functionals along References [55, 56]. We introduce several generating functionals and variables which parametrize RG flow. By considering derivative of the generating functionals about these variables, we derive exact RG equations for FRG. These equations cannot be solved as they are. Therefore we expand the exact RG equation and decompose it into coupled integro-differential equations. Finally we consider an application to the simple correlated electron systems.

2.1 Functional Renormalization Group

The functional renormalization group (FRG or fRG) method is a refinement of the conventional Wilsonian renormalization group (RG) method in the field theory [55–66]. This is also called non-perturbative renormalization group (NPRG) or exact renormalization group (ERG), depending on the context. Although FRG can be formulated in either boson fields, fermion fields, or mixtures of the two, in this dissertation we consider FRG in fermion systems in order to treat pseudo-fermion systems, which will be introduced in the next chapter. Not only in the dissertation, but in general, the problem of interacting Fermionic systems is very important in condensed matter physics, since electrons play a leading role in solid state physics. In particular, strongly correlated fermion (electron) systems cannot be solved exactly, and there are many unsolved problems including high-temperature superconductivity. Solving these systems is still a central issue in condensed matter physics today. For this reason, many computational methods for strongly correlated fermion systems have been proposed. Since the perturbation theory is no longer justified when the correlations between fermions are strong, calculations that are not rooted in the perturbation theory are necessary. In addition, various fluctuations exist in the systems with strong correlations, and furthermore, they are interdependent. Therefore, it is necessary to perform bias-free calculations that do not overestimate specific fluctuations.

Here, we consider the conventional Wilsonian RG in fermionic field theory [67]. At first, we define the (grand) partition function by functional integral with respect

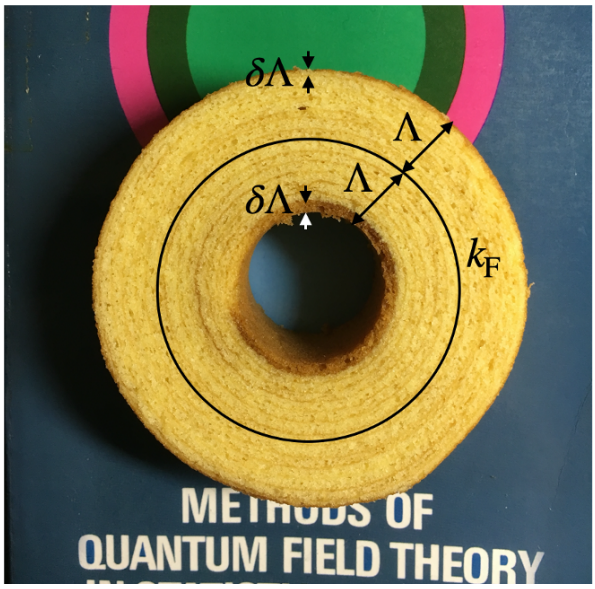

FIGURE 2.1: Picture representing momentum space Wilsonian RG procedure in fermionic field theory. k_F denotes the Fermi momentum and the circle drawn with a black line represents the Fermi surface. Like eating a Baumkuchen by peeling it off one layer at a time, we integrate and eliminate the fields contained in the width of $\delta\Lambda$. This photo was taken by me placing a Baumkuchen on top of the Fermi surface depicted on the cover of the textbook written by A. A. Abrikosov, L. P. Gorkov, and I. E. Dzyaloshinski [68].

to fermionic fields $\{\psi\}$ and $\{\overline{\psi}\}$ corresponding to the annihilation and creation operators.

$$\mathcal{Z} = \int \mathcal{D}\overline{\psi}\mathcal{D}\psi \, \mathrm{e}^{-\mathcal{S}[\overline{\psi},\psi]}, \tag{2.1}$$

where $\mathcal{S}[\overline{\psi},\psi]$ is action of the system. The details about fermionic field theory are discussed in the next section. We introduce energy cutoff scale Λ and divide the fields into those with energies greater than the cutoff ("fast fields") $\psi_>$ and those with energies less ("slow fields") $\psi_<$. We can derive the low energy effective action by integration over the fast fields. Next, we calculate how the effective action of the system changes when the cutoff is lowered from Λ to $\Lambda - \delta\Lambda$. This procedure can be written symbolically as [1]

$$\mathcal{Z} = \int^{\Lambda} \mathcal{D}\overline{\psi}\mathcal{D}\psi \, \mathrm{e}^{-\mathcal{S}^{\Lambda}[\overline{\psi},\psi]} \simeq \int^{\Lambda-\delta\Lambda} \mathcal{D}\overline{\psi}_< \mathcal{D}\psi_< \, \mathrm{e}^{-\mathcal{S}^{\Lambda-\delta\Lambda}[\overline{\psi}_<,\psi_<]}. \tag{2.2}$$

We can think of this as a procedure of integrating out the fields in the width of $\delta\Lambda$, as if we were eating a Baumkuchen by peeling it off one layer at a time. This is shown in Fig. 2.1. As shown in the Fig. 2.1, we take the Fermi energy ε_F $(= k_F^2/2m)$ as the origin of the energy, and calculating the low-energy effective action corresponds to constructing an effective theory on the Fermi surface. In this process, by calculating how the coupling constants of the interactions of the system $g_m(\Lambda)$ $(m = 1, 2, \cdots)$

[1] Precisely scale transformations are needed to keep the Gaussian measure of the functional integral invariant.

are transformed, we can obtain differential equations for them:

$$\frac{\mathrm{d}g_m(\Lambda)}{\mathrm{d}\Lambda} = C_m^{\Lambda}. \tag{2.3}$$

These are RG equations.

As shown in Eq. (2.2), the conventional Wilsonian RG is non-perturbative in concept, but when actually performing the calculation and finding the right-hand sides of the RG equations, diagrammatic calculations are required, which make it perturbative. Also, it is impossible to consider all diagrams, so only certain diagrams are taken into account. Therefore, the calculation is biased in favor of only certain processes and fluctuations. Furthermore, since only a finite number of coupling constants can be taken into account, we can consider only certain points, such as the van Hove singularity, when the Fermi surface is not isotropic. This fact also leads to a large bias.

FRG is a method that overcomes these shortcomings. As will be explained in the following sections, FRG allows us to obtain exact renormalization group equations by considering differential equations for the generating functional of the Green's functions or interacting vertices. By expanding the obtained exact renormalization group equations for fermionic fields, we can derive the renormalization group equations of each order. This expansion is exact because it is Taylor expansions for Grassmann variables, and the resulting equations include the channels of each fluctuation with equal footing. This enable us perform unbiased calculation. We also have access to the interaction vertices at every point to add the cutoff to the Gaussian measure of the functional integral. Thus, the FRG is non-perturbative in both concept and equations, and can be used even when the interactions are strong, at least in principle. When we expand the exact renormalization group equation for the generating functional for a fermionic field, an infinite hierarchy of equations appears. So we need to truncate it at a finite order, and this truncation makes the calculation approximate. The idea of considering the renormalization group for the generating functional was proposed in 1973 [69]. Later, the theory was refined, and Polchinski scheme [70], Wick-ordered scheme [57, 58], 1PI (1-particle irreducible) scheme [71], and other theories were proposed. In this dissertation, we use the 1PI scheme. This was proposed by C. Wetterich in 1993 [71] and is the convenient and most commonly used scheme. Hence, in this chapter, we mainly present the 1PI FRG scheme. Recently, a quantitative comparison of the results of the multi-loop FRG of the two-dimensional Hubbard model with those of the determinat quantum Monte Carlo method is also presented [72]. Research on improving the accuracy and extending the range of application of FRG is still being actively conducted.

2.2 Several Basics of Field Theory and Notations

This section is devoted to a very short review of the path integral (functional integral) formalism to confirm the notation and to introduce linked cluster theorem. The author referred mainly [73] and sometimes [74]. Here we use finite temperature formalism.

Here we consider a system described by the action

$$\mathcal{S}[\overline{\psi}, \psi] = \mathcal{S}_0[\overline{\psi}, \psi] + \mathcal{S}_{\mathrm{int}}[\overline{\psi}, \psi], \tag{2.4}$$

where $\mathcal{S}_0$ is the non-interacting part and $\mathcal{S}_{\rm int}$ is the interacting part of the action. ψ and $\overline{\psi}$ are Grassmann variables corresponding to annihilation and creation operators of fermions, respectively. The action is a functional of these variables. In general, the non-interacting parts of actions have the form

$$\mathcal{S}_0[\overline{\psi},\psi] = -(\overline{\psi}, G_0^{-1}\psi), \tag{2.5}$$

where G_0 represents the one-particle (one-body) Green's function[2] of the non-interacting system and $(\cdots,\cdots)$ means an "inner product" i.e. the sum: $(f,g) = \sum_x f(x)g(x)$ where f and g are functions of x. Therefore,

$$(\overline{\psi}, G_0^{-1}\psi) = \sum_x \overline{\psi}(x)(G_0^{-1}\psi)(x), \tag{2.6}$$

where

$$(G_0^{-1}\psi)(x) = \sum_{x'} G_0^{-1}(x,x')\psi(x'). \tag{2.7}$$

Here, x and x' represent sets of the appropriate quantum numbers for single-particle basis and imaginary-time/Matsubara frequency. The symbol $\sum_x$ represents summations for discrete variables in x and integrals for continuous variables in x. In addition, the sum includes appropriate prefactors such as inverse temperature β or volume Ω depend on the choice of x. We introduce the above rules for representation independent on arguments of field variables. If we consider an electron system with translational invariance and spin-rotational invariance, one of the appropriate choices of x is $x = (\mathrm{i}\omega_n, \boldsymbol{k}, m, \alpha)$. Here, i, ω_n, $\boldsymbol{k}$, m, and α are imaginary unit $\sqrt{-1}$, fermionic Matsubara frequency $(2n+1)\pi T$ $(n \in \mathbb{Z})$, momentum, band index, and spin index (spin configuration), respectively. Here $T = 1/\beta$ represents temperature. In this choice of x, the bare Green's function is

$$\begin{aligned} G_0(x,x') &= G_0(\mathrm{i}\omega_n, \boldsymbol{k}, m, \alpha;\ \mathrm{i}\omega_{n'}, \boldsymbol{k}', m', \alpha') \\ &= \beta\Omega\delta_{n,n'}\delta_{\boldsymbol{k},\boldsymbol{k}'}\delta_{m,m'}\delta_{\alpha,\alpha'}G_0(\mathrm{i}\omega_n, \boldsymbol{k}, m) \\ &= \beta\Omega\delta_{n,n'}\delta_{\boldsymbol{k},\boldsymbol{k}'}\delta_{m,m'}\delta_{\alpha,\alpha'}\frac{1}{\mathrm{i}\omega_n - \xi_{\boldsymbol{k}m}}. \end{aligned} \tag{2.8}$$

We sometimes use " ; " instead of " , " to separate sets of arguments as above. In this dissertation, we adopt a non-unitary definition of Fourier transformation which is introduced in Appendix A.

We focus on the interacting part next. Generally, two-body interaction has the form

$$\mathcal{S}_{\rm int}[\overline{\psi},\psi] = \frac{1}{4}\sum_{x_1,x_2,x_1',x_2'} V(x_1',x_2';x_1,x_2)\overline{\psi}(x_1')\overline{\psi}(x_2')\psi(x_2)\psi(x_1). \tag{2.9}$$

The factor $1/4 = 1/(2!)^2$ is due to anti-symmetrization of interacting matrix elements [68, 73]. It is anti-symmetric function by exchanges $x_1 \rightleftarrows x_2$ and $x_1' \rightleftarrows x_2'$. For example, consider a system with the interacting part of the Hamiltonian as

$$\mathcal{H}_{\rm int} = \frac{1}{2}\int \mathrm{d}^d r_1 \int \mathrm{d}^d r_2 \sum_{\alpha,\beta,\gamma,\delta} \psi_\alpha^\dagger(\boldsymbol{r}_1)\psi_\beta^\dagger(\boldsymbol{r}_2)U_{\alpha\beta,\gamma\delta}(\boldsymbol{r}_1-\boldsymbol{r}_2)\psi_\delta(\boldsymbol{r}_2)\psi_\gamma(\boldsymbol{r}_1). \tag{2.10}$$

Here $\psi_\alpha(\boldsymbol{r})$ and $\psi_\alpha^\dagger(\boldsymbol{r})$ are anihilation and creation operators of fermion at coordinate $\boldsymbol{r}$ with spin index α. U is the matrix element of interaction and d is the dimension of

[2] Sometimes it is called the Green function. We call it the Green's function here and after [75].

the system. Corresponding interacting part of the action is

$$\mathcal{S}_{\rm int} = \frac{1}{2}\int_0^\beta \mathrm{d}\tau_1 \int_0^\beta \mathrm{d}\tau_2 \int \mathrm{d}^d r_1 \int \mathrm{d}^d r_2 \sum_{\alpha,\beta,\gamma,\delta} \times \overline{\psi}_\alpha(\tau_1, \boldsymbol{r}_1)\overline{\psi}_\beta(\tau_2, \boldsymbol{r}_2) U_{\alpha\beta,\gamma\delta}(\boldsymbol{r}_1 - \boldsymbol{r}_2)\delta(\tau_1 - \tau_2)\psi_\delta(\tau_2, \boldsymbol{r}_2)\psi_\gamma(\tau_1, \boldsymbol{r}_1). \quad (2.11)$$

After anti-symmetrization, the interacting part is

$$\mathcal{S}_{\rm int} = \frac{1}{4}\int_0^\beta \mathrm{d}\tau_1' \int_0^\beta \mathrm{d}\tau_2' \int_0^\beta \mathrm{d}\tau_1 \int_0^\beta \mathrm{d}\tau_2 \int \mathrm{d}^d r_{1'} \int \mathrm{d}^d r_{2'} \int \mathrm{d}^d r_1 \int \mathrm{d}^d r_2 \sum_{\alpha_{1'},\alpha_{2'},\alpha_1,\alpha_2} \times \overline{\psi}_{\alpha_{1'}}(\tau_{1'}, \boldsymbol{r}_{1'})\overline{\psi}_{\alpha_{2'}}(\tau_{2'}, \boldsymbol{r}_{2'}) V_{\alpha_{1'}\alpha_{2'},\alpha_1\alpha_2}(\tau_{1'}\boldsymbol{r}_{1'}, \tau_{2'}\boldsymbol{r}_{2'}; \tau_1\boldsymbol{r}_1, \tau_2\boldsymbol{r}_2)\psi_{\alpha_2}(\tau_2, \boldsymbol{r}_2)\psi_{\alpha_1}(\tau_1, \boldsymbol{r}_1), \quad (2.12)$$

with

$$\begin{aligned} &V_{\alpha_{1'}\alpha_{2'},\alpha_1\alpha_2}(\tau_{1'}\boldsymbol{r}_{1'}, \tau_{2'}\boldsymbol{r}_{2'}; \tau_1\boldsymbol{r}_1, \tau_2\boldsymbol{r}_2) \\ &= U_{\alpha_{1'}\alpha_{2'},\alpha_1\alpha_2}(\boldsymbol{r}_1 - \boldsymbol{r}_2)\delta(\tau_1 - \tau_2)\delta(\boldsymbol{r}_{1'} - \boldsymbol{r}_1)\delta(\tau_{1'} - \tau_1)\delta(\boldsymbol{r}_{2'} - \boldsymbol{r}_2)\delta(\tau_{2'} - \tau_2) \\ &\quad - U_{\alpha_{2'}\alpha_{1'},\alpha_1\alpha_2}(\boldsymbol{r}_1 - \boldsymbol{r}_2)\delta(\tau_1 - \tau_2)\delta(\boldsymbol{r}_{1'} - \boldsymbol{r}_2)\delta(\tau_{1'} - \tau_2)\delta(\boldsymbol{r}_{2'} - \boldsymbol{r}_1)\delta(\tau_{2'} - \tau_1). \end{aligned} \quad (2.13)$$

The (grand) partition function is obtained by path integral (functional integral) respect to the Grassmann variables $\overline{\psi}$ and ψ:

$$\mathcal{Z} = \int \mathcal{D}\overline{\psi}\mathcal{D}\psi\, \mathrm{e}^{-\mathcal{S}[\overline{\psi},\psi]}\,. \quad (2.14)$$

The integral measure $\mathcal{D}\overline{\psi}\mathcal{D}\psi$ sometimes contains some constant prefactors if exist. We also define the non-interacting grand partition function $\mathcal{Z}_0$ as the same manner:

$$\mathcal{Z}_0 = \int \mathcal{D}\overline{\psi}\mathcal{D}\psi\, \mathrm{e}^{-\mathcal{S}_0[\overline{\psi},\psi]} = \mathrm{Det}\left[-G_0^{-1}\right]. \quad (2.15)$$

The free energy (to be precise, grand potential) is given by the natural logarithm of partition function

$$\mathcal{F} = -\frac{1}{\beta}\ln \mathcal{Z}, \quad (2.16)$$

and that without interacting part is also given by

$$\mathcal{F}_0 = -\frac{1}{\beta}\ln \mathcal{Z}_0 \left(= -\frac{1}{\beta}\ln\left[\mathrm{Det}\{-G_0^{-1}\}\right] = -\frac{1}{\beta}\mathrm{Tr}\left[\ln\{-G_0^{-1}\}\right]\right). \quad (2.17)$$

Taking logarithm means to collect only connected Feynman diagrams i.e.

$$\mathcal{F} - \mathcal{F}_0 = -\frac{1}{\beta}\sum(\text{all connected diagrams}). \quad (2.18)$$

This fact is called the Linked cluster theorem [73, 74]. We can prove it easily by replica technique introduced below.

Linked Cluster Theorem

Here we derive the theorem and introduce replica technique [73]. At first, we consider n ($\in \mathbb{N}$) replicas of the system. Since they do not interact, the grand partition

function is $\mathcal{Z}^n$. Then we expand it as

$$\mathcal{Z}^n = \mathrm{e}^{n\ln\mathcal{Z}} = 1 + n\ln\mathcal{Z} + \sum_{m=2}^{\infty}\frac{1}{m!}(n\ln\mathcal{Z})^m. \tag{2.19}$$

At last, we continue[3] n to $\mathbb{R}$ and take the limit after differentiation:

$$\lim_{n\to 0}\frac{\mathrm{d}}{\mathrm{d}n}\mathcal{Z}^n = \lim_{n\to 0}\frac{\mathrm{d}}{\mathrm{d}n}[\mathrm{e}^{n\ln\mathcal{Z}}] = \ln\mathcal{Z}. \tag{2.20}$$

To calculate $\mathcal{Z}^n$, we introduce replica index ρ which runs from 1 to n. Expanding it m-th order

$$\begin{aligned}\left(\frac{\mathcal{Z}}{\mathcal{Z}_0}\right)^n &= \frac{1}{\mathcal{Z}_0^n}\int\prod_{\rho=1}^{n}\mathcal{D}\overline{\psi}^\rho\mathcal{D}\psi^\rho\ \mathrm{e}^{-\sum_{\rho=1}^{n}(\mathcal{S}_0[\overline{\psi}^\rho,\psi^\rho]+\mathcal{S}_{\mathrm{int}}[\overline{\psi}^\rho,\psi^\rho])}\\ &= \sum_{m=0}^{\infty}\frac{(-1)^m}{m!}\sum_{\rho_1=1}^{n}\cdots\sum_{\rho_m=1}^{n}\left\langle\mathcal{S}_{\mathrm{int}}[\overline{\psi}^{\rho_1},\psi^{\rho_1}]\cdots\mathcal{S}_{\mathrm{int}}[\overline{\psi}^{\rho_m},\psi^{\rho_m}]\right\rangle_0.\end{aligned} \tag{2.21}$$

The average $\langle\cdots\rangle_0$ means $\int\mathcal{D}\overline{\psi}\mathcal{D}\psi\,\mathrm{e}^{-\mathcal{S}_0}\cdots/\int\mathcal{D}\overline{\psi}\mathcal{D}\psi\,\mathrm{e}^{-\mathcal{S}_0} = \frac{1}{\mathcal{Z}_0}\int\mathcal{D}\overline{\psi}\mathcal{D}\psi\,\mathrm{e}^{-\mathcal{S}_0}\cdots$, average by non-interacting action $\mathcal{S}_0$. We use Feynman rules and calculate sums of diagrams. Each propagator carries a replica index ρ, and each connected part of diagrams must carry the same replica index. Therefore, the sum over the all replica indices yield the factor n^{n_c} where n_c is the number of the connected part of the diagram. Replica technique introduced above pick up only n linear term, and Feynman diagrams proportional to n are those with only one connected part. Therefore, replica technique means that we pick up only connected diagrams.

2.3 Generating Functionals

In this section, we introduce several kinds of generating functionals and some important functions such as the Green's functions and the vertex functions.

Generating Functionals of the Green's Functions

At first, we consider the source term added the action

$$\mathcal{S}[\overline{\psi},\psi] \to \mathcal{S}[\overline{\psi},\psi] - (\overline{\eta},\psi) - (\overline{\psi},\eta), \tag{2.22}$$

with Grassmann variables $\overline{\eta}$, η and a functional defined by it

$$W[\overline{\eta},\eta] = \int\mathcal{D}\overline{\psi}\mathcal{D}\psi\,\mathrm{e}^{-\mathcal{S}[\overline{\psi},\psi]+(\overline{\eta},\psi)+(\overline{\psi},\eta)}. \tag{2.23}$$

Defining the *disconnected* m-body ($2m$-point, m-particle) Green's functions as

$$G_{\mathrm{dc}}^{(2m)}(x_1,\cdots,x_m;x_1',\cdots,x_m') = -\langle\psi(x_1)\cdots\psi(x_m)\overline{\psi}(x_m')\cdots\overline{\psi}(x_1')\rangle_{\mathrm{dc}}, \tag{2.24}$$

[3] This analytic continuation have very sensitive problem related to Carlson's theorem. Here we do not concern mathematically rigorous discussion, and we use replica technique only for formulation.

with $\langle\cdots\rangle_{\rm dc} = \int \mathcal{D}\overline{\psi}\mathcal{D}\psi\ \mathrm{e}^{-\mathcal{S}}\cdots$, we can see that $W[\overline{\eta},\eta]$ is a generating functional of the disconnected Green's functions:

$$G^{(2m)}_{\rm dc}(x_1,\cdots,x_m;x'_1,\cdots,x'_m) = (-1)^{m+1}\frac{\delta^{2m}W[\overline{\eta},\eta]}{\delta\overline{\eta}(x_1)\cdots\delta\overline{\eta}(x_m)\delta\eta(x'_m)\cdots\delta\eta(x'_1)}\bigg|_{\eta,\overline{\eta}=0}. \tag{2.25}$$

Disconnected Green's functions contain not only connected parts but also disconnected parts. To obtain m-body ($2m$-particle or m-particle) Green's functions, we divide (2.25) by the partition function $\mathcal{Z}$.

$$G^{(2m)}(x_1,\cdots,x_m;x'_1,\cdots,x'_m) = (-1)^{m+1}\frac{1}{\mathcal{Z}}\frac{\delta^{2m}W[\overline{\eta},\eta]}{\delta\overline{\eta}(x_1)\cdots\delta\overline{\eta}(x_m)\delta\eta(x'_m)\cdots\delta\eta(x'_1)}\bigg|_{\eta,\overline{\eta}=0}. \tag{2.26}$$

The m-body ($2m$-point or m-particle) Green's functions obtained above are defined as

$$G^{(2m)}(x_1,\cdots,x_m;x'_1,\cdots,x'_m) = -\langle\psi(x_1)\cdots\psi(x_m)\overline{\psi}(x'_m)\cdots\overline{\psi}(x'_1)\rangle, \tag{2.27}$$

with $\langle\cdots\rangle = \frac{1}{\mathcal{Z}}\int \mathcal{D}\overline{\psi}\mathcal{D}\psi\ \mathrm{e}^{-\mathcal{S}}\cdots$. These Green's functions have partial diagrams which do not necessarily connect ALL external legs although they do not have partial diagrams which are not connected to ANY external legs and cancelled by $\mathcal{Z}$ in the denominators.

Although we always use Green's functions introduced above, it is convenient to define *connected* Green's functions for systematic calculation. The connected m-body ($2m$-point or m-particle) Green's functions are defined as

$$G^{(2m)}_{\rm c}(x_1,\cdots,x_m;x'_1,\cdots,x'_m) = -\langle\psi(x_1)\cdots\psi(x_m)\overline{\psi}(x'_m)\cdots\overline{\psi}(x'_1)\rangle_{\rm c}, \tag{2.28}$$

where the subscript "c" means *connected* parts of diagrams. Here, "*connected*" means that the diagrams are connected to all external legs. By definition,

$$G^{(2)}_{\rm c} = G^{(2)}, \tag{2.29}$$

but

$$G^{(2m)}_{\rm c} \neq G^{(2m)} \text{ for } m \geq 2. \tag{2.30}$$

Hereafter, we write G instead of $G^{(2)}_{\rm c} = G^{(2)}$ for simplicity. The generating functional of the connected Green's functions is given by

$$\begin{aligned}\mathcal{G}[\overline{\eta},\eta] &= -\ln W[\overline{\eta},\eta] \\ &= -\ln\int \mathcal{D}\overline{\psi}\mathcal{D}\psi\ \mathrm{e}^{-\mathcal{S}[\overline{\psi},\psi]+(\overline{\eta},\psi)+(\overline{\psi},\eta)},\end{aligned} \tag{2.31}$$

and it is understood by replica technique. Connected m-body ($2m$-point or m-particle) Green's functions are obtained by functional derivative

$$G^{(2m)}_{\rm c}(x_1,\cdots,x_m;x'_1,\cdots,x'_m) = (-1)^{m}\frac{\delta^{2m}\mathcal{G}[\overline{\eta},\eta]}{\delta\overline{\eta}(x_1)\cdots\delta\overline{\eta}(x_m)\delta\eta(x'_m)\cdots\delta\eta(x'_1)}\bigg|_{\eta,\overline{\eta}=0}. \tag{2.32}$$

This is why $\mathcal{G}[\overline{\eta},\eta]$ is called generating functional of connected Green's functions or merely generating functional.

If there are no interactions, Gaussian integral for Grassmann variables [4] is exactly carried out and obtain the identity

$$\begin{aligned}\int \mathcal{D}\overline{\psi}\mathcal{D}\psi\, \mathrm{e}^{-\mathcal{S}_0[\overline{\psi},\psi]+(\overline{\eta},\psi)+(\overline{\psi},\eta)} &= \int \mathcal{D}\overline{\psi}\mathcal{D}\psi\, \mathrm{e}^{(\overline{\psi},G_0^{-1}\psi)}\mathrm{e}^{(\overline{\eta},\psi)+(\overline{\psi},\eta)} \\ &= \mathcal{Z}_0\mathrm{e}^{-(\overline{\eta},G_0\eta)},\end{aligned} \tag{2.35}$$

where $\mathcal{Z}_0 = \int \mathcal{D}\overline{\psi}\mathcal{D}\psi\, \mathrm{e}^{(\overline{\psi},G_0^{-1}\psi)} = \mathrm{Det}(-G_0^{-1})$. Therefore,

$$\mathcal{G}[\overline{\eta},\eta] = -\ln \mathcal{Z}_0 + (\overline{\eta}, G_0\eta). \tag{2.36}$$

In general case with interaction, expanding $\mathcal{G}[\overline{\eta},\eta]$ as a power series of the source fields, connected Green's functions are given by the coefficients of the series:

$$\mathcal{G}[\overline{\eta},\eta] = -\ln \mathcal{Z} + (\overline{\eta}, G\eta) + \frac{1}{(2!)^2}\sum_{\substack{x_1,x_2\\x_1',x_2'}} G_{\mathrm{c}}^{(4)}(x_1,x_2;x_1',x_2')\overline{\eta}(x_1)\overline{\eta}(x_2)\eta(x_2')\eta(x_1') + \cdots \tag{2.37}$$

$$\begin{aligned}&= -\ln \mathcal{Z} \\ &+ \sum_{m=1}^{\infty}\frac{1}{(m!)^2}\sum_{\substack{x_1,\cdots,x_m\\x_1',\cdots,x_m'}} G_{\mathrm{c}}^{(2m)}(x_1,\cdots,x_m;x_1',\cdots,x_m')\overline{\eta}(x_1)\cdots\overline{\eta}(x_m)\eta(x_m')\cdots\eta(x_1').\end{aligned} \tag{2.38}$$

Here we define the Taylor expansion of functions of Grassmann variables [74] as

$$f(\xi_1,\cdots,\xi_n) = \sum_{m=0}^{\infty}\frac{1}{m!}\sum_{i_1,\cdots,i_m=1}^{n}\left.\frac{\partial^m f}{\partial\xi_{i_1}\cdots\partial\xi_{i_m}}\right|_{\xi=0}\xi_{i_m}\cdots\xi_{i_1}, \tag{2.39}$$

where f is an analytic function of Grassmann variables $\{\xi_1,\cdots,\xi_n\}$. We derive the above relation between $\mathcal{G}[\overline{\eta},\eta]$ and $G_{\mathrm{c}}^{(2m)}$ based on this definition of Taylor expansion formula. The m-th order terms of the Taylor expansion of the generating functional with respect to $\{\eta\}$ are obtained by above definition,

$$\sum_{x_1',\cdots,x_m'}\frac{1}{m!}\left.\frac{\delta^m\mathcal{G}[\overline{\eta},\eta]}{\delta\eta(x_m')\cdots\delta\eta(x_1')}\right|_{\eta=0}\eta(x_1')\cdots\eta(x_m'), \tag{2.40}$$

then performing expansion with respect to $\{\overline{\eta}\}$, we obtain

$$\sum_{\substack{x_1,\cdots,x_m\\x_1',\cdots,x_m'}}\frac{1}{(m!)^2}\left.\frac{\delta^{2m}\mathcal{G}[\overline{\eta},\eta]}{\delta\overline{\eta}(x_1)\cdots\delta\overline{\eta}(x_m)\delta\eta(x_m')\cdots\delta\eta(x_1')}\right|_{\eta,\overline{\eta}=0}\eta(x_1')\cdots\eta(x_m')\overline{\eta}(x_m)\cdots\overline{\eta}(x_1). \tag{2.41}$$

[4] Gaussian integral for Grassmann variables [73, 74] is

$$\int\prod_i \mathrm{d}\overline{\psi}_i\mathrm{d}\psi_i\, \mathrm{e}^{-\sum_{i,j}\overline{\psi}_i A_{ij}\psi_j+\sum_i\overline{\eta}_i\psi_i+\sum_i\overline{\psi}_i\eta_i} = [\det A]\,\mathrm{e}^{\sum_{i,j}\overline{\eta}_i(A^{-1})_{ij}\eta_j}, \tag{2.33}$$

and

$$\det A = \int\prod_i \mathrm{d}\overline{\psi}_i\mathrm{d}\psi_i\, \mathrm{e}^{-\sum_{i,j}\overline{\psi}_i A_{ij}\psi_j}. \tag{2.34}$$

Now we consider to rearrange

$$\eta(x_1')\cdots\eta(x_m')\overline{\eta}(x_m)\cdots\overline{\eta}(x_1) \tag{2.42}$$

to

$$\overline{\eta}(x_1)\cdots\overline{\eta}(x_m)\eta(x_m')\cdots\eta(x_1') \tag{2.43}$$

in the manner below:

$$\begin{aligned}
&\eta(x_1')\cdots\eta(x_m')\overline{\eta}(x_m)\cdots\overline{\eta}(x_1)\\
&=(-1)^{2m-1}\overline{\eta}(x_1)\eta(x_1')\cdots\eta(x_m')\overline{\eta}(x_m)\cdots\overline{\eta}(x_2)\\
&=(-1)^{2m-1}(-1)^{2m-2}\overline{\eta}(x_1)\overline{\eta}(x_2)\eta(x_1')\cdots\eta(x_m')\overline{\eta}(x_m)\cdots\overline{\eta}(x_3)\\
&=\cdots\\
&=(-1)^{\sum_{k=1}^{2m-1}(2m-k)}\overline{\eta}(x_1)\cdots\overline{\eta}(x_m)\eta(x_m')\cdots\eta(x_1'),
\end{aligned} \tag{2.44}$$

where

$$\begin{aligned}
(-1)^{\sum_{k=1}^{2m-1}(2m-k)}&=(-1)^{2m(2m-1)-\frac{1}{2}\cdot 2m(2m-1)}\\
&=(-1)^{2m(2m-1)-m(2m-1)}\\
&=(-1)^{m(2m-1)}=(-1)^m.
\end{aligned} \tag{2.45}$$

Therefore,

$$\begin{aligned}
&\frac{1}{(m!)^2}\sum_{\substack{x_1,\cdots,x_m\\x_1',\cdots,x_m'}}\frac{\delta^{2m}\mathcal{G}[\overline{\eta},\eta]}{\delta\overline{\eta}(x_1)\cdots\delta\overline{\eta}(x_m)\delta\eta(x_m')\cdots\delta\eta(x_1')}\bigg|_{\eta,\overline{\eta}=0}\eta(x_1')\cdots\eta(x_m')\overline{\eta}(x_m)\cdots\overline{\eta}(x_1)\\
&=\frac{1}{(m!)^2}\sum_{\substack{x_1,\cdots,x_m\\x_1',\cdots,x_m'}}(-1)^m\frac{\delta^{2m}\mathcal{G}[\overline{\eta},\eta]}{\delta\overline{\eta}(x_1)\cdots\delta\overline{\eta}(x_m)\delta\eta(x_m')\cdots\delta\eta(x_1')}\bigg|_{\eta,\overline{\eta}=0}\overline{\eta}(x_1)\cdots\overline{\eta}(x_m)\eta(x_m')\cdots\eta(x_1')\\
&=\frac{1}{(m!)^2}\sum_{\substack{x_1,\cdots,x_m\\x_1',\cdots,x_m'}}G_{\mathrm{c}}^{(2m)}(x_1,\cdots,x_m;x_1',\cdots,x_m')\overline{\eta}(x_1)\cdots\overline{\eta}(x_m)\eta(x_m')\cdots\eta(x_1').
\end{aligned} \tag{2.46}$$

Generating Functional of the Vertex Functions

We introduce another generating functional by Legendre transformation. To define Legendre transformation of the generating functional we introduce conjugate fields $\{\tilde{\psi}\}$ and $\{\tilde{\overline{\psi}}\}$ by

$$\begin{aligned}
\tilde{\psi}(x)&=\langle\psi(x)\rangle_{\overline{\eta},\eta}\\
&=\frac{1}{W[\overline{\eta},\eta]}\int\mathcal{D}\overline{\psi}\mathcal{D}\psi\;\psi(x)\;\mathrm{e}^{-\mathcal{S}+(\overline{\eta},\psi)+(\overline{\psi},\eta)}\\
&=\frac{\delta}{\delta\overline{\eta}(x)}\ln\int\mathcal{D}\overline{\psi}\mathcal{D}\psi\;\mathrm{e}^{-\mathcal{S}+(\overline{\eta},\psi)+(\overline{\psi},\eta)}\\
&=-\frac{\delta\mathcal{G}[\overline{\eta},\eta]}{\delta\overline{\eta}(x)},
\end{aligned} \tag{2.47}$$

and

$$\begin{aligned}\tilde{\overline{\psi}}(x) &= \langle \overline{\psi}(x) \rangle_{\overline{\eta},\eta} \\ &= \frac{1}{W[\overline{\eta},\eta]} \int \mathcal{D}\overline{\psi}\mathcal{D}\overline{\psi}\ \overline{\psi}(x)\ \mathrm{e}^{-\mathcal{S}+(\overline{\eta},\psi)+(\overline{\psi},\eta)} \\ &= -\frac{\delta}{\delta\eta(x)} \ln \int \mathcal{D}\overline{\psi}\mathcal{D}\psi\ \mathrm{e}^{-\mathcal{S}+(\overline{\eta},\psi)+(\overline{\psi},\eta)} \\ &= \frac{\delta \mathcal{G}[\overline{\eta},\eta]}{\delta\eta(x)}, \end{aligned} \tag{2.48}$$

where $\langle \cdots \rangle_{\overline{\eta},\eta}$ represents the average with source term $\frac{1}{W[\overline{\eta},\eta]} \int \mathcal{D}\overline{\psi}\mathcal{D}\psi\ \mathrm{e}^{-\mathcal{S}[\overline{\psi},\psi]+(\overline{\eta},\psi)+(\overline{\psi},\eta)} \cdots$. Hereafter we write $\tilde{\overline{\psi}}$ and $\tilde{\psi}$ as $\overline{\psi}$ and ψ, respectively, for simplicity as the general manner of FRG [55] although the bare Grassmann fields and their averages under source fields are confusing because of the same notation [73].

Now we introduce the generating functional of the vertex functions by Legendre transformation:

$$\Gamma[\overline{\psi},\psi] = \mathcal{G}[\overline{\eta},\eta] + (\overline{\eta},\psi) + (\overline{\psi},\eta). \tag{2.49}$$

This $\Gamma[\overline{\psi},\psi]$ is called effective action or effective potential and it obeys the relations which are sometimes called the reciprocity relations

$$\frac{\delta\Gamma[\overline{\psi},\psi]}{\delta\psi} = -\overline{\eta}, \tag{2.50}$$

and

$$\frac{\delta\Gamma[\overline{\psi},\psi]}{\delta\overline{\psi}} = \eta. \tag{2.51}$$

These relations are easily checked by

$$\begin{aligned}&\frac{\delta}{\delta\overline{\psi}(x)}\Gamma[\overline{\psi},\psi] \\ &= \sum_{x'}\left[\frac{\delta\mathcal{G}[\overline{\eta},\eta]}{\delta\overline{\eta}(x')}\frac{\delta\overline{\eta}(x')}{\delta\overline{\psi}(x)} + \frac{\delta\mathcal{G}[\overline{\eta},\eta]}{\delta\eta(x')}\frac{\delta\eta(x')}{\delta\overline{\psi}(x)} + \frac{\delta}{\delta\overline{\psi}(x)}\left(\overline{\eta}(x')\psi(x') + \overline{\psi}(x')\eta(x')\right)\right] \\ &= \sum_{x'}\left[\frac{\delta\mathcal{G}}{\delta\overline{\eta}(x')}\frac{\delta\overline{\eta}(x')}{\delta\overline{\psi}(x)} + \frac{\delta\mathcal{G}}{\delta\eta(x')}\frac{\delta\eta(x')}{\delta\overline{\psi}(x)} + \frac{\delta\overline{\eta}(x')}{\delta\overline{\psi}(x)}\psi(x')\delta(x,x')\eta(x') - \overline{\psi}(x')\frac{\delta\eta(x')}{\delta\overline{\psi}(x)}\right] \\ &= \sum_{x'}\left[\frac{\delta\mathcal{G}}{\delta\overline{\eta}(x')}\frac{\delta\overline{\eta}(x')}{\delta\overline{\psi}(x)} + \frac{\delta\mathcal{G}}{\delta\eta(x')}\frac{\delta\eta(x')}{\delta\overline{\psi}(x)} - \frac{\delta\overline{\eta}(x')}{\delta\overline{\psi}(x)}\frac{\delta\mathcal{G}}{\delta\overline{\eta}(x')} + \delta(x,x')\eta(x') - \frac{\delta\mathcal{G}}{\delta\eta(x')}\frac{\delta\eta(x')}{\delta\overline{\psi}(x)}\right] \\ &= \eta(x), \end{aligned} \tag{2.52}$$

and

$$\begin{aligned}&\frac{\delta}{\delta\psi(x)}\Gamma[\overline{\psi},\psi] \\ &= \sum_{x'}\left[\frac{\delta\mathcal{G}}{\delta\overline{\eta}(x')}\frac{\delta\overline{\eta}(x')}{\delta\psi(x)} + \frac{\delta\mathcal{G}}{\delta\eta(x')}\frac{\delta\eta(x')}{\delta\psi(x)} + \frac{\delta\overline{\eta}(x')}{\delta\psi(x)}\psi(x') - \overline{\eta}(x')\delta(x,x') - \overline{\psi}(x')\frac{\delta\eta(x')}{\delta\psi(x)}\right] \\ &= \sum_{x'}\left[\frac{\delta\mathcal{G}}{\delta\overline{\eta}(x')}\frac{\delta\overline{\eta}(x')}{\delta\psi(x)} + \frac{\delta\mathcal{G}}{\delta\eta(x')}\frac{\delta\eta(x')}{\delta\psi(x)} - \frac{\delta\overline{\eta}(x')}{\delta\psi(x)}\frac{\delta\mathcal{G}}{\delta\overline{\eta}(x')} - \overline{\eta}(x')\delta(x,x') - \frac{\delta\mathcal{G}}{\delta\eta(x')}\frac{\delta\eta(x')}{\delta\psi(x)}\right] \\ &= -\overline{\eta}(x). \end{aligned} \tag{2.53}$$

Here we use the relations Eq. (2.47), (2.48), and (2.49). Here, $\delta(x, x')$ represents generalized delta function which is Kronecker delta for discrete variables and Dirac delta function for continuous variables. Then we define vertex functions to check that $\Gamma[\overline{\psi}, \psi]$ is the generating functional of vertices. The m-body ($2m$-point or m-particle) one-particle irreducible (1PI) vertex functions $\Gamma^{(2m)}$ are defined as coefficients of the effective (renormalized) action:

$$\mathcal{S}_{\text{eff}}[\overline{\psi}, \psi] = \sum_{m=1} \frac{(-1)^m}{(m!)^2} \sum_{\substack{x_1, \cdots, x_m \\ x'_1, \cdots, x'_m}} \Gamma^{(2m)}(x'_1, \cdots, x'_m; x_1, \cdots, x_m) \overline{\psi}(x'_1) \cdots \overline{\psi}(x'_m) \psi(x_m) \cdots \psi(x_1) + \text{const.} \tag{2.54}$$

1PI means that the diagrams cannot be disconnected by removing any single internal propagators.
We can regard the effective action $\Gamma[\overline{\psi}, \psi]$ as the "*effective action*" of the system literally as we prove later. Therefore, by definition of the vertices, we obtain the m-body 1PI vertices by functional derivative of the effective action:

$$\Gamma^{(2m)}(x'_1, \cdots, x'_m; x_1, \cdots, x_m) = \frac{\delta^{2m} \Gamma[\overline{\psi}, \psi]}{\delta\overline{\psi}(x'_1) \cdots \delta\overline{\psi}(x'_m) \delta\psi(x_m) \cdots \delta\psi(x_1)} \bigg|_{\psi, \overline{\psi}=0}. \tag{2.55}$$

Note that the terms "irreducible" and "reducible" refer different properties depending on the context. In condensed matter physics, "irreducible"(or proper) self-energy always refers 1PI self-energy, while "irreducible" vertices often refer two-particle irreducible (2PI) vertices. For instance, irreducible vertices obtained by dynamical mean-field theory (DMFT) are 2PI vertices[76]. Hence we must solve Bethe-Salpeter equation in order to obtain full ("reducible") vertices. To construct Bethe-Salpeter equation, we decompose full vertices into the integral equations of the Green's functions and the 2PI vertices from DMFT. There are three possible ways to decompose the full vertices: particle-particle channel, direct particle-hole channel, and crossed particle-hole channel; the results should be the same no matter which channel decomposition we use, if calculated 2PI vertices are exact. Of course, in the most case, calculated 2PI vertices are not exact, and the full vertices obtained from these 2PI vertices depend on its decomposition channel. Therefore, we have to choose channel appropriate to fluctuation we focus on. The full ("reducible") vertices above are 1PI but not 2PI vertices and correspond to 1PI vertices here we discuss. FRG also can be constructed by 2PI scheme [64]. The effective action in 2PI scheme is strongly related to Luttinger-Ward functional [77–79].

All connected Green's functions are constructed from tree diagrams of equal or lower order 1PI vertex functions[56, 73]. For example, 2-particle connected Green's function is represented as

$$G_{\text{c}}^{(4)}(x_1, x_2; x'_1, x'_2) = \sum_{y_1, y_2, y'_1, y'_2} G(x_1, y'_1) G(x_2, y'_2) \Gamma^{(4)}(y'_1, y'_2; y_1, y_2) G(y_1, x'_1) G(y_2, x'_2), \tag{2.56}$$

and 3-particle connected Green's function is also represented as $G_{\text{c}}^{(6)} = G^3 \Gamma^{(6)} G^3 + G^3 \Gamma^{(4)} G \Gamma^{(4)} G^3$.

Dyson Equation

Now we derive the relation between the generating functional of the Green's functional $\mathcal{G}$ and the generating functional of the vertices Γ what can be regarded as a generalized Dyson equation.
At first, we consider the functional derivatives of a general fuctional $f[\overline{\eta},\eta]$ using the chain rule:

$$\begin{aligned}\frac{\delta f[\overline{\eta},\eta]}{\delta\psi(x_1)} &= \sum_{x_2}\left[\frac{\delta f}{\delta\overline{\eta}(x_2)}\frac{\delta\overline{\eta}(x_2)}{\delta\psi(x_1)}+\frac{\delta f}{\delta\eta(x_2)}\frac{\delta\eta(x_2)}{\delta\psi(x_1)}\right]\\ &= \sum_{x_2}\left[-\frac{\delta f}{\delta\overline{\eta}(x_2)}\frac{\delta^2\Gamma}{\delta\psi(x_1)\delta\psi(x_2)}+\frac{\delta f}{\delta\eta(x_2)}\frac{\delta^2\Gamma}{\delta\psi(x_1)\overline{\psi}(x_2)}\right]\\ &= \sum_{x_2}\left[+\frac{\delta f}{\delta\overline{\eta}(x_2)}\frac{\delta^2\Gamma}{\delta\psi(x_2)\delta\psi(x_1)}-\frac{\delta f}{\delta\eta(x_2)}\frac{\delta^2\Gamma}{\delta\overline{\psi}(x_2)\psi(x_1)}\right],\end{aligned} \tag{2.57}$$

$$\begin{aligned}\frac{\delta f[\overline{\eta},\eta]}{\delta\overline{\psi}(x_1)} &= \sum_{x_2}\left[\frac{\delta f}{\delta\overline{\eta}(x_2)}\frac{\delta\overline{\eta}(x_2)}{\delta\overline{\psi}(x_1)}+\frac{\delta f}{\delta\eta(x_2)}\frac{\delta\eta(x_2)}{\delta\overline{\psi}(x_1)}\right]\\ &= \sum_{x_2}\left[-\frac{\delta f}{\delta\overline{\eta}(x_2)}\frac{\delta^2\Gamma}{\delta\overline{\psi}(x_1)\delta\psi(x_2)}+\frac{\delta f}{\delta\eta(x_2)}\frac{\delta^2\Gamma}{\delta\overline{\psi}(x_1)\overline{\psi}(x_2)}\right]\\ &= \sum_{x_2}\left[+\frac{\delta f}{\delta\overline{\eta}(x_2)}\frac{\delta^2\Gamma}{\delta\psi(x_2)\delta\overline{\psi}(x_1)}-\frac{\delta f}{\delta\eta(x_2)}\frac{\delta^2\Gamma}{\delta\overline{\psi}(x_2)\overline{\psi}(x_1)}\right].\end{aligned} \tag{2.58}$$

If $f[\overline{\eta},\eta]=\psi(x_3)[\overline{\eta},\eta]$ in Eq. (2.57),

$$\begin{aligned}\delta(x_3,x_1) &= \frac{\delta\psi(x_3)}{\delta\psi(x_1)}\\ &= \sum_{x_2}\left[\frac{\delta\psi(x_3)}{\delta\overline{\eta}(x_2)}\frac{\delta^2\Gamma}{\delta\psi(x_2)\delta\psi(x_1)}-\frac{\delta\psi(x_3)}{\delta\eta(x_2)}\frac{\delta^2\Gamma}{\delta\overline{\psi}(x_2)\delta\psi(x_1)}\right]\\ &= \sum_{x_2}\left[-\frac{\delta^2\mathcal{G}}{\delta\overline{\eta}(x_2)\delta\overline{\eta}(x_3)}\frac{\delta^2\Gamma}{\delta\psi(x_2)\delta\psi(x_1)}+\frac{\delta^2\mathcal{G}}{\delta\eta(x_2)\delta\overline{\eta}(x_3)}\frac{\delta^2\Gamma}{\delta\overline{\psi}(x_2)\delta\psi(x_1)}\right]\\ &= \sum_{x_2}\left[\frac{\delta^2\mathcal{G}}{\delta\overline{\eta}(x_3)\delta\overline{\eta}(x_2)}\frac{\delta^2\Gamma}{\delta\psi(x_2)\delta\psi(x_1)}-\frac{\delta^2\mathcal{G}}{\delta\overline{\eta}(x_3)\delta\eta(x_2)}\frac{\delta^2\Gamma}{\delta\overline{\psi}(x_2)\delta\psi(x_1)}\right]\\ &= \sum_{x_2}\left[-\frac{\delta^2\mathcal{G}}{\delta\overline{\eta}(x_3)\delta\eta(x_2)}\frac{\delta^2\Gamma}{\delta\overline{\psi}(x_2)\delta\psi(x_1)}+\frac{\delta^2\mathcal{G}}{\delta\overline{\eta}(x_3)\delta\overline{\eta}(x_2)}\frac{\delta^2\Gamma}{\delta\psi(x_2)\delta\psi(x_1)}\right].\end{aligned} \tag{2.59}$$

In the same manner as above:
if $f[\overline{\eta},\eta]=\overline{\psi}(x_3)$ in Eq. (2.57),

$$\begin{aligned}0&=\frac{\delta\overline{\psi}(x_3)}{\delta\psi(x_1)}\\&=\sum_{x_2}\left[\frac{\delta\overline{\psi}(x_3)}{\delta\overline{\eta}(x_2)}\frac{\delta^2\Gamma}{\delta\psi(x_2)\delta\psi(x_1)}-\frac{\delta\overline{\psi}(x_3)}{\delta\eta(x_2)}\frac{\delta^2\Gamma}{\delta\overline{\psi}(x_2)\psi(x_1)}\right]\\&=\sum_{x_2}\left[\frac{\delta^2\mathcal{G}}{\delta\overline{\eta}(x_2)\delta\eta(x_3)}\frac{\delta^2\Gamma}{\delta\psi(x_2)\delta\psi(x_1)}-\frac{\delta^2\mathcal{G}}{\delta\eta(x_2)\delta\eta(x_3)}\frac{\delta^2\Gamma}{\delta\overline{\psi}(x_2)\psi(x_1)}\right]\\&=\sum_{x_2}\left[\frac{\delta^2\mathcal{G}}{\delta\eta(x_3)\delta\eta(x_2)}\frac{\delta^2\Gamma}{\delta\overline{\psi}(x_2)\psi(x_1)}+\frac{\delta^2\mathcal{G}}{\delta\eta(x_3)\delta\overline{\eta}(x_2)}\frac{\delta^2\Gamma}{\delta\psi(x_2)\delta\psi(x_1)}\right],\end{aligned}\tag{2.60}$$

if $f[\overline{\eta},\eta]=\overline{\psi}(x_2)$ in Eq. (2.58),

$$\begin{aligned}\delta(x_3,x_1)&=\frac{\delta\overline{\psi}(x_3)}{\delta\overline{\psi}(x_1)}\\&=\sum_{x_2}\left[\frac{\delta\overline{\psi}(x_3)}{\delta\overline{\eta}(x_2)}\frac{\delta^2\Gamma}{\delta\psi(x_2)\delta\overline{\psi}(x_1)}-\frac{\delta\overline{\psi}(x_3)}{\delta\eta(x_2)}\frac{\delta^2\Gamma}{\delta\overline{\psi}(x_2)\delta\overline{\psi}(x_1)}\right]\\&=\sum_{x_2}\left[-\frac{\delta^2\mathcal{G}}{\delta\eta(x_3)\delta\overline{\eta}(x_2)}\frac{\delta^2\Gamma}{\delta\psi(x_2)\delta\overline{\psi}(x_1)}+\frac{\delta^2\mathcal{G}}{\delta\eta(x_3)\delta\eta(x_2)}\frac{\delta^2\Gamma}{\delta\overline{\psi}(x_2)\delta\overline{\psi}(x_1)}\right],\end{aligned}\tag{2.61}$$

if $f[\overline{\eta},\eta]=\psi(x_3)$ in Eq. (2.58),

$$\begin{aligned}0&=\frac{\delta\psi(x_3)}{\delta\overline{\psi}(x_1)}\\&=\sum_{x_2}\left[\frac{\delta\psi(x_3)}{\delta\overline{\eta}(x_2)}\frac{\delta^2\Gamma}{\delta\psi(x_2)\delta\overline{\psi}(x_1)}-\frac{\delta\psi(x_3)}{\delta\eta(x_2)}\frac{\delta^2\Gamma}{\delta\overline{\psi}(x_2)\delta\overline{\psi}(x_1)}\right]\\&=\sum_{x_2}\left[\frac{\delta^2\mathcal{G}}{\delta\overline{\eta}(x_3)\delta\overline{\eta}(x_2)}\frac{\delta^2\Gamma}{\delta\psi(x_2)\delta\overline{\psi}(x_1)}-\frac{\delta^2\mathcal{G}}{\delta\overline{\eta}(x_3\delta\eta(x_2)}\frac{\delta^2\Gamma}{\delta\overline{\psi}(x_2)\delta\overline{\psi}(x_1)}\right]\\&=\sum_{x_2}\left[-\frac{\delta^2\mathcal{G}}{\delta\overline{\eta}(x_3)\delta\eta(x_2)}\frac{\delta^2\Gamma}{\delta\overline{\psi}(x_2)\delta\overline{\psi}(x_1)}+\frac{\delta^2\mathcal{G}}{\delta\overline{\eta}(x_3)\delta\overline{\eta}(x_2)}\frac{\delta^2\Gamma}{\delta\psi(x_2)\delta\overline{\psi}(x_1)}\right].\end{aligned}\tag{2.62}$$

These equations can be represented in matrix form

$$-\sum_{x_2}\begin{pmatrix}\frac{\delta^2\mathcal{G}}{\delta\overline{\eta}(x_3)\delta\eta(x_2)} & -\frac{\delta^2\mathcal{G}}{\delta\overline{\eta}(x_3)\delta\overline{\eta}(x_2)}\\ -\frac{\delta^2\mathcal{G}}{\delta\eta(x_3)\delta\eta(x_2)} & \frac{\delta^2\mathcal{G}}{\delta\eta(x_3)\delta\overline{\eta}(x_3)}\end{pmatrix}\begin{pmatrix}\frac{\delta^2\Gamma}{\delta\overline{\psi}(x_2)\delta\psi(x_1)} & \frac{\delta^2\Gamma}{\delta\overline{\psi}(x_2)\delta\overline{\psi}(x_1)}\\ \frac{\delta^2\Gamma}{\delta\psi(x_2)\delta\psi(x_1)} & \frac{\delta^2\Gamma}{\delta\psi(x_2)\delta\overline{\psi}(x_1)}\end{pmatrix}=\delta(x_3,x_1)\begin{pmatrix}1&0\\0&1\end{pmatrix},\tag{2.63}$$

more simply, we write symbolically

$$\{-\delta^2\mathcal{G}[\overline{\eta},\eta]\}\{\delta^2\Gamma[\overline{\psi},\psi]\}=\mathbf{1}.\tag{2.64}$$

Therefore,

$$\{-\delta^2\mathcal{G}[\overline{\eta},\eta]\}=\{\delta^2\Gamma[\overline{\psi},\psi]\}^{-1}.\tag{2.65}$$

We will use this relation later.

Then, we derive the standard Dyson equation from the above relation (2.65). We set $\overline{\psi} = \psi = 0$ (It implies $\overline{\eta} = \eta = 0$. It is explained later.), and obtain a relation between the Green's function and the 1-particle vertex function,

$$\sum_{x_2} \mathbf{G}(x_1, x_2)\mathbf{\Gamma}^{(2)}(x_2, x_3) = \mathbf{1}\delta(x_1, x_3). \tag{2.66}$$

Here, we define the matrices

$$\begin{aligned}\mathbf{G}(x, x') = -\delta^2\mathcal{G}[\overline{\eta}, \eta] &= -\begin{pmatrix} \frac{\delta^2\mathcal{G}}{\delta\overline{\eta}(x)\delta\eta(x')} & -\frac{\delta^2\mathcal{G}}{\delta\overline{\eta}(x)\delta\overline{\eta}(x')} \\ -\frac{\delta^2\mathcal{G}}{\delta\eta(x)\delta\eta(x')} & \frac{\delta^2\mathcal{G}}{\delta\eta(x)\delta\overline{\eta}(x')} \end{pmatrix}\Bigg|_{\overline{\eta}=\eta=0} \\ &= \begin{pmatrix} -\langle\psi(x)\overline{\psi}(x')\rangle & -\langle\psi(x)\psi(x')\rangle \\ -\langle\overline{\psi}(x)\overline{\psi}(x')\rangle & -\langle\overline{\psi}(x)\psi(x')\rangle \end{pmatrix}\end{aligned} \tag{2.67}$$

and

$$\mathbf{\Gamma}^{(2)}(x', x) = \delta\Gamma[\overline{\psi}, \psi] = \begin{pmatrix} \frac{\delta^2\Gamma}{\delta\overline{\psi}(x')\delta\psi(x)} & \frac{\delta^2\Gamma}{\delta\overline{\psi}(x')\delta\overline{\psi}(x)} \\ \frac{\delta^2\Gamma}{\delta\psi(x')\delta\psi(x)} & \frac{\delta^2\Gamma}{\delta\psi(x')\delta\overline{\psi}(x)} \end{pmatrix}\Bigg|_{\overline{\psi}=\psi=0} \tag{2.68}$$

We use the bold font to represent matrices in particle-hole (Nambu) space here, not vectors.
From Eq. (2.66),

$$\mathbf{\Gamma}^{(2)} = \mathbf{G}^{-1}. \tag{2.69}$$

If there are no U(1) symmetry breaking,

$$\Gamma^{(2)}(x', x) = \frac{\delta^2\Gamma}{\delta\overline{\psi}(x')\delta\psi(x)}\Bigg|_{\overline{\psi}=\psi=0} = G^{-1}(x', x). \tag{2.70}$$

We define the self-energy from 1-particle vertex function:

$$-\mathbf{\Sigma} = \mathbf{\Gamma}^{(2)} - \mathbf{\Gamma}_0^{(2)} \tag{2.71}$$

$$= \mathbf{\Gamma}^{(2)} - \mathbf{G}_0^{-1} \tag{2.72}$$

$$= \mathbf{G}^{-1} - \mathbf{G}_0^{-1}, \tag{2.73}$$

and then, Dyson equation is obtained:

$$\mathbf{G}(x_1, x_2) = \mathbf{G}_0(x_1, x_2) + \sum_{x_3, x_4} \mathbf{G}_0(x_1, x_3)\mathbf{\Sigma}(x_3, x_4)\mathbf{G}(x_4, x_2). \tag{2.74}$$

Here, $\mathbf{\Gamma}_0^{(2)}$ represents the 1-particle vertex function of the non-interacting system.
In single-band system with translation invariance and spin-rotation invariance, $x = (k, \sigma)$ is one of appropriate choices of quantum numbers and

$$\mathbf{G}(k) = \mathbf{G}_0(k) + \mathbf{G}_0(k)\mathbf{\Sigma}(k)\mathbf{G}(k), \tag{2.75}$$

with a shorthand notation $k = (\mathrm{i}\omega_n, \boldsymbol{k})$. This is the well-known form of the Dyson equation.

Another Generating Functional: Effective Interaction

We introduce one more useful generating functional called effective interaction [55, 57]:

$$\mathcal{V}[\overline{\chi},\chi] = -\ln\left[\frac{1}{\mathcal{Z}_0}\int \mathcal{D}\overline{\psi}\mathcal{D}\psi\, \mathrm{e}^{-\mathcal{S}_0[\overline{\psi},\psi]-\mathcal{S}_{\mathrm{int}}[\overline{\psi}+\overline{\chi},\psi+\chi]}\right]. \tag{2.76}$$

Performing the substitution

$$\chi = G_0\eta \quad \text{and} \quad \overline{\chi} = G_0^{\mathrm{T}}\overline{\eta}, \tag{2.77}$$

with $G_0^{\mathrm{T}}(x,x') = G_0(x',x)$, we obtain

$$\mathcal{V}[\overline{\chi},\chi] = \mathcal{G}[\overline{\eta},\eta] + \ln\mathcal{Z}_0 - (\overline{\eta}, G_0\eta). \tag{2.78}$$

Since the last two terms cancel the non-interacting part of $\mathcal{G}[\overline{\eta},\eta]$, functional derivatives of the effective interaction $\mathcal{V}[\overline{\chi},\chi]$ generate connected Green's functions with bare propagators amputated from external legs. Therefore,

$$\mathcal{S}_{\mathrm{int}}[\overline{\psi},\psi] = 0 \quad \Longrightarrow \quad \mathcal{V}[\overline{\chi},\chi] = 0. \tag{2.79}$$

We expressed $\mathcal{V}$ by not only integration but also derivative:

$$\begin{aligned}
\mathrm{e}^{-\mathcal{V}[\overline{\chi},\chi]} &= \frac{1}{\mathcal{Z}_0}\int \mathcal{D}\overline{\psi}\mathcal{D}\psi\, \mathrm{e}^{-\mathcal{S}_0[\overline{\psi},\psi]-\mathcal{S}_{\mathrm{int}}[\overline{\psi}+\overline{\chi},\psi+\chi]} \\
&= \frac{1}{\mathcal{Z}_0}\mathrm{e}^{-\mathcal{S}_{\mathrm{int}}[\delta_\eta,\delta_{\overline{\eta}}]}\int \mathcal{D}\overline{\psi}\mathcal{D}\psi\, \mathrm{e}^{(\overline{\psi},G_0^{-1}\psi)}\mathrm{e}^{(\overline{\eta},\psi+\chi)+(\eta,\overline{\psi}+\overline{\chi})}\Big|_{\overline{\eta},\eta=0} \\
&= \frac{1}{\mathcal{Z}_0}\mathrm{e}^{-\mathcal{S}_{\mathrm{int}}[\delta_\eta,\delta_{\overline{\eta}}]}\int \mathcal{D}\overline{\psi}\mathcal{D}\psi\, \mathrm{e}^{(\overline{\psi},G_0^{-1}\psi)}\mathrm{e}^{(\overline{\eta},\psi)-(\overline{\psi},\eta)}\mathrm{e}^{(\overline{\eta},\chi)+(\eta,\overline{\chi})}\Big|_{\overline{\eta},\eta=0} \\
&= \frac{1}{\mathcal{Z}_0}\mathrm{e}^{-\mathcal{S}_{\mathrm{int}}[\delta_\eta,\delta_{\overline{\eta}}]}\int \mathcal{D}\overline{\psi}\mathcal{D}\psi\, \mathrm{e}^{-(\overline{\psi},G_0^{-1}\psi)}\mathrm{e}^{(\overline{\eta},\psi)+(\overline{\psi},\eta)}\mathrm{e}^{(\overline{\eta},\chi)+(\eta,\overline{\chi})}\Big|_{\overline{\eta},\eta=0} \\
&= \mathrm{e}^{-\mathcal{S}_{\mathrm{int}}[\delta_\eta,\delta_{\overline{\eta}}]}\mathrm{e}^{(\overline{\eta},G_0\eta)}\mathrm{e}^{(\overline{\eta},\chi)+(\eta,\overline{\chi})}\Big|_{\overline{\eta},\eta=0} \\
&= \mathrm{e}^{-\mathcal{S}_{\mathrm{int}}[\delta_\eta,\delta_{\overline{\eta}}]}\mathrm{e}^{(\delta_\chi,G_0\delta_{\overline{\chi}})}\mathrm{e}^{(\overline{\eta},\chi)+(\eta,\overline{\chi})}\Big|_{\overline{\eta},\eta=0} \\
&= \mathrm{e}^{\Delta_{G_0}}\mathrm{e}^{-\mathcal{S}_{\mathrm{int}}[\overline{\chi},\chi]},
\end{aligned} \tag{2.80}$$

where we define the functional Laplacian as

$$\Delta_{G_0} = (\delta_\chi, G_0\delta_{\overline{\chi}}) = \sum_{x,x'}\frac{\delta}{\delta\chi(x)}G_0(x,x')\frac{\delta}{\delta\overline{\chi}(x')}. \tag{2.81}$$

2.4 Derivation of Exact Flow Equations

In this section we derive the exact flow equations of the FRG. It is a paramount equation of this dissertation. As mentioned before, considering flow equations of the generating functionals makes it possible to obtain exact flow equations in FRG. At first, we introduce flow parameters which play as a cutoff for mode elimination of Wilsonian renormalization procedure. Then we derive the exact flow equations by differential with respect to the flow parameter. Finally, we obtain the exact flow

equations for each vertex function by expansion of the exact flow equation of the effective action.

Flow Parameters

Recalling the general functional integral form of the partition function:

$$\begin{aligned}\mathcal{Z} &= \int \mathcal{D}\overline{\psi}\mathcal{D}\psi\ \mathrm{e}^{-\mathcal{S}_0[\overline{\psi},\psi]-\mathcal{S}_{\mathrm{int}}[\overline{\psi},\psi]} \\ &= \int \mathcal{D}\overline{\psi}\mathcal{D}\psi\ \mathrm{e}^{(\overline{\psi},G_0^{-1}\psi)}\mathrm{e}^{-\mathcal{S}_{\mathrm{int}}[\overline{\psi},\psi]} \\ &= \mathcal{Z}_0\left\langle \mathrm{e}^{-\mathcal{S}_{\mathrm{int}}[\overline{\psi},\psi]}\right\rangle_0,\end{aligned} \tag{2.82}$$

we can see that the inverse of the bare Green's function G_0^{-1} plays the role of the measure of the functional integral. Here we define $\langle\cdots\rangle_0$ as the average in non-interacting systems i.e. $\langle\cdots\rangle_0 = \int \mathcal{D}\overline{\psi}\mathcal{D}\psi\ \mathrm{e}^{-\mathcal{S}_0[\overline{\psi},\psi]}\cdots / \int \mathcal{D}\overline{\psi}\mathcal{D}\psi\ \mathrm{e}^{-\mathcal{S}_0[\overline{\psi},\psi]}$. For standard Wilsonian renormalization group procedure, we introduce momentum or energy cutoff Λ and divide field variables into slow ($<\Lambda$) and fast ($>\Lambda$) parts: $\psi = \psi_< + \psi_>$, then perform successive mode elimination by integration with respect to fast modes $\psi_>$. In FRG, we also introduce cutoff Λ. However, we attach the cutoff not to field variables but to integral measure:

$$G_0^{-1} \ \to [G_0^\Lambda]^{-1} = Q^\Lambda, \tag{2.83}$$

where $Q = G_0^{-1}$ (also $Q^\Lambda = (G_0^\Lambda)^{-1}$) and,

$$G_0^\Lambda = \theta^\Lambda G_0. \tag{2.84}$$

Here θ^Λ is called a cutoff function. In general, the cut off functions are required to satisfy the condition

$$G_0^\Lambda \sim \begin{cases} 0 & \text{for } \Lambda = \Lambda_{\mathrm{UV}}, \\ G_0 & \text{for } \Lambda = \Lambda_{\mathrm{IR}}. \end{cases} \tag{2.85}$$

There are some choices for the cutoff function. For example, we consider the bare Green's function of the single-band system which has translation and spin rotation invariance. We choose a label of the 1-particle states as $x = (\mathrm{i}\omega_n, \boldsymbol{k}, \sigma)$, the bare Green's function has the form

$$\begin{aligned}G_0(\mathrm{i}\omega_n,\boldsymbol{k},\sigma;\mathrm{i}\omega_{n'},\boldsymbol{k}',\sigma') &= \beta\Omega\delta_{\sigma\sigma'}\delta_{n,n'}\delta(\boldsymbol{k}-\boldsymbol{k}')\ G_0(\mathrm{i}\omega_n,\boldsymbol{k}) \\ &= \beta\Omega\delta_{\sigma\sigma'}\delta_{n,n'}\delta(\boldsymbol{k}-\boldsymbol{k}')\ \frac{1}{\mathrm{i}\omega_n-\xi_{\boldsymbol{k}}}.\end{aligned} \tag{2.86}$$

Therefore, there is the infrared (IR) singularity at Fermi surface $\mathrm{i}\omega_n \to \omega(+\mathrm{i}0) = 0$ and $\xi_{\boldsymbol{k}} = 0$ which is corresponding to the non-interacting Fermi surface. The flow parameter is introduced as the cutoff to avoid this singularity as

$$G_0^\Lambda(\mathrm{i}\omega_n,\boldsymbol{k}) = \frac{\theta^\Lambda(\boldsymbol{k})}{\mathrm{i}\omega_n-\xi_{\boldsymbol{k}}}, \tag{2.87}$$

where $\theta^\Lambda(\boldsymbol{k})$ is a function that vanishes for $|\xi_{\boldsymbol{k}}| \ll \Lambda$ and approaches to unity for $|\xi_{\boldsymbol{k}}| \gg \Lambda$. In the beginning of the flow we set the ultraviolet (UV) cutoff $\Lambda_{\mathrm{UV}} = W$, where W is the band width (sometimes $W = \infty$ e.g. for electron gas). During

renormalization flow we gradually reduce Λ to IR limit Λ_{IR}. Here, $\Lambda_{\mathrm{IR}} = 0$ and it corresponds non-interacting Fermi surface. This is called momentum cutoff scheme. One of the simplest and often used form for the cutoff function is

$$\theta^{\Lambda}(\boldsymbol{k}) = \Theta(|\xi_{\boldsymbol{k}}| - \Lambda), \tag{2.88}$$

where Θ is a step function (Heaviside function).
In momentum cutoff scheme sometimes we can perform Matsubara frequency summation analytically. However, it has some drawbacks: firstly if deformation of the Fermi surface due to self-energy occurs, non-interacting Fermi surface is no longer a good goals of the flow; secondly if the system has no translation invariance, fourier transformation to momentum representation is ill-defined; in addition, the processes with small momentum transfer are suppressed in the flow calculation. We can also use another choice called frequency cutoff scheme:

$$G_0^{\Lambda}(\mathrm{i}\omega_n, \boldsymbol{k}) = \frac{\theta^{\Lambda}(\omega_n)}{\mathrm{i}\omega_n - \xi_{\boldsymbol{k}}}. \tag{2.89}$$

It is useful in the case that the system lacks translation invariance. In frequency cutoff scheme, $\Lambda_{\mathrm{UR}} = \infty$ and $\Lambda_{\mathrm{IR}} = 0$. For example, sharp frequency cutoff $\theta^{\Lambda}(\omega_n) = \Theta(|\omega_n| - \Lambda)$. In addition, mixing momentum and frequency cutoff

$$G_0^{\Lambda}(\mathrm{i}\omega_n, \boldsymbol{k}) = \frac{\theta^{\Lambda}\left(\sqrt{\omega_n^2 + \xi_{\boldsymbol{k}}^2}\right)}{\mathrm{i}\omega_n - \xi_{\boldsymbol{k}}}, \tag{2.90}$$

is also used. This scheme is useful for mathematical literatures because in this scheme momentum and Matsubara frequency treated equally and it is convenient for power counting.
More smooth functions are often used for numerics while sharp cutoff functions are useful for analytical calculation. It is required to apply appropriate cutoff scheme and form of cutoff functions depending on the properties of the systems, phenomena, and calculation methods. The important fact is that the details of the Λ-dependency of G_0^{Λ} do not matter to derive the exact flow equation, as shown later.
We denote $\mathcal{S}^{\Lambda}$ as the bare action with G_0^{Λ} instead of G_0, and the generating functional $\mathcal{G}^{\Lambda}$ is defined by $\mathcal{S}^{\Lambda}$ as

$$\mathcal{G}^{\Lambda}[\overline{\eta}, \eta] = -\ln W^{\Lambda}[\overline{\eta}, \eta] = -\ln \int \mathcal{D}\overline{\psi}\mathcal{D}\psi \, \mathrm{e}^{-\mathcal{S}^{\Lambda}[\overline{\psi},\psi]+(\overline{\eta},\psi)+(\overline{\psi},\eta)}, \tag{2.91}$$

with

$$W^{\Lambda}[\overline{\eta}, \eta] = \int \mathcal{D}\overline{\psi}\mathcal{D}\psi \, \mathrm{e}^{-\mathcal{S}^{\Lambda}[\overline{\psi},\psi]+(\overline{\eta},\psi)+(\overline{\psi},\eta)}. \tag{2.92}$$

The effective action with the flow parameter is defined in the same manner before:

$$\Gamma^{\Lambda}[\overline{\psi}, \psi] = \mathcal{G}^{\Lambda}[\overline{\eta}^{\Lambda}, \eta^{\Lambda}] + (\overline{\eta}^{\Lambda}, \psi) + (\overline{\psi}, \eta^{\Lambda}), \tag{2.93}$$

with the conjugate fields

$$\overline{\psi} = \frac{\delta \mathcal{G}^{\Lambda}}{\delta \eta}, \tag{2.94}$$

and

$$\psi = -\frac{\delta \mathcal{G}^\Lambda}{\delta \overline{\eta}}. \tag{2.95}$$

Here $\overline{\psi}$ and ψ do not depend on Λ. Moreover, the source fields $\overline{\eta}$ and η are Λ-dependent in the Legendre transformation above although they do not depend on Λ in the definition of $\mathcal{G}^\Lambda$ (2.93).
More precisely, the Legendre transformation is written as

$$\Gamma^\Lambda[\overline{\psi}, \psi] = \mathcal{G}^\Lambda[\overline{\eta}^\Lambda[\overline{\psi}, \psi], \eta^\Lambda[\overline{\psi}, \psi]] + (\overline{\eta}^\Lambda[\overline{\psi}, \psi], \psi) + (\overline{\psi}, \eta^\Lambda[\overline{\psi}, \psi]). \tag{2.96}$$

And it means "if the values of ψ and $\overline{\psi}$ are given, find the values $\overline{\eta}$ and η which satisfy the relation

$$\psi = -\frac{\delta \mathcal{G}^\Lambda[\overline{\eta}, \eta]}{\delta \overline{\eta}}, \quad \overline{\psi} = \frac{\delta \mathcal{G}^\Lambda[\overline{\eta}, \eta]}{\delta \eta}, \tag{2.97}$$

and define them as $\overline{\eta}^\Lambda[\overline{\psi}, \psi]$ and $\eta^\Lambda[\overline{\psi}, \psi]$. Then, we define the values of $\Gamma^\Lambda[\overline{\psi}, \psi]$ by substituting the values of $\overline{\eta}^\Lambda$ and η^Λ for the right-hand side $\mathcal{G}^\Lambda[\overline{\eta}^\Lambda, \eta^\Lambda] + (\overline{\eta}^\Lambda, \psi) + (\overline{\psi}, \eta^\Lambda)$."
Therefore, $\overline{\eta}$ and η are Λ-dependent in the definition of Γ^Λ. This is important to derive the exact flow equation of $\Gamma^\Lambda[\overline{\psi}, \psi]$. The reciprocity relations are

$$\eta^\Lambda = \frac{\delta \Gamma^\Lambda}{\delta \overline{\psi}}, \quad \overline{\eta}^\Lambda = -\frac{\delta \Gamma^\Lambda}{\delta \psi}. \tag{2.98}$$

At the first of the renormalization flow $\Lambda = \Lambda_{\mathrm{UV}}$, Γ^Λ corresponds to the regularized bare action of the system $\Gamma^{\Lambda_{\mathrm{UV}}} = \mathcal{S}^{\Lambda_{\mathrm{UV}}}$. Then high energy contributions to the action is renormalized in Γ^Λ along the renormalization flow. At last, Γ^Λ reaches the genuine effective action $\Gamma^{\Lambda_{\mathrm{IR}}} = \Gamma$ describing physical phenomena at low energy scale.

The vertex functions are obtained by

$$\Gamma^{\Lambda(2m)}(x'_1, \cdots, x'_m; x_1, \cdots, x_m) = \left. \frac{\delta^{2m} \Gamma^\Lambda[\overline{\psi}, \psi]}{\delta \overline{\psi}(x'_1) \cdots \delta \overline{\psi}(x'_m) \delta \psi(x_m) \cdots \delta \psi(x_1)} \right|_{\overline{\psi}, \psi = 0}, \tag{2.99}$$

and the Dyson equation is

$$\begin{aligned} -\mathbf{\Sigma}^\Lambda &= \mathbf{\Gamma}^{\Lambda(2)} - [\mathbf{G}_0^\Lambda]^{-1} \\ &= [\mathbf{G}^\Lambda]^{-1} - [\mathbf{G}_0^\Lambda]^{-1}. \end{aligned} \tag{2.100}$$

In addition, we introduce the inverse bare propagator

$$Q^\Lambda(x, x') = [G_0^\Lambda(x, x')]^{-1}, \tag{2.101}$$

for a simple form of the flow equation.
Finally, we expand the effective potential:

$$\Gamma^\Lambda[\overline{\psi}, \psi] = \sum_{m=0}^{\infty} \mathcal{A}^{(2m)\Lambda}[\overline{\psi}, \psi]. \tag{2.102}$$

In the same manner of expansion Eq. (2.37), we perform Taylor expansion of the functionals of Grassmann variables and obtain

$$\mathcal{A}^{(2m)\Lambda}[\overline{\psi}.\psi] = \frac{(-1)^m}{(m!)^2} \sum_{\substack{x_1,\cdots,x_m \\ x'_1,\cdots,x'_m}} \Gamma^{(2m)\Lambda}(x'_1,\cdots,x'_m;x_1,\cdots,x_m)\overline{\psi}(x'_1)\cdots\overline{\psi}(x'_m)\psi(x_m)\cdots\psi(x_1), \tag{2.103}$$

for $m \geq 1$. Then, we calculate

$$\mathcal{A}^{(0)\Lambda} = \Gamma^{\Lambda}[0,0]. \tag{2.104}$$

We consider the Legendre transformation again:

$$\Gamma^{\Lambda}[\overline{\psi},\psi] = \mathcal{G}^{\Lambda}[\overline{\eta}^{\Lambda},\eta^{\Lambda}] + (\overline{\eta}^{\Lambda},\psi) + (\overline{\psi},\eta^{\Lambda}). \tag{2.105}$$

We set $\overline{\psi} = \psi = 0$, and remember the meaning of the Legendre transformation. We find values of $\overline{\eta}^{\Lambda}$ and η^{Λ} satisfying

$$\begin{aligned} \frac{\delta\mathcal{G}^{\Lambda}}{\delta\eta} &= \langle\overline{\psi}\rangle = 0, \\ \frac{\delta\mathcal{G}^{\Lambda}}{\delta\overline{\eta}} &= -\langle\psi\rangle = 0. \end{aligned} \tag{2.106}$$

The expectation values of single field variable are zero if source fields do not exist $\overline{\eta} = \eta = 0$. Remembering $\mathcal{G}^{\Lambda}[0,0] = -\ln\mathcal{Z}^{\Lambda}$,

$$\mathcal{A}^{(0)\Lambda} = \Gamma^{\Lambda}[0,0] = -\ln\mathcal{Z}^{\Lambda}. \tag{2.107}$$

Therefore,

$$\begin{aligned} &\Gamma^{\Lambda}[\overline{\psi},\psi] \\ &= -\ln\mathcal{Z}^{\Lambda} - (\overline{\psi},\Gamma^{(2)\Lambda}\psi) + \frac{1}{4}\sum_{x_1,x_2,x'_1,x'_2}\Gamma^{(4)\Lambda}(x'_1,x'_2;x_1,x_2)\overline{\psi}(x'_1)\overline{\psi}(x'_2)\psi(x_2)\psi(x_1) + \cdots \\ &= -\ln\mathcal{Z}^{\Lambda} - (\overline{\psi},[G^{\Lambda}]^{-1}\psi) + \frac{1}{4}\sum_{x_1,x_2,x'_1,x'_2}\Gamma^{(4)\Lambda}(x'_1,x'_2;x_1,x_2)\overline{\psi}(x'_1)\overline{\psi}(x'_2)\psi(x_2)\psi(x_1) + \cdots \\ &= -\ln\mathcal{Z}^{\Lambda} - (\overline{\psi},\{[G_0^{\Lambda}]^{-1} - \Sigma^{\Lambda}\}\psi) \\ &\qquad + \frac{1}{4}\sum_{x_1,x_2,x'_1,x'_2}\Gamma^{(4)\Lambda}(x'_1,x'_2;x_1,x_2)\overline{\psi}(x'_1)\overline{\psi}(x'_2)\psi(x_2)\psi(x_1) + \cdots. \end{aligned} \tag{2.108}$$

This has the form corresponding to action. At initial condition ($\Lambda = \Lambda_{\mathrm{UV}}$), $\Sigma^{\Lambda_{\mathrm{UV}}}$=0, $[G^{\Lambda_{\mathrm{UV}}}]^{-1} = [G_0^{\Lambda_{\mathrm{UV}}}]^{-1} = Q^{\Lambda_{\mathrm{UV}}}$, $\Gamma^{(4)\Lambda_{\mathrm{UV}}} = V$, and $\Gamma^{(2m)\Lambda_{\mathrm{UV}}} = 0$ ($m \geq 3$, $m \in \mathbb{N}$). V is the anti-symmetrized 2-particle interaction of the model.
Here, let us prove

$$\Gamma^{\Lambda}[\overline{\psi},\psi] \longrightarrow \mathcal{S}^{\Lambda}[\overline{\psi},\psi] + \text{const.}\ (\Lambda \to \Lambda_{\mathrm{UV}}). \tag{2.109}$$

The proof is below:

$$\begin{aligned} \mathrm{e}^{-\Gamma^{\Lambda}[\tilde{\overline{\psi}},\tilde{\psi}]} &= \exp\left(-\mathcal{G}^{\Lambda}[\overline{\eta},\eta] - (\overline{\eta},\tilde{\psi}) - (\tilde{\overline{\psi}},\eta)\right) \\ &= \int \mathcal{D}\overline{\psi}\mathcal{D}\psi\, \mathrm{e}^{-\mathcal{S}^{\Lambda}[\overline{\psi},\psi]+(\overline{\eta},\psi)+(\overline{\psi},\eta)-(\overline{\eta},\tilde{\psi})-(\tilde{\overline{\psi}},\eta)} \end{aligned} \tag{2.110}$$

Here, we introduce variable translation:

$$\begin{aligned} \psi &\to \psi + \tilde{\psi}, \\ \overline{\psi} &\to \overline{\psi} + \tilde{\overline{\psi}}. \end{aligned} \tag{2.111}$$

Then,

$$\begin{aligned} &\int \mathcal{D}\overline{\psi}\mathcal{D}\psi\, \mathrm{e}^{-\mathcal{S}^{\Lambda}[\overline{\psi}+\tilde{\overline{\psi}},\psi+\tilde{\psi}]} \\ &= \int \mathcal{D}\overline{\psi}\mathcal{D}\psi\, \mathrm{e}^{-\mathcal{S}_0^{\Lambda}[\overline{\psi},\psi]-\mathcal{S}_0^{\Lambda}[\tilde{\overline{\psi}},\tilde{\psi}]-\mathcal{S}_{\mathrm{int}}[\overline{\psi}+\tilde{\overline{\psi}},\psi+\tilde{\psi}]}\mathrm{e}^{(\overline{\psi},Q^{\Lambda}\tilde{\psi})+(\tilde{\overline{\psi}},Q^{\Lambda}\psi)} \\ &= \mathrm{e}^{-\mathcal{S}_0^{\Lambda}[\tilde{\overline{\psi}},\tilde{\psi}]} \underbrace{\int \mathcal{D}\overline{\psi}\mathcal{D}\psi\, \mathrm{e}^{-\mathcal{S}_0^{\Lambda}[\overline{\psi},\psi]-\mathcal{S}_{\mathrm{int}}[\overline{\psi}+\tilde{\overline{\psi}},\psi+\tilde{\psi}]}}_{\mathcal{Z}_0\times\mathrm{e}^{-\mathcal{V}^{\Lambda}[\tilde{\overline{\psi}},\tilde{\psi}]}\ \to\ \mathrm{e}^{-\mathcal{S}_{\mathrm{int}}[\tilde{\overline{\psi}},\tilde{\psi}]+\mathrm{const.}}\ (\Lambda\to\Lambda_{\mathrm{UV}})} \underbrace{\mathrm{e}^{(\overline{\psi},Q^{\Lambda}\tilde{\psi})+(\tilde{\overline{\psi}},Q^{\Lambda}\psi)}}_{\to\ 0\ (\Lambda\to\Lambda_{\mathrm{UV}})} \\ &\longrightarrow \mathrm{e}^{-\mathcal{S}_0^{\Lambda}[\tilde{\overline{\psi}},\tilde{\psi}]-\mathcal{S}_{\mathrm{int}}[\tilde{\overline{\psi}},\tilde{\psi}]} + \mathrm{const.}\ (\Lambda\to\Lambda_{\mathrm{UV}}). \end{aligned} \tag{2.112}$$

There are other options for flow parameters and we introduce temperature flow scheme and interaction flow scheme in appendix B.

Direct Derivation

At first, we derive the flow equation of the generating functional $\mathcal{G}^{\Lambda}[\overline{\eta},\eta]$ directly by Λ-derivative [55, 65]. We can obtain simple form of Λ-derivative by using functional

derivative.

$$
\begin{aligned}
\frac{\mathrm{d}}{\mathrm{d}\Lambda}\mathcal{G}^{\Lambda}[\overline{\eta},\eta] &= -\mathrm{e}^{\mathcal{G}^{\Lambda}[\overline{\eta},\eta]}\frac{\mathrm{d}}{\mathrm{d}\Lambda}\mathrm{e}^{-\mathcal{G}^{\Lambda}[\overline{\eta},\eta]} \\
&= -\mathrm{e}^{\mathcal{G}^{\Lambda}[\overline{\eta},\eta]}\frac{\mathrm{d}}{\mathrm{d}\Lambda}\int \mathcal{D}\overline{\psi}\mathcal{D}\psi\, \mathrm{e}^{(\overline{\psi},[G_0^{\Lambda}]^{-1}\psi)-\mathcal{S}_{\mathrm{int}}[\overline{\psi},\psi]+(\overline{\eta},\psi)+(\overline{\psi},\eta)} \\
&= -\mathrm{e}^{\mathcal{G}^{\Lambda}[\overline{\eta},\eta]}\int \mathcal{D}\overline{\psi}\mathcal{D}\psi\, (\overline{\psi},[\dot{G}_0^{\Lambda}]^{-1}\psi)\mathrm{e}^{-\mathcal{S}^{\Lambda}[\overline{\psi},\psi]+(\overline{\eta},\psi)+(\overline{\psi},\eta)} \\
&= -\mathrm{e}^{\mathcal{G}^{\Lambda}[\overline{\eta},\eta]}\left(-\frac{\delta}{\delta\eta},[\dot{G}_0^{\Lambda}]^{-1}\frac{\delta}{\delta\overline{\eta}}\right)\int \mathcal{D}\overline{\psi}\mathcal{D}\psi\, \mathrm{e}^{-\mathcal{S}^{\Lambda}[\overline{\psi},\psi]+(\overline{\eta},\psi)+(\overline{\psi},\eta)} \\
&= \mathrm{e}^{\mathcal{G}^{\Lambda}[\overline{\eta},\eta]}\left(\frac{\delta}{\delta\eta},[\dot{G}_0^{\Lambda}]^{-1}\frac{\delta}{\delta\overline{\eta}}\right)\mathrm{e}^{-\mathcal{G}^{\Lambda}[\overline{\eta},\eta]} \\
&= \mathrm{e}^{\mathcal{G}^{\Lambda}[\overline{\eta},\eta]}\left(\frac{\delta}{\delta\eta},\dot{\mathcal{Q}}^{\Lambda}\frac{\delta}{\delta\overline{\eta}}\right)\mathrm{e}^{-\mathcal{G}^{\Lambda}[\overline{\eta},\eta]} \\
&= \mathrm{e}^{\mathcal{G}^{\Lambda}[\overline{\eta},\eta]}\left(\frac{\delta}{\delta\eta},\dot{\mathcal{Q}}^{\Lambda}(-1)\frac{\delta\mathcal{G}^{\Lambda}[\overline{\eta},\eta]}{\delta\overline{\eta}}\right)\mathrm{e}^{-\mathcal{G}^{\Lambda}[\overline{\eta},\eta]} \\
&= \mathrm{e}^{\mathcal{G}^{\Lambda}[\overline{\eta},\eta]}\left[-\sum_{x,x'}\dot{\mathcal{Q}}^{\Lambda}(x,x')\frac{\delta^2\mathcal{G}^{\Lambda}[\overline{\eta},\eta]}{\delta\eta(x)\delta\overline{\eta}(x')}+\left(\frac{\delta\mathcal{G}^{\Lambda}[\overline{\eta},\eta]}{\delta\eta},\dot{\mathcal{Q}}^{\Lambda}\frac{\delta\mathcal{G}^{\Lambda}[\overline{\eta},\eta]}{\delta\overline{\eta}}\right)\right]\mathrm{e}^{-\mathcal{G}^{\Lambda}[\overline{\eta},\eta]} \\
&= \left(\frac{\delta\mathcal{G}^{\Lambda}[\overline{\eta},\eta]}{\delta\eta},\dot{\mathcal{Q}}^{\Lambda}\frac{\delta\mathcal{G}^{\Lambda}[\overline{\eta},\eta]}{\delta\overline{\eta}}\right)+\sum_{x,x'}\dot{\mathcal{Q}}^{\Lambda}(x,x')\frac{\delta^2\mathcal{G}^{\Lambda}[\overline{\eta},\eta]}{\delta\overline{\eta}(x')\delta\eta(x)} \\
&= \left(\frac{\delta\mathcal{G}^{\Lambda}[\overline{\eta},\eta]}{\delta\eta},\dot{\mathcal{Q}}^{\Lambda}\frac{\delta\mathcal{G}^{\Lambda}[\overline{\eta},\eta]}{\delta\overline{\eta}}\right)+\mathrm{Tr}\left(\dot{\mathcal{Q}}^{\Lambda}\frac{\delta^2\mathcal{G}^{\Lambda}[\overline{\eta},\eta]}{\delta\overline{\eta}\delta\eta}\right).
\end{aligned}
\tag{2.113}
$$

This is an exact flow equation. We use the dot symbol " $\cdot$ " by representing Λ-derivative hereafter. As shown before, the generating functional is expanded in the series of source field whose coefficients are connected many-body Green's functions. Therefore we can obtain an infinite hierarchy of functional differential equations for connected many-body Green's functions. However, the isolated propagators can lead to technical problems within scheme described here [80]. In addition, the flow equation for Green's functions contains one-particle reducible term, which require more care [55].

Another choice is the exact flow equation of the effective action, which generates 1PI vertex functions. Now we consider Λ-derivative of $\Gamma^{\Lambda}[\overline{\psi},\psi]$ using Eq. (2.96):

$$
\frac{\mathrm{d}}{\mathrm{d}\Lambda}\Gamma^{\Lambda}[\tilde{\overline{\psi}},\tilde{\psi}] = \frac{\mathrm{d}}{\mathrm{d}\Lambda}\mathcal{G}^{\Lambda}[\overline{\eta}^{\Lambda},\eta^{\Lambda}]+\left(\tilde{\overline{\psi}},\frac{\mathrm{d}\eta^{\Lambda}}{\mathrm{d}\Lambda}\right)+\left(\frac{\mathrm{d}\overline{\eta}^{\Lambda}}{\mathrm{d}\Lambda},\tilde{\psi}\right). \tag{2.114}
$$

Unlike the above derivation of the flow equation of $\mathcal{G}^\Lambda[\overline{\eta},\eta]$, the arguments $\overline{\eta}^\Lambda$ and η^Λ of the generating functional are Λ-dependent. As in the same manner above,

$$
\begin{aligned}
&\frac{\mathrm{d}}{\mathrm{d}\Lambda}\mathcal{G}^\Lambda[\overline{\eta}^\Lambda,\eta^\Lambda] \\
&= -\mathrm{e}^{\mathcal{G}^\Lambda[\overline{\eta}^\Lambda,\eta^\Lambda]}\frac{\mathrm{d}}{\mathrm{d}\Lambda}\mathrm{e}^{-\mathcal{G}^\Lambda[\overline{\eta}^\Lambda,\eta^\Lambda]} \\
&= -\mathrm{e}^{\mathcal{G}^\Lambda[\overline{\eta}^\Lambda,\eta^\Lambda]}\frac{\mathrm{d}}{\mathrm{d}\Lambda}\int\mathcal{D}\overline{\psi}\mathcal{D}\psi\,\mathrm{e}^{(\overline{\psi},Q^\Lambda\psi)-\mathcal{S}_{\mathrm{int}}[\overline{\psi},\psi]+(\overline{\eta}^\Lambda,\psi)+(\overline{\psi},\eta^\Lambda)} \\
&= -\mathrm{e}^{\mathcal{G}^\Lambda[\overline{\eta}^\Lambda,\eta^\Lambda]}\int\mathcal{D}\overline{\psi}\mathcal{D}\psi\left\{(\overline{\psi},\dot{Q}^\Lambda\psi)+\left(\frac{\mathrm{d}\overline{\eta}^\Lambda}{\mathrm{d}\Lambda},\psi\right)+\left(\overline{\psi},\frac{\mathrm{d}\eta^\Lambda}{\mathrm{d}\Lambda}\right)\right\}\mathrm{e}^{-\mathcal{S}^\Lambda[\overline{\psi},\psi]+(\overline{\eta}^\Lambda,\psi)+(\overline{\psi},\eta^\Lambda)} \\
&= \frac{\mathrm{d}}{\mathrm{d}\Lambda}\mathcal{G}^\Lambda[\overline{\eta}^\Lambda,\eta^\Lambda]\Big|_{\overline{\eta}^\Lambda,\eta^\Lambda:\mathrm{fixed}} \\
&\quad -\mathrm{e}^{\mathcal{G}^\Lambda[\overline{\eta}^\Lambda,\eta^\Lambda]}\left\{\left(\frac{\mathrm{d}\overline{\eta}^\Lambda}{\mathrm{d}\Lambda},\frac{\delta}{\delta\overline{\eta}^\Lambda}\right)+\left(-\frac{\delta}{\delta\eta^\Lambda},\frac{\mathrm{d}\eta^\Lambda}{\mathrm{d}\Lambda}\right)\right\}\mathrm{e}^{-\mathcal{G}^\Lambda[\overline{\eta},\eta]} \\
&= \frac{\mathrm{d}}{\mathrm{d}\Lambda}\mathcal{G}^\Lambda[\overline{\eta}^\Lambda,\eta^\Lambda]\Big|_{\overline{\eta}^\Lambda,\eta^\Lambda:\mathrm{fixed}} \\
&\quad -\left(\frac{\mathrm{d}\overline{\eta}^\Lambda}{\mathrm{d}\Lambda},-\frac{\delta\mathcal{G}^\Lambda[\overline{\eta}^\Lambda,\eta^\Lambda]}{\delta\overline{\eta}^\Lambda}\right)+\left(\frac{\delta\mathcal{G}^\Lambda[\overline{\eta}^\Lambda,\eta^\Lambda]}{\delta\eta^\Lambda},\frac{\mathrm{d}\eta^\Lambda}{\mathrm{d}\Lambda}\right).
\end{aligned}
\tag{2.115}
$$

Here, we remember the relation Eq. (2.94) and Eq. (2.95), we obtain

$$
\frac{\mathrm{d}}{\mathrm{d}\Lambda}\mathcal{G}^\Lambda[\overline{\eta}^\Lambda,\eta^\Lambda]=\frac{\mathrm{d}}{\mathrm{d}\Lambda}\mathcal{G}^\Lambda[\overline{\eta}^\Lambda,\eta^\Lambda]\Big|_{\overline{\eta}^\Lambda,\eta^\Lambda:\mathrm{fixed}}-\left(\frac{\mathrm{d}\overline{\eta}^\Lambda}{\mathrm{d}\Lambda},\tilde{\psi}\right)-\left(\tilde{\overline{\psi}},\frac{\mathrm{d}\eta^\Lambda}{\mathrm{d}\Lambda}\right).
\tag{2.116}
$$

Substituting it into $\mathrm{d}\Gamma^\Lambda[\tilde{\overline{\psi}},\tilde{\psi}]/\mathrm{d}\Lambda$, we obtain

$$
\begin{aligned}
\frac{\mathrm{d}}{\mathrm{d}\Lambda}\Gamma^\Lambda[\tilde{\overline{\psi}},\tilde{\psi}] &= \frac{\mathrm{d}}{\mathrm{d}\Lambda}\mathcal{G}^\Lambda[\overline{\eta}^\Lambda,\eta^\Lambda]\Big|_{\overline{\eta}^\Lambda,\eta^\Lambda:\mathrm{fixed}} \\
&= \left(\frac{\delta\mathcal{G}^\Lambda[\overline{\eta}^\Lambda,\eta^\Lambda]}{\delta\eta^\Lambda},\dot{Q}^\Lambda\frac{\delta\mathcal{G}^\Lambda[\overline{\eta}^\Lambda,\eta^\Lambda]}{\delta\overline{\eta}^\Lambda}\right)+\mathrm{Tr}\left(\dot{Q}^\Lambda\frac{\delta^2\mathcal{G}^\Lambda[\overline{\eta}^\Lambda,\eta^\Lambda]}{\delta\overline{\eta}^\Lambda\delta\eta^\Lambda}\right).
\end{aligned}
\tag{2.117}
$$

Rewriting the right-hand-side by $\overline{\psi}$ and ψ (we omit "$\sim$" for simplicity),

$$
\begin{aligned}
\frac{\mathrm{d}}{\mathrm{d}\Lambda}\Gamma^\Lambda[\overline{\psi},\psi] &= -(\overline{\psi},\dot{Q}^\Lambda\psi)+\mathrm{Tr}\left(\dot{Q}^\Lambda\frac{\delta^2\mathcal{G}^\Lambda[\overline{\eta}^\Lambda,\eta^\Lambda]}{\delta\overline{\eta}^\Lambda\delta\eta^\Lambda}\right) \\
&= -(\overline{\psi},\dot{Q}^\Lambda\psi)+\sum_{x,x'}\dot{Q}^\Lambda(x,x')\frac{\delta^2\mathcal{G}^\Lambda[\overline{\eta},\eta^\Lambda]}{\delta\overline{\eta}^\Lambda(x')\delta\eta^\Lambda(x)} \\
&= -(\overline{\psi},\dot{Q}^\Lambda\psi)+\frac{1}{2}\sum_{x,x'}\left\{\dot{Q}^\Lambda(x,x')\frac{\delta^2\mathcal{G}^\Lambda[\overline{\eta}^\Lambda,\eta^\Lambda]}{\delta\overline{\eta}^\Lambda(x')\delta\eta^\Lambda(x)}+\dot{Q}^\Lambda(x',x)\frac{\delta^2\mathcal{G}^\Lambda[\overline{\eta}^\Lambda,\eta^\Lambda]}{\delta\overline{\eta}^\Lambda(x)\delta\eta^\Lambda}(x')\right\} \\
&= -(\overline{\psi},\dot{Q}^\Lambda\psi)+\frac{1}{2}\mathrm{Tr}(\dot{\mathbf{Q}}^\Lambda\delta^2\mathcal{G}^\Lambda[\overline{\eta}^\Lambda,\eta^\Lambda]) \\
&= -(\overline{\psi},\dot{Q}^\Lambda\psi)-\frac{1}{2}\mathrm{Tr}\{\dot{\mathbf{Q}}^\Lambda(\delta^2\Gamma^\Lambda[\overline{\psi},\psi])^{-1}\}.
\end{aligned}
\tag{2.118}
$$

Here

$$
\mathbf{Q}^\Lambda=\begin{pmatrix}Q^\Lambda & 0\\ 0 & -(Q^\Lambda)^{\mathrm{T}}\end{pmatrix}.
\tag{2.119}
$$

and

$$[Q^\Lambda(x,x')]^{\mathrm{T}} = Q^\Lambda(x',x). \tag{2.120}$$

This equation Eq. (2.118) is the exact flow equation of the effective action. Sometimes it is also called Wetterich equation [71]. This Wetterich equation is a primal equation in FRG.

Effective Average Action

Here, we introduce another version of the Wetterich equation. We define one more generating functional of vertex functions

$$\Gamma_R^\Lambda[\overline{\psi},\psi] = \Gamma^\Lambda[\overline{\psi},\psi] + (\overline{\psi}, R^\Lambda\psi), \tag{2.121}$$

whose analog for bosonic fields is called effective average action [60, 71]. R^Λ is called a regulator function defined

$$R^\Lambda = Q^\Lambda - Q, \tag{2.122}$$

and its derivative is

$$\dot{R}^\Lambda = \frac{\mathrm{d}}{\mathrm{d}\Lambda}R^\Lambda = \frac{\mathrm{d}}{\mathrm{d}\Lambda}(Q^\Lambda - Q) = \dot{Q}^\Lambda. \tag{2.123}$$

When we consider flow equation of Γ_R^Λ, the additional term $(\overline{\psi}, R\psi)$ cancel the first term of the Wetterich equation Eq. (2.118). Moreover, the second derivative of $\Gamma_R^\Lambda[\overline{\psi},\psi]$ is

$$\begin{aligned}\frac{\delta^2\Gamma_R^\Lambda[\overline{\psi},\psi]}{\delta\overline{\psi}(x_1)\delta\psi(x_1')} &= \frac{\delta^2\Gamma^\Lambda[\overline{\psi},\psi]}{\delta\overline{\psi}(x_1)\delta\psi(x_1')} - \frac{\delta}{\delta\psi(x_1')}\sum_x\left(\overline{\psi}(x)R^\Lambda(x,x_1')\right)\\ &= \frac{\delta^2\Gamma^\Lambda[\overline{\psi},\psi]}{\delta\overline{\psi}(x_1)\delta\psi(x_1')} - R^\Lambda(x_1,x_1').\end{aligned} \tag{2.124}$$

Using this relation, the flow equation is rewritten as

$$\frac{\mathrm{d}}{\mathrm{d}\Lambda}\Gamma_R^\Lambda[\overline{\psi},\psi] = -\frac{1}{2}\mathrm{Tr}\{\dot{\mathbf{R}}^\Lambda(\delta^2\Gamma_R^\Lambda[\overline{\psi},\psi] + \mathbf{R}^\Lambda)^{-1}\}, \tag{2.125}$$

where $\mathbf{R}^\Lambda = \mathrm{diag}(R^\Lambda, -(R^\Lambda)^{\mathrm{T}})$. This is fermionic counterpart of the original form of the Wetterich equation [71] [5].
At the initial condition $\Lambda = \Lambda_{\mathrm{UV}}$,

$$\begin{aligned}\Gamma_R^{\Lambda_{\mathrm{UV}}}[\overline{\psi},\psi] &= \Gamma^{\Lambda_{\mathrm{UV}}}[\overline{\psi},\psi] + (\overline{\psi}, R^{\Lambda_{\mathrm{UV}}}\psi)\\ &= \mathcal{S}^{\Lambda_{\mathrm{UV}}}[\overline{\psi},\psi] + (\overline{\psi}, R^{\Lambda_{\mathrm{UV}}}\psi) + \mathrm{const.}\\ &= -(\overline{\psi}, Q^{\Lambda_{\mathrm{UV}}}\psi) + \mathcal{S}_{\mathrm{int}}[\overline{\psi},\psi] + (\overline{\psi}, R^{\Lambda_{\mathrm{UV}}}\psi) + \mathrm{const.}\\ &= -(\overline{\psi}, Q\psi) - (\overline{\psi}, (Q^{\Lambda_{\mathrm{UV}}} - Q)\psi) + \mathcal{S}_{\mathrm{int}}[\overline{\psi},\psi] + (\overline{\psi}, R^{\Lambda_{\mathrm{UV}}}\psi) + \mathrm{const.}\\ &= \mathcal{S}[\overline{\psi},\psi] - (\overline{\psi}, R^{\Lambda_{\mathrm{UV}}}\psi) + (\overline{\psi}, R^{\Lambda_{\mathrm{UV}}}\psi) + \mathrm{const.}\\ &= \mathcal{S}[\overline{\psi},\psi] + \mathrm{const.}\end{aligned} \tag{2.126}$$

As shown above, the effective average action Γ_R^Λ interpolates smoothly between the (unregularized) bare action $\mathcal{S}$ and the final effective action Γ, while the effective

[5] Interestingly, in the paper proposing the Wetterich equation, "FRG" is written as the country name in the column of the affiliation to which Wetterich belongs. Here, "FRG" is an abbreviation of Federal Republic of Germany in English and does not mean a functional renormalization group.

action Γ^Λ interpolates between the regularized bare action $\mathcal{S}^\Lambda$ and the final effective action Γ. One may think that we should always use the effective average action Γ_R^Λ. However, the effective action Γ^Λ is also useful because the inverse of the second functional derivative of Γ^Λ is the exactly Green's function G^Λ without addition of R^Λ.

Derivation by the Effective Interaction

In addition, we derive the exact flow equation of the effective interaction $\mathcal{V}$ and we show another derivation of the flow equation of $\mathcal{G}$ using it.
With a cutoff Λ, the effective interaction is represented as

$$\mathrm{e}^{-\mathcal{V}^\Lambda} = \mathrm{e}^{\Delta_{G_0^\Lambda}} \mathrm{e}^{-\mathcal{S}_{\mathrm{int}}}. \tag{2.127}$$

At the initial condition or the highest energy scale $\Lambda = \Lambda_{\mathrm{UV}}$, the bare Green's function is zero due to regularization: $G_0^{\Lambda_{\mathrm{UV}}} = 0$. Thus $\mathcal{V}^{\Lambda_{\mathrm{UV}}} = \mathcal{S}_{\mathrm{int}}$. From this fact, we can know that the effective interaction $\mathcal{V}^\Lambda$ smoothly interpolates between the interaction part of the bare action $\mathcal{S}_{\mathrm{int}}$ and the final effective interaction $\mathcal{V}$.
The relation between $\mathcal{V}^\Lambda$ and $\mathcal{V}$ is obtained as

$$\mathrm{e}^{-\mathcal{V}} = \mathrm{e}^{\Delta_{G_0}} \mathrm{e}^{-\mathcal{S}_{\mathrm{int}}} = \mathrm{e}^{\Delta_{\overline{G}_0^\Lambda} + \Delta_{G_0^\Lambda}} \mathrm{e}^{-\mathcal{S}_{\mathrm{int}}} = \mathrm{e}^{\Delta_{\overline{G}_0^\Lambda}} \mathrm{e}^{-\mathcal{V}^\Lambda}, \tag{2.128}$$

with the soft mode bare propagator defined as

$$\overline{G}_0^\Lambda = G_0 - G_0^\Lambda. \tag{2.129}$$

Now, we derive the exact flow equation of the effective interaction. In the same manner as Eq. (2.113), we can obtain

$$\begin{aligned}
\frac{\mathrm{d}}{\mathrm{d}\Lambda}\mathcal{V}^\Lambda[\overline{\chi},\chi] &= -\mathrm{e}^{\mathcal{V}^\Lambda}\frac{\mathrm{d}}{\mathrm{d}\Lambda}\mathrm{e}^{-\mathcal{V}^\Lambda} \\
&= -\mathrm{e}^{\mathcal{V}^\Lambda}\frac{\mathrm{d}}{\mathrm{d}\Lambda}[\mathrm{e}^{\Delta_{G_0^\Lambda}}\mathrm{e}^{-\mathcal{S}_{\mathrm{int}}}] \\
&= -\mathrm{e}^{\mathcal{V}^\Lambda}\Delta_{\dot{G}_0^\Lambda}\mathrm{e}^{-\mathcal{V}^\Lambda} \\
&= -\mathrm{e}^{\mathcal{V}^\Lambda}\sum_{x,x'}\frac{\delta}{\delta\chi(x)}\left[\dot{G}_0^\Lambda(x,x')\frac{\delta}{\delta\overline{\chi}(x')}\mathrm{e}^{-\mathcal{V}^\Lambda}\right] \\
&= -\mathrm{e}^{\mathcal{V}^\Lambda}\sum_{x,x'}\frac{\delta}{\delta\chi(x)}\left[-\dot{G}_0^\Lambda(x,x')\mathrm{e}^{-\mathcal{V}^\Lambda}\frac{\delta\mathcal{V}^\Lambda}{\delta\overline{\chi}(x')}\right] \\
&= -\sum_{x,x'}\left[+\frac{\delta\mathcal{V}^\Lambda}{\delta\chi(x)}\dot{G}_0^\Lambda(x,x')\frac{\delta\mathcal{V}^\Lambda}{\delta\overline{\chi}(x')} - \dot{G}_0^\Lambda(x,x')\frac{\delta^2\mathcal{V}^\Lambda}{\delta\chi(x)\delta\overline{\chi}(x')}\right] \\
&= -\sum_{x,x'}\left[+\frac{\delta\mathcal{V}^\Lambda}{\delta\chi(x)}\dot{G}_0^\Lambda(x,x')\frac{\delta\mathcal{V}^\Lambda}{\delta\overline{\chi}(x')} + \dot{G}_0^\Lambda(x,x')\frac{\delta^2\mathcal{V}^\Lambda}{\delta\overline{\chi}(x')\delta\chi(x)}\right] \\
&= -\left(\frac{\delta\mathcal{V}^\Lambda}{\delta\chi}, \dot{G}_0^\Lambda\frac{\delta\mathcal{V}^\Lambda}{\delta\overline{\chi}}\right) - \mathrm{Tr}\left(\dot{G}_0^\Lambda\frac{\delta^2\mathcal{V}^\Lambda}{\delta\overline{\chi}\delta\chi}\right).
\end{aligned} \tag{2.130}$$

This is Polchinski equation [70] which is the exact flow equation for the effective interaction. Using the relation between $\mathcal{V}[\overline{\chi},\chi]$ and $\mathcal{G}[\overline{\eta},\eta]$ Eq. (2.78) and $\chi = G\eta$, $\overline{\chi} = G^{\mathrm{T}}\overline{\eta}$, we also obtain the flow equation for $\mathcal{G}^\Lambda[\overline{\eta},\eta]$ Eq. (2.113).

2.5 Hierarchy of the Flow Equation

While the exact flow equation Eq. (2.118) can be solved directly only for a few systems, we are usually interested in a few number of 1PI vertex functions in practice. Therefore, we perform the Taylor expansion of the flow equation in powers of the fields to obtain the hierarchy of the equations. Note that the Taylor expansions with respect to fermion variables are exact thanks to the nilpotent property of Grassmann variables. Hence expanded flow equations are yet "exact".
We introduced the expansion of $\Gamma^\Lambda[\overline{\psi},\psi]$ before. Hence, the left-hand side (LHS) of Eq. (2.118)

$$(\mathrm{LHS}) = \frac{\mathrm{d}}{\mathrm{d}\Lambda}\Gamma^\Lambda[\overline{\psi},\psi] = \sum_{m=0}^{\infty}\frac{\mathrm{d}}{\mathrm{d}\Lambda}\mathcal{A}^{(2m)\Lambda}[\overline{\psi},\psi]. \tag{2.131}$$

To expand the right-hand side (RHS) of Eq. (2.118) systematically, we introduce the matrix

$$\begin{aligned}\mathbf{U}^\Lambda[\overline{\psi},\psi] &= \delta^2\Gamma^\Lambda[\overline{\psi},\psi]\Big|_{\overline{\psi}=\psi=0} - \delta^2\Gamma^\Lambda[\overline{\psi},\psi] \\ &= [\mathbf{G}^\Lambda]^{-1} - \delta^2\Gamma^\Lambda[\overline{\psi},\psi] \\ &= -\sum_{m=2}^{\infty}\delta^2\mathcal{A}^{(2m)\Lambda}[\overline{\psi},\psi] \\ &= -(\delta^2\mathcal{A}^{(4)\Lambda} + \delta^2\mathcal{A}^{(6)\Lambda} + \delta^2\mathcal{A}^{(8)\Lambda} + \cdots).\end{aligned} \tag{2.132}$$

Using this matrix and expanding as geometric series[6],

$$\begin{aligned}(\delta^2\Gamma^\Lambda[\overline{\psi},\psi])^{-1} &= \Big([\mathbf{G}^\Lambda]^{-1} - \mathbf{U}^\Lambda[\overline{\psi},\psi]\Big)^{-1} \\ &= \Big\{[\mathbf{G}^\Lambda]^{-1}\Big(\mathbf{1} - \mathbf{G}^\Lambda\mathbf{U}^\Lambda[\overline{\psi},\psi]\Big)\Big\}^{-1} \\ &= (\mathbf{1} - \mathbf{G}^\Lambda\mathbf{U}^\Lambda[\overline{\psi},\psi])^{-1}\mathbf{G}^\Lambda \\ &= (\mathbf{1} + \mathbf{G}^\Lambda\mathbf{U}^\Lambda + \mathbf{G}^\Lambda\mathbf{U}^\Lambda\mathbf{G}^\Lambda\mathbf{U}^\Lambda + \cdots)\mathbf{G}^\Lambda.\end{aligned} \tag{2.135}$$

[6]Here we use the formula for inverse matrix:

$$(AB)^{-1} = B^{-1}A^{-1}, \tag{2.133}$$

which is proved as

$$(AB)^{-1}AB = B^{-1}A^{-1}AB = B^{-1}B = 1. \tag{2.134}$$

Substituting this into the Wetterich equation Eq. (2.118),

$$\begin{aligned}\frac{\mathrm{d}}{\mathrm{d}\Lambda}\Gamma^{\Lambda}[\overline{\psi},\psi] &= \sum_{m=0}^{\infty}\frac{\mathrm{d}}{\mathrm{d}\Lambda}\mathcal{A}^{(2m)\Lambda}[\overline{\psi},\psi] \\ &= -(\overline{\psi},\dot{Q}^{\Lambda}\psi) - \frac{1}{2}\mathrm{Tr}\Big(\dot{\mathbf{Q}}^{\Lambda}(\mathbf{1}+\mathbf{G}^{\Lambda}\mathbf{U}^{\Lambda}+\mathbf{G}^{\Lambda}\mathbf{U}^{\Lambda}\mathbf{G}^{\Lambda}\mathbf{U}^{\Lambda}+\cdots)\mathbf{G}^{\Lambda}\Big) \\ &= -(\overline{\psi},\dot{Q}^{\Lambda}\psi) - \mathrm{Tr}(\dot{Q}^{\Lambda}G^{\Lambda}) - \frac{1}{2}\mathrm{Tr}\Big(\mathbf{G}^{\Lambda}\dot{\mathbf{Q}}^{\Lambda}(\mathbf{G}^{\Lambda}\mathbf{U}^{\Lambda}+\mathbf{G}^{\Lambda}\mathbf{U}^{\Lambda}\mathbf{G}^{\Lambda}\mathbf{U}^{\Lambda}+\cdots)\Big) \\ &= -(\overline{\psi},\dot{Q}^{\Lambda}\psi) - \mathrm{Tr}(\dot{Q}^{\Lambda}G^{\Lambda}) - \frac{1}{2}\mathrm{Tr}\Big(\mathbf{G}^{\Lambda}\dot{\mathbf{Q}}^{\Lambda}\mathbf{G}^{\Lambda}(\mathbf{U}^{\Lambda}+\mathbf{U}^{\Lambda}\mathbf{G}^{\Lambda}\mathbf{U}^{\Lambda}+\cdots)\Big) \\ &= -(\overline{\psi},\dot{Q}^{\Lambda}\psi) - \mathrm{Tr}(\dot{Q}^{\Lambda}G^{\Lambda}) + \frac{1}{2}\mathrm{Tr}\Big(\mathbf{S}^{\Lambda}(\mathbf{U}^{\Lambda}+\mathbf{U}^{\Lambda}\mathbf{G}^{\Lambda}\mathbf{U}^{\Lambda}+\cdots)\Big).\end{aligned} \tag{2.136}$$

Here we define the single-scale propagator

$$\mathbf{S}^{\Lambda} = \mathrm{diag}(S^{\Lambda},-[S^{\Lambda}]^{\mathrm{T}}) = -\mathbf{G}^{\Lambda}\dot{\mathbf{Q}}^{\Lambda}\mathbf{G}^{\Lambda}, \tag{2.137}$$

with

$$S^{\Lambda} = -G^{\Lambda}\dot{Q}^{\Lambda}G^{\Lambda}. \tag{2.138}$$

It is called the single-scale propagator because it has the factor $\partial_{\Lambda}\theta^{\Lambda}(ik_0,\boldsymbol{k})$. It is obtained by the derivative with fixing self-energy as below. From the Dyson's equation

$$[\mathbf{G}^{\Lambda}]^{-1} = [\mathbf{G}_0^{\Lambda}]^{-1} - \mathbf{\Sigma}^{\Lambda}, \tag{2.139}$$

we can obtain the single-scale propagator [7]

$$\begin{aligned}\frac{\mathrm{d}}{\mathrm{d}\Lambda}\mathbf{G}^{\Lambda}\Big|_{\mathbf{\Sigma}^{\Lambda}:\mathrm{fixed}} &= \frac{\mathrm{d}}{\mathrm{d}\Lambda}([\mathbf{G}_0^{\Lambda}]^{-1}-\mathbf{\Sigma}^{\Lambda})^{-1}\Big|_{\mathbf{\Sigma}^{\Lambda}:\mathrm{fixed}} \\ &= \frac{\mathrm{d}}{\mathrm{d}\Lambda}(\mathbf{Q}^{\Lambda}-\mathbf{\Sigma}^{\Lambda})^{-1}\Big|_{\mathbf{\Sigma}^{\Lambda}:\mathrm{fixed}} \\ &= -(\mathbf{Q}^{\Lambda}-\mathbf{\Sigma}^{\Lambda})^{-1}\dot{\mathbf{Q}}^{\Lambda}(\mathbf{Q}^{\Lambda}-\mathbf{\Sigma}^{\Lambda})^{-1} \\ &= -\mathbf{G}^{\Lambda}\dot{\mathbf{Q}}^{\Lambda}\mathbf{G}^{\Lambda} \\ &= \mathbf{S}^{\Lambda}.\end{aligned} \tag{2.143}$$

[7] Here we use the derivative of inverse matrix. From

$$A^{-1}(x)A(x) = 1, \tag{2.140}$$

$$\frac{\mathrm{d}A^{-1}(x)}{\mathrm{d}x}A(x) + A^{-1}(x)\frac{\mathrm{d}A(x)}{\mathrm{d}x} = 0. \tag{2.141}$$

Thus,

$$\frac{\mathrm{d}A^{-1}(x)}{\mathrm{d}x} = -A^{-1}\frac{\mathrm{d}A(x)}{\mathrm{d}x}A^{-1}. \tag{2.142}$$

Finally, we compare the same order term in LHS and RHS and obtain the infinite hierarchy of the flow equation:

$$\frac{\mathrm{d}}{\mathrm{d}\Lambda}\mathcal{A}^{(0)\Lambda} = -\mathrm{Tr}(\dot{Q}^{\Lambda}G^{\Lambda}), \tag{2.144}$$

$$\frac{\mathrm{d}}{\mathrm{d}\Lambda}\mathcal{A}^{(2)\Lambda} = -(\overline{\psi}, \dot{Q}^{\Lambda}\psi) - \frac{1}{2}\mathrm{Tr}(\mathbf{S}^{\Lambda}\delta^2\mathcal{A}^{(4)\Lambda}), \tag{2.145}$$

$$\frac{\mathrm{d}}{\mathrm{d}\Lambda}\mathcal{A}^{(4)\Lambda} = -\frac{1}{2}\mathrm{Tr}(\mathbf{S}^{\Lambda}\delta^2\mathcal{A}^{(6)\Lambda}) + \frac{1}{2}\mathrm{Tr}(\mathbf{S}^{\Lambda}\delta^2\mathcal{A}^{(4)\Lambda}\mathbf{G}^{\Lambda}\delta^2\mathcal{A}^{(4)\Lambda}), \tag{2.146}$$

$$\begin{aligned}\frac{\mathrm{d}}{\mathrm{d}\Lambda}\mathcal{A}^{(6)\Lambda} = &-\frac{1}{2}\mathrm{Tr}(\mathbf{S}^{\Lambda}\delta^2\mathcal{A}^{(8)\Lambda}) + \frac{1}{2}\mathrm{Tr}(\mathbf{S}^{\Lambda}\delta^2\mathcal{A}^{(6)\Lambda}\mathbf{G}^{\Lambda}\delta^2\mathcal{A}^{(4)\Lambda}) \\ &+ \frac{1}{2}\mathrm{Tr}(\mathbf{S}^{\Lambda}\delta^2\mathcal{A}^{(4)\Lambda}\mathbf{G}^{\Lambda}\delta^2\mathcal{A}^{(6)\Lambda}) - \frac{1}{2}\mathrm{Tr}(\mathbf{S}^{\Lambda}\delta^2\mathcal{A}^{(4)\Lambda}\mathbf{G}^{\Lambda}\delta^2\mathcal{A}^{(4)\Lambda}\mathbf{G}^{\Lambda}\delta^2\mathcal{A}^{(4)\Lambda}),\end{aligned} \tag{2.147}$$

$$\cdots .$$

From zero-th order equation Eq. (2.144), we obtain the flow equation for the free energy (grand potential):

$$\begin{aligned}\frac{\mathrm{d}}{\mathrm{d}\Lambda}\mathcal{F}^{\Lambda} &= -\frac{1}{\beta}\mathrm{Tr}(\dot{Q}^{\Lambda}G^{\Lambda}) \\ &= -\frac{1}{\beta}\sum_{x,x'}\dot{Q}^{\Lambda}(x',x)G^{\Lambda}(x,x').\end{aligned} \tag{2.148}$$

Then, we calculate the flow equation for 1-particle vertex Eq. (2.145).

$$\begin{aligned}(\mathrm{LHS}) = \frac{\mathrm{d}}{\mathrm{d}\Lambda}\mathcal{A}^{(2)\Lambda}[\overline{\psi},\psi] &= -\frac{\mathrm{d}}{\mathrm{d}\Lambda}\sum_{x,x'}\Gamma^{(2)\Lambda}(x',x)\overline{\psi}(x')\psi(x) \\ &= -\frac{\mathrm{d}}{\mathrm{d}\Lambda}\sum_{x,x'}\Big\{Q^{\Lambda}(x',x) - \Sigma^{\Lambda}(x',x)\Big\}\overline{\psi}(x')\psi(x) \\ &= -(\overline{\psi},\dot{Q}^{\Lambda}\psi) + \sum_{x,x'}\frac{\mathrm{d}}{\mathrm{d}\Lambda}\Sigma^{\Lambda}(x',x)\overline{\psi}(x')\psi(x),\end{aligned} \tag{2.149}$$

and

$$
\begin{aligned}
(\mathrm{RHS}) &= -(\overline{\psi}, \dot{Q}^{\Lambda}\psi) - \frac{1}{2}\mathrm{Tr}(\mathbf{S}^{\Lambda}\delta^2\mathcal{A}^{(4)\Lambda}) \\
&= -(\overline{\psi}, \dot{Q}^{\Lambda}\psi) - \frac{1}{2}\mathrm{Tr}(S^{\Lambda}\overline{\delta}\delta\mathcal{A}^{(4)\Lambda}[\overline{\psi},\psi] - (S^{\Lambda})^{\mathrm{T}}\delta\overline{\delta}\mathcal{A}^{(4)\Lambda}) \\
&= -(\overline{\psi}, \dot{Q}^{\Lambda}\psi) - \frac{1}{2}\sum_{y,y'}\left(S^{\Lambda}(y,y')\overline{\delta}_{y'}\delta_{y}\mathcal{A}^{(4)\Lambda} - S^{\Lambda}(y',y)\delta_{y'}\overline{\delta}_{y}\mathcal{A}^{(4)\Lambda}\right) \\
&= -(\overline{\psi}, \dot{Q}^{\Lambda}\psi) - \frac{1}{2}\sum_{y,y'}\left(S^{\Lambda}(y,y')\overline{\delta}_{y'}\delta_{y}\mathcal{A}^{(4)\Lambda} + S^{\Lambda}(y',y)\overline{\delta}_{y}\delta_{y'}\mathcal{A}^{(4)\Lambda}\right) \\
&= -(\overline{\psi}, \dot{Q}^{\Lambda}\psi) - \sum_{y,y'}S^{\Lambda}(y,y')\overline{\delta}_{y'}\delta_{y}\mathcal{A}^{(4)\Lambda} \\
&= -(\overline{\psi}, \dot{Q}^{\Lambda}\psi) - \frac{1}{4}\sum_{y,y'}\sum_{\substack{x_1,x_2\\x_1',x_2'}}S^{\Lambda}(y,y')\overline{\delta}_{y'}\delta_{y}\Gamma^{(4)\Lambda}(x_1',x_2';x_1,x_2)\overline{\psi}(x_1')\overline{\psi}(x_2')\psi(x_2)\psi(x_1) \\
&= -(\overline{\psi}, \dot{Q}^{\Lambda}\psi) - \frac{1}{4}\sum_{y,y'}S^{\Lambda}(y,y') \\
&\quad\times\left(-\sum_{x,x'}\Gamma^{(4)\Lambda}(y',x';y,x)\overline{\psi}(x')\psi(x)\right. \\
&\quad+\sum_{x,x'}\Gamma^{(4)\Lambda}(y',x';x,y)\overline{\psi}(x')\psi(x) \\
&\quad+\sum_{x,x'}\Gamma^{(4)\Lambda}(x',y';y,x)\overline{\psi}(x')\psi(x) \\
&\quad\left.-\sum_{x,x'}\Gamma^{(4)\Lambda}(x',y';x,y)\overline{\psi}(x')\psi(x)\right).
\end{aligned}
\tag{2.150}
$$

Here, from the definition of $\Gamma^{(4)}$ and the anti-commutation relation of Grassmann variable derivative,

$$\Gamma^{(4)\Lambda}(y',x';y,x) = \Gamma^{(4)\Lambda}(x',y';x,y), \tag{2.151}$$

$$\Gamma^{(4)\Lambda}(y',x';x,y) = -\Gamma^{(4)\Lambda}(x',y';x,y), \tag{2.152}$$

$$\Gamma^{(4)\Lambda}(x',y';y,x) = -\Gamma^{(4)\Lambda}(x',y';x,y). \tag{2.153}$$

Using these relations,

$$(\mathrm{RHS}) = -(\overline{\psi}, \dot{Q}^{\Lambda}\psi) + \sum_{y,y'}\sum_{x,x'}S^{\Lambda}(y,y')\Gamma^{(4)\Lambda}(x',y';x,y)\overline{\psi}(x')\psi(x). \tag{2.154}$$

Therefore, we obtain the flow equation for the self-energy

$$\frac{\mathrm{d}}{\mathrm{d}\Lambda}\Sigma^{\Lambda}(x',x) = \sum_{y,y'}S^{\Lambda}(y,y')\Gamma^{(4)\Lambda}(x',y';x,y). \tag{2.155}$$

In the next step, we calculate the quartic term,

$$(\mathrm{LHS}) = \frac{\mathrm{d}}{\mathrm{d}\Lambda}\mathcal{A}^{(4)\Lambda} = \frac{1}{4}\sum_{\substack{x_1,x_2\\x_1',x_2'}}\frac{\mathrm{d}}{\mathrm{d}\Lambda}\Gamma^{(4)\Lambda}(x_1',x_2';x_1,x_2)\overline{\psi}(x_1')\overline{\psi}(x_2')\psi(x_2)\psi(x_1), \tag{2.156}$$

and

$$
\begin{aligned}
&(\mathrm{RHS}) \\
&= -\frac{1}{2}\mathrm{Tr}(\mathbf{S}^{\Lambda}\delta^2\mathcal{A}^{(6)\Lambda}) + \frac{1}{2}\mathrm{Tr}[\mathbf{S}^{\Lambda}\delta^2\mathcal{A}^{(4)\Lambda}\mathbf{G}^{\Lambda}\delta^2\mathcal{A}^{(4)\Lambda}] \\
&= -\mathrm{Tr}(S^{\Lambda}\bar{\delta}\delta\mathcal{A}^{(6)\Lambda}) \\
&+ \frac{1}{2}\mathrm{Tr}\left[\begin{pmatrix} S^{\Lambda} & 0 \\ 0 & -(S^{\Lambda})^{\mathrm{T}} \end{pmatrix}\begin{pmatrix} \bar{\delta}\delta\mathcal{A}^{(4)\Lambda} & \bar{\delta}\bar{\delta}\mathcal{A}^{(4)\Lambda} \\ \delta\delta\mathcal{A}^{(4)\Lambda} & \delta\bar{\delta}\mathcal{A}^{(4)\Lambda} \end{pmatrix}\begin{pmatrix} G^{\Lambda} & 0 \\ 0 & -(G^{\Lambda})^{\mathrm{T}} \end{pmatrix}\begin{pmatrix} \bar{\delta}\delta\mathcal{A}^{(4)\Lambda} & \bar{\delta}\bar{\delta}\mathcal{A}^{(4)\Lambda} \\ \delta\delta\mathcal{A}^{(4)\Lambda} & \delta\bar{\delta}\mathcal{A}^{(4)\Lambda} \end{pmatrix}\right] \\
&= -\mathrm{Tr}(S^{\Lambda}\bar{\delta}\delta\mathcal{A}^{(6)\Lambda}) \\
&\quad + \frac{1}{2}\mathrm{Tr}[S^{\Lambda}\bar{\delta}\delta\mathcal{A}^{(4)\Lambda}G^{\Lambda}\bar{\delta}\delta\mathcal{A}^{(4)\Lambda} + (S^{\Lambda})^{\mathrm{T}}\delta\bar{\delta}\mathcal{A}^{(4)\Lambda}(G^{\Lambda})^{\mathrm{T}}\delta\bar{\delta}\mathcal{A}^{(4)\Lambda}] \\
&\qquad - \mathrm{Tr}[S^{\Lambda}\bar{\delta}\bar{\delta}\mathcal{A}^{(4)\Lambda}G^{\Lambda}\delta\delta\mathcal{A}^{(4)\Lambda} + (S^{\Lambda})^{\mathrm{T}}\delta\delta\mathcal{A}^{(4)\Lambda}G^{\Lambda}\bar{\delta}\bar{\delta}\mathcal{A}^{(4)\Lambda}] \\
&= -\mathrm{Tr}(S^{\Lambda}\bar{\delta}\delta\mathcal{A}^{(6)\Lambda}) \\
&\quad + \mathrm{Tr}[S^{\Lambda}\bar{\delta}\delta\mathcal{A}^{(4)\Lambda}G^{\Lambda}\bar{\delta}\delta\mathcal{A}^{(4)\Lambda}] \\
&\quad - \mathrm{Tr}[S^{\Lambda}\bar{\delta}\bar{\delta}\mathcal{A}^{(4)\Lambda}G^{\Lambda}\delta\delta\mathcal{A}^{(4)\Lambda} + (S^{\Lambda})^{\mathrm{T}}\delta\delta\mathcal{A}^{(4)\Lambda}G^{\Lambda}\bar{\delta}\bar{\delta}\mathcal{A}^{(4)\Lambda}]. \qquad (2.157)
\end{aligned}
$$

Performing functional derivative in the same manner as equation for the self-energy above,

$$
\begin{aligned}
&\frac{\mathrm{d}}{\mathrm{d}\Lambda}\Gamma^{(4)\Lambda}(x_1', x_2'; x_1, x_2) \\
&= -\sum_{\substack{y_1, y_2 \\ y_1', y_2'}} G^{\Lambda}(y_1, y_1')S^{\Lambda}(y_2, y_2')\Big[\Gamma^{(4)\Lambda}(x_1', x_2'; y_1, y_2)\Gamma^{(4)\Lambda}(y_1', y_2'; x_1, x_2) \\
&\quad - \left\{\Gamma^{(4)\Lambda}(x_1', y_2'; x_1, y_1)\Gamma^{(4)\Lambda}(y_1', x_2'; y_2, x_2) + \Gamma^{(4)\Lambda}(x_1', y_1'; x_1, y_2)\Gamma^{(4)\Lambda}(y_2', x_2'; y_1, x_2)\right\} \\
&\quad + \left\{\Gamma^{(4)\Lambda}(x_2', y_2'; x_1, y_1)\Gamma^{(4)\Lambda}(y_1', x_1'; y_2, x_2) + \Gamma^{(4)\Lambda}(x_2', y_1'; x_1, y_2)\Gamma^{(4)\Lambda}(y_2', x_1'; y_1, x_2)\right\}\Big] \\
&\quad - \sum_{y, y'} S^{\Lambda}(y, y')\Gamma^{(6)\Lambda}(x_1', x_2', y'; x_1, x_2, y). \qquad (2.158)
\end{aligned}
$$

The first, second, and third line of Eq. (2.158) is particle-particle (PP) channel term, direct particle-hole (direct PH) channel term, and exchange (crossed) particle-hole (exchange PH) channel term, respectively.

Finally, using the relation

$$
\Gamma^{(4)\Lambda}(x_1', x_2'; x_3, x_4) = -\Gamma^{(4)\Lambda}(x_1', x_2'; x_4, x_3) = -\Gamma^{(4)\Lambda}(x_2', x_1'; x_3, x_4) = \Gamma^{(4)\Lambda}(x_2', x_1'; x_4, x_3), \qquad (2.159)
$$

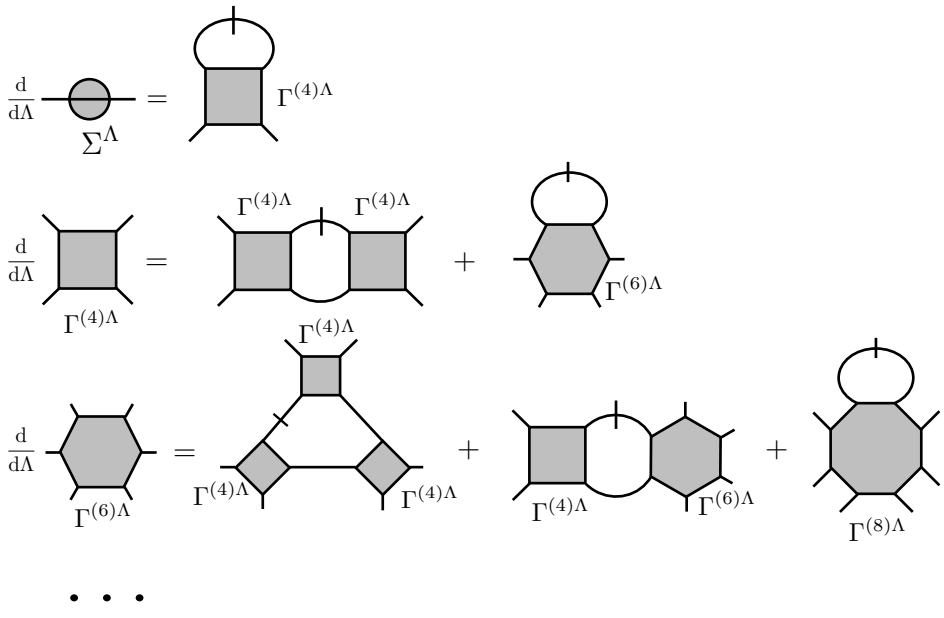

FIGURE 2.2: Diagrammatic representation of the hierarchy of the flow equations. The thick lines denote Green's functions and the slashed thick lines represent the single-scale propagators. The flow equation of $2m$-particle vertex contains a tadpole diagram consisting of $2(m+1)$-particle vertex. Therefore the hierarchy of equations does not close within finite order.

we can rewrite Eq. (2.158), as

$$\begin{aligned}
&\frac{\mathrm{d}}{\mathrm{d}\Lambda}\Gamma^{(4)\Lambda}(x_1', x_2'; x_1, x_2) \\
&= -\sum_{\substack{y_1,y_2\\ y_1',y_2'}} L^{\Lambda}(y_1, y_1'; y_2, y_2')\Big[\frac{1}{2}\Gamma^{(4)\Lambda}(x_1', x_2'; y_1, y_2)\Gamma^{(4)\Lambda}(y_1', y_2'; x_1, x_2) \\
&\qquad\qquad - \Gamma^{(4)\Lambda}(x_1', y_2'; x_1, y_1)\Gamma^{(4)\Lambda}(y_1', x_2'; y_2, x_2) \\
&\qquad\qquad + \Gamma^{(4)\Lambda}(x_2', y_2'; x_1, y_1)\Gamma^{(4)\Lambda}(y_1', x_1'; y_2, x_2)\Big] \\
&\quad - \sum_{y,y'} S^{\Lambda}(y, y')\Gamma^{(6)\Lambda}(x_1', x_2', y'; x_1, x_2, y),
\end{aligned} \tag{2.160}$$

with

$$L^{\Lambda}(y_1, y_1'; y_2, y_2') = G^{\Lambda}(y_1, y_1')S^{\Lambda}(y_2, y_2') + S^{\Lambda}(y_1, y_1')G^{\Lambda}(y_2, y_2'). \tag{2.161}$$

These hierarchy of the flow equations does not close at any finite orders because the flow equation for $\Gamma^{(2m)\Lambda}$ has the tadpole-like diagram with $\Gamma^{(2m+2)\Lambda}$. The schematic figure of these hierarchy of flow equations are shown in Figure 2.2. The full propagators are represented by thick lines and the single-scale propagators are shown by thick slashed lines. Therefore, in numerical calculation we need truncation of the infinite hierarchy. One of the natural truncation schemes is, so called, level-m_0 truncation. In this truncation scheme, we neglect all flows for $\Gamma^{(2m)\Lambda}$ for $m > m_0$. The level-m_0 truncation contains all perturbative contributions up to m_0-th order in the bare interaction. In level-1 truncation scheme, for instance, we only consider

the flow for self-energy (& free energy), and replace $\Gamma^{(4)\Lambda}$ to $\Gamma^{(4)\Lambda_{\mathrm{UV}}}$ in the tadpole-like diagram. This truncation is extremely simple, however it is useful and good sometimes in calculation of the quantum transport phenomena [55]. More generally used scheme is level-2 truncation in which the RG flows for $\Gamma^{(2m)\Lambda}$ ($m \geq 3$) are neglected and $\Gamma^{(6)\Lambda}$ in the tadpole-like diagram in the flow for $\Gamma^{(4)\Lambda}$ is replaced to its bare value, i.e. zero, in most cases. We will adopt another truncation scheme called Katanin truncation [81] later. In addition, level-2 truncation FRG is also called as one-loop FRG because the diagrams contain one internal fermion loop in momentum space [56].

The level-2 truncation FRG framework is closely related to parquet equations. Parquet framework [82–87] is an exact and self-consistent framework for the 2-particle vertex and the self-energy. In the framework we decompose the 1PI vertex (full vertex) as $\Gamma^{(4)} = R + \gamma^{(4)}_{\mathrm{PH}} + \gamma^{(4)}_{\overline{\mathrm{PH}}} + \gamma^{(4)}_{\mathrm{PP}}$, where R is the fully irreducible vertex and $\gamma^{(4)}_r$ ($r = \mathrm{PH}, \overline{\mathrm{PH}}, \mathrm{PP}$) represent the reducible (2PI) vertices of each channel (here PH, $\overline{\mathrm{PH}}$, and PP mean direct particle-hole, crossed particle-hole, and particle-particle channels, respectively). We suppress their arguments here for ease of reading. These reducible (2PI) vertices are reducible (2PI) only in their own channels, i.e. they are 2-particle irreducible for other channels. Thus we define irreducible vertices in each channel as $I_r = R + \sum_{r' \neq r} \gamma^{(4)}_{r'}$. These reducible (2PI) vertices are obtained by solving self-consistent Bethe-Salpeter equations in each channel. The Bethe-Salpeter equations are represented schematically as the second line in Fig. 2.2 without $\mathrm{d}/\mathrm{d}\Lambda$ in the left-hand side and the $\Gamma^{(6)\Lambda}$ term in the right-hand side. In addition, the single-scale propagator and two 2-particle vertices in the right-hand side are replaced by the full propagator G, I_r, and $\Gamma^{(4)}$, respectively. Obtained vertices are used to calculate the self-energy in Schwinger-Dyson equation and calculated self-energy is fed back to the Bethe-Salpeter equations through G. This self-consistent procedure is the parquet formalism. In practice, we replace the fully irreducible vertex R with the bare 2-particle vertex $\Gamma^{(4)\Lambda_{\mathrm{IR}}}$. This is called parquet approximation or first-order parquet equation. The level-2 truncation FRG has the same diagrams as we can see in Fig. 2.2. The multi-loop FRG extension is based on this fact [85–87]. The multi-loop contributions are implemented through the parquet diagrams. In 2020, using that multi-loop extension, a quantitative comparison between the numerical results of multi-loop FRG and the deterministic quantum Monte Carlo method for the Hubbard model on the square lattice was performed [72]. Moreover, it is discussed that the parquet approximation with the bare propagators and one-loop FRG are equivalent through the problem of the X-ray absorption in metals recently [88].

2.6 Example: Single-Band Spin-Rotation and Translation Invariant Systems

At the end of this chapter, we introduce FRG flow equations of fermions in single-band spin-rotation and translation invariant systems [55, 59] as an example. It is also the purpose of this section to show concrete forms of the regularized Green's functions and the single-scale propagators.

Full and Single-Scale Propagators

At first, we consider the regularized bare propagator G_0^Λ Here, $x = (\mathrm{i}\omega_n, \boldsymbol{k}, \alpha)$ and

$$G_0^\Lambda(\mathrm{i}\omega_n, \boldsymbol{k}, \alpha; \mathrm{i}\omega_{n'}, \boldsymbol{k}', \alpha') = \beta\Omega\delta_{n,n'}\delta_{\boldsymbol{k},\boldsymbol{k}'}\delta_{\alpha,\alpha'}G_0^\Lambda(\mathrm{i}\omega_n, \boldsymbol{k}), \tag{2.162}$$

with

$$G_0^\Lambda(\mathrm{i}\omega_n, \boldsymbol{k}) = \theta^\Lambda(\omega_n, \boldsymbol{k}) G_0(\mathrm{i}\omega_n, \boldsymbol{k}) = \frac{\theta^\Lambda(\omega_n, \boldsymbol{k})}{\mathrm{i}\omega_n - \xi_k}. \tag{2.163}$$

Here $\theta^\Lambda(\omega_n, \boldsymbol{k})$ is a general cutoff function. We can obtain the form of the regularized full propagator G^Λ with the self-energy Σ^Λ by Dyson equation:

$$\begin{aligned}
[G^\Lambda(\mathrm{i}\omega_n, \boldsymbol{k})]^{-1} &= [G_0^\Lambda(\mathrm{i}\omega_n, \boldsymbol{k})]^{-1} - \Sigma^\Lambda(\mathrm{i}\omega_n, \boldsymbol{k}) \\
&= [\theta^\Lambda(\mathrm{i}\omega_n, \boldsymbol{k})]^{-1} [G_0(\mathrm{i}\omega_n, \boldsymbol{k})]^{-1} - \Sigma^\Lambda(\mathrm{i}\omega_n, \boldsymbol{k}) \\
&= [\theta^\Lambda(\mathrm{i}\omega_n, \boldsymbol{k})]^{-1} \Big([G_0(\mathrm{i}\omega_n, \boldsymbol{k})]^{-1} - \theta^\Lambda(\mathrm{i}\omega_n, \boldsymbol{k}) \Sigma^\Lambda(\mathrm{i}\omega_n, \boldsymbol{k}) \Big).
\end{aligned} \tag{2.164}$$

Therefore,

$$\begin{aligned}
\therefore G^\Lambda(\mathrm{i}\omega_n, \boldsymbol{k}) &= \theta^\Lambda(\mathrm{i}\omega_n, \boldsymbol{k}) \Big([G_0(\mathrm{i}\omega_n, \boldsymbol{k})]^{-1} - \theta^\Lambda(\mathrm{i}\omega_n, \boldsymbol{k}) \Sigma^\Lambda(\mathrm{i}\omega_n, \boldsymbol{k}) \Big)^{-1} \\
&= \frac{\theta^\Lambda(\mathrm{i}\omega_n, \boldsymbol{k})}{\mathrm{i}\omega_n - \xi_k - \theta^\Lambda(\mathrm{i}\omega_n, \boldsymbol{k}) \Sigma^\Lambda(\mathrm{i}\omega_n, \boldsymbol{k})}.
\end{aligned} \tag{2.165}$$

In the next step, we derive the single-scale propagator S^Λ from its definition

$$S^\Lambda(\mathrm{i}\omega_n, \boldsymbol{k}) = -G^\Lambda(\mathrm{i}\omega_n, \boldsymbol{k}) \dot{Q}^\Lambda(\mathrm{i}\omega_n, \boldsymbol{k}) G^\Lambda(\mathrm{i}\omega_n, \boldsymbol{k}). \tag{2.166}$$

The regularized inverse bare propagator and its derivative are

$$Q^\Lambda(\mathrm{i}\omega_n, \boldsymbol{k}) = [G_0^\Lambda(\mathrm{i}\omega_n, \boldsymbol{k})]^{-1} = [\theta^\Lambda(\mathrm{i}\omega_n, \boldsymbol{k})]^{-1} [G_0(\mathrm{i}\omega_n, \boldsymbol{k})]^{-1} = [\theta^\Lambda(\mathrm{i}\omega_n, \boldsymbol{k})]^{-1} [\mathrm{i}\omega_n - \xi_k], \tag{2.167}$$

and

$$\dot{Q}^\Lambda(\mathrm{i}\omega_n, \boldsymbol{k}) = \frac{\mathrm{d}}{\mathrm{d}\Lambda} Q^\Lambda(\mathrm{i}\omega_n, \boldsymbol{k}) = -\Big(\partial_\Lambda \theta^\Lambda(\mathrm{i}\omega_n, \boldsymbol{k}) \Big) [\theta^\Lambda(\mathrm{i}\omega_n, \boldsymbol{k})]^{-2} [\mathrm{i}\omega_n - \xi_k]. \tag{2.168}$$

Therefore, the single-scale propagator is

$$\begin{aligned}
S^\Lambda(\mathrm{i}\omega_n, \boldsymbol{k}) &= -G^\Lambda(\mathrm{i}\omega_n, \boldsymbol{k}) \dot{Q}^\Lambda(\mathrm{i}\omega_n, \boldsymbol{k}) G^\Lambda(\mathrm{i}\omega_n, \boldsymbol{k}) \\
&= \left[\frac{\theta^\Lambda(\mathrm{i}\omega_n, \boldsymbol{k})}{\mathrm{i}\omega_n - \xi_k - \theta^\Lambda(\mathrm{i}\omega_n, \boldsymbol{k}) \Sigma^\Lambda(\mathrm{i}\omega_n, \boldsymbol{k})} \right]^2 \Big(\partial_\Lambda \theta^\Lambda(\mathrm{i}\omega_n, \boldsymbol{k}) \Big) [\theta^\Lambda(\mathrm{i}\omega_n, \boldsymbol{k})]^{-2} [\mathrm{i}\omega_n - \xi_k] \\
&= \frac{(\mathrm{i}\omega_n - \xi_k) \partial_\Lambda \theta^\Lambda(\mathrm{i}\omega_n, \boldsymbol{k})}{[\mathrm{i}\omega_n - \xi_k - \theta^\Lambda(\mathrm{i}\omega_n, \boldsymbol{k}) \Sigma^\Lambda(\mathrm{i}\omega_n, \boldsymbol{k})]^2}.
\end{aligned} \tag{2.169}$$

Now we specify the cutoff function as a sharp step function of frequency [8]

$$\theta^\Lambda(\omega_n, \boldsymbol{k}) = \theta^\Lambda(\omega_n) = \Theta(|\omega_n| - \Lambda). \tag{2.170}$$

The single-scale propagator is ill-defined with this choice due to the coexistence of delta peak in the numerator

$$\partial_\Lambda \theta^\Lambda(\omega_n) = \partial_\Lambda \Theta(|\omega_n| - \Lambda) = -\delta(|\omega_n| - \Lambda), \tag{2.171}$$

[8] Later we consider zero temperature limit and Matsubara frequency become a continuous variable strictly in the limit.

and a discontinuity in its denominator, while this sharp cutoff function is convenient for analytical calculation. One of the prescriptions is to choose the sharp regularized step function $\Theta_\epsilon(x)$ as a cutoff function. Suppose that $\Theta_\epsilon(x)$ has limit ($\epsilon > 0$)

$$\Theta_\epsilon(x) \xrightarrow{\epsilon\to 0} \Theta(x), \tag{2.172}$$

and satisfies

$$\partial_x \Theta_\epsilon(x) = \delta_\epsilon(x) \xrightarrow{\epsilon\to 0} \delta(x). \tag{2.173}$$

Thanks to properties above, the sharp regularized step function satisfies the relation

$$\delta_\epsilon(x) f(x, \Theta_\epsilon(x)) \xrightarrow{\epsilon\to 0} \delta(x) \int_0^1 \mathrm{d}u\, f(0, u), \tag{2.174}$$

for any continuous functions f. This relation does not depend on the detailed shape of $\Theta_\epsilon(x)$. This is sometimes called as Morris lemma [80]. Using this lemma, the single-scale propagator is obtained as

$$\begin{aligned} S^\Lambda(\mathrm{i}\omega, \boldsymbol{k}) &= -\frac{(\mathrm{i}\omega_n - \xi_{\boldsymbol{k}})\partial_\Lambda \delta_\epsilon(|\omega_n| - \Lambda)}{[\mathrm{i}\omega_n - \xi_{\boldsymbol{k}} - \Theta_\epsilon(\mathrm{i}\omega_n)\Sigma^\Lambda(\mathrm{i}\omega_n, \boldsymbol{k})]^2} \\ &\xrightarrow{\epsilon\to 0} -(\mathrm{i}\omega_n - \xi_{\boldsymbol{k}})\delta(|\omega_n| - \Lambda) \int_0^1 \mathrm{d}u \frac{1}{[\mathrm{i}\omega_n - \xi_{\boldsymbol{k}} - u\Sigma^\Lambda(\mathrm{i}\omega_n, \boldsymbol{k})]^2} \\ &= -[\Sigma^\Lambda(\mathrm{i}\omega_n, \boldsymbol{k})]^{-1}(\mathrm{i}\omega_n - \xi_{\boldsymbol{k}})\delta(|\omega_n| - \Lambda)\left(\frac{1}{\mathrm{i}\omega_n - \xi_{\boldsymbol{k}} - \Sigma^\Lambda(\mathrm{i}\omega_n, \boldsymbol{k})} - \frac{1}{\mathrm{i}\omega_n - \xi_{\boldsymbol{k}}}\right) \\ &= -\frac{\delta(|\omega_n| - \Lambda)}{\mathrm{i}\omega_n - \xi_{\boldsymbol{k}} - \Sigma^\Lambda(\mathrm{i}\omega_n, \boldsymbol{k})}. \end{aligned} \tag{2.175}$$

There is no longer the coexistence of delta peak and discontinuity.

Spin Independent Flow Equation

For derivation of flow equations, we have to parametrize the vertex functions as well as propagators. In general, if the system has full spin-rotational symmetry, the vertex functions can be written as [56, 65]

$$\begin{aligned} &\Gamma^{(2m)\Lambda}(\tilde{x}'_1\alpha'_1, \cdots, \tilde{x}'_m\alpha'_m; \tilde{x}_1\alpha_1, \cdots, \tilde{x}_m\alpha_m) \\ &\quad = \sum_{P\in\mathfrak{S}_m} \mathrm{sgn}(P)\, V^{(2m)\Lambda}(\tilde{x}'_1, \cdots, \tilde{x}'_m; \tilde{x}_{P(1)}, \cdots, \tilde{x}_{P(m)})\delta_{\alpha'_1,\alpha_{P(1)}} \cdots \delta_{\alpha'_m,\alpha'_{P(m)}}. \end{aligned} \tag{2.176}$$

Here, $\mathfrak{S}_m$ is the symmetric group and P represents its elements. $\tilde{x}$ denotes the set of appropriate quantum numbers and frequency(time) without spin projection: $x = (\tilde{x}, \alpha)$. For the choice of labels in this section, $\tilde{x} = (\mathrm{i}\omega_n, \boldsymbol{k})$. $V^{(2m)}$ is m-particle ($2m$-point) spin-independent vertex function.
Specifying $m = 1$,

$$\begin{aligned} \Gamma^{(2)\Lambda}(\tilde{x}'\alpha'; \tilde{x}\alpha) &= V^{(2)\Lambda}(\tilde{x}'; \tilde{x})\delta_{\alpha,\alpha'} \\ &= \Big[Q^\Lambda(\tilde{x}'; \tilde{x}) - \Sigma^\Lambda(\tilde{x}'; \tilde{x})\Big]\delta_{\alpha,\alpha'}, \end{aligned} \tag{2.177}$$

and $m = 2$ [59] [9],

$$\Gamma^{(4)\Lambda}(\tilde{x}_1'\alpha_1', \tilde{x}_2'\alpha_2'; \tilde{x}_1\alpha_1, \tilde{x}_2\alpha_2) = V^{(4)\Lambda}(\tilde{x}_1', \tilde{x}_2'; \tilde{x}_1, \tilde{x}_2)\delta_{\alpha_1',\alpha_1}\delta_{\alpha_2',\alpha_2} - V^{(4)}(\tilde{x}_1', \tilde{x}_2'; \tilde{x}_2, \tilde{x}_1)\delta_{\alpha_1',\alpha_2}\delta_{\alpha_2',\alpha_1}. \tag{2.178}$$

Substituting these relations into 1st and 2nd order flow equations Eq. (2.155) and Eq. (2.160) (assuming $\Gamma^{(6)} = 0$ with level-2 truncation in mind) and performing summations over spin variables, we can obtain spin-independent flow equations. For $m = 1$

$$\frac{\mathrm{d}}{\mathrm{d}\Lambda}\Sigma^{\Lambda}(\tilde{x}', \tilde{x}) = \sum_{\tilde{y},\tilde{y}'} S^{\Lambda}(\tilde{y}, \tilde{y}')[V^{(4)\Lambda}(\tilde{x}', \tilde{y}'; \tilde{y}, \tilde{x}) - 2V^{(4)\Lambda}(\tilde{x}', \tilde{y}'; \tilde{x}, \tilde{y})], \tag{2.179}$$

and, the flow equation of $\Gamma^{(4)\Lambda}$ is decomposed into a part proportional to $\delta_{\alpha_1',\alpha_1}\delta_{\alpha_2',\alpha_2}$ and a part proportional to $\delta_{\alpha_1',\alpha_2}\delta_{\alpha_2',\alpha_1}$. These parts are equivalent and from former part we can obtain

$$\begin{aligned}
&\frac{\mathrm{d}}{\mathrm{d}\Lambda}V^{(4)\Lambda}(\tilde{x}_1', \tilde{x}_2'; \tilde{x}_1, \tilde{x}_2) \\
&= -\sum_{\substack{\tilde{y}_1,\tilde{y}_2 \\ \tilde{y}_1',\tilde{y}_2'}} L^{\Lambda}(\tilde{y}_1, \tilde{y}_1'; \tilde{y}_2, \tilde{y}_2')\Big[V^{(4)\Lambda}(\tilde{x}_1', \tilde{x}_2'; \tilde{y}_1, \tilde{y}_2)V^{(4)\Lambda}(\tilde{y}_1', \tilde{y}_2'; \tilde{x}_1, \tilde{x}_2) \\
&\qquad + \Big\{-2V^{(4)\Lambda}(\tilde{x}_1', \tilde{y}_2'; \tilde{x}_1, \tilde{y}_1)V^{(4)\Lambda}(\tilde{y}_1', \tilde{x}_2'; \tilde{y}_2, \tilde{x}_2) \\
&\qquad\quad + V^{(4)\Lambda}(\tilde{x}_1', \tilde{y}_2'; \tilde{x}_1, \tilde{y}_1)V^{(4)\Lambda}(\tilde{y}_1', \tilde{x}_2'; \tilde{x}_2, \tilde{y}_2) \\
&\qquad\quad + V^{(4)\Lambda}(\tilde{x}_1', \tilde{y}_2'; \tilde{y}_1, \tilde{x}_1)V^{(4)\Lambda}(\tilde{y}_1', \tilde{x}_2'; \tilde{y}_2, \tilde{x}_2)\Big\} \\
&\qquad + V^{(4)\Lambda}(\tilde{x}_2', \tilde{y}_2'; \tilde{y}_1, \tilde{x}_1)V^{(4)\Lambda}(\tilde{y}_1', \tilde{x}_1'; \tilde{x}_2, \tilde{y}_2)\Big].
\end{aligned} \tag{2.180}$$

The first and the last lines of RHS are PP channel and exchange (crossed) PH channel contributions, respectively. The second to forth lines, enclosed in parentheses, are the contributions of the direct PH channel. At last, we parametrize Green's functions and vertices as

$$S^{\Lambda}(\tilde{x}, \tilde{x}') = S^{\Lambda}(K) \times \beta\Omega\delta(K - K'), \tag{2.181}$$
$$G^{\Lambda}(\tilde{x}, \tilde{x}') = G^{\Lambda}(K) \times \beta\Omega\delta(K - K'), \tag{2.182}$$
$$\Sigma^{\Lambda}(\tilde{x}, \tilde{x}') = \Sigma^{\Lambda}(K) \times \beta\Omega\delta(K - K'), \tag{2.183}$$
$$V^{(4)\Lambda}(\tilde{x}_1', \tilde{x}_2'; \tilde{x}_1, \tilde{x}_2) = V^{(4)\Lambda}(K_1', K_2', K_1) \times \beta\Omega\delta(K_1' + K_2' - K_1 - K_2). \tag{2.184}$$

Here we use simplified notation for generalized 4-component momemta $K = (\mathrm{i}\omega_n, \boldsymbol{k})$ and $\delta(K - K') = \delta_{n,n'}\delta(\boldsymbol{k} - \boldsymbol{k}')$. These delta functions come from Fourier transformation (see Appendix A), and reflect energy and momentum conservation laws. Substituting these parametrization into spin-independent flow equations Eq. (2.180) and Eq. (2.180), we obtain

$$\frac{\mathrm{d}}{\mathrm{d}\Lambda}\Sigma^{\Lambda}(K) = \int \mathrm{d}P\Big[V^{(4)\Lambda}(K, P, P) - 2V^{(4)\Lambda}(K, P, K)\Big]S^{\Lambda}(P), \tag{2.185}$$

[9] We can also decompose 2-particle vertex into spin-singlet part and spin-triplet part instead of decomposition in the main text [89].

and

$$\frac{\mathrm{d}}{\mathrm{d}\Lambda}V^{(4)\Lambda}(K_1', K_2', K_1) = \mathcal{T}^{\Lambda}_{\mathrm{PP}}(K_1', K_2', K_1) + \mathcal{T}^{\Lambda}_{\mathrm{PH,d}}(K_1', K_2', K_1) + \mathcal{T}^{\Lambda}_{\mathrm{PH,cr}}(K_1', K_2', K_1), \tag{2.186}$$

with

$$\mathcal{T}^{\Lambda}_{\mathrm{PP}}(K_1', K_2', K_1) = -\int \mathrm{d}P\; V^{(4)\Lambda}(K_1', K_2', P)V^{(4)\Lambda}(P, K_s - P, K_1)L^{\Lambda}(P, K_s - P), \tag{2.187}$$

$$\begin{aligned}\mathcal{T}^{\Lambda}_{\mathrm{PH,d}}(K_1', K_2', K_1) = -\int \mathrm{d}P \Big\{ &-2V^{(4)\Lambda}(K_1', P, K_1)V^{(4)\Lambda}(P + K_t, K_2', P) \\ &+ V^{(4)\Lambda}(K_1', P, K_1)V^{(4)\Lambda}(P_2', P + K_t, P) \\ &+ V^{(4)\Lambda}(K_1', P, P + K_t)V^{(4)\Lambda}(P + K_t, K_2', P)\Big\}L^{\Lambda}(P, P + K_t),\end{aligned} \tag{2.188}$$

and

$$\mathcal{T}^{\Lambda}_{\mathrm{PH,cr}}(K_1', K_2', K_1) = -\int \mathrm{d}P\; V^{(4)\Lambda}(K_1', P - K_u, P)V^{(4)\Lambda}(P, K_2', K_1)L^{\Lambda}(P, P - K_u). \tag{2.189}$$

We defined Mandelstam-like variables

$$\begin{aligned} K_s &= K_1' + K_2' = K_1 + K_2, \\ K_t &= K_1' - K_1 = K_2 - K_2', \\ K_u &= K_1' - K_2 = K_1 - K_2', \end{aligned} \tag{2.190}$$

and K_s, K_t, and K_u are transfer energy/momentum of PP channel, direct PH channel, and exchange (crossed) PH channel, respectively. In addition,

$$L^{\Lambda}(K, K') = G^{\Lambda}(K)S^{\Lambda}(K') + S^{\Lambda}(K)G^{\Lambda}(K'). \tag{2.191}$$

2.7 Summary of This Chapter

In this chapter, we have reviewed the general framework of 1PI scheme FRG for interacting fermion systems. First, we defined the generating functionals of the many-particle Green's functions and vertices. Then, in order to consider the Wilsonian renormalization group, the infrared cutoff was introduced as the flow parameter, and the exact renormalization group equation was obtained by performing the flow parameter derivative on the functional.

Then, in order to consider the Wilsonian renormalization group, we introduced the infrared cutoff as the flow parameter, and differentiated the generating functionals with respect to it to derive the exact renormalization group equation. By Taylor expansion of both sides of the equation for Grassmann field, we derive the flow equations for the vertices of each order, which we have to solve in practice.

Finally, as a typical example, we presented an application to single-band systems with spin-rotational and translational symmetries. The Hubbard model, which is a

typical model of strongly correlated electron systems, is included in this example. This provides the basis for the PFFRG that we use in this doctoral dissertation.

Chapter 3

Pseudo-Fermion Functional Renormalization Group

In this chapter, we explain pseudo-fermion functional renormalization group (PFFRG or pf-FRG) approach [53, 54, 90], used to obtain most results in this dissertation, which is a calculation method for unraveling frustrated quantum magnetism. At first, we give a brief overview of FRG for quantum spin systems. In section 2 and subsequent sections, we review pseudo-fermion representation of quantum spins and the formulation of FRG for pseudo-fermions. Some of our definitions of functions and ways to explain may be little different from Johannes Reuther's original formulation in Ref [91]. However the resultant flow equations are the same. Although there have been several studies applying PFFRG to models with Kitaev-type interactions, there is no literature describing the PFFRG flow equations for the case with these interactions explicitly. In this dissertation, we will perform calculations for models with Kitaev-type interactions, so we will derive explicit flow equations for these models in this chapter.

3.1 FRG for Spin Systems

Since the FRG can be applied if the generating functionals can be defined, it can also be applied in systems described classical fields. Studies on the analysis of classical spins using FRGs formulated in multicomponent classical fields have been continued mainly in the context of statistical mechanics [56, 60, 64, 66]. In a similar context, quantum XY spin systems have been studied as hard-core boson model and quantum O(2) model [92–94].

Although FRG for quantum spin systems have not been established in the context of condensed matter physics, the pseudo-fermion functional renormalization group (PFFRG) method was proposed in 2010 by J. Reuther and P. Wölfle [1], and has been applied to many systems [53, 54, 90, 91]. As we will discuss in detail in the following section, we applies FRG to fermion systems by rewriting the quantum spins as auxiliary fermions (Abrikosov fermions [98]) in PFFRG. This allows us to discuss the competition between different ordered states and between ordered and quantum spin liquid states in quantum spin systems without bias, at least in principle, because the different interaction channels in the fermion systems are treated with equal footings in FRG, as discussed in Chap. 2. PFFRG is a relatively new method for quantum spin systems and its extensions are still being intensively studied. We briefly review these developments in Sec. 3.7.

[1] They were originally working on the diagrammatic study of quantum spin systems using Abrikosov fermions [53, 54, 95–97].

Although not dealt with in this paper, another FRG for spin systems called spin functional renormalization group (SFRG) [2] has recently been proposed and is beginning to be used [101–104]. In SFRG, we consider the renormalization group equations for the generating functionals of the Green's functions of the spin operators. Although the Wick decomposition of the spin Green's function is complicated, the systematic treatment can be achieved by functional differentiation. In SFRG, unlike the FRG introduced so far, we introduce the flow parameter Λ as a deformation parameter of the interaction term in the Hamiltonian. There is no interaction At the initial condition ($\Lambda = 0$), and as Λ increases, the interaction is incorporated. Finally, the results for the original Hamiltonian are recovered at the end of the flow ($\Lambda = 1$). The SFRG also has the advantage that it can be applied directly to spin systems with arbitrary spin length S.

Furthermore, in the end of 2020/the beginning of 2021[3], a new FRG for quantum spin systems emerged in arXiv server: pseudo-Majorana functional renormalization group (PMFRG) [105]. In this FRG, quantum spins are rewritten by SO(3) Majorana operators and Majorana fermion FRG are performed at both zero and finite temperature. The results are good agreement with that from exact diagonalization and high-temperature series expansion. Despite its accuracy, PMFRG has the problem that the flow diverges around $T = 0$. In order to reduce that divergence, multi-loop expansion implementation is to be required.

While we are looking forward to the future development of SFRG and PMFRG as well as PFFRG, now we return to PFFRG and explain the detailed formulation of it that we use in this dissertation in the following section.

3.2 Auxiliary Fermion Representation

The difficulty of systematic calculations based on spin Green's function is due to the fact that the commutators of spin operators are not numbers but operators:

$$[S^\mu, S^\nu] = \mathrm{i} \sum_\lambda \epsilon^{\mu\nu\lambda} S^\lambda, \tag{3.1}$$

where $\epsilon^{\mu\nu\lambda}$ is a Levi-Civita symbol. Here, μ, ν, and λ are indices of spin components (x, y, z). Especially, Wick theorem of spin operators is more complicated than that of bosons and fermions [106]. Therefore, bosonization or fermionization is desired for systematic field theoretical calculation. A general way for bosonization is Schwinger-Wigner representation [107]:

$$S^\mu = \frac{1}{2} \sum_{\alpha,\alpha'} b^\dagger_{\alpha'} \sigma^\mu_{\alpha'\alpha} b_\alpha, \tag{3.2}$$

with bosonic creation and annihilation operators $b^\dagger_\alpha$ and b_α ($\alpha, \alpha' = \uparrow$ or $\downarrow$) which satisfy

$$[b_\alpha, b^\dagger_{\alpha'}] = \delta_{\alpha,\alpha'}. \tag{3.3}$$

This representation is applicable to spins with arbitrary S and holds the spin commutation relation Eq. (3.1). However the Hilbert space is enlarged by this representation and it contains unphysical subspace. Hence it is required to restrict Hilbert space to

[2] PFFRG was also sometimes referred to as spin-FRG for a while after it was proposed [99, 100].

[3] The paper was submitted on December 29th in 2020, and it emerged on the arXiv web page on January 1st in 2021.

physical subspace satisfying

$$b_\uparrow^\dagger b_\uparrow + b_\downarrow^\dagger b_\downarrow = 2S. \tag{3.4}$$

This condition is derived from the relation

$$\boldsymbol{S}^2 = (S^x)^2 + (S^y)^2 + (S^z)^2 = \left(\frac{b_\uparrow^\dagger b_\uparrow + b_\downarrow^\dagger b_\downarrow}{2}\right)\left[\left(\frac{b_\uparrow^\dagger b_\uparrow + b_\downarrow^\dagger b_\downarrow}{2}\right) + 1\right], \tag{3.5}$$

and the identity for the quantum spin

$$\boldsymbol{S}^2 = S(S+1). \tag{3.6}$$

Boson operators in Eq. (3.2) can be replaced by fermion operators $f_\alpha^\dagger$ and f_α only when $S = 1/2$:

$$S^\mu = \frac{1}{2}\sum_{\alpha,\alpha'} f_{\alpha'}^\dagger \sigma_{\alpha'\alpha}^\mu f_\alpha, \tag{3.7}$$

and

$$\{f_\alpha, f_{\alpha'}^\dagger\} = \delta_{\alpha,\alpha'}. \tag{3.8}$$

A fermionic counterpart of the relationship Eq. (3.5) is

$$\boldsymbol{S}^2 = \frac{3}{4}\left(f_\uparrow^\dagger f_\uparrow - f_\downarrow^\dagger f_\downarrow\right)^2 = \frac{3}{4}\left(f_\uparrow^\dagger f_\uparrow + f_\downarrow^\dagger f_\downarrow\right). \tag{3.9}$$

We use the fact that fermion occupation number is 1 or 0: $(f_\alpha^\dagger f_\alpha)^2 = f_\alpha^\dagger f_\alpha$ and the fermion commutation relation Eq. (3.8). Therefore we have to restrict the Hilbert space to its subspace satisfying half-filling condition

$$f_\uparrow^\dagger f_\uparrow + f_\downarrow^\dagger f_\downarrow = 1. \tag{3.10}$$

In most cases we deal with problems with $S = 1/2$ and since the fermions are easier to handle in numerical calculations based on field theory, PFFRG adopts this fermionization sometimes called Abrikosov fermion representation [98]. Fermionic Green's function based on it has been used for Feynman-diagrammatic studies of quantum spin systems [95–97]. This fermionization is also used for RVB mean-field theory of the quantum spin liquid where f_α and $f_\alpha^\dagger$ represent the spinon degrees of freedom; sometimes called "parton construction" [1, 5, 6] [4].
Hamiltonians of the $S = 1/2$ quantum spin systems treated in this dissertation in general have the form

$$\mathcal{H} = \frac{1}{2}\sum_{i,j}\sum_{\mu,\nu} J_{ij}^{\mu\nu} S_i^\mu S_j^\nu, \tag{3.11}$$

where i and j are site indices.
For example, in the case of the nearest-neighbor antiferromagnetic (AFM) Heisenberg model ($J > 0$)

$$J_{ij}^{\mu\nu} = J_{ij}\delta^{\mu\nu} = \begin{cases} J\delta^{\mu\nu} & i \text{ and } j \text{ are nearest-neighbors} \\ 0 & \text{otherwise} \end{cases}, \tag{3.12}$$

[4] "Parton" is firstly introduced by Richard P. Feynman to interpret high-energy hadron collisions [108].

and in the case of the ferromagnetic (FM) Kitaev model ($J_x, Jy, J_z > 0$)

$$J_{ij}^{\mu\nu} = J_{ij}^{\mu}\delta^{\mu\nu} = \begin{cases} -J_x\delta^{\mu x}\delta^{\mu\nu} & \text{bond between } i \text{ and } j \text{ is } x\text{-bond} \\ -J_y\delta^{\mu y}\delta^{\mu\nu} & \text{bond between } i \text{ and } j \text{ is } y\text{-bond} \\ -J_z\delta^{\mu z}\delta^{\mu\nu} & \text{bond between } i \text{ and } j \text{ is } z\text{-bond} \\ 0 & \text{otherwise} \end{cases}. \tag{3.13}$$

In PFFRG, we represent quantum spins on each site like Eq. (3.7):

$$S_i^{\mu} = \frac{1}{2}\sum_{\alpha,\alpha'} f_{i\alpha'}^{\dagger}\sigma_{\alpha'\alpha}^{\mu} f_{i\alpha}. \tag{3.14}$$

Fermionic creators and annihilators satisfy the commutation relation as Eq. (3.8)

$$\{f_{i\alpha}, f_{i'\alpha'}^{\dagger}\} = \delta_{i,i'}\delta_{\alpha,\alpha'}. \tag{3.15}$$

Due to the fermionization of spins Eq. (3.14), the Hilbert space is enlarged. Each site has four fermionic states:

$$|0\rangle_i, \quad |\uparrow\rangle_i, \quad |\downarrow\rangle_i, \quad |\uparrow\downarrow\rangle_i. \tag{3.16}$$

The first empty state $|0\rangle_i$ and the last doubly-occupied state $|\uparrow\downarrow\rangle_i$ are unphysical ($S = 0$) and it is required to restrict states to those corresponding to the original spin states $|\uparrow\rangle_i$ and $|\downarrow\rangle_i$, which satisfy the local half-filling constraint

$$Q_i = 1 \qquad \text{with} \quad Q_i = f_{\uparrow}^{\dagger}f_{\uparrow} + f_{\downarrow}^{\dagger}f_{\downarrow} \quad \text{(at each site)}. \tag{3.17}$$

Writing the Hamiltonian Eq. (3.11) by the pseudo-fermions Eq. (3.14), we obtain a fermionic Hamiltonian which we directly treat by FRG:

$$\mathcal{H} = \frac{1}{2}\sum_{i,j}\sum_{\substack{\alpha,\beta \\ \alpha',\beta'}}\sum_{\mu,\nu}\frac{J_{ij}^{\mu\nu}}{4}\sigma_{\alpha'\alpha}^{\mu}\sigma_{\beta'\beta}^{\nu} f_{i\alpha'}^{\dagger} f_{j\beta'}^{\dagger} f_{j\beta} f_{i\alpha}. \tag{3.18}$$

For projection to physical sector of the pseudo-fermion Hilbert space fulfilling the condition Eq. (3.17), we adopt grand canonical ensemble and introduce chemical potential

$$\mathcal{H} \to \mathcal{H} - \mu\sum_i Q_i. \tag{3.19}$$

In one of the exact projection schemes, we set the chemical potential

$$\mu = -\lambda, \tag{3.20}$$

and perform the limitation $\lambda \to \infty$ after differential of the grand partition function with respect to the fugacity in order to obtain the exact projected partition function. This scheme was used for Kondo effect and mixed-valence problem [109, 110]. Unfortunately, this projection is not applicable for lattice model considered in this dissertation and it can be performed only in models like Kondo model and Anderson impurity exactly [91]. Another exact projection scheme proposed by Popov and Fedotov is realized by setting imaginary-valued chemical potential [111]

$$\mu = -\frac{\mathrm{i}\pi T}{2}. \tag{3.21}$$

In this scheme, the expectation value of an arbitrary physical quantity $\mathcal{O}$ calculated with the original spin Hamiltonian $\langle\mathcal{O}\rangle$ is equal to that calculated with the chemical potential Eq. (3.21) $\langle\mathcal{O}\rangle_{\mathrm{ppv}}$ due to cancellation between unphysical contribution of the $Q_i = 0$ (empty) sector and that of the $Q_i = 2$ (doubly-occupied) sector. Note that for unphysical operators i.e. operators ill-defined by the original spin operators the expectation values of them are meaningless and $\langle\mathcal{O}\rangle \neq \langle\mathcal{O}\rangle_{\mathrm{ppv}}$ even if calculated. With imaginary-valued chemical potentials the grand canonical Hamiltonian is no longer hermitian and requires more computation costs than average projection scheme introduced below although it is applicable for the lattice model considered here [112, 113]. In order to calculate more simply, we adopt an average projection scheme where the local half-filling condition Eq. (3.17) is replaced by the average condition

$$\langle Q_i \rangle = 1. \tag{3.22}$$

Due to the particle-hole symmetry (particle-hole gauge redundancy more precisely) , this average constraint can be implemented by

$$\mu = 0. \tag{3.23}$$

In ordinal PFFRG calculation, we consider the absolute zero limit for a simpler calculation (we will mention finite temperature calculation later). At first glance, exact projection proposed by Popov and Fedotov ($\mu = -\mathrm{i}\pi T/2$) and average projection ($\mu = 0$) appear to be equivalent in the $T \to 0$ limit, but the average under $\mu = -\mathrm{i}\pi T/2$ and the limit $T \to 0$ do not necessarily commute. Nevertheless both projections are expected to be identical at $T = 0$ here. It is because pseudo-fermion number fluctuations are not allowed energetically at $T = 0$ [54, 91].

3.3 Parametrization of Functions

For implementation of FRG for quantum spin systems, we have to parametrize propagators and vertices for the quantum numbers carried by pseudo-fermions constructing spins and have to introduce some methodological modifications to FRG schemes shown in previous chapter. In ordinal FRG for fermion systems, especially electron systems, described in the previous section, we parametrize functions in momentum space except some cases, for instance, for transport phenomena [114–116] and for inhomogeneous systems [117]. It is the same for bosonic systems [56]. In PFFRG for the spin Hamiltonian Eq. (3.11), we adopt real space representation i.e. pseudo-fermions carry site indices in addition to spin indices. Therefore we take the set of quantum numbers that specify one-particle states and frequency (or time) x as $x = (\omega, i, \alpha)$: ω, i, and α are Matsubara frequency, site index, and spin index, respectively. Corresponding it, the summation is replaced as $\sum_x = \sum_i \sum_\alpha \int \frac{\mathrm{d}\omega}{2\pi}$. Remember that we write Matsubara frequency as ω hereafter because of its simplicity and continuity of the Matsubara frequency due to zero temperature limit $\frac{1}{\beta}\sum_\omega \to \int \frac{\mathrm{d}\omega}{2\pi}$.

Parametrization of Propagators and Self-Energy

Due to absence of a kinetic term in pseudo-fermion Hamiltonian Eq. (3.18), pseudo-fermions are strictly localized and its bare Green's function has the form

$$\begin{aligned} G_0(x,x') = G_0(\mathrm{i}\omega, i, \alpha; \mathrm{i}\omega', i', \alpha') &= G_{0i\alpha}(\omega) \times \beta\delta(\omega-\omega')\delta_{i,i'}\delta_{\alpha,\alpha'} \\ &= G_0(\omega) \times \beta\delta(\omega-\omega')\delta_{i,i'}\delta_{\alpha,\alpha'}, \end{aligned} \tag{3.24}$$

with

$$G_0(\omega) = \frac{1}{\mathrm{i}\omega}. \tag{3.25}$$

Hereafter we adopt the average projection scheme $\mu = 0$ and $T \to 0$ limit. In addition, we assume that all lattice sites are equivalent and omit the site indices of propagators hereafter. This is trivial for the bare propagator and it is applicable to all models in this dissertation. This locality of the Green's function is also understood by the local U(1) gauge redundancy [118, 119]. We can parametrize the full propagator and pseudo-fermion self energy as the bare propagator:

$$\begin{aligned} G(x,x') = G(\mathrm{i}\omega, i, \alpha; \mathrm{i}\omega', i', \alpha') &= G_{i\alpha}(\omega) \times \beta\delta(\omega-\omega')\delta_{i,i'}\delta_{\alpha,\alpha'} \\ &= G(\omega) \times \beta\delta(\omega-\omega')\delta_{i,i'}\delta_{\alpha,\alpha'}, \end{aligned} \tag{3.26}$$

and

$$\Sigma(x,x') = \Sigma(\omega) \times \beta\delta(\omega-\omega')\delta_{i,i'}\delta_{\alpha,\alpha'}. \tag{3.27}$$

Combining them, we can write

$$G(\omega) = \frac{1}{\mathrm{i}\omega - \Sigma(\omega)}. \tag{3.28}$$

Thanks to the particle-hole symmetry, a spectral function of the pseudo-fermions is even function $A(\varepsilon) = A(-\varepsilon)$ for real variable ε. From the Lehmann representation of the Green's function,

$$\begin{aligned} G(\omega) &= \int_{-\infty}^{\infty} \mathrm{d}\varepsilon \frac{A(\varepsilon)}{\mathrm{i}\omega - \varepsilon} \\ &= \int_{-\infty}^{\infty} \mathrm{d}\varepsilon \frac{A(\varepsilon) \times (-\mathrm{i}\omega - \varepsilon)}{\omega^2 + \varepsilon^2} \\ &= -\mathrm{i}\omega \int_{-\infty}^{\infty} \mathrm{d}\varepsilon \frac{A(\varepsilon)}{\omega^2 + \varepsilon^2} - \int_{-\infty}^{\infty} \mathrm{d}\varepsilon \frac{A(\varepsilon)\varepsilon}{\omega^2 + \varepsilon^2} \\ &= -\mathrm{i}\omega \int_{-\infty}^{\infty} \mathrm{d}\varepsilon \frac{A(\varepsilon)}{\omega^2 + \varepsilon^2}. \end{aligned} \tag{3.29}$$

Therefore, we can conclude that the Green's function is odd function of the Matsubara frequency and a pure imaginary function:

$$G(-\omega) = -G(\omega), \tag{3.30}$$

$$G(\omega) \in \mathrm{i}\mathbb{R}. \tag{3.31}$$

The self-energy should have the same symmetry due to Dyson equation:

$$\Sigma(-\omega) = -\Sigma(\omega), \tag{3.32}$$

$$\Sigma(\omega) \in \mathrm{i}\mathbb{R}. \tag{3.33}$$

From these properties, we define a real-valued self-energy

$$\Sigma(\omega) = -\mathrm{i}\gamma(\omega). \tag{3.34}$$

It corresponds to damping constant of the pseudo-fermions. From the above discussion, the pseudo-fermion Green's function with damping constant γ has the form

$$G(\omega) = \frac{1}{\mathrm{i}\omega + \mathrm{i}\gamma\mathrm{sgn}(\omega)}. \tag{3.35}$$

Note that the damping constant involves a sign function of the Matsubara frequency in the denominator. The retarded Green's function G^{R} is

$$G^{\mathrm{R}}(\varepsilon) = \frac{1}{\varepsilon + \mathrm{i}\gamma}, \tag{3.36}$$

with real frequency variable ε. And in real-time representation,

$$G^{\mathrm{R}}(t) = \frac{\Theta(t)}{\mathrm{i}} \mathrm{e}^{-t/\tau}, \tag{3.37}$$

with the pseudo-fermion lifetime $\tau = 1/\gamma$.

For FRG flow equation, we introduce IR cutoff Λ. In ordinary PFFRG calculation we adopt sharp frequency cutoff scheme i.e. we choose

$$\theta^{\Lambda}(\omega) = \Theta(|\omega| - \Lambda) \tag{3.38}$$

as a cutoff function. With this function, the regularized bare propagator is

$$G_0^{\Lambda}(\omega) = \frac{\Theta(|\omega| - \Lambda)}{\mathrm{i}\omega}, \tag{3.39}$$

and it satisfies

$$G_0^{\Lambda}(\omega) = \begin{cases} 0 & \Lambda = \Lambda_{\mathrm{UV}} = \infty \\ G_0(\omega) & \Lambda = \Lambda_{\mathrm{IR}} = 0. \end{cases} \tag{3.40}$$

In the same manner as in section 2.6, the full propagator is

$$\begin{aligned} G^{\Lambda}(\omega) &= \frac{\Theta(|\omega| - \Lambda)}{\mathrm{i}\omega - \Theta(|\omega| - \Lambda)\Sigma^{\Lambda}(\omega)} \\ &= \frac{\Theta(|\omega| - \Lambda)}{\mathrm{i}\omega - \Sigma^{\Lambda}(\omega)} \\ &= \frac{\Theta(|\omega| - \Lambda)}{\mathrm{i}\omega + \mathrm{i}\gamma^{\Lambda}(\omega)}. \end{aligned} \tag{3.41}$$

In addition, the single-scale propagator can be parametrized as

$$S^{\Lambda}(x, x') = S^{\Lambda}(\omega) \times \beta\delta(\omega - \omega')\delta_{i,i'}\delta_{\alpha,\alpha'}, \tag{3.42}$$

and has the properties as

$$S^{\Lambda}(-\omega) = -S^{\Lambda}(\omega), \tag{3.43}$$

$$S^{\Lambda}(\omega) \in \mathrm{i}\mathbb{R}, \tag{3.44}$$

due to those of the Green's function. We can obtain a simple formula for the single-scale propagator by Morris lemma [80] in the same way as section 2.6,

$$\begin{aligned} S^{\Lambda}(\omega) &= -G^{\Lambda}(\omega)\dot{Q}^{\Lambda}(\omega)G^{\Lambda}(\omega) \\ &= -\frac{\delta(|\omega|-\Lambda)}{\mathrm{i}\omega - \Sigma^{\Lambda}(\omega)} \\ &= -\frac{\delta(|\omega|-\Lambda)}{\mathrm{i}\omega + \mathrm{i}\gamma^{\Lambda}(\omega)}. \end{aligned} \tag{3.45}$$

Parametrization of Vertices

We also have to parametrize vertices, especially 2-particle vertex function. By strict locality of all propagators, the site indices of incoming legs of vertices and corresponding indices of outgoing legs have to be identical. This is also understood by the local U(1) gauge redundancy [118, 119]. Therefore we can parametrize site indices dependence of the 2-particle vertex as

$$\begin{aligned} \Gamma^{(4)\Lambda}(x_1', x_2'; x_1, x_2) =& \Gamma^{\Lambda}_{i_1 i_2}(\omega_1'\alpha_1', \omega_2'\alpha_2'; \omega_1\alpha_1, \omega_2\alpha_2)\delta_{i_1', i_1}\delta_{i_2', i_2} \\ &- \Gamma^{\Lambda}_{i_1 i_2}(\omega_2'\alpha_2', \omega_1'\alpha_1'; \omega_1\alpha_1, \omega_2\alpha_2)\delta_{i_2' i_1}\delta_{i_1' i_2}. \end{aligned} \tag{3.46}$$

We omit the suffix (4) for parametrized 2-particle (4-point) vertex. Because it is simpler to write and we do not treat $\Gamma^{(2m)}$ $(m \geq 3)$ hereafter.
Applying it to the flow equations of the self-energy Eq. (2.155) and 2-particle vertex Eq. (2.160), then we perform the summation of site indices and extract only the terms proportional to $\delta_{i_1', i_1}\delta_{i_2', i_2}$ not to $\delta_{i_2', i_1}\delta_{i_1', i_2}$ for the equation of Γ^{Λ}, we obtain

$$\begin{aligned} &\frac{\mathrm{d}}{\mathrm{d}\Lambda}(-\mathrm{i})\gamma^{\Lambda}(\omega_1) \times 2\pi\delta(\omega_1' - \omega_1)\delta_{\alpha_1', \alpha} \\ &\qquad = \int \frac{\mathrm{d}\omega'}{2\pi} \sum_{\alpha'} S^{\Lambda}(\omega') \Bigg[\sum_{j} \Gamma^{\Lambda}_{i_1 j}(\omega'\alpha', \omega_1'\alpha_1'; \omega_1\alpha_1, \omega'\alpha') \\ &\qquad\qquad - \Gamma^{\Lambda}_{i_1 i_1}(\omega_1'\alpha_1', \omega'\alpha'; \omega_1\alpha_1, \omega'\alpha') \Bigg], \end{aligned} \tag{3.47}$$

and

$$\begin{aligned} &\frac{\mathrm{d}}{\mathrm{d}\Lambda}\Gamma^{\Lambda}_{i_1 i_2}(\omega_1'\alpha_1', \omega_2'\alpha_2; \omega_1\alpha_1, \omega_2\alpha_2) \\ &= -\int \frac{\mathrm{d}\omega_3}{2\pi}\frac{\mathrm{d}\omega_4}{2\pi} \sum_{\alpha_3, \alpha_4} L^{\Lambda}(\omega_3, \omega_4) \\ &\quad \times \Big[\Gamma^{\Lambda}_{i_1 i_2}(\omega_1'\alpha_1, \omega_2'\alpha_2'; \omega_3\alpha_3, \omega_4\alpha_4)\Gamma^{\Lambda}_{i_1 i_2}(\omega_3\alpha_3, \omega_4\alpha_4; \omega_1\alpha_1, \omega_2\alpha_2) \\ &\qquad - \sum_{j} \Gamma^{\Lambda}_{i_1 j}(\omega_1'\alpha_1', \omega_4\alpha_4; \omega_1\alpha_1, \omega_3\alpha_3)\Gamma^{\Lambda}_{j i_2}(\omega_3\alpha_3, \omega_2'\alpha_2'; \omega_4\alpha_4, \omega_2\alpha_2) \\ &\qquad + \Gamma^{\Lambda}_{i_1 i_2}(\omega_1'\alpha_1', \omega_4\alpha_4; \omega_1\alpha_1, \omega_3\alpha_3)\Gamma^{\Lambda}_{i_2 i_2}(\omega_2'\alpha_2', \omega_3\alpha_3; \omega_4\alpha_4, \omega_2\alpha_2) \\ &\qquad + \Gamma^{\Lambda}_{i_1 i_1}(\omega_4\alpha_4, \omega_1'\alpha_1'; \omega_1\alpha_1, \omega_3\alpha_3)\Gamma^{\Lambda}_{i_1 i_2}(\omega_3\alpha_3, \omega_2'\alpha_2'; \omega_4\alpha_4, \omega_2\alpha_2) \\ &\qquad + \Gamma^{\Lambda}_{i_1 i_2}(\omega_4\alpha_4, \omega_2'\alpha_2'; \omega_1\alpha_1, \omega_3\alpha_3)\Gamma^{\Lambda}_{i_1 i_2}(\omega_1'\alpha_1', \omega_3\alpha_3; \omega_4\alpha_4, \omega_2\alpha_2) \Big], \end{aligned} \tag{3.48}$$

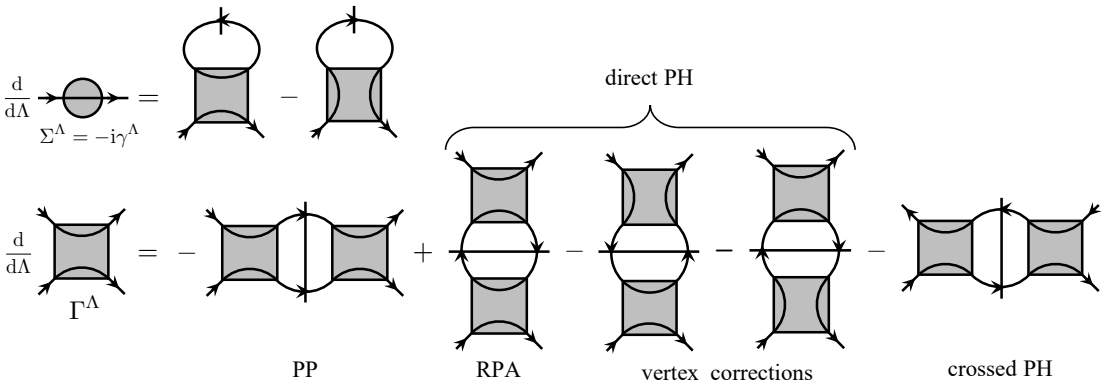

FIGURE 3.1: Diagrams representing PFFRG flow equations Eq. (3.47) and Eq. (3.48). The gray circle and the grey square correspond the self-energy $\Sigma^\Lambda = -i\gamma^\Lambda$ and the 2-particle vertex Γ^Λ, respectively. In the diagram for the self-energy, the slashed line denotes the single-scale propagator S^Λ. The pair of slashed lines represents $L^\Lambda(\omega', \omega'')$ defined in Eq. (3.49).

with

$$L^\Lambda(\omega_3, \omega_4) = G^\Lambda(\omega_3)S^\Lambda(\omega_4) + S^\Lambda(\omega_3)G^\Lambda(\omega_4). \tag{3.49}$$

In order to simplify the first term in the RHS of Eq. (3.47) (PP term), We use the fact that the integrand is symmetrical with respect to ω_3 and ω_4, and the relation

$$\Gamma^\Lambda_{i_1 i_2}(\omega_1'\alpha_1', \omega_2'\alpha_2'; \omega_1\alpha_1, \omega_2\alpha_2) = \Gamma^\Lambda_{i_2 i_1}(\omega_2'\alpha_2', \omega_1'\alpha_1'; \omega_2\alpha_2, \omega_1\alpha_1). \tag{3.50}$$

This relation is derived from the identity

$$\Gamma^\Lambda(x_1', x_2'; x_1, x_2) = \Gamma^\Lambda(x_2', x_1'; x_2, x_1), \tag{3.51}$$

that we can prove by the functional differentiation of the effective action. Applying Eq. (3.46) to the above identity and comparing the terms proportional to $\delta_{i_1', i_1}\delta_{i_2', i_2}$ in both sides, we can prove the relation Eq. (3.50). Diagrammatic representations of Eq. (3.47) and Eq. (3.48) are shown in Figure 3.1. The fist and last terms in the RHS of Eq. (3.48) are PP and PH ladder, respectively. The second term contains an internal summation over all sites and it corresponds to a RPA (random phase approximation) bubble term. This internal summation is also in the first term in the RHS of Eq. (3.47). Remaining the third and forth terms of Eq. (3.48) are vertex correction terms.

In the RPA term, the summation with respect to the site index of the fermion bubble (j) runs over entire lattice and induce spin correlations. Therefore this term induces magnetic orders, i. e., it contains the leading term in $1/S$-expansion. In the limit $S \to \infty$, this is equivalent to the spin mean-field theory of classical spins [54, 91, 95, 120]. On the other hand, PP and PH ladder terms contain the leading contribution of $1/N$ expansion for SU(N) quantum spin systems [54, 91, 120]. In the $N \to \infty$ limit, these contributions are identical to RVB mean-field theory [121, 122]. These contributions involve quantum fluctuations and induce short-range dimerization and its superposition. Hence their effects compete with long-range magnetic ordering tendencies stabilized by the RPA term and stabilize VBC (valence bond

crystal) states, RVB states, or spin liquid states. The vertex correction terms combine these contributions. Note that the above descriptions of terms are based on the discussions in which we only consider equation with a single channel contribution with neglecting other terms. In PFFRG with all terms, we consider the contributions of each term unbiasedly and those of the diagrams corresponding combinations of those contributions.
In the next step, we perform more detailed parametrization of the vertex function. We can parametrize the vertex for the general spin Hamiltonian Eq. (3.18) or Eq. (3.18) including off-diagonal spin interactions as

$$\Gamma^{\Lambda}_{i_1 i_2}(\omega_1'\alpha_1', \omega_2'\alpha_2'; \omega_1\alpha_1, \omega_2\alpha_2) = \sum_{\tilde{\mu},\tilde{\nu}} \Gamma^{\tilde{\mu}\tilde{\nu},\Lambda}_{i_1 i_2}(s,t,u)\sigma^{\tilde{\mu}}_{\alpha_1',\alpha_1}\sigma^{\tilde{\nu}}_{\alpha_2',\alpha_2} \times 2\pi\delta(\omega_1' + \omega_2' - \omega_1 - \omega_2). \tag{3.52}$$

The number of independent frequencies is three and one of four frequencies is restricted by energy conservation law. We can confirm this fact by the Fourier transformation, see Appendix 3.7. We define independent Mandelstam-like frequency variables s, t, and u from frequency arguments as

$$s = \omega_1' + \omega_2' = \omega_1 + \omega_2, \tag{3.53}$$
$$t = \omega_1' - \omega_1 = \omega_2 - \omega_2', \tag{3.54}$$
$$u = \omega_1' - \omega_2 = \omega_1 - \omega_2'. \tag{3.55}$$

These variables have properties similar to Mandelstam variables [123]. s, t, and u are transfer frequencies of PP, direct PH, and exchange (crossed) PH channel, respectively. Equations (3.53), (3.54), and (3.55) can be rewritten as

$$\omega_1' = \frac{1}{2}(s+t+u), \tag{3.56}$$
$$\omega_2' = \frac{1}{2}(s-t-u), \tag{3.57}$$
$$\omega_1 = \frac{1}{2}(s-t+u), \tag{3.58}$$
$$\omega_2 = \frac{1}{2}(s+t-u). \tag{3.59}$$

In Eq. (3.52), we introduce 4-valued variables $\tilde{\mu}$, $\tilde{\nu} = 0, 1, 2, 3$. Recall that we introduced μ, $\nu = x, y, z$ before. Here, $\sigma^1 = \sigma^x$, $\sigma^2 = \sigma^y$, $\sigma^3 = \sigma^z$, and $\sigma^0 = \mathbb{1}_{2\times 2}$: it 2-dimensional represents an identity matrix and $\sigma^0_{\alpha_1',\alpha_1} = \delta_{\alpha_1',\alpha_1}$.
Fully parametrized 2-particle vertices in Eq. (3.52) obey the following symmetry relations [119]:

$$\Gamma^{\tilde{\mu}\tilde{\nu},\Lambda}_{i_1 i_2}(s,t,u) \in \begin{cases} \mathbb{R} & \text{if } \xi(\tilde{\mu})\xi(\tilde{\nu}) = 1 \\ \mathrm{i}\mathbb{R} & \text{if } \xi(\tilde{\mu})\xi(\tilde{\nu}) = -1 \end{cases}, \tag{3.60}$$
$$\Gamma^{\tilde{\mu}\tilde{\nu},\Lambda}_{i_1 i_2}(s,t,u) = \Gamma^{\tilde{\nu}\tilde{\mu},\Lambda}_{i_2 i_1}(-s,t,u), \tag{3.61}$$
$$\Gamma^{\tilde{\mu}\tilde{\nu},\Lambda}_{i_1 i_2}(s,t,u) = \xi(\tilde{\mu})\xi(\tilde{\nu})\Gamma^{\tilde{\mu}\tilde{\nu},\Lambda}_{i_1 i_2}(s,-t,u), \tag{3.62}$$
$$\Gamma^{\tilde{\mu}\tilde{\nu},\Lambda}_{i_1 i_2}(s,t,u) = \xi(\tilde{\mu})\xi(\tilde{\nu})\Gamma^{\tilde{\nu}\tilde{\mu},\Lambda}_{i_2 i_1}(s,t,-u), \tag{3.63}$$
$$\Gamma^{\tilde{\mu}\tilde{\nu},\Lambda}_{i_1 i_2}(s,t,u) = -\xi(\tilde{\nu})\Gamma^{\tilde{\mu}\tilde{\nu},\Lambda}_{i_1 i_2}(u,t,s), \tag{3.64}$$

where

$$\xi(\tilde{\mu}) = \begin{cases} +1 & \text{if } \tilde{\mu} = 0 \\ -1 & \text{otherwise} \end{cases}. \tag{3.65}$$

In this dissertation, we only consider diagonal spin interactions. Therefore, it is sufficient to consider a simpler parametrization

$$\begin{aligned} &\Gamma^{\Lambda}_{i_1 i_2}(\omega_1' \alpha_1', \omega_2' \alpha_2'; \omega_1 \alpha_1, \omega_2 \alpha_2) \\ &\quad = \left\{ \sum_{\mu} \Gamma^{\mu,\Lambda}_{i_1 i_2}(s,t,u) \sigma^{\mu}_{\alpha_1',\alpha_1} \sigma^{\mu}_{\alpha_2',\alpha_2} + \Gamma^{\mathrm{d},\Lambda}_{i_1 i_2}(s,t,u) \delta_{\alpha_1',\alpha_1} \delta_{\alpha_2',\alpha_2} \right\} \times 2\pi\delta(\omega_1' + \omega_2' - \omega_1 - \omega_2). \end{aligned} \tag{3.66}$$

Corresponding the symmetry relations (3.60)-(3.64),

$$\Gamma^{\mu,\Lambda}_{i_1 i_2}(s,t,u),\ \Gamma^{\mathrm{d},\Lambda}_{i_1 i_2}(s,t,u) \in \mathbb{R}, \tag{3.67}$$

$$\Gamma^{\mu,\Lambda}_{i_1 i_2}(s,t,u) = \Gamma^{\mu,\Lambda}_{i_2 i_1}(-s,t,u), \tag{3.68}$$

$$\Gamma^{\mu,\Lambda}_{i_1 i_2}(s,t,u) = \Gamma^{\mu,\Lambda}_{i_1 i_2}(s,-t,u), \tag{3.69}$$

$$\Gamma^{\mu,\Lambda}_{i_1 i_2}(s,t,u) = \Gamma^{\mu,\Lambda}_{i_2 i_1}(s,t,-u), \tag{3.70}$$

$$\Gamma^{\mu,\Lambda}_{i_1 i_2}(s,t,u) = \Gamma^{\mu,\Lambda}_{i_1 i_2}(u,t,s), \tag{3.71}$$

$$\Gamma^{\mathrm{d},\Lambda}_{i_1 i_2}(s,t,u) = -\Gamma^{\mathrm{d},\Lambda}_{i_1 i_2}(u,t,s). \tag{3.72}$$

For Kitaev interaction,

$$\Gamma^{x,\Lambda} \neq \Gamma^{y,\Lambda} \neq \Gamma^{z,\Lambda}, \tag{3.73}$$

for XXZ interaction,

$$\Gamma^{x,\Lambda} = \Gamma^{y,\Lambda} \neq \Gamma^{z,\Lambda}, \tag{3.74}$$

and for Heisenberg interaction,

$$\Gamma^{x,\Lambda} = \Gamma^{y,\Lambda} = \Gamma^{z,\Lambda}, \tag{3.75}$$

as examples. From the above symmetry relations, all $\Gamma^{\mu,\Lambda}$ are real.
The second term in Eq. (3.66) is a pseudo-fermion density-density interaction term. Contribution from this term is generated through the RG flow and $\Gamma^{\mathrm{d},\Lambda}$ becomes finite although a density-density interaction term is absent in the pseudo-fermion Hamiltonian Eq. (3.18). This $\Gamma^{\mathrm{d},\Lambda}$ corresponds $\Gamma^{00,\Lambda}$ in parametrized vertices for general spin interaction Eq. (3.52). Furthermore spin-density interaction terms like $\Gamma^{\mu 0,\Lambda}$ and $\Gamma^{0\nu,\Lambda}$ become finite if the Hamiltonian has non-diagonal spin interactions.

Initial Condition

Now we parametrized all functions in the flow equations. Finally, we refer to the initial condition. We rewrite the general pseudo-fermion Hamiltonian Eq. (3.18) as

$$\mathcal{H} = \frac{1}{4} \sum_{\substack{i_1,i_2 \\ i_1',i_2'}} \sum_{\substack{\alpha_1,\alpha_2 \\ \alpha_1',\alpha_2'}} \sum_{\mu,\nu} \frac{J^{\mu\nu}_{i_1 i_2}}{4} \left(\sigma^{\mu}_{\alpha_1',\alpha_1} \sigma^{\nu}_{\alpha_2',\alpha_2} \delta_{i_1',i_1} \delta_{i_2',i_2} - \sigma^{\mu}_{\alpha_2',\alpha_1} \sigma^{\nu}_{\alpha_1',\alpha_2} \delta_{i_2',i_1} \delta_{i_1',i_2} \right) f^{\dagger}_{i_1'\alpha_1'} f^{\dagger}_{i_2'\alpha_2'} f_{i_2\alpha_2} f_{i_1\alpha_1}. \tag{3.76}$$

The corresponding pseudo-fermion action is

$$\mathcal{S}[\overline{\psi},\psi] = \mathcal{S}_0[\overline{\psi},\psi] + \mathcal{S}_{\text{int}}[\overline{\psi},\psi], \tag{3.77}$$

with

$$\mathcal{S}_0[\overline{\psi},\psi] = \int \frac{\mathrm{d}\omega_1'}{2\pi}\frac{\mathrm{d}\omega_1}{2\pi}\sum_{i_1',i_1}\sum_{\alpha_1',\alpha}\overline{\psi}_{i_1'\alpha_1'}(\omega_1')\left[-\mathrm{i}\omega_1\right]\psi_{i_1\alpha_1}(\omega_1)\times 2\pi\delta_{i_1',i_1}\delta_{\alpha_1',\alpha_1}\delta(\omega_1'-\omega_1), \tag{3.78}$$

and

$$\begin{aligned}\mathcal{S}_{\text{int}}[\overline{\psi},\psi] = \frac{1}{4}\int \frac{\mathrm{d}\omega_1'}{2\pi}\frac{\mathrm{d}\omega_2'}{2\pi}\frac{\mathrm{d}\omega_1}{2\pi}\frac{\mathrm{d}\omega_2}{2\pi}\sum_{\substack{i_1',i_2'\\ i_1,i_2}}\sum_{\substack{\alpha_1',\alpha_2'\\ \alpha_1,\alpha_2}}\sum_{\mu,\nu}\frac{J^{\mu\nu}_{i_1i_2}}{4}\Big(\sigma^{\mu}_{\alpha_1',\alpha_1}\sigma^{\nu}_{\alpha_2',\alpha_2}\delta_{i_1',i_1}\delta_{i_2',i_2}-\sigma^{\mu}_{\alpha_2',\alpha_1}\sigma^{\nu}_{\alpha_1',\alpha_2}\delta_{i_2',i_1}\delta_{i_1',i_2}\Big)\\ \times\overline{\psi}_{i_1'\alpha_1'}(\omega_1')\overline{\psi}_{i_2'\alpha_2'}(\omega_2')\psi_{i_2\alpha_2}(\omega_2)\psi_{i_1\alpha_1}(\omega_1)\times 2\pi\delta(\omega_1'+\omega_2'-\omega_1-\omega_2).\end{aligned} \tag{3.79}$$

Therefore, the initial conditions for the self-energy and vertices in Eq. (3.52) of the PFFRG flow equations are

$$\gamma^{\Lambda_{\text{UV}}}(\omega) = 0, \tag{3.80}$$

$$\Gamma^{\mu\nu,\Lambda_{\text{UV}}}_{i_1i_2}(s,t,u) = \frac{J^{\mu\nu}_{i_1i_2}}{4}, \tag{3.81}$$

$$\Gamma^{\mu 0,\Lambda_{\text{UV}}}_{i_1i_2}(s,t,u) = \Gamma^{0\nu,\Lambda_{\text{UV}}}_{i_1i_2}(s,t,u) = 0, \tag{3.82}$$

$$\Gamma^{00,\Lambda_{\text{UV}}}_{i_1i_2}(s,t,u) = 0. \tag{3.83}$$

It is obvious that the self-energy and pseudo-fermion spin-density and density-density interaction terms are zero in the initial pseudo-fermion action. If there is only diagonal interactions, the initial conditions for the functions parametrized in Eq. (3.66) are flow equations are

$$\gamma^{\Lambda_{\text{UV}}}(\omega) = 0, \tag{3.84}$$

$$\Gamma^{\mu,\Lambda_{\text{UV}}}_{i_1i_2}(s,t,u) = \frac{J^{\mu\mu}_{i_1i_2}}{4}, \tag{3.85}$$

$$\Gamma^{\text{d},\Lambda_{\text{UV}}}_{i_1i_2}(s,t,u) = 0. \tag{3.86}$$

Although the vertex functions have no frequency dependence at the beginning of the RG flow, the frequency dependence of vertices is generated along the flow.

3.4 Explicit Flow Equations

We apply the parametrization introduced in the previous section Eq. (3.66) to the flow equations Eq. (3.47) and Eq. (3.48). Then we perform summations with respect to spin indices and frequency integration in order to derive the flow equations for fully parametrized vertices. Here we show the obtained flow equations explicitly.

In the self-energy flow Eq. (3.47), the integration with respect to (Matsubara) frequency ω' can be done analytically thanks to sharp frequency cutoff:

$$\begin{aligned}\int \mathrm{d}\omega'\, S^{\Lambda}(\omega')\Big[\cdots\Big] &= -\int \mathrm{d}\omega'\, \frac{\delta(|\omega'|-\Lambda)}{\mathrm{i}\omega' + \mathrm{i}\gamma^{\Lambda}(\omega')}\Big[\cdots\Big] \\ &= \mathrm{i}\sum_{\omega'=\pm\Lambda} \frac{1}{\omega' + \gamma^{\Lambda}(\omega')}\Big[\cdots\Big]. \end{aligned} \tag{3.87}$$

An explicit form of flow equation for self-energy (pseudo-fermion damping) is

$$\begin{aligned}\frac{\mathrm{d}}{\mathrm{d}\Lambda}\gamma^{\Lambda}(\omega) = \frac{1}{2\pi}\frac{1}{\Lambda+\gamma^{\Lambda}(\Lambda)}\Bigg[&-2\sum_{j}\Big\{\Gamma^{\mathrm{d},\Lambda}_{i_1 j}(\omega+\Lambda,0,\omega-\Lambda) - \Gamma^{\mathrm{d},\Lambda}_{i_1 j}(\omega-\Lambda,0,\omega+\Lambda)\Big\} \\ &+\sum_{\mu}\Big\{\Gamma^{\mu,\Lambda}_{i_1 i_1}(\omega+\Lambda,\omega-\Lambda,0) - \Gamma^{\mu,\Lambda}_{i_1 i_1}(\omega-\Lambda,\omega+\Lambda,0)\Big\} \\ &+\Gamma^{\mathrm{d},\Lambda}_{i_1 i_1}(\omega+\Lambda,\omega-\Lambda,0) - \Gamma^{\mathrm{d},\Lambda}_{i_1 i_1}(\omega-\Lambda,\omega+\Lambda,0)\Bigg]. \end{aligned} \tag{3.88}$$

For isotropic ($J_x = J_y = J_z$) Kitaev(-Heisenberg) model

$$\Gamma^{x,\Lambda}_{i_1 i_1} = \Gamma^{y,\Lambda}_{i_1 i_1} = \Gamma^{z,\Lambda}_{i_1 i_1}, \tag{3.89}$$

due to simultaneous lattice and spin $3\pi/2$ rotation. Hence we can simplify Eq. (3.88) as

$$\begin{aligned}\frac{\mathrm{d}}{\mathrm{d}\Lambda}\gamma^{\Lambda}(\omega) = \frac{1}{2\pi}\frac{1}{\Lambda+\gamma^{\Lambda}(\Lambda)}\Bigg[&-2\sum_{j}\Big\{\Gamma^{\mathrm{d},\Lambda}_{i_1 j}(\omega+\Lambda,0,\omega-\Lambda) - \Gamma^{\mathrm{d},\Lambda}_{i_1 j}(\omega-\Lambda,0,\omega+\Lambda)\Big\} \\ &+3\Big\{\Gamma^{z,\Lambda}_{i_1 i_1}(\omega+\Lambda,\omega-\Lambda,0) - \Gamma^{z,\Lambda}_{i_1 i_1}(\omega-\Lambda,\omega+\Lambda,0)\Big\} \\ &+\Gamma^{\mathrm{d},\Lambda}_{i_1 i_1}(\omega+\Lambda,\omega-\Lambda,0) - \Gamma^{\mathrm{d},\Lambda}_{i_1 i_1}(\omega-\Lambda,\omega+\Lambda,0)\Bigg]. \end{aligned} \tag{3.90}$$

Each term in RHS of the vertex flow Eq. (3.48) has two frequency integrals. We can carry out one of two frequency integrations analytically on account of these delta functions. Therefore, only one frequency integral is left in each explicit flow equations for vertices. Explicit formulae of flow equations for $\Gamma^{x,\Lambda}$, $\Gamma^{y,\Lambda}$, $\Gamma^{z,\Lambda}$, and $\Gamma^{\mathrm{d},\Lambda}$ are shown below:

$$\begin{aligned}\frac{\mathrm{d}}{\mathrm{d}\Lambda}\Gamma^{z,\Lambda}_{i_1 i_2}(s,t,u) = \int_{-\infty}^{\infty}\frac{\mathrm{d}\omega'}{2\pi}\Bigg[&L^{\Lambda}(\omega',\omega'+s)\tilde{\mathcal{T}}^{z,\Lambda}_{\mathrm{PP}}(s,t,u;\omega') \\ &+L^{\Lambda}(\omega',\omega'+t)\tilde{\mathcal{T}}^{z,\Lambda}_{\mathrm{PH,d}}(s,t,u;\omega') \\ &+L^{\Lambda}(\omega',\omega'+u)\tilde{\mathcal{T}}^{z,\Lambda}_{\mathrm{PH,cr}}(s,t,u;\omega')\Bigg], \end{aligned} \tag{3.91}$$

with

$$\begin{aligned}\tilde{\mathcal{T}}^{z,\Lambda}_{\mathrm{PP}}(s,t,u;\omega') =& -\Gamma^{x,\Lambda}_{i_1 i_2}(s,-\omega_2'-\omega',\omega_1'+\omega')\Gamma^{y,\Lambda}_{i_1 i_2}(s,\omega_2+\omega',\omega_1+\omega')\\ &-\Gamma^{y,\Lambda}_{i_1 i_2}(s,-\omega_2'-\omega',\omega_1'+\omega')\Gamma^{x,\Lambda}_{i_1 i_2}(s,\omega_2+\omega',\omega_1+\omega')\\ &+\Gamma^{z,\Lambda}_{i_1 i_2}(s,-\omega_2'-\omega',\omega_1'+\omega')\Gamma^{\mathrm{d},\Lambda}_{i_1 i_2}(s,\omega_2+\omega',\omega_1+\omega')\\ &+\Gamma^{\mathrm{d},\Lambda}_{i_1 i_2}(s,-\omega_2'-\omega',\omega_1'+\omega')\Gamma^{z,\Lambda}_{i_1 i_2}(s,\omega_2+\omega',\omega_1+\omega'),\end{aligned} \tag{3.92}$$

$$\begin{aligned}\tilde{\mathcal{T}}^{z,\Lambda}_{\mathrm{PH,d}}(s,t,u;\omega') =& 2\sum_j \Gamma^{z,\Lambda}_{i_1 j}(\omega_1'+\omega',t,\omega_1-\omega')\Gamma^{z,\Lambda}_{j i_2}(\omega_2+\omega',t,-\omega_2'+\omega')\\ &+\Gamma^{z,\Lambda}_{i_1 i_2}(\omega_1'+\omega',t,\omega_1-\omega')\Gamma^{x,\Lambda}_{i_2 i_2}(\omega_2+\omega',-\omega_2'+\omega',t)\\ &+\Gamma^{z,\Lambda}_{i_1 i_2}(\omega_1'+\omega',t,\omega_1-\omega')\Gamma^{y,\Lambda}_{i_2 i_2}(\omega_2+\omega',-\omega_2'+\omega',t)\\ &-\Gamma^{z,\Lambda}_{i_1 i_2}(\omega_1'+\omega',t,\omega_1-\omega')\Gamma^{z,\Lambda}_{i_2 i_2}(\omega_2+\omega',-\omega_2'+\omega',t)\\ &-\Gamma^{z,\Lambda}_{i_1 i_2}(\omega_1'+\omega',t,\omega_1-\omega')\Gamma^{\mathrm{d},\Lambda}_{i_2 i_2}(\omega_2+\omega',-\omega_2'+\omega',t)\\ &+\Gamma^{x,\Lambda}_{i_1 i_1}(\omega_1'+\omega',\omega_1-\omega',t)\Gamma^{z,\Lambda}_{i_1 i_2}(\omega_2+\omega',t,-\omega_2'+\omega')\\ &+\Gamma^{y,\Lambda}_{i_1 i_1}(\omega_1'+\omega',\omega_1-\omega',t)\Gamma^{z,\Lambda}_{i_1 i_2}(\omega_2+\omega',t,-\omega_2'+\omega')\\ &-\Gamma^{z,\Lambda}_{i_1 i_1}(\omega_1'+\omega',\omega_1-\omega',t)\Gamma^{z,\Lambda}_{i_1 i_2}(\omega_2+\omega',t,-\omega_2'+\omega')\\ &-\Gamma^{\mathrm{d},\Lambda}_{i_1 i_1}(\omega_1'+\omega',\omega_1-\omega',t)\Gamma^{z,\Lambda}_{i_1 i_2}(\omega_2+\omega',t,-\omega_2'+\omega'),\end{aligned} \tag{3.93}$$

$$\begin{aligned}\tilde{\mathcal{T}}^{z,\Lambda}_{\mathrm{PH,cr}}(s,t,u;\omega') =& -\Gamma^{x,\Lambda}_{i_1 i_2}(\omega_2'-\omega',-\omega_1-\omega',u)\Gamma^{y,\Lambda}_{i_1 i_2}(\omega_2-\omega',\omega_1'+\omega',u)\\ &-\Gamma^{y,\Lambda}_{i_1 i_2}(\omega_2'-\omega',-\omega_1-\omega',u)\Gamma^{x,\Lambda}_{i_1 i_2}(\omega_2-\omega',\omega_1'+\omega',u)\\ &-\Gamma^{z,\Lambda}_{i_1 i_2}(\omega_2'-\omega',-\omega_1-\omega',u)\Gamma^{\mathrm{d},\Lambda}_{i_1 i_2}(\omega_2-\omega',\omega_1'+\omega',u)\\ &-\Gamma^{\mathrm{d},\Lambda}_{i_1 i_2}(\omega_2'-\omega',-\omega_1-\omega',u)\Gamma^{z,\Lambda}_{i_1 i_2}(\omega_2-\omega',\omega_1'+\omega',u),\end{aligned} \tag{3.94}$$

and

$$L^{\Lambda}(\omega',\omega'') = G^{\Lambda}(\omega')S^{\Lambda}(\omega'') + S^{\Lambda}(\omega')G^{\Lambda}(\omega''). \tag{3.95}$$

Here we show only $\Gamma^{z,\Lambda}$ flow equation. In the case of $\Gamma^{x,\Lambda}$ and $\Gamma^{y,\Lambda}$, we can obtain their flow equations by cyclic permutation of spin component suffixes $x \to y \to z \to x$ on both sides of the above explicit formulae.
The explicit formula of the flow equation for $\Gamma^{\mathrm{d},\Lambda}$ is

$$\begin{aligned}\frac{\mathrm{d}}{\mathrm{d}\Lambda}\Gamma^{\mathrm{d},\Lambda}_{i_1 i_2}(s,t,u) = \int_{-\infty}^{\infty}\frac{\mathrm{d}\omega'}{2\pi}\Big[& L^{\Lambda}(\omega',\omega'+s)\tilde{\mathcal{T}}^{\mathrm{d},\Lambda}_{\mathrm{PP}}(s,t,u;\omega')\\ &+ L^{\Lambda}(\omega',\omega'+t)\tilde{\mathcal{T}}^{\mathrm{d},\Lambda}_{\mathrm{PH,d}}(s,t,u;\omega')\\ &+ L^{\Lambda}(\omega',\omega'+u)\tilde{\mathcal{T}}^{\mathrm{d},\Lambda}_{\mathrm{PH,cr}}(s,t,u;\omega')\Big],\end{aligned} \tag{3.96}$$

with

$$\begin{aligned}\tilde{\mathcal{T}}^{\mathrm{d},\Lambda}_{\mathrm{PP}}(s,t,u;\omega') =&\Gamma^{x,\Lambda}_{i_1i_2}(s,-\omega_2'-\omega',\omega_1'+\omega')\Gamma^{x,\Lambda}_{i_1i_2}(s,\omega_2+\omega',\omega_1+\omega')\\&+\Gamma^{y,\Lambda}_{i_1i_2}(s,-\omega_2'-\omega',\omega_1'+\omega')\Gamma^{y,\Lambda}_{i_1i_2}(s,\omega_2+\omega',\omega_1+\omega')\\&+\Gamma^{z,\Lambda}_{i_1i_2}(s,-\omega_2'-\omega',\omega_1'+\omega')\Gamma^{z,\Lambda}_{i_1i_2}(s,\omega_2+\omega',\omega_1+\omega')\\&+\Gamma^{\mathrm{d},\Lambda}_{i_1i_2}(s,-\omega_2'-\omega',\omega_1'+\omega')\Gamma^{\mathrm{d},\Lambda}_{i_1i_2}(s,\omega_2+\omega',\omega_1+\omega'),\end{aligned}\tag{3.97}$$

$$\begin{aligned}\tilde{\mathcal{T}}^{\mathrm{d},\Lambda}_{\mathrm{PH,d}}(s,t,u;\omega') =&2\sum_j\Gamma^{\mathrm{d},\Lambda}_{i_1j}(\omega_1'+\omega',t,\omega_1-\omega')\Gamma^{\mathrm{d},\Lambda}_{ji_2}(\omega_2+\omega',t,-\omega_2'+\omega')\\&-\Gamma^{\mathrm{d},\Lambda}_{i_1i_2}(\omega_1'+\omega',t,\omega_1-\omega')\Gamma^{x,\Lambda}_{i_2i_2}(\omega_2+\omega',-\omega_2'+\omega',t)\\&-\Gamma^{\mathrm{d},\Lambda}_{i_1i_2}(\omega_1'+\omega',t,\omega_1-\omega')\Gamma^{y,\Lambda}_{i_2i_2}(\omega_2+\omega',-\omega_2'+\omega',t)\\&-\Gamma^{\mathrm{d},\Lambda}_{i_1i_2}(\omega_1'+\omega',t,\omega_1-\omega')\Gamma^{z,\Lambda}_{i_2i_2}(\omega_2+\omega',-\omega_2'+\omega',t)\\&-\Gamma^{\mathrm{d},\Lambda}_{i_1i_2}(\omega_1'+\omega',t,\omega_1-\omega')\Gamma^{\mathrm{d},\Lambda}_{i_2i_2}(\omega_2+\omega',-\omega_2'+\omega',t)\\&-\Gamma^{x,\Lambda}_{i_1i_1}(\omega_1'+\omega',\omega_1-\omega',t)\Gamma^{\mathrm{d},\Lambda}_{i_1i_2}(\omega_2+\omega',t,-\omega_2'+\omega')\\&-\Gamma^{y,\Lambda}_{i_1i_1}(\omega_1'+\omega',\omega_1-\omega',t)\Gamma^{\mathrm{d},\Lambda}_{i_1i_2}(\omega_2+\omega',t,-\omega_2'+\omega')\\&-\Gamma^{z,\Lambda}_{i_1i_1}(\omega_1'+\omega',\omega_1-\omega',t)\Gamma^{\mathrm{d},\Lambda}_{i_1i_2}(\omega_2+\omega',t,-\omega_2'+\omega')\\&-\Gamma^{\mathrm{d},\Lambda}_{i_1i_1}(\omega_1'+\omega',\omega_1-\omega',t)\Gamma^{\mathrm{d},\Lambda}_{i_1i_2}(\omega_2+\omega',t,-\omega_2'+\omega'),\end{aligned}\tag{3.98}$$

and

$$\begin{aligned}\tilde{\mathcal{T}}^{\mathrm{d},\Lambda}_{\mathrm{PH,cr}}(s,t,u;\omega') =&-\Gamma^{x,\Lambda}_{i_1i_2}(\omega_2'-\omega',-\omega_1-\omega',u)\Gamma^{x,\Lambda}_{i_1i_2}(\omega_2-\omega',\omega_1'+\omega',u)\\&-\Gamma^{y,\Lambda}_{i_1i_2}(\omega_2'-\omega',-\omega_1-\omega',u)\Gamma^{y,\Lambda}_{i_1i_2}(\omega_2-\omega',\omega_1'+\omega',u)\\&-\Gamma^{z,\Lambda}_{i_1i_2}(\omega_2'-\omega',-\omega_1-\omega',u)\Gamma^{z,\Lambda}_{i_1i_2}(\omega_2-\omega',\omega_1'+\omega',u)\\&-\Gamma^{\mathrm{d},\Lambda}_{i_1i_2}(\omega_2'-\omega',-\omega_1-\omega',u)\Gamma^{\mathrm{d},\Lambda}_{i_1i_2}(\omega_2-\omega',\omega_1'+\omega',u).\end{aligned}\tag{3.99}$$

We have to solve the differential equation for γ^Λ Eq. (3.88) and the integlo-differential equations for $\Gamma^{x,\Lambda}$, $\Gamma^{y,\Lambda}$, $\Gamma^{z,\Lambda}$, and $\Gamma^{\mathrm{d},\Lambda}$ simultaneously.

Taking Heisenberg limit (SU(2) limit) Eq. (3.75), the above equations coincide with equations for Heisenberg spin systems shown in Ref. [54]. In addition, in the case of XXZ limit Eq. (3.74), the above explicit equations reproduce the PFFRG equations for XXZ models in Ref. [100].

3.5 Correlation Functions

Even if we finish to solve the flow equations Eq. (3.47) and Eq. (3.48), we cannot get the information of original spin systems directly from vertices. Consequently, we should calculate observables of the original systems from the obtained vertices. One of the most important observables is spin susceptibility (spin-spin correlation function), and we can calculate it via Kubo formula as

$$\chi^{\mu\nu}_{ij}(\mathrm{i}\nu)=\int_0^\infty \mathrm{d}\tau\,\mathrm{e}^{\mathrm{i}\nu\tau}\langle T_\tau S^\mu_i(\tau)S^\nu_j(0)\rangle,\tag{3.100}$$

where νs as suffixes of χ and S_j are spin component suffixes but other nus represent bosonic Matsubara frequency. Note that we consider $T \to 0$ limit here, so Matsubara frequency is continuous. This is why the upper limit of the integral is infinity ($\beta = 1/T \to \infty$). If the spin susceptibility diverges, the system undergoes phase transition to magnetic phase with ordering vectors corresponding with wave vectors at which susceptibility diverges. Therefore we can investigate ordering tendency of the system by calculation of the susceptibility and it is a central information we can obtain from PFFRG. To calculate the spin susceptibility from PFFRG, we have to represent it in pseudo-fermion language. We introduced fermionic FRG scheme based on fermion path-integral in the previous chapter. Hence we derive the path-integral representation of the spin susceptibility in the pseudo-fermion field theory and then rewrite it using vertices obtained PFFRG calculation.

Although we do not embark on, recently another way to utilize vertices calculated by PFFRG was proposed by Hering *et al*. By replacing the interaction and Green's function in the self-consistent equation in the pseudo-fermion mean-field theory of the quantum spin liquid with those calculated by PFFRG, we can obtain the spinon band dispersion that incorporates the effect beyond the mean-field theory [124].

Path-Integral Representation of the Spin Susceptibility

Consider a general pseudo-fermion action $\mathcal{S}[\overline{\psi}, \psi]$. As defined in the previous chapter, the (grand) partition function is obtained by

$$\mathcal{Z} = \int \mathcal{D}\overline{\psi}\mathcal{D}\psi \, \mathrm{e}^{-\mathcal{S}[\overline{\psi},\psi]}, \tag{3.101}$$

and free energy (thermodynamic potential) is given by

$$\mathcal{F} = -\frac{1}{\beta} \ln \mathcal{Z}. \tag{3.102}$$

Here we do not take the zero temperature limit explicitly for consistency with the formulae in the previous section. In addition, because formulae shown here hold at arbitrary temperature.
Now we introduce a spin-conjugate field $\boldsymbol{h}$ as

$$\mathcal{Z}[\boldsymbol{h}] = \int \mathcal{D}\overline{\psi}\mathcal{D}\psi \, \mathrm{e}^{-\mathcal{S}[\overline{\psi},\psi]-(\boldsymbol{h},\boldsymbol{S})}, \tag{3.103}$$

and

$$\mathcal{F}[\boldsymbol{h}] = -\frac{1}{\beta} \ln \mathcal{Z}[\boldsymbol{h}]. \tag{3.104}$$

$\mathcal{Z}[\boldsymbol{h}]$ and $\mathcal{F}[\boldsymbol{h}]$ are partition function and free energy of the system with source field $\boldsymbol{h}$, respectively. The above $\boldsymbol{S}$ represents the pseudo-fermion spins. This source field $\boldsymbol{h}$ corresponds "magnetic field": in the electron systems Zeeman term is

$$\mathcal{H}_{\text{Zeeman}} = -g\mu_{\text{B}} \sum_i \boldsymbol{S}_i \cdot \boldsymbol{H}_i, \tag{3.105}$$

where g, μ_{B}, $\boldsymbol{S}_i$, and $\boldsymbol{H}_i$ are electron g-factor, Bohr magneton, electron spin on the site i, and magnetic field at the site i, respectively. Note that the minus sign is from negative electric charge of the electrons. We consider the field derivative of the free

energy

$$
\begin{aligned}
-\beta\frac{\delta\mathcal{F}[\boldsymbol{h}]}{\delta h^{\mu}(x)} &= \frac{\delta \ln \mathcal{Z}[\boldsymbol{h}]}{\delta h^{\mu}(x)} \\
&= \frac{1}{\mathcal{Z}[\boldsymbol{h}]}\frac{\delta \mathcal{Z}[\boldsymbol{h}]}{\delta h^{\mu}(x)}, \qquad (3.106)\\
-\beta\frac{\delta^2\mathcal{F}[\boldsymbol{h}]}{\delta h^{\mu}(x)\delta h^{\nu}(x')} &= \frac{\delta^2 \ln \mathcal{Z}[\boldsymbol{h}]}{\delta h^{\mu}(x)\delta h^{\nu}(x')} \\
&= \frac{1}{\mathcal{Z}[\boldsymbol{h}]}\frac{\delta^2 \mathcal{Z}[\boldsymbol{h}]}{\delta h^{\mu}(x)\delta h^{\nu}(x')} - \frac{1}{\mathcal{Z}[\boldsymbol{h}]}\frac{\delta \mathcal{Z}[\boldsymbol{h}]}{\delta h^{\mu}(x)}\frac{1}{\mathcal{Z}[\boldsymbol{h}]}\frac{\delta \mathcal{Z}[\boldsymbol{h}]}{\delta h^{\nu}(x')}. \qquad (3.107)
\end{aligned}
$$

From this, we can define spin susceptibility by functional derivative [74]:

$$
\begin{aligned}
\chi^{\mu\nu}(x,x') &= -\beta\frac{\delta^2\mathcal{F}[\boldsymbol{h}]}{\delta h^{\mu}(x)\delta h^{\nu}(x')}\bigg|_{\boldsymbol{h}=0} \\
&= \frac{\delta^2 \ln \mathcal{Z}[\boldsymbol{h}]}{\delta h^{\mu}(x)\delta h^{\nu}(x')}\bigg|_{\boldsymbol{h}=0} \\
&= \frac{1}{\mathcal{Z}[\boldsymbol{h}]}\frac{\delta^2 \mathcal{Z}[\boldsymbol{h}]}{\delta h^{\mu}(x)\delta h^{\nu}(x')}\bigg|_{\boldsymbol{h}=0} - \frac{1}{\mathcal{Z}[\boldsymbol{h}]}\frac{\delta \mathcal{Z}[\boldsymbol{h}]}{\delta h^{\mu}(x)}\frac{1}{\mathcal{Z}[\boldsymbol{h}]}\frac{\delta \mathcal{Z}[\boldsymbol{h}]}{\delta h^{\nu}(x')}\bigg|_{\boldsymbol{h}=0} \\
&= \langle S^{\mu}(x)S^{\nu}(x')\rangle - \langle S^{\mu}(x)\rangle\langle S^{\nu}(x')\rangle. \qquad (3.108)
\end{aligned}
$$

We only consider the states which have no magnetization i.e. $\langle S^{\mu}\rangle = 0$, and that $x = (\tau, i)$ represents imaginary time and site index, so

$$
\chi^{\mu\nu}_{ij}(\tau_1,\tau_2) = \langle S^{\mu}_i(\tau_1)S^{\nu}_j(\tau_2)\rangle. \qquad (3.109)
$$

This is a path-integral derivation of the pseudo-fermion spin susceptibility.

Rewrite of the Susceptibility by Vertices

For further discussion we have to represent the susceptibility by the Grassmann variables corresponding to the creation and annihilation operators of pseudo-fermions explicitly. Substituting the Grassmann variable counterpart of Eq. (3.14)

$$
S^{\mu}_i = \frac{1}{2}\sum_{\alpha',\alpha} f^{\dagger}_{i\alpha'}\sigma^{\mu}_{\alpha',\alpha}f_{i\alpha} \;\rightarrow\; S^{\mu}_i(\tau) = \frac{1}{2}\sum_{\alpha',\alpha}\overline{\psi}_{i\alpha'}(\tau)\sigma^{\mu}_{\alpha',\alpha}\psi_{i\alpha}(\tau), \qquad (3.110)
$$

the susceptibility Eq. (3.109) can be expressed by the pseudo-fermion 2-particle Green's function:

$$
\begin{aligned}
\chi^{\mu\nu}_{ij}(\tau_1,\tau_2) &= \langle S^{\mu}_i(\tau_1)S^{\nu}_j(\tau_2)\rangle \\
&= \frac{1}{4}\sum_{\substack{\alpha_1,\alpha_2\\ \alpha_1',\alpha_2'}}\langle \overline{\psi}_{i\alpha_1'}(\tau_1)\sigma^{\mu}_{\alpha_1',\alpha_1}\psi_{i\alpha_1}(\tau_1)\overline{\psi}_{j\alpha_2'}(\tau_2)\sigma^{\nu}_{\alpha_2',\alpha_2}\psi_{j\alpha_2}(\tau_2)\rangle \\
&= \frac{1}{4}\sum_{\substack{\alpha_1,\alpha_2\\ \alpha_1',\alpha_2'}}\langle \psi_{i\alpha_1}(\tau_1)\psi_{j\alpha_2}(\tau_2)\overline{\psi}_{j\alpha_2'}(\tau_2)\overline{\psi}_{i\alpha_1'}(\tau_1)\rangle\sigma^{\mu}_{\alpha_1',\alpha_1}\sigma^{\nu}_{\alpha_2',\alpha_2} \\
&= -\frac{1}{4}\sum_{\substack{\alpha_1,\alpha_2\\ \alpha_1',\alpha_2'}} G^{(4)}(\tau_1 i\alpha_1,\tau_2 j\alpha_2;\tau_1 i\alpha_1',\tau_2 j\alpha_2')\sigma^{\mu}_{\alpha_1',\alpha_1}\sigma^{\nu}_{\alpha_2',\alpha_2}. \qquad (3.111)
\end{aligned}
$$

We can decompose the 2-particle Green's function by the relation

$$G^{(4)}(x_1,x_2;x_1',x_2') = -G(x_1,x_1')G(x_2,x_2') + G(x_1,x_2')G(x_2,x_1') + G_{\mathrm{c}}^{(4)}(x_1,x_2;x_1',x_2'), \tag{3.112}$$

and the 2-particle connected Green's function is obtained from the 2-particle vertex function by the relation Eq. (2.56). As a result, we can write 2-particle Green's function only by 1-particle Green's function and 2-particle 1PI vertex function

$$\begin{aligned} G^{(4)}(x_1,x_2;x_1',x_2') = &-G(x_1,x_1')G(x_2,x_2') + G(x_1,x_2')G(x_2,x_1') \\ &+ \sum_{\substack{y_1,y_2\\ y_1',y_2'}} G(x_1,y_1')G(x_2,y_2')\Gamma^{(4)}(y_1',y_2';y_1,y_2)G(y_2,x_2')G(y_1,x_1'). \end{aligned} \tag{3.113}$$

Therefore,

$$\begin{aligned} &-G^{(4)}(\tau_1 i\alpha_1,\tau_2 j\alpha_2;\tau_1 i\alpha_1',\tau_2 j\alpha_2') \\ &= G(\tau_1 i\alpha_1,\tau_1 i\alpha_1')G(\tau_2 j\alpha_2,\tau_2 j\alpha_2') - G(\tau_1 i\alpha_1,\tau_2 j\alpha_2')G(\tau_2 j\alpha_2,\tau_1 i\alpha_1') \\ &\quad - \sum_{\substack{\beta_1,\beta_2\\ \beta_1',\beta_2'}}\sum_{\substack{i_1,i_2\\ i_1',i_2'}}\int_0^\beta \mathrm{d}\tau_3\mathrm{d}\tau_3'\mathrm{d}\tau_4\mathrm{d}\tau_4'\, G(\tau_1 i\alpha_1,\tau_3 i_1\beta_1)G(\tau_2 j\alpha_2,\tau_4 i_2\beta_2) \\ &\qquad \times \Gamma^{(4)}(\tau_3 i_1\beta_1,\tau_4 i_2\beta_2;\tau_3' i_1'\beta_1',\tau_4' i_2'\beta_2')G(\tau_3' i_1'\beta_1',\tau_1 i\alpha_1')G(\tau_4' i_2'\beta_2',\tau_2 j\alpha_2') \\ &= G(\tau_1,\tau_1)G(\tau_2,\tau_2)\delta_{\alpha_1\alpha_1'}\delta_{\alpha_2\alpha_2'} - G(\tau_1,\tau_2)G(\tau_2,\tau_1)\delta_{ij}\delta_{\alpha_1\alpha_2'}\delta_{\alpha_2\alpha_1'} \\ &\quad - \sum_{\substack{\beta_1,\beta_2\\ \beta_1',\beta_2'}}\sum_{\substack{i_1,i_2\\ i_1',i_2'}}\int_0^\beta \mathrm{d}\tau_3\mathrm{d}\tau_3'\mathrm{d}\tau_4\mathrm{d}\tau_4'\, G(\tau_1,\tau_3)G(\tau_2,\tau_4)\Gamma^{(4)}(\tau_3 i_1\beta_1,\tau_4 i_2\beta_2;\tau_3' i_1'\beta_1',\tau_4' i_2'\beta_2') \\ &\qquad \times G(\tau_3',\tau_1)G(\tau_4',\tau_2)\delta_{ii_1}\delta_{ji_2}\delta_{i_1'i}\delta_{i_2'j}\delta_{\alpha_1\beta_1}\delta_{\alpha_2\beta_2}\delta_{\beta_1'\alpha_1'}\delta_{\beta_2'\alpha_2'} \\ &= G(\tau_1,\tau_1)G(\tau_2,\tau_2)\delta_{\alpha_1\alpha_1'}\delta_{\alpha_2\alpha_2'} - G(\tau_1,\tau_2)G(\tau_2,\tau_1)\delta_{ij}\delta_{\alpha_1\alpha_2'}\delta_{\alpha_2\alpha_1'} \\ &\quad - \int_0^\beta \mathrm{d}\tau_3\mathrm{d}\tau_3'\mathrm{d}\tau_4\mathrm{d}\tau_4'\, G(\tau_1,\tau_3)G(\tau_2,\tau_4)\Gamma^{(4)}(\tau_3 i\alpha_1,\tau_4 j\alpha_2;\tau_3' i\alpha_1',\tau_4 j\alpha_2')G(\tau_3',\tau_1)G(\tau_4',\tau_2). \end{aligned} \tag{3.114}$$

We used Eq. (3.29) above. Substituting this into susceptibility formula and summing over spin indices, we obtain

$$
\begin{aligned}
&\chi_{ij}^{\mu\nu}(\tau_1,\tau_2) \\
&\quad= -\frac{1}{4}\sum_{\substack{\alpha_1,\alpha_2\\ \alpha_1',\alpha_2'}} G^{(4)}(\tau_1 i\alpha_1,\tau_2 j\alpha_2;\tau_1 i\alpha_1',\tau_2 j\alpha_2')\sigma^{\mu}_{\alpha_1'\alpha_1}\sigma^{\nu}_{\alpha_2'\alpha_2} \\
&\quad= \frac{1}{4}G(\tau_1,\tau_1)G(\tau_2,\tau_2)\underbrace{\sum_{\substack{\alpha_1,\alpha_2\\ \alpha_1',\alpha_2'}}\delta_{\alpha_1\alpha_1'}\delta_{\alpha_2\alpha_2'}\sigma^{\mu}_{\alpha_1'\alpha_1}\sigma^{\nu}_{\alpha_2'\alpha_2}}_{\sum_{\alpha_1,\alpha_2}\sigma^{\mu}_{\alpha_1\alpha_1}\sigma^{\nu}_{\alpha_2\alpha_2}=\mathrm{tr}[\sigma^{\mu}]\mathrm{tr}[\sigma^{\nu}]=0\ \text{(traceless)}} \\
&\qquad -\frac{1}{4}G(\tau_1,\tau_2)G(\tau_2,\tau_1)\underbrace{\sum_{\substack{\alpha_1,\alpha_2\\ \alpha_1',\alpha_2'}}\delta_{\alpha_1\alpha_2'}\delta_{\alpha_2\alpha_1'}\sigma^{\mu}_{\alpha_1'\alpha_1}\sigma^{\nu}_{\alpha_2'\alpha_2}}_{\sum_{\alpha_1,\alpha_2}\sigma^{\mu}_{\alpha_2\alpha_1}\sigma^{\nu}_{\alpha_1\alpha_2}=\mathrm{tr}(\sigma^{\mu}\sigma^{\nu})=\mathrm{tr}[\sigma^0\delta^{\mu\nu}+\mathrm{i}\sum_{\lambda=1}^{3}\epsilon^{\mu\nu\lambda}\sigma^{\lambda}]=2\delta^{\mu\nu}}\delta_{ij} \\
&\qquad -\frac{1}{4}\sum_{\substack{\alpha_1,\alpha_2\\ \alpha_1',\alpha_2'}}\int_0^{\beta}\mathrm{d}\tau_3\mathrm{d}\tau_3'\mathrm{d}\tau_4\mathrm{d}\tau_4'\,G(\tau_1,\tau_3)G(\tau_2,\tau_4)\Gamma^{(4)}(\tau_3 i\alpha_1,\tau_4 j\alpha_2;\tau_3' i\alpha_1',\tau_4' j\alpha_2') \\
&\qquad\qquad \times G(\tau_3',\tau_1)G(\tau_4',\tau_2)\sigma^{\mu}_{\alpha_1'\alpha_1}\sigma^{\nu}_{\alpha_2'\alpha_2} \\
&\quad= -\frac{1}{2}G(\tau_1,\tau_2)G(\tau_2,\tau_1)\delta^{\mu\nu}\delta_{ij} \\
&\qquad -\frac{1}{4}\sum_{\substack{\alpha_1,\alpha_2\\ \alpha_1',\alpha_2'}}\int_0^{\beta}\mathrm{d}\tau_3\mathrm{d}\tau_3'\mathrm{d}\tau_4\mathrm{d}\tau_4'\,G(\tau_1,\tau_3)G(\tau_2,\tau_4)G(\tau_3',\tau_1)G(\tau_4',\tau_2) \\
&\qquad\qquad \times \Gamma^{(4)}(\tau_3 i\alpha_1,\tau_4 j\alpha_2;\tau_3' i\alpha_1',\tau_4' j\alpha_2')\sigma^{\mu}_{\alpha_1'\alpha_1}\sigma^{\nu}_{\alpha_2'\alpha_2}.
\end{aligned}
\tag{3.115}
$$

We formulate PFFRG in Matsubara frequency representation and calculate vertices in Matsubara frequency space. Hence we need transform the susceptibility to Frequency space. Fourier expansion of the Green's functions and the vertex function

give

$$
\begin{aligned}
&\chi^{\mu\nu}_{ij}(\tau_1,\tau_2)\\
&\quad= -\frac{1}{2}\frac{1}{\beta^4}\sum_{\substack{\omega_1,\omega_2\\ \omega_1',\omega_2'}} \mathrm{e}^{-\mathrm{i}\omega_1\tau_1+\mathrm{i}\omega_2\tau_2}\mathrm{e}^{-\mathrm{i}\omega_1'\tau_2+\mathrm{i}\omega_2'\tau_1}G(\omega_1,\omega_2)G(\omega_1',\omega_2')\delta^{\mu\nu}\delta_{ij}\\
&\quad-\frac{1}{4}\frac{1}{\beta^{12}}\int_0^\beta \mathrm{d}\tau_3\mathrm{d}\tau_3'\mathrm{d}\tau_4\mathrm{d}\tau_4' \sum_{\substack{\omega_1,\omega_2,\omega_3,\omega_4,\omega_5,\omega_6\\ \omega_1',\omega_2',\omega_3',\omega_4',\omega_5',\omega_6'}} \mathrm{e}^{-\mathrm{i}\omega_1\tau_1+\mathrm{i}\omega_1'\tau_3}\mathrm{e}^{-\mathrm{i}\omega_2\tau_2+\mathrm{i}\omega_2'\tau_4}\mathrm{e}^{-\mathrm{i}\omega_3\tau_3'+\mathrm{i}\omega_3'\tau_1}\mathrm{e}^{-\mathrm{i}\omega_4\tau_4'+\mathrm{i}\omega_4'\tau_2}\\
&\qquad\times \mathrm{e}^{-\mathrm{i}\omega_5\tau_3-\mathrm{i}\omega_6\tau_4+\mathrm{i}\omega_5'\tau_3'+\mathrm{i}\omega_6'\tau_4'}G(\omega_1,\omega_1')G(\omega_2,\omega_2')G(\omega_3,\omega_3')G(\omega_4,\omega_4')\\
&\qquad\quad\times\sum_{\substack{\alpha_1,\alpha_2\\ \alpha_1',\alpha_2'}}\Gamma^{(4)}(\omega_5 i\alpha_1,\omega_6 j\alpha_2;\omega_5' i\alpha_1',\omega_6' j\alpha_2')\sigma^{\mu}_{\alpha_1'\alpha_1}\sigma^{\nu}_{\alpha_2'\alpha_2}\\
&\quad= -\frac{1}{2}\frac{1}{\beta^2}\sum_{\omega_1,\omega_1'}\mathrm{e}^{-\mathrm{i}(\omega_1-\omega_1')\tau_1}\mathrm{e}^{-\mathrm{i}(\omega_1'-\omega_1)\tau_2}G(\omega_1)G(\omega_1')\delta^{\mu\nu}\delta_{ij}\\
&\quad-\frac{1}{4}\frac{1}{\beta^4}\sum_{\substack{\omega_1,\omega_2\\ \omega_3,\omega_4}}\mathrm{e}^{-\mathrm{i}(\omega_1-\omega_3)\tau_1}\mathrm{e}^{-\mathrm{i}(\omega_2-\omega_4)\tau_2}G(\omega_1)G(\omega_2)G(\omega_3)G(\omega_4)\\
&\qquad\quad\times\sum_{\substack{\alpha_1,\alpha_2\\ \alpha_1',\alpha_2'}}\Gamma^{(4)}(\omega_1 i\alpha_1,\omega_2 j\alpha_2;\omega_3 i\alpha_1',\omega_4 j\alpha_2')\sigma^{\mu}_{\alpha_1'\alpha_1}\sigma^{\nu}_{\alpha_2'\alpha_2}.
\end{aligned}
\tag{3.116}
$$

Remember the parametrization of the Green's function with respect to Matsubara frequency Eq. (3.29). Then we conduct the Fourier transformation of the susceptibility and parametrize the spin susceptibility with respect to Matsubara frequency arguments:

$$\chi^{\mu\nu}_{ij}(\mathrm{i}\nu,\mathrm{i}\nu') = \chi^{\mu\nu}_{ij}(\mathrm{i}\nu)\times\beta\delta(\nu+\nu'), \tag{3.117}$$

$$= \int_0^\beta \mathrm{d}\tau_1\mathrm{d}\tau_2\,\mathrm{e}^{\mathrm{i}\nu\tau_1+\mathrm{i}\nu'\tau_2}\chi^{\mu\nu}_{ij}(\tau_1,\tau_2). \tag{3.118}$$

Performing the integration of the second line, we obtain Matsubara frequency representation of the susceptibility

$$\begin{aligned}
&\int_0^\beta \mathrm{d}\tau_1 \mathrm{d}\tau_2\, \mathrm{e}^{\mathrm{i}\nu(\tau_1-\tau_2)} \chi_{ij}^{\mu\nu}(\tau_1,\tau_2) \\
&= -\frac{1}{2\beta^2} \sum_{\omega_1,\omega_1'} \underbrace{\int_0^\beta \mathrm{d}\tau_1 \mathrm{d}\tau_2\, \mathrm{e}^{-\mathrm{i}(\omega_1-\omega_1'-\nu)\tau_1} \mathrm{e}^{-\mathrm{i}(\omega_1'-\omega_1-\nu')\tau_2}}_{=\beta^2\delta(\omega_1-\omega_1'-\nu)\delta(\nu+\nu')} G(\omega_1)G(\omega_1')\delta^{\mu\nu}\delta_{ij} \\
&\quad - \frac{1}{4\beta^4} \sum_{\substack{\omega_1,\omega_2\\ \omega_3,\omega_4}} \underbrace{\int_0^\beta \mathrm{d}\tau_1 \mathrm{d}\tau_2\, \mathrm{e}^{-\mathrm{i}(\omega_1-\omega_3-\nu)\tau_1} \mathrm{e}^{-\mathrm{i}(\omega_2-\omega_4+\nu)\tau_2}}_{=\beta^2\delta(\omega_1-\omega_3-\nu)\delta(\omega_4-\omega_2+\nu')} G(\omega_1)G(\omega_2)G(\omega_3)G(\omega_4) \\
&\quad \times \sum_{\substack{\alpha_1,\alpha_2\\ \alpha_1',\alpha_2'}} \Gamma^{(4)}(\omega_1 i\alpha_1, \omega_2 j\alpha_2; \omega_3 i\alpha_1', \omega_4 j\alpha_2') \sigma^\mu_{\alpha_1'\alpha_1} \sigma^\nu_{\alpha_2'\alpha_2} \\
&= -\frac{1}{2}\sum_\omega G(\omega)G(\omega+\nu)\delta(\nu+\nu')\delta^{\mu\nu}\delta_{ij} \\
&\quad - \frac{1}{4\beta^2} \sum_{\omega,\omega'} G(\omega)G(\omega+\nu)G(\omega')G(\omega'-\nu') \\
&\qquad \times \sum_{\substack{\alpha_1,\alpha_2\\ \alpha_1',\alpha_2'}} \Gamma^{(4)}(\omega+\nu i\alpha_1, \omega' j\alpha_2; \omega i\alpha_1', \omega'-\nu' j\alpha_2') \sigma^\mu_{\alpha_1'\alpha_1} \sigma^\nu_{\alpha_2'\alpha_2}.
\end{aligned} \tag{3.119}$$

Remember that $\Gamma^{(4)}(\omega+\nu i\alpha_1, \omega' j\alpha_2; \omega i\alpha_1', \omega'-\nu' j\alpha_2') \propto \beta\delta(\omega+\nu+\omega'-\omega-\omega'+\nu') = \beta\delta(\nu+\nu')$ from the parametrization Eq. (3.52) or Eq. (3.66), we can find that both term of Eq. (3.119) are proportional to $\beta\delta(\nu+\nu')$ as well as RHS of Eq. (3.117). Thereby, we can write

$$\begin{aligned}
\chi_{ij}^{\mu\nu}(\mathrm{i}\nu) &= -\frac{1}{2\beta}\sum_\omega G(\omega)G(\omega+\nu)\delta^{\mu\nu}\delta_{ij} \\
&\quad - \frac{1}{4\beta^2} \sum_{\omega,\omega'} G(\omega)G(\omega+\nu)G(\omega')G(\omega'+\nu) \\
&\qquad \times \sum_{\substack{\alpha_1,\alpha_2\\ \alpha_1',\alpha_2'}} \tilde{\Gamma}^{(4)}(\omega+\nu i\alpha_1, \omega' j\alpha_2; \omega i\alpha_1', \omega'+\nu j\alpha_2') \sigma^\mu_{\alpha_1'\alpha_1} \sigma^\nu_{\alpha_2'\alpha_2}.
\end{aligned} \tag{3.120}$$

Here we use the relation $\nu' = -\nu$ and define $\tilde{\Gamma}^{(4)} = \Gamma^{(4)}/\beta\delta(\nu+\nu)$. Now the susceptibility is no longer dependent on ν'. Finally, we use Eq. (3.46) and take $T \to 0$ limit. Then we can conclude

$$\begin{aligned}
\chi_{ij}^{\mu\nu}(\mathrm{i}\nu) &= -\frac{1}{4\pi}\int_{-\infty}^{\infty} \mathrm{d}\omega\, G(\omega)G(\omega+\nu)\delta^{\mu\nu}\delta_{ij} \\
&\quad - \frac{1}{16\pi^2} \int_{-\infty}^{\infty} \mathrm{d}\omega \mathrm{d}\omega'\, G(\omega)G(\omega+\nu)G(\omega')G(\omega'+\nu) \\
&\qquad \times \sum_{\substack{\alpha_1,\alpha_2\\ \alpha_1',\alpha_2'}} \Big\{ \tilde{\Gamma}_{ij}(\omega+\nu\alpha_1, \omega'\alpha_2; \omega\alpha_1', \omega'+\nu\alpha_2') \\
&\qquad\qquad - \tilde{\Gamma}_{ii}(\omega'\alpha_2, \omega+\nu\alpha_1; \omega\alpha_1', \omega'+\nu\alpha_2')\delta_{ij} \Big\} \sigma^\mu_{\alpha_1'\alpha_1} \sigma^\nu_{\alpha_2'\alpha_2}.
\end{aligned} \tag{3.121}$$

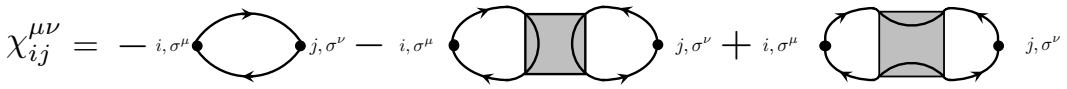

FIGURE 3.2: Diagram representing Eq. (3.121). Oriented black thick lines and gray squares correspond the Green's functions G and the vertices $\tilde{\Gamma}_{ij}$, respectively. The black dots express the Pauli matrices σ. Each connected thick line has one site index i or j.

We show a diagrammatic representation of Eq. (3.121) in Fig. (3.2).

Explicit Formula of the Susceptibility

Moreover, we show more explicit formula of the spin susceptibility for diagonal spin interactions and rewrite its integration to reduce calculation costs. Now we consider the cutoff Λ again although we have ignored it from the beginning of this section. The parametrization Eq. (3.66) for $\tilde{\Gamma}^{\Lambda}$ is

$$\tilde{\Gamma}^{\Lambda}_{i_1 i_2}(\omega_1'\alpha_1', \omega_2'\alpha_2'; \omega_1\alpha_1, \omega_2\alpha_2) = \sum_{\mu} \tilde{\Gamma}^{\mu,\Lambda}_{i_1 i_2}(s,t,u)\sigma^{\mu}_{\alpha_1',\alpha_1}\sigma^{\mu}_{\alpha_2',\alpha_2} + \tilde{\Gamma}^{\mathrm{d},\Lambda}_{i_1 i_2}(s,t,u)\delta_{\alpha_1',\alpha_1}\delta_{\alpha_2',\alpha_2}. \tag{3.122}$$

Substituting the above parametrization for diagonal interactions, which we treated in this dissertation, into Eq. (3.121) and performing the summations over spin indices, we can obtain the explicit formula $\chi^{\mu\nu} = \chi^{\mu\mu}\delta^{\mu\nu}$, with

$$\begin{aligned}
&\chi_{ij}^{\mu\mu,\Lambda}(\mathrm{i}\nu) \\
&= -\frac{1}{4\pi}\int_{-\infty}^{\infty} \mathrm{d}\omega\, G^{\Lambda}(\omega)G^{\Lambda}(\omega+\nu)\delta_{ij} \\
&\quad - \frac{1}{8\pi^2}\int_{-\infty}^{\infty} \mathrm{d}\omega\mathrm{d}\omega'\, G^{\Lambda}(\omega)G^{\Lambda}(\omega+\nu)G^{\Lambda}(\omega')G^{\Lambda}(\omega'+\nu) \\
&\qquad \times \Bigg[2\Gamma_{ij}^{\mu,\Lambda}(\omega+\omega'+\nu, \nu, \omega-\omega') \\
&\qquad\quad + \Bigg\{ -\Gamma_{ii}^{\mu,\Lambda}(\omega+\omega'+\nu, \omega-\omega', \nu) + \sum_{\nu\neq\mu}\Gamma_{ii}^{\nu,\Lambda}(\omega+\omega'+\nu, \omega-\omega', \nu) \\
&\qquad\qquad - \Gamma_{ii}^{\mathrm{d},\Lambda}(\omega+\omega'+\nu, \omega-\omega', \nu) \Bigg\}\delta_{ij} \Bigg].
\end{aligned} \tag{3.123}$$

Taking Heisenberg limit Eq. (3.75), this equation corresponds to that for the Heisenberg model in Ref. [91]. Moreover the XXZ limit Eq. (3.74) of this formula is identical to the susceptibility of the XXZ models in Ref. [100].
For isotropic Kitaev (-Heisenberg) case, we can use the relation Eq. (3.89) and the

above formula can be simplified as

$$\begin{aligned}
&\chi_{ij}^{\mu\mu,\Lambda}(\mathrm{i}\nu) \\
&= -\frac{1}{4\pi}\int_{-\infty}^{\infty} \mathrm{d}\omega\, G^{\Lambda}(\omega)G^{\Lambda}(\omega+\nu)\delta_{ij} \\
&\quad - \frac{1}{8\pi^2}\int_{-\infty}^{\infty} \mathrm{d}\omega\mathrm{d}\omega'\, G^{\Lambda}(\omega)G^{\Lambda}(\omega+\nu)G^{\Lambda}(\omega')G^{\Lambda}(\omega'+\nu) \\
&\qquad \times \Bigg[2\Gamma_{ij}^{\mu,\Lambda}(\omega+\omega'+\nu,\nu,\omega-\omega') \\
&\qquad\quad + \left\{ \Gamma_{ii}^{\mu,\Lambda}(\omega+\omega'+\nu,\omega-\omega',\nu) - \Gamma_{ii}^{\mathrm{d},\Lambda}(\omega+\omega'+\nu,\omega-\omega',\nu) \right\}\delta_{ij} \Bigg].
\end{aligned} \tag{3.124}$$

Note that all terms except Γ_{ij} in the above equation are local ($\propto \delta_{ij}$). Only Γ_{ij} term describes spacial dependence of the susceptibility.

The spin susceptibility is the main result of PFFRG. Especially, we can elucidate the full spacial structure of the static (elastic) component ($\mathrm{i}\nu = 0$) directly. Later we perform Fourier transformation of the susceptibility $\chi_{ij}(\mathrm{i}\nu) \to \chi(\boldsymbol{k},\mathrm{i}\nu)$ in order to clarify its momentum dependence. The phase transition to magnetic ordered phases can be detected by the divergence of the static susceptibility. On the other hand, we cannot obtain the dynamical (inelastic) components because our formulation is based on imaginary-time (Matsubara frequency) formulation. We have to conduct analytic continuation to obtain inelastic components of the susceptibility from $\mathrm{i}\nu \neq 0$ components. Note that the "static" susceptibility means $\chi(\boldsymbol{k}) = \chi(\boldsymbol{k},\mathrm{i}\nu = 0) = \chi^{\mathrm{R}}(\boldsymbol{k},\omega = 0)$, where ω is a real frequency and the suffix R represents retarded correlation function, although the "static" structure factor stands for $\mathcal{S}(\boldsymbol{k}) = \int_{-\infty}^{\infty}\mathrm{d}\omega\, \mathcal{S}(\boldsymbol{k},\omega)$. Former means "time-averaged" and latter "static" is identical to "equal-time" (e.g. equal-time correlation function).

Furthermore, we use the explicit form of the regularized Green's function shown in Eq. (3.41) to make susceptibility formula simpler. If we only consider the static component,

$$\begin{aligned}
&\chi_{ij}^{\mu\mu,\Lambda}(\mathrm{i}\nu = 0) \\
&= \frac{1}{2\pi}\int_{\Lambda}^{\infty} \mathrm{d}\omega \left[\frac{1}{\omega+\gamma^{\Lambda}(\omega)}\right]^2 \delta_{ij} \\
&\quad - \frac{1}{2\pi^2}\int_{\Lambda}^{\infty} \mathrm{d}\omega \int_{\Lambda}^{\omega} \mathrm{d}\omega' \left[\frac{1}{\omega+\gamma^{\Lambda}(\omega)}\right]^2 \left[\frac{1}{\omega'+\gamma^{\Lambda}(\omega')}\right]^2 \\
&\qquad \times \Bigg[4\Gamma_{ij}^{\mu,\Lambda}(\omega+\omega',0,\omega-\omega') \\
&\qquad\quad + \Bigg\{ -\Gamma_{ii}^{\mu,\Lambda}(\omega+\omega',\omega-\omega',0) - \Gamma_{ii}^{\mu,\Lambda}(\omega-\omega',\omega+\omega',0) \\
&\qquad\qquad + \sum_{\nu\neq\mu}\Gamma_{ii}^{\nu,\Lambda}(\omega+\omega',\omega-\omega',0) + \sum_{\nu\neq\mu}\Gamma_{ii}^{\nu,\Lambda}(\omega-\omega',\omega+\omega',0) \\
&\qquad\qquad - \Gamma_{ii}^{\mathrm{d},\Lambda}(\omega+\omega',\omega-\omega',0) - \Gamma_{ii}^{\mathrm{d},\Lambda}(\omega-\omega',\omega+\omega',0) \Bigg\}\delta_{ij} \Bigg].
\end{aligned} \tag{3.125}$$

Here we use the fact that $\gamma^{\Lambda}(\omega)$ is an odd function of ω and the symmetry Eq. (3.71).

In addition, we rewrite the integration symmetric about ω and ω' into the anti-symmetric one. This reduces numerical cost for integration.

Susceptibility in the Momentum Space

Finally, we obtain the susceptibility in momentum space by Fourier transformation.

In ordinary Fourier transformation for itinerant fermion systems on periodic lattices, the coordinates of underlying Bravais lattices and the position in the unit cells are considered separately. We consider all lattice sites identical in PFFRG. The fourier transformation of the susceptibility calculated by PFFRG is

$$\begin{aligned}\chi^{\mu\nu,\Lambda}(\boldsymbol{k},\mathrm{i}\nu) &= \frac{1}{N}\sum_{i,j}\mathrm{e}^{-\boldsymbol{k}\cdot(\boldsymbol{r}_i-\boldsymbol{r}_j)}\chi_{ij}^{\mu\nu,\Lambda}(\mathrm{i}\nu) \\ &= \frac{1}{N_{\mathrm{sub}}}\sum_{i\in\mathrm{u.c.}}\sum_{j}\mathrm{e}^{-\boldsymbol{k}\cdot(\boldsymbol{r}_i-\boldsymbol{r}_j)}\chi_{ij}^{\mu\nu,\Lambda}(\mathrm{i}\nu),\end{aligned} \tag{3.126}$$

where N, N_{sub}, and $\sum_{i\in\mathrm{u.c.}}$ is the number of all lattice sites, the number of sub lattices, and the summation over sites in an arbitrary unit cell in contrast to the summation over all sites $\sum_j$, respectively. For monoatomic cells $N_{\mathrm{sub}} = 1$ in which the entire lattice corresponds to the underlying Bravais lattice, the susceptibility is periodic with respect to the first Brillouin zone. For polyatomic cells $N_{\mathrm{sub}} \geq 2$, the susceptibility is no longer periodic with respect to the first Brillouin zone, but to the N_{sub}-th Brillouin zone often called extended Brillouin zone. The structure of the susceptibility within the first Brillouin zone reflects spin patterns on underlying Bravais lattice and that within the extended Brillouin zone reflects spin structures in the unit cell.
Here we parametrize the susceptibility in momentum space like in frequency space: $\chi(\boldsymbol{k},\boldsymbol{k}';\mathrm{i}\nu) = \chi(\boldsymbol{k},\mathrm{i}\nu)\times N\delta(\boldsymbol{k}+\boldsymbol{k})$. The prefactor $1/N$ in the first line of the above equation is from this parametrization.

We trace the static susceptibility $\chi^{\mu\nu,\Lambda}(\boldsymbol{k}) = \chi^{\mu\nu,\Lambda}(\boldsymbol{k},\mathrm{i}\nu = 0)$, along the RG flow and we can regard the divergence of it as signals of the onset magnetic long-range order. The momenta at which the susceptibility diverges are characterized spin patterns of the magnetic orders. The ordering scale, also called critical cutoff, Λ_{c} at which the susceptibility diverges can be interpreted as critical temperature. As we prove later, there is approximate relationship $T \simeq \frac{\pi}{2}\Lambda$. Note that the divergence of the susceptibility often appears as a breakdown of the susceptibility due to the discrete frequency mesh in numerical calculations (we now consider $T \to 0$ limit and Matsubara frequency is continuous). In contrast, signals of non-magnetic states appear as smooth continuous susceptibility flows without significant changes to the end of flows. We show these behaviors of the susceptibility in Fig. 3.3 schematically.

3.6 Truncation Schemes for PFFRG

We have introduced PFFRG scheme based on level-2 truncation flow. For investigation of order competition in electron systems, level-2 truncation or static level-2 truncation are often used [55, 65] and it has achieved some success. However, for spin systems those are not enough because frustration effect and quantum fluctuation are not sufficiently taken into account. They shorten the pseudo-fermion lifetime and affect the flow through the self-energy. We must therefore incorporate self-energy feedback into the flows beyond the level-2 truncation. A prescription

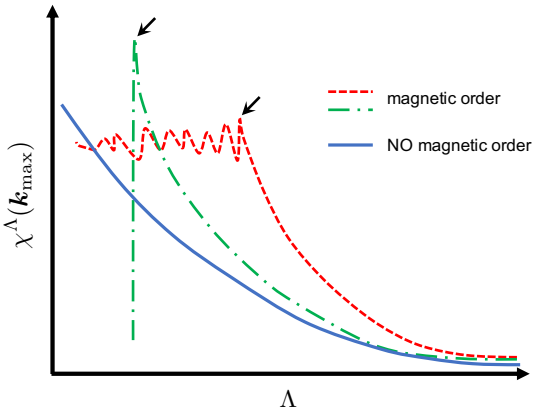

FIGURE 3.3: Schematic figure showing typical behaviors of the spin susceptibility. $\boldsymbol{k}_{\max}$ means the point in the momentum space at which the susceptibility has the maximum value. The red dashed line and green dashed dotted line indicate the phase transition to magnetic ordering phases. The small black arrows indicate the breakdown points of the flow and those signal the onset of the magnetic orders. The blue continuous line shows no breakdown. It means that there are no magnetic order.

for this is known as Katanin truncation [81], which is used in ordinary PFFRG. In this section, we review static approximation and level-2 truncation for our PFFRG equations first. Then we introduce Katanin truncation.

Static PFFRG

Static approximation is the simplest approximation we can come up with first. In this approximation we ignore the frequency dependence of the vertices:

$$\gamma^{\Lambda}(\omega) \;\to\; \gamma^{\Lambda}, \tag{3.127}$$

$$\Gamma^{\mu,\Lambda}_{i_1 i_2}(s,t,u) \;\to\; \Gamma^{\mu,\Lambda}_{i_1 i_2}, \tag{3.128}$$

$$\Gamma^{\mathrm{d},\Lambda}_{i_1 i_2}(s,t,u) \;\to\; \Gamma^{\mathrm{d},\Lambda}_{i_1 i_2}. \tag{3.129}$$

As a result, from Eq. (3.88) we can obtain the equation

$$\frac{\mathrm{d}}{\mathrm{d}\Lambda}\gamma^{\Lambda} = 0. \tag{3.130}$$

We remember that at the beginning of the flow $\gamma^{\Lambda_{\mathrm{UV}}} = 0$ in Eq. (3.84). Hence

$$\gamma^{\Lambda} = 0 \quad \text{for all} \quad \Lambda. \tag{3.131}$$

This is consistent to the fact $\gamma^{\Lambda}(\omega)$ is an odd function of ω. Then

$$\begin{aligned}\int_{-\infty}^{\infty} \mathrm{d}\omega'\, L^{\Lambda}(\omega',\omega') &= 2\int_{-\infty}^{\infty} \mathrm{d}\omega'\, G^{\Lambda}(\omega')S^{\Lambda}(\omega) \\ &= 2\int_{-\infty}^{\infty} \mathrm{d}\omega'\, \frac{\Theta(|\omega'|-\Lambda)}{\omega'}\frac{\delta(|\omega'|-\Lambda)}{\omega'} \\ &= 2\int_{-\infty}^{\infty} \mathrm{d}\omega'\, \frac{\delta(|\omega'|-\Lambda)}{\omega'^2}\int_0^1 \mathrm{d}u\, u \\ &= 2\sum_{\omega'=\pm\Lambda}\frac{1}{2\omega'^2} \\ &= \frac{2}{\Lambda^2}. \end{aligned} \tag{3.132}$$

Here we use Morris lemma Eq. (2.174) to transform into the third line. Using this relation to Eq. (3.96), we can also conclude that the density vertex $\Gamma^{\mathrm{d},\Lambda}$ is zero at any Λ. From Eq. (3.96), a frequency independent flow equation is

$$\frac{\mathrm{d}}{\mathrm{d}\Lambda}\Gamma^{\mathrm{d},\Lambda}_{i_1 i_2} = \frac{2}{\pi\Lambda^2}\left[\sum_j \Gamma^{\mathrm{d},\Lambda}_{i_1 j}\Gamma^{\mathrm{d},\Lambda}_{j i_2} - \Gamma^{\mathrm{d},\Lambda}_{i_1 i_2}\Big(\sum_{\mu}\Gamma^{\mu,\Lambda}_{i_1 i_1} + \Gamma^{\mathrm{d},\Lambda}_{i_1 i_1}\Big)\right]. \tag{3.133}$$

Due to the initial condition in Eq. (3.86), the right-hand side of the above equation is zero. Therefore no finite contribution to $\Gamma^{\mathrm{d},\Lambda}$ is generated along the flow. Consequently,

$$\Gamma^{\mathrm{d},\Lambda}_{i_1 i_2} = 0 \quad \text{for all} \quad \Lambda. \tag{3.134}$$

Finally, we substitute the above results in Eq. (3.91) and derive the simplified equation

$$\frac{\mathrm{d}}{\mathrm{d}\Lambda}\Gamma^{z,\Lambda}_{i_1 i_2} = \frac{2}{\pi\Lambda^2}\left[\sum_j \Gamma^{z,\Lambda}_{i_1 j}\Gamma^{z,\Lambda}_{j i_2} - 2\Gamma^{x,\Lambda}_{i_1 i_2}\Gamma^{y,\Lambda}_{i_1 i_2} + \Gamma^{z,\Lambda}_{i_1 i_2}\big(\Gamma^{x,\Lambda}_{i_1 i_1} + \Gamma^{y,\Lambda}_{i_1 i_1} - \Gamma^{z,\Lambda}_{i_1 i_1}\big)\right]. \tag{3.135}$$

We only show the equation for $\Gamma^{z,\Lambda}_{i_1 i_2}$ and counterparts for $\Gamma^{x,\Lambda}_{i_1 i_2}$ and $\Gamma^{y,\Lambda}_{i_1 i_2}$ can be obtained by cyclic permutation $x \to y \to z \to x$. We have to solve only these equations.

In addition, we simplify the formula of the susceptibility Eq. (3.125) as

$$\chi^{\mu\mu,\Lambda}_{ij} = \frac{1}{2\pi\Lambda}\delta_{ij} - \frac{1}{2\pi^2\Lambda^2}\left[2\Gamma^{\mu,\Lambda}_{ij} + \big(-\Gamma^{\mu,\Lambda}_{ii} + \sum_{\nu\neq\mu}\Gamma^{\nu,\Lambda}_{ii}\big)\delta_{ij}\right]. \tag{3.136}$$

As we mentioned above, quantum fluctuation and frustration are incorporated through the frequency dependence of the vertices. Thereby the static approximation is almost equivalent to the classical approximation. The resulting phase diagrams also suggests it [125]. Recall that the RPA term corresponding to the first term in the right-hand side of Eq. (3.135) causes the ordering tendency and is a dominant term in static approximation. On the other hand, particle-partile and particle-hole ladder terms corresponding to the second term in the right-hand side of Eq. (3.135) contain the leading term of $1/N$ expansion and these terms contribute only small fluctuation effect in static approximation. The vertex correction terms corresponding to the third terms in the right-hand side of Eq. (3.135) connect these bubble and ladder diagrammatic contributions. Furthermore, we later introduce PFFRG extension for general spin length S, and only RPA terms in vertex flow equations and non-local

terms in the susceptibility remain for classical spin limit $S \to \infty$. An approximation leaving only RPA term in Eq. (3.135) and non-local term in Eq. (3.136) corresponds to the mean-field approximation with the classical spin approximation:

$$\frac{\mathrm{d}}{\mathrm{d}\Lambda}\Gamma^{z,\Lambda}_{i_1 i_2} = \frac{2}{\pi\Lambda^2}\sum_j \Gamma^{z,\Lambda}_{i_1 j}\Gamma^{z,\Lambda}_{j i_2}, \tag{3.137}$$

and

$$\chi^{\mu\mu,\Lambda}_{ij} = \frac{1}{2\pi\Lambda}\delta_{ij} - \frac{1}{\pi^2\Lambda^2}\Gamma^{\mu,\Lambda}_{ij}. \tag{3.138}$$

Level-2 Truncation

In level-2 truncation, we solve Eq. (3.88), Eq. (3.91), and Eq. (3.96) simultaneously with the single-scale propagator shown in Eq. (3.45).
Thanks to the delta function in the single-scale propagator $S^\Lambda(\omega)$ (see Eq. (3.45)), We can perform the integration in Eq. (3.91) and Eq. (3.96) analytically. For example, PP channel terms of Eq. (3.91) and Eq. (3.96) have the form

$$\int_{-\infty}^{\infty}\frac{\mathrm{d}\omega'}{2\pi}\, L^\Lambda(\omega', \omega'+s)\tilde{\mathcal{T}}^\Lambda_{\mathrm{PP}}(s,t,u;\omega'). \tag{3.139}$$

Substituting the explicit formula of L^Λ in Eq. (3.95), the above integration is performed as

$$\begin{aligned}
&\int_{-\infty}^{\infty}\frac{\mathrm{d}\omega'}{2\pi}\left[\frac{\delta(|\omega'|-\Lambda)}{\omega'+\gamma^\Lambda(\omega')}\frac{\Theta(|\omega'+s|-\Lambda)}{\omega'+s+\gamma^\Lambda(\omega'+s)}\tilde{\mathcal{T}}^\Lambda_{\mathrm{PP}}(s,t,u;\omega')\right.\\
&\qquad\left.+\frac{\delta(|\omega'+s|-\Lambda)}{\omega'+s+\gamma^\Lambda(\omega'+s)}\frac{\Theta(|\omega'|-\Lambda)}{\omega'+\gamma^\Lambda(\omega')}\tilde{\mathcal{T}}^\Lambda_{\mathrm{PP}}(s,t,u;\omega')\right]\\
&=\frac{1}{\Lambda+\gamma^\Lambda(\Lambda)}\left[\frac{\Theta(|\Lambda+s|-\Lambda)}{\Lambda+s+\gamma^\Lambda(\Lambda+s)}\left\{\tilde{\mathcal{T}}^\Lambda_{\mathrm{PP}}(s,t,u;\Lambda)+\tilde{\mathcal{T}}^\Lambda_{\mathrm{PP}}(s,t,u;-\Lambda-s)\right\}\right.\\
&\qquad\left.+\frac{\Theta(|\Lambda-s|-\Lambda)}{\Lambda-s+\gamma^\Lambda(\Lambda-s)}\left\{\tilde{\mathcal{T}}^\Lambda_{\mathrm{PP}}(s,t,u;-\Lambda)+\tilde{\mathcal{T}}^\Lambda_{\mathrm{PP}}(s,t,u;\Lambda-s)\right\}\right].
\end{aligned} \tag{3.140}$$

We think about the contribution of the step functions $\Theta(|\Lambda+s|-\Lambda)$ and $\Theta(|\Lambda-s|-\Lambda)$. These are non-zero (i.e. 1) if

$$\Theta(|\Lambda+s|-\Lambda)=1:\ \text{if}\ \begin{cases} s>0 \\ s<-2\Lambda \end{cases}, \tag{3.141}$$

and

$$\Theta(|\Lambda-s|-\Lambda)=1:\ \text{if}\ \begin{cases} s<0 \\ s>2\Lambda \end{cases}. \tag{3.142}$$

Owing to the frequency symmetries Eq. (3.68), (3.69), and (3.70), it is sufficient to consider positive frequencies $s,t,u \geq 0$. Hence, $\Theta(|\Lambda+s|-\Lambda)$ is always 1, and

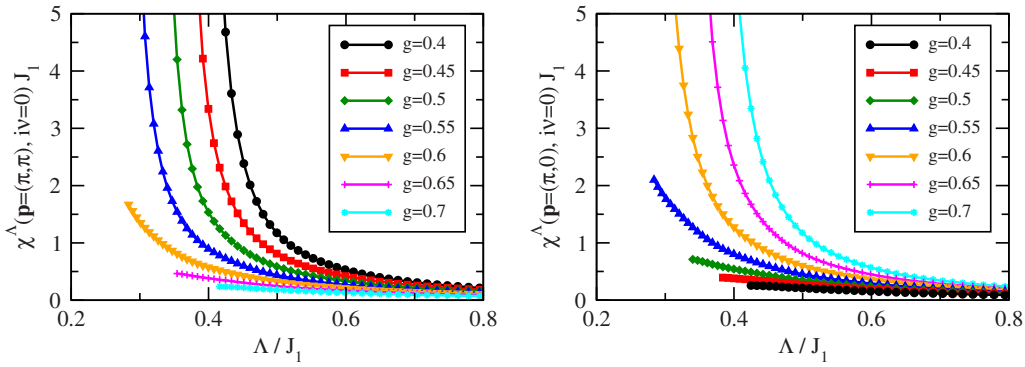

FIGURE 3.4: Flows of the static Néel (left) and collinear (right) susceptibilities of J_1-J_2 Heisenberg model calculated by level-2 truncation. Reprinted with permission from Ref. [54] © 2010 by the American Physical Society.

$\Theta(|\Lambda - s| - \Lambda)$ can be replaced by $\Theta(s - 2\Lambda)$. Therefore,

$$\begin{aligned}
&\int_{-\infty}^{\infty} \frac{d\omega'}{2\pi} L^{\Lambda}(\omega', \omega' + s) \tilde{\mathcal{T}}_{\mathrm{PP}}^{\Lambda}(s, t, u; \omega') \\
&= \frac{1}{\Lambda + \gamma^{\Lambda}(\Lambda)} \left[\frac{1}{\Lambda + s + \gamma^{\Lambda}(\Lambda + s)} \left\{ \tilde{\mathcal{T}}_{\mathrm{PP}}^{\Lambda}(s, t, u; \Lambda) + \tilde{\mathcal{T}}_{\mathrm{PP}}^{\Lambda}(s, t, u; -\Lambda - s) \right\} \right. \\
&\qquad \left. + \frac{\Theta(s - 2\Lambda)}{\Lambda - s + \gamma^{\Lambda}(\Lambda - s)} \left\{ \tilde{\mathcal{T}}_{\mathrm{PP}}^{\Lambda}(s, t, u; -\Lambda) + \tilde{\mathcal{T}}_{\mathrm{PP}}^{\Lambda}(s, t, u; \Lambda - s) \right\} \right].
\end{aligned} \tag{3.143}$$

In direct PH terms and crossed PH terms, we can execute integrals analytically in the same manner. After these procedures, the integro-differential equations Eq. (3.91) and Eq. (3.96) no longer contain integrals and we can reduce the computation costs for integration.

Here we mention the result for J_1-J_2 Heisenberg model on the square lattice [54]. The J_1-J_2 Heisenberg model is described the Hamiltonian ($J_1,\ J_2 > 0$)

$$\mathcal{H} = J_1 \sum_{\langle i,j \rangle} \boldsymbol{S}_i \cdot \boldsymbol{S}_j + J_2 \sum_{\langle\langle i,j \rangle\rangle} \boldsymbol{S}_i \cdot \boldsymbol{S}_j, \tag{3.144}$$

where $\sum_{\langle i,j \rangle}$ denotes a summation over all nearest-neighbor site pairs i, j and $\sum_{\langle\langle i,j \rangle\rangle}$ represents a summation over all next nearest-neighbor sites i, j. Since both terms are antiferromagnetic, this model has strong frustration. We take J_1 as an energy scale and define $g = J_2/J_1$ here. The susceptibility calculated by level-2 PFFRG is shown in Fig. 3.4 from Ref. [54]. The left panel shows the flow of the susceptibility at $\boldsymbol{k} = (\pi, \pi)$ and the right exhibits that at $\boldsymbol{k} = (\pi, 0)$. These wave vectors correspond Néel antiferromagnetic (AFM) and collinear AFM orders respectively.

From Fig. 3.4, we may conclude that the ground state is in Néel antiferromagnetic phase if $0 \leq g \leq 0.55$ and collinear antiferromagnetic phase if $0.6 \leq g$. However, calculations in studies by other methods suggest there is non-magnetic phase between the two phases [126–131]. Some papers conclude that this additional non-magnetic phase is quantum spin liquid state. In level-2 truncation in PFFRG, the effects of quantum fluctuation and frustration are not included sufficiently in order to detect non-magnetic phases. Level-2 truncation PFFRG overestimates ordering tendency.

Katanin Truncation

The level-2 truncation is the most commonly used approximation in the FRG of itinerant electron systems [55, 65]. As mention before this truncation is not sufficient to PFFRG,unfortunately. The pseudo-fermion lifetime is shortened by quantum fluctuation and frustration. Since this effect appears in the frequency dependence of the self-energy, feedback of the self-energy must be incorporated into the flow equation beyond the level-2 truncation. An efficient way to improve the flow was proposed by A. A. Katanin originally in context of the improvement of the fulfillment of Word identities in FRG for itinerant elecrons [81]. Improved flow violates Ward identities only by the terms with overlapping loops of fourth order in the 2-particle vertices although unimproved level-2 truncated flow satisfies only in the third order. In Katanin truncation scheme, we include 2-loop contributions partially in flow equations. Here we consider Hamiltonians only with 2-particle terms i.e. quadratic for the operators. In the pseudo-fermion language it means we only consider 2-particle interaction $\sim \overline{\psi}\overline{\psi}\psi\psi$. Therefore there is no bare 3-particle term and 3-particle vertex $\Gamma^{(6)\Lambda}$ is generated by $m < 3$ contributions γ^Λ and $\Gamma^{(4)\Lambda}$. We generate a part of 3-particle contributions by replacement of the single-scale propagator $S^\Lambda(\omega)$. In Eq. (2.143) we defined the single-scale propagator by Λ-derivative of the Green's function while fixing the self-energy. In Katanin truncation we replace the single-scale propagators in $\Gamma^{(4)\Lambda}$ flow with full Λ-derivative of the Green's function:

$$\begin{aligned}
\mathbf{S}^\Lambda_{\mathrm{Kat}} = \frac{\mathrm{d}}{\mathrm{d}\Lambda}\mathbf{G}^\Lambda &= \frac{\mathrm{d}}{\mathrm{d}\Lambda}([\mathbf{G}_0^\Lambda]^{-1} - \mathbf{\Sigma}^\Lambda)^{-1} \\
&= \frac{\mathrm{d}}{\mathrm{d}\Lambda}(\mathbf{Q}^\Lambda - \mathbf{\Sigma}^\Lambda)^{-1} \\
&= -(\mathbf{Q}^\Lambda - \mathbf{\Sigma}^\Lambda)^{-1}\dot{\mathbf{Q}}^\Lambda(\mathbf{Q}^\Lambda - \mathbf{\Sigma}^\Lambda)^{-1} + (\mathbf{Q}^\Lambda - \mathbf{\Sigma}^\Lambda)^{-1}\dot{\mathbf{\Sigma}}^\Lambda(\mathbf{Q}^\Lambda - \mathbf{\Sigma}^\Lambda)^{-1} \\
&= -\mathbf{G}^\Lambda\dot{\mathbf{Q}}^\Lambda\mathbf{G}^\Lambda + \mathbf{G}^\Lambda\dot{\mathbf{\Sigma}}^\Lambda\mathbf{G}^\Lambda \\
&= \mathbf{S}^\Lambda + \mathbf{G}^\Lambda\dot{\mathbf{\Sigma}}^\Lambda\mathbf{G}^\Lambda.
\end{aligned} \tag{3.145}$$

In PFFRG, we have to replace

$$\begin{aligned}
S^\Lambda(\omega) \to S^\Lambda_{\mathrm{Kat}}(\omega) &= \frac{\mathrm{d}}{\mathrm{d}\Lambda}G^\Lambda(\omega) \\
&= S^\Lambda(\omega) + \left[G^\Lambda(\omega)\right]^2(-\mathrm{i})\frac{\mathrm{d}}{\mathrm{d}\Lambda}\gamma^\Lambda(\omega),
\end{aligned} \tag{3.146}$$

in the flow for 2-particle vertices. We show the result of this replacement diagramatically in Fig. 3.5.

This procedure generates a part of $\Gamma^{(6)\Lambda}$ tadpole contributions to $\Gamma^{(4)\Lambda}$ flow (see Fig. 3.5). We can rewrite $L^\Lambda(\omega', \omega'')$ defined in Eq. (3.95) as

$$\begin{aligned}
L^\Lambda_{\mathrm{Kat}}(\omega', \omega'') &= G^\Lambda(\omega')S^\Lambda_{\mathrm{Kat}}(\omega'') + S^\Lambda_{\mathrm{Kat}}(\omega')G^\Lambda(\omega) \\
&= G^\Lambda(\omega')\left[\frac{\mathrm{d}}{\mathrm{d}\Lambda}G^\Lambda(\omega'')\right] + \left[\frac{\mathrm{d}}{\mathrm{d}\Lambda}G^\Lambda(\omega')\right]G^\Lambda(\omega) \\
&= \frac{\mathrm{d}}{\mathrm{d}\Lambda}\left[G^\Lambda(\omega')G^\Lambda(\omega'')\right].
\end{aligned} \tag{3.147}$$

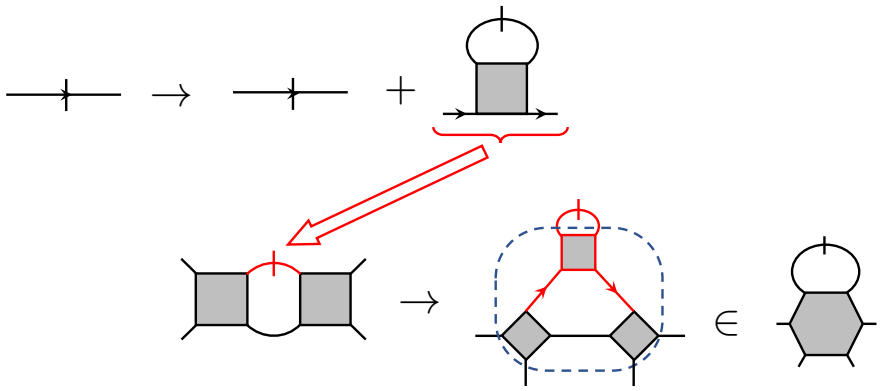

FIGURE 3.5: Diagrammatic representation of the replacement in Eq. (3.146) for Katanin truncation and 2-loop contribution generated from it. The single-scale propagators in the equation for Γ^{Λ} are replaced by $\mathrm{d}\Gamma^{\Lambda}/\mathrm{d}\Lambda$. This replacement generates a part of the 3-particle vertex contributions.

This form is useful for formulation. We can also rewrite it as another useful form for calculation,

$$
\begin{aligned}
&L^{\Lambda}_{\mathrm{Kat}}(\omega',\omega'') \\
&= G^{\Lambda}(\omega')S^{\Lambda}_{\mathrm{Kat}}(\omega'') + S^{\Lambda}_{\mathrm{Kat}}(\omega')G^{\Lambda}(\omega) \\
&= G^{\Lambda}(\omega')\left\{S^{\Lambda}(\omega'') + \left[G^{\Lambda}(\omega'')\right]^2(-\mathrm{i})\frac{\mathrm{d}}{\mathrm{d}\Lambda}\gamma^{\Lambda}(\omega'')\right\} \\
&\qquad + \left\{S^{\Lambda}(\omega') + \left[G^{\Lambda}(\omega')\right]^2(-\mathrm{i})\frac{\mathrm{d}}{\mathrm{d}\Lambda}\gamma^{\Lambda}(\omega')\right\}G^{\Lambda}(\omega'') \\
&= L^{\Lambda}(\omega',\omega'') \\
&\quad + G^{\Lambda}(\omega')\left\{-\mathrm{i}\frac{\mathrm{d}}{\mathrm{d}\Lambda}\gamma^{\Lambda}(\omega'')\right\}\left[G^{\Lambda}(\omega'')\right]^2 + \left[G^{\Lambda}(\omega')\right]^2\left\{-\mathrm{i}\frac{\mathrm{d}}{\mathrm{d}\Lambda}\gamma^{\Lambda}(\omega')\right\}G^{\Lambda}(\omega'').
\end{aligned}
\tag{3.148}
$$

The first term in the above equation is the same as $L^{\Lambda}(\omega',\omega'')$ in Eq. (3.95) in level-2 truncation. Hence in numerical calculation, we can perform frequency integration analytically for the first term and the result corresponds to level-2 truncation flow equations, and for the second term we substitute the right-hand side in the self-energy flow Eq. (3.88) and execute integration numerically.
Note that we replace the single-scale propagators only in the flow of $\Gamma^{(4)\Lambda}$. In other words we do not change the self-energy flow equation.

If we apply an approximation in which we only leave RPA terms in flow equations for 2-particle vertices, Katanin truncation leads dressed RPA approximation [56, 61, 65, 91].

For example, we show the susceptibilities of J_1-J_2 Heisenberg model calculated by Katanin truncation in Ref. [54] in Fig. 3.6. Each panel shows the flow of Néel and collinear AFM susceptibilities at $g = 0.2$ (left), $g = 0.55$ (center), and $g = 0.8$ (right). Although at $g = 0.2$ and $g = 0.8$, Néel and collinear spin susceptibilities diverge, respectively, as calculated in level-2 truncation scheme shown in Fig. 3.4, at $g = 0.55$ spin susceptibilities do not diverge and stay finite without significant changes even in $\Lambda \to \Lambda_{\mathrm{IR}} = 0$. This means there is no magnetic long-range order.

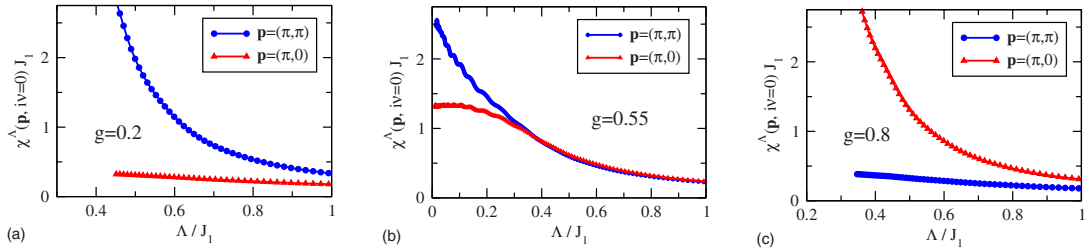

FIGURE 3.6: Flow of the Néel and collinear susceptibilities at $g = 0.2$ (left), $g = 0.55$ (center), and $g = 0.8$ (right). The wave vectors $\boldsymbol{k} = (\pi, \pi)$ and $\boldsymbol{k} = (\pi, 0)$ are correspond to Néel and collinear AFM order, respectively. Reprinted with permission from Ref. [54] © 2010 by the American Physical Society.

Comparison with Other Methods

Now we present a brief comparison of the results of PFFRG and other numerical methods. First of all, we show the temperature dependence of the uniform susceptibilities obtained by PFFRG and high-temperature series expansion (HTSE) in Fig. 3.7. Figure (a) and (b) show uniform susceptibility of the Heisenberg model on the hyperkagome lattice with ferromagnetic (FM) and antiferromagnetic (AFM) exchanges, respectively. In both figures, pf-FRG, high-T series, and dlog Pade represent pseudo-fermion functional renormalization group (PFFRG), 16th-order high-temperature series expansion, and high-order differential Dlog Padé approximations to the high-temperature series, respectively. Temperature dependence of the PFFRG susceptibilities are calculated by the relation Eq. (3.150) in the next section. The inset of Fig. 3.7 (b) shows the comparison in a wide temperature range. All lines overlap and no differences can be seen. We can conclude that in the high temperature region, PFFRG is in good agreement with the results of HTSE from these comparisons.

Second, we show a comparison of the susceptibilities obtained with PFFRG and exact diagonalization (ED) in Fig. 3.8. Figure (a) and (b) show the temperature dependence of the susceptibilities of a AFM Heisenberg dimer and a J_1-J_2 Heisenberg hexamer with $J_1 = 1$ and $J_2 = 0.5$, respectively. We can see that the susceptibility of PFFRG is quantitatively different from that in ED at low temperature.

Moreover, we calculate susceptibility of the Kitaev model by PFFRG and compare the result with the uniform susceptibility from quantum Monte Carlo + continuous-time quantum Monte Carlo (QMC+CTQMC) calculation in Ref. [133]. The results is shown in Fig. 3.9. We use the same calculation condition in Sec. 5.6 and consider isotropic ($J_x = J_y = J_z = J$) FM Kitaev model with the energy unit J. Λ-dependence of the results from PFFRG is rescaled by the relation between Λ and T in Eq. (3.150). The data from QMC+CTQMC in Ref. [133] are extracted by WebPlotDigitizer [134]. As we can see in the figure, $T = 0$ PFFRG (1-loop + Katanin truncation) cannot describe the decrease of the susceptibility in low temperature.

From comparisons above, we can conclude that the susceptibilities calculated by PFFRG (1-loop + Katanin truncation) are consistent with other methods at high temperatures, but have a quantitative (sometimes qualitative) discrepancy at low temperature. For further comparison, next, we show a comparison of the phase boundaries obtained by PFFRG and quantum Monte Carlo (QMC) in Fig. 3.10. This figure

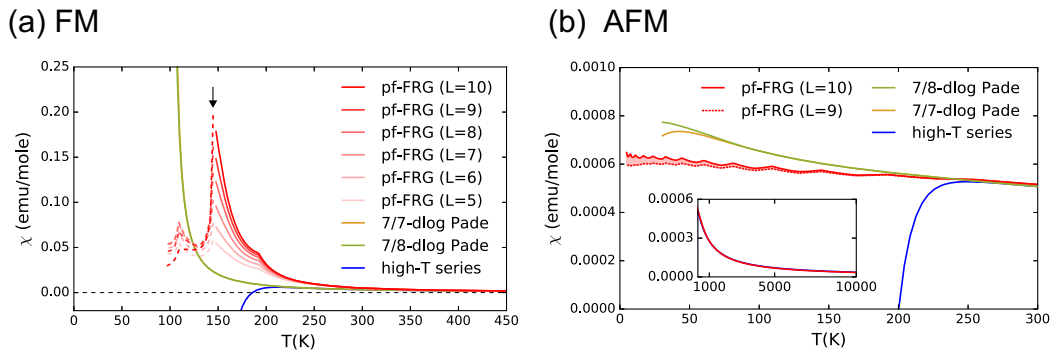

FIGURE 3.7: Temperature dependence of the uniform susceptibilities calculated by PFFRG and HTSE of the Heisenberg model with (a) FM and (b) AFM couplings on the hyperkagome lattice. pf-FRG, high-T series, and dlog Pade mean pseudo-fermion functional renormalization group (PFFRG), 16th-order high-temperature series expansion, and high-order differential Dlog Padé approximations to the high-temperature series, respectively. The inset shows the comparison in a wide temperature range. Reprinted with permission from Ref. [132] © 2016 by the American Physical Society.

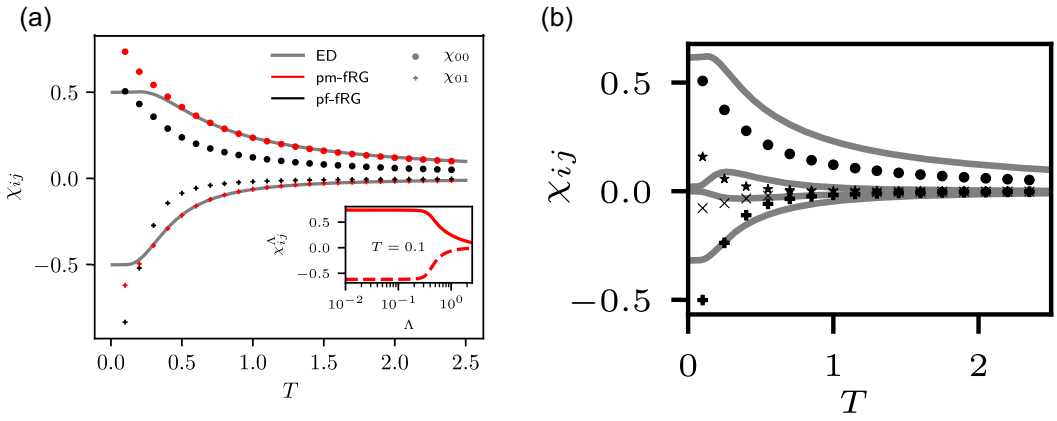

FIGURE 3.8: Temperature dependence of the susceptibilities calculated by PFFRG and ED of a (a) AFM Heisenberg dimer and a (b) J_1-J_2 Heisenberg hexamer with $J_1 = 1$ and $J_2 = 0.5$. In figure (a), pf-fRG and pm-fRG represent pseudo-fermion functional renormalization group (PFFRG) and pseudo-Majorana functional renormalization group, respectively. In figure (b), the same legend as in figure (a) is applied (There are only ED and pf-fRG plots). These figures are from Ref. [105].

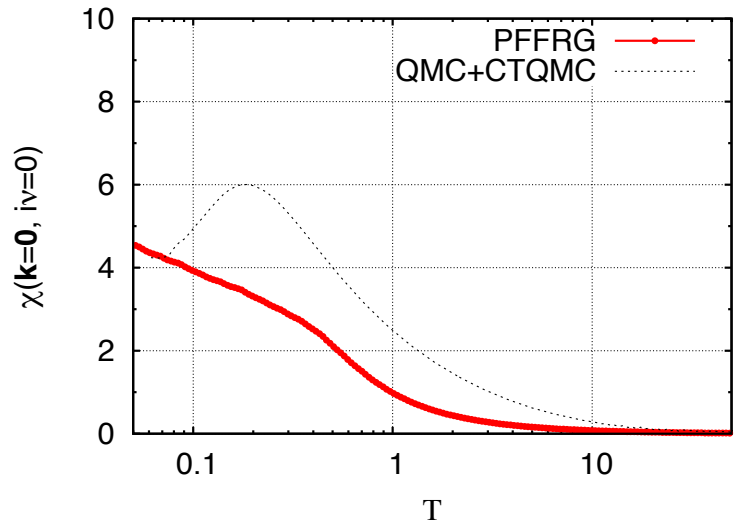

FIGURE 3.9: A comparison of temperature dependence of the uniform susceptibilities of the isotropic FM Kitaev model obtained by PFFRG and QMC+CTQMC. QMC+CTQMC data is from Ref. [133] and we extract data from the article by WebPlotDigitizer [134].

shows a Λ-Δ phase diagram of the antiferromagnetic XXZ model on the square lattice. Hamiltonian of the AFM XXZ model is given as

$$\mathcal{H} = J \sum_{\langle i,j \rangle} (S_i^x S_j^x + S_i^y S_j^y + \Delta S_i^z S_j^z). \tag{3.149}$$

FRG, RPA0, RPA+, and QMC in the figure represent PFFRG, PFFRG with only RPA diagrams without the self-energy, PFFRG with only RPA diagrams with the self-energy, and quantum Monte Carlo, respectively. It can be seen that PFFRG overestimates the phase boundary at finite Λ (or temperature). In addition, the XXZ model defined in Eq. (3.149) acquires full SU(2) symmetry and becomes the Heisenberg model at $\Delta = 1$. Therefore finite temperature phase transitions are prohibited, as claimed by Mermin-Wagner theorem. The phase boundaries obtained by QMC reflect this properties. As we can see in Fig. 3.10, solutions by PFFRG (with 1-loop + Katanin truncation) violate Mermin-Wagner theorem near $\Delta = 1$.

However, the T_c (Λc) obtained by PFFRG is in good agreement with the results of QMC. In order to support that, we present another example. We show in Tab. 3.1 a comparison of the Néel temperatures of the J_1-J_3 AFM Heisenberg model on the simple cubic lattice obtained by PFFRG and QMC from the previous study in Ref. [135]. J_1 and J_3 are the nearest-neighbor and third-nearest-neighbor AFM Heisenberg exchanges, respectively. For PFFRG results, the relation Eq. (3.150) is used to obtain T_c from Λ_c. We can see that Néel temperatures from PFFRG and QMC are in good agreement with the results. The calculation results by PFFRG can generally reproduce the relative differences in Λ_c due to the differences in parameters. This feature is proven numerically also for other models. Furthermore, it is known that the solution calculated PFFRG well reproduce the ground state phase boundaries between magnetic ordered phases and between ordered phase and magnetically disordered phase e.g. VBC, nematic, and spin liquid phases (e.g. in Ref. [136], see also the comparison in the Chap. 5).

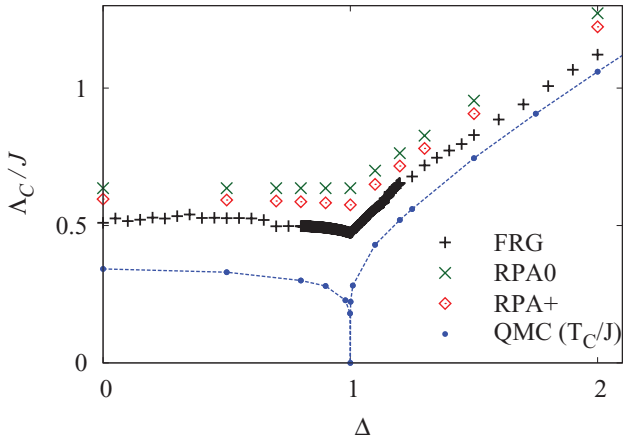

FIGURE 3.10: Λ-Δ phase diagram of the AFM XXZ model on the square lattice obtained PFFRG and QMC. FRG, RPA0, RPA+, and QMC in the figure represent PFFRG, PFFRG with only RPA diagrams without the self-energy, PFFRG with only RPA diagrams with the self-energy, and quantum Monte Carlo, respectively. Reprinted with permission from Ref. [99] © 2012 by the American Physical Society.

TABLE 3.1: Néel temperature T_c of the J_1-J_3 AFM Heisenberg model on the simple cubic lattice obtained by PFFRG and QMC. Reprinted with permission from Ref. [135] © 2016 by the American Physical Society.

J_3/J_1	0	0.20	0.40	0.60	0.80
PFFRG	1.05(5)	1.43(7)	1.67(8)	1.94(9)	2.36(10)
QMC	0.946(1)	1.371(1)	1.7675(10)	2.143(1)	2.5039(5)

3.7 Futher Extensions

We have introduced PFFRG scheme for Hamiltonian with $S = 1/2$ and only diagonal spin interactions. Our PFFRG is formulated at zero temperature (but using Matsubara frequency representation) and zero magnetic field. We adopt 1-loop + Katanin truncation scheme and therefore we cannot calculate expectation value of the product of three or more spin operators directly. In this section, we mention further extensions of PFFRG. The following two subsections for finite temperature and spin-S systems are relevant to this dissertation, and in particular the extension to the spin-S systems is used to study the spin-S Kitaev-Heisenberg model in chapter 5. The remaining parts of this section is devoted to mention other extensions beyond scheme we delivered through this chapter.

Finite Temperature

PFFRG is formulated in Matsubara frequency representation but we take the limit $T \to 0$. Therefore PFFRG calculation is executed at zero temperature and entropic effect is not included. PFFRG was extended to finite temperature in J. Reuther's doctoral dissertation [91]. In $T \neq 0$ we cannot use average projection $\mu = 0$ and we must use $\mu = -\frac{i\pi T}{2}$. This projection breaks time-reversal symmetry and hermitian property of the pseudo-fermion Hamiltonian. Because of this the computational costs increase enormously. However, qualitative behavior of the susceptibility is not changed. This is the reason why finite temperature PFFRG has not been used after Reuther's dissertation.

As we mentioned before, there is an approximate relation between

$$T \simeq \frac{\pi}{2}\Lambda, \tag{3.150}$$

in our PFFRG scheme. This relation is mentioned in Ref. [135]. In this paper the factor $\pi/2$ is obtained by the comparison between PFFRG with only RPA terms and conventional mean-field theory in spin language (this is argued in the note in the reference list). In appendix C, we develop this argument further and prove that the factor is valid not only in mean-field theory but also in the leading order of high-temperature expansion. In addition, in Ref. [118, 137] PFFRG for SU(N) Heisenberg model is formulated (as mentioned later) and Eq. (3.150) is also proved in $N \to \infty$ limit.

Spin-S Systems

The pseudo-fermion representation of spin Eq. (3.14) can be applied only to $S = 1/2$ spins. For spins with $S \geq 1/2$ it is suggested to introduce multi-flavor fermions with $2S + 1$ flavors [138]. In this Hilbert space single-occupancy condition and half-filling condition is not the same for $S > 1/2$, unfortunately. Therefore we cannot use average projection $\mu = 0$. A simpler and more convenient for PFFRG extension is proposed by M. Baez and J. Reuther [139]. In this extension, we put $2S$ spins with $S = 1/2$ on each site and construct spins with S by superposition of those like

$$\boldsymbol{S}_i = \sum_{\kappa=1}^{2S} \boldsymbol{S}_{i,\kappa}, \tag{3.151}$$

where κ is flavor index. In this formulation, we consider extended Hilbert space and require the projection to the subspace satisfying highest weight condition $|\boldsymbol{S}_i| = S$. To represent spins by fermions we introduce pseudo-fermion operators like Eq. (3.14),

$$S_i^\mu = \frac{1}{2}\sum_{\alpha,\alpha'}\sum_{\kappa=1}^{M} f_{i\alpha'\kappa}^\dagger \sigma_{\alpha'\alpha}^\mu f_{i\alpha\kappa}, \tag{3.152}$$

with $M = 2S$. Those fermion operators satisfy the anti-commutation relation like Eq. (3.15)

$$\{f_{i\alpha\kappa}, f_{i'\alpha'\kappa'}^\dagger\} = \delta_{ii'}\delta_{\alpha\alpha'}\delta_{\kappa\kappa}. \tag{3.153}$$

There are two constraints: (i) maximal spin length condition $|\boldsymbol{S}_i| = S$ and (ii) single-occupancy condition $Q_{i\kappa} = 1$. Though both constraints can be implemented by imaginary-value chemical potential [140], we adopt more simpler projection. The latter is easily implemented $\mu = 0$ as the same manner as $S = 1/2$ PFFRG. For fulfillment of the former constraint we introduce a level repulsion term later. We consider PFFRG for fermions with flavor indices $f_{i\alpha\kappa}$ and $f_{i\alpha\kappa}^\dagger$.
As can seen in Eq. (3.152) and Eq. (3.153), the flavor indices behave like site indices. Thereby we can conclude that it is sufficient that $\delta_{i'i} \to \delta_{i'i}\delta_{\kappa'\kappa}$ for all parametrization and we can obtain the almost same flow equations for $S = 1/2$ Eq. (3.88), Eq. (3.91), and Eq. (3.96). Then we assume that the vertices do not depend on flavor indices like their initial conditions:

$$\Gamma^{\mu,\Lambda}_{i_1 i_2,\kappa_1\kappa_2} \to \Gamma^{\mu,\Lambda}_{i_1 i_2}, \tag{3.154}$$

$$\Gamma^{\mathrm{d},\Lambda}_{i_1 i_2,\kappa_1\kappa_2} \to \Gamma^{\mathrm{d},\Lambda}_{i_1 i_2}. \tag{3.155}$$

The remaining internal summations over flavor indices can be performed easily

$$\sum_{\kappa=1}^{M} \to M. \tag{3.156}$$

As a result, there is no flavor index in the entire flow, while the term contains site summation in Eq. (3.88) and the RPA term in Eq. (3.91) and Eq. (3.96) obtain additional prefactor M. In classical limit $S \to \infty$, M also becomes infinite because $M = 2S$ and the flow equations diverge. Therefore it is required to rescale the vertices. For system with M we rescale

$$\Gamma \to \bar{\Gamma} = M\Gamma. \tag{3.157}$$

Finally we obtain the explicit flow equations corresponding to Eq. (3.88), Eq. (3.91), and Eq. (3.96) as,

$$\begin{aligned}\frac{\mathrm{d}}{\mathrm{d}\Lambda}\gamma^\Lambda(\omega) = \frac{1}{2\pi}\frac{1}{\Lambda+\gamma^\Lambda(\Lambda)}\Bigg[&-2\sum_j\left\{\bar{\Gamma}^{\mathrm{d},\Lambda}_{i_1 j}(\omega+\Lambda,0,\omega-\Lambda) - \bar{\Gamma}^{\mathrm{d},\Lambda}_{i_1 j}(\omega-\Lambda,0,\omega+\Lambda)\right\} \\ &+\frac{1}{M}\sum_\mu\left\{\bar{\Gamma}^{\mu,\Lambda}_{i_1 i_1}(\omega+\Lambda,\omega-\Lambda,0) - \bar{\Gamma}^{\mu,\Lambda}_{i_1 i_1}(\omega-\Lambda,\omega+\Lambda,0)\right\} \\ &+\frac{1}{M}\left\{\bar{\Gamma}^{\mathrm{d},\Lambda}_{i_1 i_1}(\omega+\Lambda,\omega-\Lambda,0) - \bar{\Gamma}^{\mathrm{d},\Lambda}_{i_1 i_1}(\omega-\Lambda,\omega+\Lambda,0)\right\}\Bigg],\end{aligned} \tag{3.158}$$

$$\frac{\mathrm{d}}{\mathrm{d}\Lambda}\bar{\Gamma}^{z,\Lambda}_{i_1 i_2}(s,t,u) = \int_{-\infty}^{\infty}\frac{\mathrm{d}\omega'}{2\pi}\Big[L^{\Lambda}(\omega',\omega'+s)\tilde{\mathcal{T}}^{z,\Lambda}_{\mathrm{PP}}(s,t,u;\omega') + L^{\Lambda}(\omega',\omega'+t)\tilde{\mathcal{T}}^{z,\Lambda}_{\mathrm{PH,d}}(s,t,u;\omega') + L^{\Lambda}(\omega',\omega'+u)\tilde{\mathcal{T}}^{z,\Lambda}_{\mathrm{PH,cr}}(s,t,u;\omega')\Big], \tag{3.159}$$

with

$$\begin{aligned}\tilde{\mathcal{T}}^{z,\Lambda}_{\mathrm{PP}}(s,t,u;\omega') = \frac{1}{M}\Big\{ &-\bar{\Gamma}^{x,\Lambda}_{i_1 i_2}(s,-\omega_2'-\omega',\omega_1'+\omega')\bar{\Gamma}^{y,\Lambda}_{i_1 i_2}(s,\omega_2+\omega',\omega_1+\omega')\\ &-\bar{\Gamma}^{y,\Lambda}_{i_1 i_2}(s,-\omega_2'-\omega',\omega_1'+\omega')\bar{\Gamma}^{x,\Lambda}_{i_1 i_2}(s,\omega_2+\omega',\omega_1+\omega')\\ &+\bar{\Gamma}^{z,\Lambda}_{i_1 i_2}(s,-\omega_2'-\omega',\omega_1'+\omega')\bar{\Gamma}^{\mathrm{d},\Lambda}_{i_1 i_2}(s,\omega_2+\omega',\omega_1+\omega')\\ &+\bar{\Gamma}^{\mathrm{d},\Lambda}_{i_1 i_2}(s,-\omega_2'-\omega',\omega_1'+\omega')\bar{\Gamma}^{z,\Lambda}_{i_1 i_2}(s,\omega_2+\omega',\omega_1+\omega')\Big\},\end{aligned} \tag{3.160}$$

$$\begin{aligned}\tilde{\mathcal{T}}^{z,\Lambda}_{\mathrm{PH,d}}(s,t,u;\omega') =& 2\sum_j \bar{\Gamma}^{z,\Lambda}_{i_1 j}(\omega_1'+\omega',t,\omega_1-\omega')\bar{\Gamma}^{z,\Lambda}_{j i_2}(\omega_2+\omega',t,-\omega_2'+\omega')\\ &+\frac{1}{M}\Big\{\bar{\Gamma}^{z,\Lambda}_{i_1 i_2}(\omega_1'+\omega',t,\omega_1-\omega')\bar{\Gamma}^{x,\Lambda}_{i_2 i_2}(\omega_2+\omega',-\omega_2'+\omega',t)\\ &+\bar{\Gamma}^{z,\Lambda}_{i_1 i_2}(\omega_1'+\omega',t,\omega_1-\omega')\bar{\Gamma}^{y,\Lambda}_{i_2 i_2}(\omega_2+\omega',-\omega_2'+\omega',t)\\ &-\bar{\Gamma}^{z,\Lambda}_{i_1 i_2}(\omega_1'+\omega',t,\omega_1-\omega')\bar{\Gamma}^{z,\Lambda}_{i_2 i_2}(\omega_2+\omega',-\omega_2'+\omega',t)\\ &-\bar{\Gamma}^{z,\Lambda}_{i_1 i_2}(\omega_1'+\omega',t,\omega_1-\omega')\bar{\Gamma}^{\mathrm{d},\Lambda}_{i_2 i_2}(\omega_2+\omega',-\omega_2'+\omega',t)\\ &+\bar{\Gamma}^{x,\Lambda}_{i_1 i_1}(\omega_1'+\omega',\omega_1-\omega',t)\bar{\Gamma}^{z,\Lambda}_{i_1 i_2}(\omega_2+\omega',t,-\omega_2'+\omega')\\ &+\bar{\Gamma}^{y,\Lambda}_{i_1 i_1}(\omega_1'+\omega',\omega_1-\omega',t)\bar{\Gamma}^{z,\Lambda}_{i_1 i_2}(\omega_2+\omega',t,-\omega_2'+\omega')\\ &-\bar{\Gamma}^{z,\Lambda}_{i_1 i_1}(\omega_1'+\omega',\omega_1-\omega',t)\bar{\Gamma}^{z,\Lambda}_{i_1 i_2}(\omega_2+\omega',t,-\omega_2'+\omega')\\ &-\bar{\Gamma}^{\mathrm{d},\Lambda}_{i_1 i_1}(\omega_1'+\omega',\omega_1-\omega',t)\bar{\Gamma}^{z,\Lambda}_{i_1 i_2}(\omega_2+\omega',t,-\omega_2'+\omega')\Big\},\end{aligned} \tag{3.161}$$

$$\begin{aligned}\tilde{\mathcal{T}}^{z,\Lambda}_{\mathrm{PH,cr}}(s,t,u;\omega') = \frac{1}{M}\Big\{ &-\bar{\Gamma}^{x,\Lambda}_{i_1 i_2}(\omega_2'-\omega',-\omega_1-\omega',u)\bar{\Gamma}^{y,\Lambda}_{i_1 i_2}(\omega_2-\omega',\omega_1'+\omega',u)\\ &-\bar{\Gamma}^{y,\Lambda}_{i_1 i_2}(\omega_2'-\omega',-\omega_1-\omega',u)\bar{\Gamma}^{x,\Lambda}_{i_1 i_2}(\omega_2-\omega',\omega_1'+\omega',u)\\ &-\bar{\Gamma}^{z,\Lambda}_{i_1 i_2}(\omega_2'-\omega',-\omega_1-\omega',u)\bar{\Gamma}^{\mathrm{d},\Lambda}_{i_1 i_2}(\omega_2-\omega',\omega_1'+\omega',u)\\ &-\bar{\Gamma}^{\mathrm{d},\Lambda}_{i_1 i_2}(\omega_2'-\omega',-\omega_1-\omega',u)\bar{\Gamma}^{z,\Lambda}_{i_1 i_2}(\omega_2-\omega',\omega_1'+\omega',u)\Big\},\end{aligned} \tag{3.162}$$

and

$$\frac{\mathrm{d}}{\mathrm{d}\Lambda}\bar{\Gamma}^{\mathrm{d},\Lambda}_{i_1 i_2}(s,t,u) = \int_{-\infty}^{\infty}\frac{\mathrm{d}\omega'}{2\pi}\Big[L^{\Lambda}(\omega',\omega'+s)\tilde{\mathcal{T}}^{\mathrm{d},\Lambda}_{\mathrm{PP}}(s,t,u;\omega') + L^{\Lambda}(\omega',\omega'+t)\tilde{\mathcal{T}}^{\mathrm{d},\Lambda}_{\mathrm{PH,d}}(s,t,u;\omega') + L^{\Lambda}(\omega',\omega'+u)\tilde{\mathcal{T}}^{\mathrm{d},\Lambda}_{\mathrm{PH,cr}}(s,t,u;\omega')\Big], \tag{3.163}$$

with

$$\begin{aligned}\tilde{\mathcal{T}}^{\mathrm{d},\Lambda}_{\mathrm{PP}}(s,t,u;\omega') = \frac{1}{M}\Big\{&\bar{\Gamma}^{x,\Lambda}_{i_1 i_2}(s,-\omega_2'-\omega',\omega_1'+\omega')\bar{\Gamma}^{x,\Lambda}_{i_1 i_2}(s,\omega_2+\omega',\omega_1+\omega')\\ &+\bar{\Gamma}^{y,\Lambda}_{i_1 i_2}(s,-\omega_2'-\omega',\omega_1'+\omega')\bar{\Gamma}^{y,\Lambda}_{i_1 i_2}(s,\omega_2+\omega',\omega_1+\omega')\\ &+\bar{\Gamma}^{z,\Lambda}_{i_1 i_2}(s,-\omega_2'-\omega',\omega_1'+\omega')\bar{\Gamma}^{z,\Lambda}_{i_1 i_2}(s,\omega_2+\omega',\omega_1+\omega')\\ &+\bar{\Gamma}^{\mathrm{d},\Lambda}_{i_1 i_2}(s,-\omega_2'-\omega',\omega_1'+\omega')\bar{\Gamma}^{\mathrm{d},\Lambda}_{i_1 i_2}(s,\omega_2+\omega',\omega_1+\omega')\Big\},\end{aligned} \tag{3.164}$$

$$\begin{aligned}\tilde{\mathcal{T}}^{\mathrm{d},\Lambda}_{\mathrm{PH,d}}(s,t,u;\omega') =& 2\sum_j \bar{\Gamma}^{\mathrm{d},\Lambda}_{i_1 j}(\omega_1'+\omega',t,\omega_1-\omega')\bar{\Gamma}^{\mathrm{d},\Lambda}_{j i_2}(\omega_2+\omega',t,-\omega_2'+\omega')\\ &+\frac{1}{M}\Big\{-\bar{\Gamma}^{\mathrm{d},\Lambda}_{i_1 i_2}(\omega_1'+\omega',t,\omega_1-\omega')\bar{\Gamma}^{x,\Lambda}_{i_2 i_2}(\omega_2+\omega',-\omega_2'+\omega',t)\\ &-\bar{\Gamma}^{\mathrm{d},\Lambda}_{i_1 i_2}(\omega_1'+\omega',t,\omega_1-\omega')\bar{\Gamma}^{y,\Lambda}_{i_2 i_2}(\omega_2+\omega',-\omega_2'+\omega',t)\\ &-\bar{\Gamma}^{\mathrm{d},\Lambda}_{i_1 i_2}(\omega_1'+\omega',t,\omega_1-\omega')\bar{\Gamma}^{z,\Lambda}_{i_2 i_2}(\omega_2+\omega',-\omega_2'+\omega',t)\\ &-\bar{\Gamma}^{\mathrm{d},\Lambda}_{i_1 i_2}(\omega_1'+\omega',t,\omega_1-\omega')\bar{\Gamma}^{\mathrm{d},\Lambda}_{i_2 i_2}(\omega_2+\omega',-\omega_2'+\omega',t)\\ &-\bar{\Gamma}^{x,\Lambda}_{i_1 i_1}(\omega_1'+\omega',\omega_1-\omega',t)\bar{\Gamma}^{\mathrm{d},\Lambda}_{i_1 i_2}(\omega_2+\omega',t,-\omega_2'+\omega')\\ &-\bar{\Gamma}^{y,\Lambda}_{i_1 i_1}(\omega_1'+\omega',\omega_1-\omega',t)\bar{\Gamma}^{\mathrm{d},\Lambda}_{i_1 i_2}(\omega_2+\omega',t,-\omega_2'+\omega')\\ &-\bar{\Gamma}^{z,\Lambda}_{i_1 i_1}(\omega_1'+\omega',\omega_1-\omega',t)\bar{\Gamma}^{\mathrm{d},\Lambda}_{i_1 i_2}(\omega_2+\omega',t,-\omega_2'+\omega')\\ &-\bar{\Gamma}^{\mathrm{d},\Lambda}_{i_1 i_1}(\omega_1'+\omega',\omega_1-\omega',t)\bar{\Gamma}^{\mathrm{d},\Lambda}_{i_1 i_2}(\omega_2+\omega',t,-\omega_2'+\omega')\Big\},\end{aligned} \tag{3.165}$$

$$\begin{aligned}\tilde{\mathcal{T}}^{\mathrm{d},\Lambda}_{\mathrm{PH,cr}}(s,t,u;\omega') = \frac{1}{M}\Big\{&-\bar{\Gamma}^{x,\Lambda}_{i_1 i_2}(\omega_2'-\omega',-\omega_1-\omega',u)\bar{\Gamma}^{x,\Lambda}_{i_1 i_2}(\omega_2-\omega',\omega_1'+\omega',u)\\ &-\bar{\Gamma}^{y,\Lambda}_{i_1 i_2}(\omega_2'-\omega',-\omega_1-\omega',u)\bar{\Gamma}^{y,\Lambda}_{i_1 i_2}(\omega_2-\omega',\omega_1'+\omega',u)\\ &-\bar{\Gamma}^{z,\Lambda}_{i_1 i_2}(\omega_2'-\omega',-\omega_1-\omega',u)\bar{\Gamma}^{z,\Lambda}_{i_1 i_2}(\omega_2-\omega',\omega_1'+\omega',u)\\ &-\bar{\Gamma}^{\mathrm{d},\Lambda}_{i_1 i_2}(\omega_2'-\omega',-\omega_1-\omega',u)\bar{\Gamma}^{\mathrm{d},\Lambda}_{i_1 i_2}(\omega_2-\omega',\omega_1'+\omega',u)\Big\}.\end{aligned} \tag{3.166}$$

For the formula of the susceptibility Eq. (3.123), we adopt the above treatment in the same manner as the flow equations. In the rescale of the susceptibility, we pay attention to the relationship $\chi\Gamma$ being dimensionless. Therefore we rescale χ so as

not to break this relationship:

$$\chi\Gamma = \frac{\chi}{M} M\Gamma = \bar{\chi}\bar{\Gamma}. \tag{3.167}$$

The susceptibility is rescaled as $\chi \to \bar{\chi} = \chi/M$. The explicit formula is

$$\begin{aligned}
&\bar{\chi}_{ij}^{\mu\mu,\Lambda}(\mathrm{i}\nu) \\
&= -\frac{1}{4\pi}\int_{-\infty}^{\infty} \mathrm{d}\omega\, G^{\Lambda}(\omega)G^{\Lambda}(\omega+\nu)\delta_{ij} \\
&\quad - \frac{1}{8\pi^2}\int_{-\infty}^{\infty} \mathrm{d}\omega\mathrm{d}\omega'\, G^{\Lambda}(\omega)G^{\Lambda}(\omega+\nu)G^{\Lambda}(\omega')G^{\Lambda}(\omega'+\nu) \\
&\qquad \times \Bigg[2\bar{\Gamma}_{ij}^{\mu,\Lambda}(\omega+\omega'+\nu,\nu,\omega-\omega') \\
&\qquad\quad + \frac{1}{M}\Bigg\{ -\bar{\Gamma}_{ii}^{\mu,\Lambda}(\omega+\omega'+\nu,\omega-\omega',\nu) + \sum_{\nu\neq\mu}\bar{\Gamma}_{ii}^{\nu,\Lambda}(\omega+\omega'+\nu,\omega-\omega',\nu) \\
&\qquad\qquad - \bar{\Gamma}_{ii}^{\mathrm{d},\Lambda}(\omega+\omega'+\nu,\omega-\omega',\nu)\Bigg\}\delta_{ij}\Bigg].
\end{aligned} \tag{3.168}$$

In the classical limit $S \to \infty$, only the terms containing site summations in the flow equations and the non-local term in the susceptibility remain finite and it is consistent to the approximation introduced to static PFFRG.
If $\Lambda \to \Lambda_{\mathrm{IR}} = 0$, these flow equations correspond to Luttinger-Tisza method [141, 142]. This equivalence is proved in Ref. [139, 143].

For example, we consider antiferromagnetic (AFM) Heisenberg model with general S on honeycomb lattice [139]. The Hamiltonian is

$$\mathcal{H} = J_1 \sum_{\langle i,j\rangle} \boldsymbol{S}_i \cdot \boldsymbol{S}_j, \tag{3.169}$$

where $\sum_{\langle i,j\rangle}$ denotes a summation over all nearest-neighbor site pairs i, j. We rewrite this Hamiltonian using Eq. (3.151) and Eq. (3.152),

$$\mathcal{H} = J_1 \sum_{\langle i,j\rangle} \left(\sum_{\kappa=1}^{M} \boldsymbol{S}_{i,\kappa}\right)\cdot\left(\sum_{\kappa'=1}^{M} \boldsymbol{S}_{j,\kappa'}\right) + A\sum_{i}\left(\sum_{\kappa=1}^{M} \boldsymbol{S}_{i,\kappa}\right)^2. \tag{3.170}$$

The additional last term is level repulsion term with $A \leq 0$ and it projects systems onto $|\boldsymbol{S}_i| = S$ sector.
The calculated static susceptibilities are shown in Fig. 3.11 from the paper written by Baez and Reuhter [139]. Fig. 3.11 (a) show the static susceptibility of $S = 3/2$ system at the momentum at which $\chi^{\Lambda}(\boldsymbol{k})$ has the maximum value with some values of A. Fig. 3.11 (b) is the counterpart of $S = 1/2$ system. In both figures, the energy unit is J_1. One may think that the level repulsion term does not affect to $S = 1/2$ systems although in Fig. 3.11 (b) the susceptibility varies slightly for different values of A. This is true for the original spins. However in pseudo-fermion representation, pseudo-fermions interact via density-density channel as well as spin-spin channel, and the susceptibility difference is generated from pseudo-fermion interactions. In other words, the difference of the value A corresponds to the difference of the initial value of the vertices in pseudo-fermion language although in $S = 1/2$ spin representation the level repulsion term is merely constant energy shift. Each inset shows

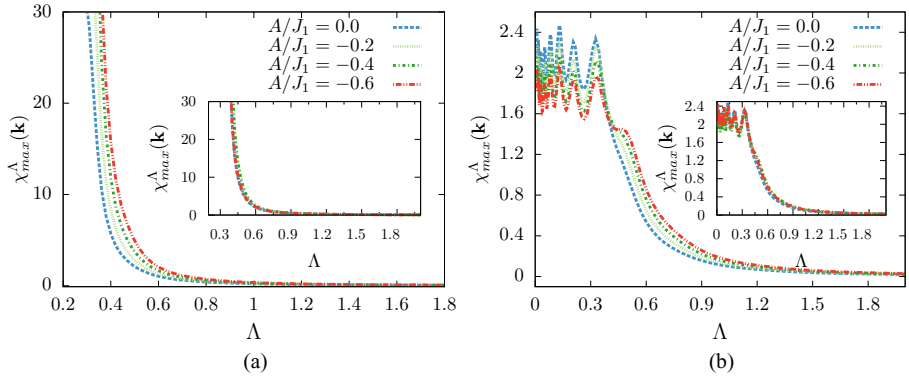

FIGURE 3.11: (a) $S = 3/2$ and (b) $S = 1/2$ PFFRG susceptibility of AFM Heisenberg model on the honeycomb lattice with various A. Energy unit is the Heisenberg interaction J_1. Insets show re-calculated susceptibilities with energy unit $\sqrt{J_1^2 + A^2}$. Reprinted with permission from Ref. [139] © 2017 by the American Physical Society.

the susceptibilities re-calculated by rescaling the energy unit $J_1 \to \sqrt{J_1^2 + A^2}$. As we can see in the inset, the calculated susceptibility curves for all A correspond to the curve for A = 0. Hence we can conclude that even without the additional level repulsion term, a projection to the largest-S subspace is made naturally to maximize the energy gain of the magnetic interaction. Additional calculations confirm this conclusion [139].

Other Extensions

At last, we mention other extensions briefly.

- **Off-diagonal spin interaction**
  In this dissertation we treat only diagonal spin interactions. Therefore we cannot apply our PFFRG to systems with non-diagonal spin interactions like Γ terms in extended Kitaev-Heisenberg model and Dzyaloshinskii-Moriya interaction directly. The Dzyaloshinskii-Moriya interaction was partially included in PFFRG by M. Hering and J. Reuther in 2017 [144, 145]. Then in 2019, F. L. Buessen and his collaborators extended PFFRG to treat general non-diagonal interactions [119].

- **Dynamical susceptibility**
  In PFFRG study, the dynamical susceptibility is calculated in probably only one literature [146]. PFFRG is formulated in Matsubara frequency representation and it can calculate $\chi_{ij}^{\mu\nu,\Lambda}(i\nu)$ directly. Thus we have to perform analytic continuation numerically to obtain retarded susceptibility. In Ref. [146], it was done by Padé approximation, but there are inevitable artificial discontinuities. Therefore the authors of that paper assumed the formula of the dynamical susceptibility and performed fitting to obtain it.

- **Cluster PFFRG**
  We consider an infinite system and assume that all sites are identical in our formulation. In 2014, J. Reuther and R. Thomale studied the bilayer Heisenberg model by extending PFFRG to cluster systems [146]. This cluster PFFRG uses

small spin clusters as the staring point of the flow. Another extension was proposed by D. Roscher and his collaborators in 2019 [147].

- **Magnetic field and magnetization**
  We do not consider magnetic field in PFFRG introduced in this chapter (see our general Hamiltonian Eq. (3.11)). In addition, we cannot calculate magnetization and susceptibility in ordered phase because we formulate FRG in phases with no symmetry breaking. PFFRG in magnetic field and ordered phase was conducted only in J. Reuther's dissertation [91]. In this case, we have to add magnetization terms proportional to the Pauli matrices to the self-energy, which is proportional to an identity matrix in spin space. Besides, the numerical costs increase greatly due to broken time-reversal symmetry. It is said that the computational complexity is 2048 times that of ordinary PFFRG for Heisenberg interaction [119].

- **SU(N) Heisenberg model**
  PFFRG for SU(N) Heisenberg spin systems are extended by F. L. Buessen and D. Roscher and their collaborators in real space [137] and in momentum space [148] in 2018. We can implement the real space extension by replacement of prefactors in flow equations as the same manner of spin-S extension we present above.

- **VBC and nematic order**
  We calculate only 1-particle and 2-particle vertices in 1-loop FRG even if we use Katanin truncation to include 2-loop correction partially. In general, m-particle Green's function can be obtained from tree diagrams composed of Green's functions and vertices of m-th order or less. Because this, we cannot calculate the susceptibility of the ordered state where the order operator is given by the product of two or more spins, directly. However, prescriptions for calculating those order, valence-bond crystal (VBC) order and nematic order for example, have been presented since the proposal of PFFRG [54]. In this prescription, we add a spin quadratic perturbation term corresponding to order which we investigate. For example, we consider the plaquette order in J_1-J_2 Heisenberg model on the square lattice described by the Hamiltonian Eq. (3.144). The perturbation term is

$$\mathcal{H}_{\mathrm{p}} = \delta \sum_{i_x,i_y} \left[(-1)^{i_x} \boldsymbol{S}_{i_x,i_y} \cdot \boldsymbol{S}_{i_x+1,i_y} + (-1)^{i_y} \boldsymbol{S}_{i_x,i_y} \cdot \boldsymbol{S}_{i_x,i_y+1}\right], \tag{3.171}$$

  where i_x and i_y are site indices along the x-axis and y-axis, respectively. We set the perturbative energy δ is much smaller than J_1 and J_2. The expectation value $\left\langle \sum_{i_x,i_y} \left[(-1)^{i_x} \boldsymbol{S}_{i_x,i_y} \cdot \boldsymbol{S}_{i_x+1,i_y} + (-1)^{i_y} \boldsymbol{S}_{i_x,i_y} \cdot \boldsymbol{S}_{i_x,i_y+1}\right] \right\rangle$ is the order parameter of the plaquette order. We define the susceptibility as

$$\chi_{\mathrm{p}}^{\Lambda} = \frac{J_1}{\delta} \frac{|C_1^{\Lambda} - C_2^{\Lambda}|}{C_1^{\Lambda} + C_2^{\Lambda}}, \tag{3.172}$$

  with the equal-time correlation function

$$C_1^{\Lambda} = \langle \boldsymbol{S}_{i_x,i_y} \cdot \boldsymbol{S}_{i_x+1,i_y} \rangle_{\mathrm{p}}, \tag{3.173}$$

$$C_2^{\Lambda} = \langle \boldsymbol{S}_{i_x+1,i_y} \cdot \boldsymbol{S}_{i_x+2,i_y} \rangle_{\mathrm{p}}, \tag{3.174}$$

where the expectation $\langle \cdots \rangle_{\mathrm{p}}$ means expectation value under the Hamiltonian $\mathcal{H} + \mathcal{H}_{\mathrm{p}}$. We calculate RG flow with the Hamiltonian $\mathcal{H} + \mathcal{H}_{\mathrm{p}}$ and trace the susceptibility of the plaquette order Eq. (3.172) along the flow. If this susceptibility diverges we conclude that there is onset of the plaquette order. This method have been used to investigate various orders [54, 135, 149–153].

- **Multi-loop PFFRG**
  In 2018, PFFRG was extended to include 2-loop contributions by M. Rück and T. Reuther [154]. Then, multi-loop extension is done by J. Thoenniss and his collaborators [155] and D. Kiese and his collaborators [156] simultaneously in 2020. Recently, multi-loop FRG for itinerant electron systems showed results which quantitatively coincide with the results by parquet approximation and deterministic quantum Monte Carlo [72]. It is expected that the accuracy of PFFRG also will be improved by multi-loop extension.

3.8 Summary of This Chapter

This chapter have been devoted to a detailed review to the PFFRG we used. First, we introduced the auxiliary fermionic representation of quantum spins, and discussed the projection from the enlarged Hilbert space to its physical subspace. Second, we parametrized the Green's functions and the vertices. Unlike the examples in Sec. 2.6, in PFFRG we use real-space representation. Based on this parametrization, we derive the explicit PFFRG flow equations for the models with the Kitaev-type interactions which are treated in this dissertation.

Then, We have also introduced Katanin truncation in order to incorporate the effects of frustration and quantum fluctuations into the flow equations. The static limit was also discussed. The main result calculated by PFFRG is the spin susceptibility. We define the spin susceptibility in a path integral representation and derive its formula using the Green functions and the vertices obtained by PFFRG.

Finally, a short review of each of the PFFRG extensions was given. In particular, the extensions for the finite temperature case and for the general spin-S case were explained in detail. These extensions are used in studies in the dissertation.

Chapter 4

Dipolar Kitaev Systems

In this chapter, we discuss the realization of Kitaev quantum spin liquids in systems of molecular gases pinned in optical lattices rather than in solids. We can design various interactions in the polar molecular systems due to its high controllability. First, we confirm that these systems can be used as quantum simulators for the Heisenberg model. This model has a long-range interaction which has roots in the dipolar-dipolar interaction between polar molecules. Therefore it is required to use numerical methods for large-size calculation. We then introduce previous studies by PFFRG. Next, we mention the implementation of Kitaev type interaction using microwave dressing proposed in 2013 [34, 35]. And then, we define the dipolar Kitaev model based on these proposals and reveal the ground state phase diagram of the model using PFFRG. The main part of this chapter will be submitted as Ref. [157].

4.1 Ultracold Polar Molecules as Quantum Simulators

Ultracold polar molecular systems are one of the "hot" themes in condensed matter physics [158–161]. Experimental study on the control of ultracold polar molecules has made great progress since 2000s [162–181]. Various bialkali molecules have been created by Feshbach resonance: KRb [162], Cs_2 [163], Rb_2 [164], LiCs [165, 166], RbCs [174, 175], NaK [176, 179, 180] , NaRb [177], and NaLi [178]. Even in the last few years, new molecules have been produced intensively. Since 2006, before the production of these molecules, the research using these polar molecules as quantum simulators, by manipulating their interactions, has been carried out [34, 35, 182–191]. The idea of a quantum simulator is to simulate one quantum system using another controllable quantum system. The basic idea originated from Richard P. Feynman [192]. As another application of polar molecules, their application to quantum computation is also expected and being intensively studied [193–199].

This chapter focuses in particular on the application of ultracold polar molecular systems trapped in optical lattices as quantum simulators of the spin systems. Here we introduce a model called "dipolar Heisenberg (XXZ) model" which is ultracold polar molecular realization of the quantum Heisenberg (XXZ) model and we mention calculation for it by PFFRG. Then we refer to the realization of Kitaev-type interaction in those systems and our calculation for "dipolar Kitaev model", which is the implementation of the Kitaev model in polar molecular system, to clarify feasibility of the Kitaev quantum spin liquid. Before we discuss the feasibility of it, we examine the size dependence of PFFRG results and check how large system size we should take. After that, we discuss the realization of the quantum spin liquid by calculating the spin susceptibilities with changing the parameters.

4.2 Dipolar Heisenberg Model

We consider an ultracold polar molecular (KRb or LiCs, for example) system confined to a two dimensional plane and each molecule is pinned in a deep optical lattice. [34, 35, 185, 191] In order to simulate spin systems, here the optical lattice is deep enough to localize each molecule in each site although generally we can consider Hubbard [182, 187] and t-J [185, 186, 200] -type models to allow molecules to hop. The non-interacting Hamiltonian describing each molecule is

$$\mathcal{H}_0 = B_v \boldsymbol{N} - E d^z. \tag{4.1}$$

Each molecule can be treated by a rigid motor with angular momentum $\boldsymbol{N}$, dipole moment $\boldsymbol{d}$, and rotational constant B_v. The symbol E in Eq. (4.1) represents DC electric field along z-axis. We assume the system extends in the xy-plane with the z-axis oriented perpendicular to it. In $E = 0$, we can take the simultaneous eigenstates of the square of the total angular momentum $\boldsymbol{N}^2$ and the z-component of the angular momentum N^z with each eigenvalue $N(N+1)$ and M, respectively, as eigenstates of the Hamiltonian Eq. (4.1). We denote these eigenstates as $|N, M\rangle$. If we turn on E, the eigenstates $|N, M\rangle_{E=0}$ adiabatically connect $|N, M\rangle_{E\neq 0}$. There is dipole-dipole interaction between molecules and its Hamiltonian is written as

$$\mathcal{H}_{\text{d-d}} = \frac{1}{2} \sum_{i,j}^{i\neq j} H_{ij}, \tag{4.2}$$

with

$$H_{ij} = \frac{\boldsymbol{d}_i \cdot \boldsymbol{d}_j - 3(\boldsymbol{d}_i \cdot \hat{\boldsymbol{r}}_{ij})(\boldsymbol{d}_j \cdot \hat{\boldsymbol{r}}_{ij})}{r_{ij}^3}. \tag{4.3}$$

Here, $\boldsymbol{r}_{ij}$ is the vector connecting the site i and the site j, and r_{ij} is its norm denoting the distance between sites i and j. In addition, $\hat{\boldsymbol{r}}_{ij}$ is normalized vector $\hat{\boldsymbol{r}}_{ij} = \boldsymbol{r}_{ij}/r_{ij}$. This H_{ij} can be expanded with the spherical harmonics as

$$H_{ij} = -\frac{\sqrt{6}}{r_{ij}^3} \sum_{m=-2}^{2} (-1)^m C^2_{-m}(\theta_{ij}, \phi_{ij}) T^2_m(\boldsymbol{d}_i, \boldsymbol{d}_j), \tag{4.4}$$

where

$$C^l_m(\theta_{ij}, \phi_{ij}) = \sqrt{\frac{4\pi}{2l+1}} Y_{lm}(\theta_{ij}, \phi_{ij}). \tag{4.5}$$

The components of $\boldsymbol{r}_{ij}$ in the spherical coordinates are denoted as $(r_{ij}, \theta_{ij}, \phi_{ij})$ and $Y_{lm}(\theta_{ij}, \phi_{ij})$ is spherical harmonics with polar angle θ_{ij} and azimuthal angle ϕ_{ij}. T^2_m is an operator defined as

$$T^2_{\pm 2}(\boldsymbol{d}_i, \boldsymbol{d}_j) = d_i^{\pm} d_j^{\pm}, \tag{4.6}$$

$$T^2_{\pm 1}(\boldsymbol{d}_i, \boldsymbol{d}_j) = \frac{d_i^0 d_j^{\pm} + d_i^{\pm} d_j^0}{\sqrt{2}}, \tag{4.7}$$

$$T^2_0(\boldsymbol{d}_i, \boldsymbol{d}_j) = \frac{d_i^+ d_j^- + d_i^- d_j^+ + 2 d_i^0 d_j^0}{\sqrt{6}}, \tag{4.8}$$

with ladder operators

$$d_i^{\pm} = \mp \frac{d_i^x + \mathrm{i} d_j^y}{\sqrt{2}}, \tag{4.9}$$

$$d_i^0 = d_i^z. \tag{4.10}$$

Therefore, the operator $T_m^2(\boldsymbol{d}_i, \boldsymbol{d}_j)$ changes M of the two molecules on the sites i and j by m. According to Ref. [34], for $r \sim 0.4$ μm, $d^2/r^3 \sim 1$ (100) kHz in KRb (LiCs) molecules, and $B_v \sim 1$ GHz from Ref. [185]. We have to select two rotational states and regard them as "spin" degrees of freeedom, for example $|\uparrow\rangle = |1,0\rangle$ and $|\downarrow\rangle = |0,0\rangle$, to derive a spin Hamiltonian (with $S = 1/2$). Finally, it is required to project Hilbert space to the subspace spanned by $\{|\uparrow\rangle, |\downarrow\rangle\}$ and it is justified by sufficient large E. According to Ref. [185], this condition is achievable for ^{40}K^{87}Rb, and for ^{7}Li^{133}Cs required E is even lower. We define the spin operator $\boldsymbol{S}_i = (S_i^x, S_i^y, S_i^z)$ as the usual spin operator with $S = 1/2$. In this case, the terms in the Hamiltonian Eq. (4.4) not conserving S_i^z are strongly off-resonant. Hence we can drop these terms and only C_0^2 term contributes. As a result, we obtain

$$H_{ij} = -\frac{\sqrt{6}}{r_{ij}^3} \cdot (-1)^0 \cdot \sqrt{\frac{4\pi}{5}} \cdot \underbrace{\sqrt{\frac{5}{16\pi}}(3\cos^2\theta_{ij} - 1)}_{Y_{20}(\theta_{ij},\phi_{ij})} \cdot \underbrace{\frac{2}{\sqrt{6}}\left\{\frac{1}{2}\left(S_i^+ S_j^- + S_i^- S_j^+\right) + S_i^0 S_j^0\right\}}_{T_0^2(\boldsymbol{d}_i,\boldsymbol{d}_j)}$$

$$= (1 - 3\cos^2\theta_{ij})\boldsymbol{S}_i \cdot \boldsymbol{S}_j. \tag{4.11}$$

Here, our lattice expands in xy-plane and $\theta_{ij} = \pi/2$. Therefore,

$$\mathcal{H}_{\text{eff}} = \frac{1}{2}\sum_{i,j}^{i\neq j} \frac{\boldsymbol{S}_i \cdot \boldsymbol{S}_j}{r_{ij}^3}. \tag{4.12}$$

This is a dipolar antiferromagnetic Heisenberg Hamiltonian.

4.3 Numrical Study for Quantum Dipolar Spin Systems

In 2017, H. Zou, E. Zhao, and V. Liu defined the dipolar XXZ ($\eta \neq 1$) and Heisenberg ($\eta = 1$) model on the square lattice as

$$\mathcal{H} = \frac{J}{2}\sum_{i,j}^{i\neq j} \frac{1 - 3(\hat{\boldsymbol{r}}_{ij} \cdot \hat{\boldsymbol{d}})}{r_{ij}^3}(S_i^x S_j^x + S_i^y S_j^y + \eta S_i^z S_j^z), \tag{4.13}$$

with the exchange anisotropy η, and performed tensor renormalization group (TRG) calculation as well as spin wave and Schwinger boson mean-field calculation [201]. Here, they considered the case DC electric field points in the general direction called "dipole tilting angle" (θ, ϕ) and introduced the vector $\hat{\boldsymbol{d}} = (\cos\phi\sin\theta, \sin\phi\sin\theta, \cos\theta)$. $\hat{\boldsymbol{d}}$ controls spatial anisotropy of interaction. They calculated phase diagram mainly for $\eta = 1$ (dipolar Heisenberg model) by changing θ and ϕ as parameters, and found 4 phases; Néel AFM, stripe, spiral, and quantum paramagnetism. As well, Y. N. Yao and his collaborators perform density matrix renormalization (DMRG) calculation for the Hamiltonian Eq. (4.13) on the Kagome and triangular lattice and they found quantum spin liquid behavior near $\eta = 1$ and $\theta = 0$ in 2018 [191]. However, in both

TRG and DMRG, calculation is limited to small system size due to (quasi-) long-range property of the dipole interaction [1]. We have to truncate interaction for unit cell size L and the bond dimension D [201] and small cluster size and small bond dimension are insufficient to describe spiral orders in which the ordering wave vector locates incommensurate points. Indeed, Zou and his collaborators could not perform TRG calculation beyond $\phi \sim 20^\circ$ due to that. Later, E. Zhao who is one of the authors of the above paper Ref. [201], conducted studies to clarify the ground state phase diagrams of the dipolar Heisenberg model on the square lattice [202] and the triangular lattice [125] by PFFRG together with A. Keleş, in order to overcome this limitation. By PFFRG, they calculated the spin susceptibility in all range of θ and ϕ (the range of ϕ was reduced by lattice symmerty) and elucidated that there are competing orders Néel AFM, stripe, and spiral order and spin liquid phase near the boundary between Néel AFM and stripe/spiral orders on the square lattice, and in the triangular lattice there is no 120° AFM order phase and there is quantum paramagnetic phase instead of that phase. As shown by them, PFFRG is good numerical method for quantum dipolar spin systems because we can treat large size systems in 2 or 3 dimension to consider (quasi-) long-range interaction and describe incommemsulate magnetic orders. There is no difference in computational costs between to treat a system with nearest-neighbor interaction and to treat a systems with long-range interaction, for PFFRG if the system sizes are the same. For these reasons, in this chapter we choose PFFRG as a numerical method to investigate quantum dipolar spin systems.

4.4 Realization of Kitaev-type Interactions

For the realization of the quantum spin systems in the ultracold polar molecular systems described above, we can only obtain limited variety of interactions. In 2013, it was proposed that we can control each coefficient C^2_{-m} in Eq. (4.4) independently by making linear combinations of molecular rotation states by microwave radiation [34, 35]. In addition, a general spin-S Hamiltonian can also be realized by selecting $2S+1$ disjoint sets of $|N, M\rangle$ for each molecule and coupling them within each set by microwave fields. Therefore, we can obtain a large variety of spin Hamiltonians by microwave dressing. As an example, $S = 1/2$ Kitaev-like bond-dependent Ising-type interaction is realized by controling the coefficients C^2_{-m} and coupling 25 rotational states [34, 35]: the states $|\uparrow\rangle$ and $|\downarrow\rangle$ are made by linear coupling of 12 and 13 states

$$\begin{aligned}\big\{&|2,-1\rangle,\ |2,0\rangle,\ |2,2\rangle,\ |3,-1\rangle,\ |3,1\rangle,\ |3,2\rangle,\\ &|3,3\rangle,\ |4,-4\rangle,\ |4,-3\rangle,\ |4,-1\rangle,\ |4,1\rangle,\ |4,3\rangle\big\},\end{aligned} \tag{4.15}$$

and

$$\begin{aligned}\big\{&|0,0\rangle,\ |1,-1\rangle,\ |1,0\rangle,\ |1,1\rangle,\ |2,-2\rangle,\ |2,1\rangle,\ |3,-3\rangle,\\ &|3,-2\rangle,\ |3,0\rangle,\ |4,-2\rangle,\ |4,0\rangle,\ |4,2\rangle,\ |4,4\rangle\big\},\end{aligned} \tag{4.16}$$

[1] In 2-dimensional systems, the dipole interaction $\sim 1/r^3$ is quasi-long-range, strictly speaking:

$$\lim_{R\to\infty}\int_a^R \mathrm{d}^2 r\ \frac{1}{r^3} \tag{4.14}$$

converge, where a is a lattice constant as a natural short-range (ultraviolet) cutoff.

respectively. The coefficients and more detailed procedures are written in Ref. [35]. In the next chapter we define "dipolar Kitaev model" based on the proposal in this paper. The realization of Kitaev model in polar molecular systems was also suggested in 2006 [183]. This realization is perturbative although the implementation in Ref. [35] is based on dipole-dipole interaction directly. Thereby, the latter implementation has stronger interaction and easier to access experimentally. Note that the interactions are still long-range in the implementation of spin-spin interactions described in this chapter because these interactions have roots in the dipole-dipole interaction between polar molecules. The dipole Kitaev model is not exception (see Eq. (4.17) in the next section) as well as the dipolar Heisenberg (XXZ) model Eq. (4.13). Consequently it has long-range interaction in addition to nearest-neighbor Kitaev-type interaction. It is not clear whether Kitaev quantum spin liquid is stabilized or not in the model with long-range interaction because spin-spin correlations beyond nearest-neighbors strictly vanish in the original Kitaev model [13, 29]. In Ref. [35], authors remark on this point:

> *While in some cases long-range corrections are weak enough to ensure the survival of the desired phases, it is an open question whether this holds for the present example.*

There is no studies on the phase diagram of the proposed model and it has not been clarified whether quantum spin liquid is realized until now. The goal in this chapter is to unravel whether Kitaev quantum spin liquid realizes in dipolar model and polar molecules can be used as a quantum simulator of the Kitaev model, by PFFRG calculation. If so, we also have to clarify the difference with the quantum spin liquid state in the original Kitaev model. If not, it is also our aim to clarify what happens in the dipolar model and to suggest modified implementation for the realization of Kitaev quantum spin liquid in ultracold polar molecular systems.

4.5 Dipolar Kitaev Model

In this section, we define the dipolar Kitaev model based on the works in Ref. [34, 35] as a model for a $S = 1/2$ quantum simulator realized in ultracold polar molecular systems trapped in deep hexagonal optical lattice:

$$\begin{aligned}\mathcal{H} &= \frac{1}{2}\sum_{i,j}^{i\neq j} H_{ij}, \\ H_{ij} &= -\frac{1}{3r_{ij}^3}\Big\{ J_x[1-2\cos\Big(2\Phi_{ij}-\frac{4\pi}{3}\Big)]S_i^xS_j^x \\ &\qquad + J_y[1-2\cos\Big(2\Phi_{ij}-\frac{2\pi}{3}\Big)]S_i^yS_j^y \\ &\qquad + J_z[1-2\cos\left(2\Phi_{ij}\right)]S_i^zS_j^z\Big\}. \end{aligned} \tag{4.17}$$

We modify two points from a suggested Hamiltonian in Ref. [35]. First, we consider the case $J_x \neq J_y \neq J_z$ though $J_x = J_y = J_z$ in Ref. [35]. It can be considered that anisotropic $J_x \neq J_y \neq J_z$ is easily implemented thanks to the controllability of the polar molecular systems. Second, we relabel the bond directions (x, y, z) for convenience in numerical calculations. Here, $\boldsymbol{r}_{ij}$ is the vector connecting from site i to site j and $r_{ij} = |\boldsymbol{r}_{ij}|$ is its norm, as defined in Sec. 4.2. We set the lattice constant

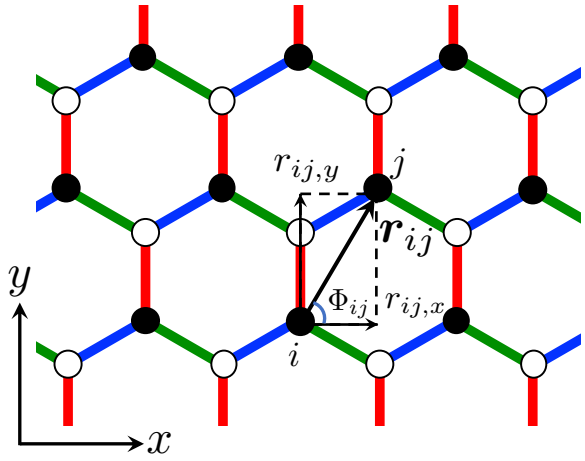

FIGURE 4.1: Schematic figure showing the definition of $\boldsymbol{r}_{ij}$ and Φ_{ij} in the dipolar Kitaev model Eq. (4.17)

as unity. Here we define the lattice constant as a length of a bond, not as a length of the primitive vectors of underlying Bravais lattice. The angle Φ_{ij} is defined as the angle of $\boldsymbol{r}_{ij}$ measured from the x-axis. These definitions are shown in Fig. 4.1. Another representation of Φ_{ij} is the argument of the complex number $r_{ij,x} + \mathrm{i}r_{ij,y}$ i.e. $\mathrm{Arg}(r_{ij,x} + \mathrm{i}r_{ij,y})$ in the complex $x + \mathrm{i}y$ plane where $r_{ij,x}$ and $r_{ij,y}$ are the x- and y-component of the vector $\boldsymbol{r}_{ij}$ (see Fig. 4.1). The summation $\sum_{i,j}$ runs over all sites with the constraint $i \neq j$. This model has the angle-dependent Ising-type interaction which is dipolar generalization of the original Kitaev model. Let us focus on the site labeled i in Fig. 4.1 and consider the interaction between nearest-neighbors sites. At first, we consider the nearest-neighbor site connected with the site i by a blue bond. In this case, $r_{ij} = 1$ and $\Phi_{ij} = -\frac{5\pi}{6}$ and

$$1 - 2\cos\left(2\Phi_{ij} - \frac{4\pi}{3}\right) = 3, \tag{4.18}$$

$$1 - 2\cos\left(2\Phi_{ij} - \frac{2\pi}{3}\right) = 0, \tag{4.19}$$

$$1 - 2\cos\left(2\Phi_{ij}\right) = 0. \tag{4.20}$$

Hence the two-site interaction Hamiltonian in Eq. (4.17) is $H_{ij} = -J_x S_i^x S_j^x$. In the same manner, the interactions between the site i and the nearest-neighbor site connected by a green ($\Phi_{ij} = -\frac{\pi}{6}$) and red ($\Phi_{ij} = \frac{\pi}{2}$) bond are $H_{ij} = -J_y S_i^y S_j^y$ and $H_{ij} = -J_z S_i^z S_j^z$, respectively. Therefore, the interactions between nearest-neighbor sites are consistent with the original Kitaev model [13]. Then we consider the interaction between the next-nearest-neighbors. As an example, we focus on the site labeled as j in Fig. 4.1. The distance between two sites is $r_{ij} = \sqrt{3}$ and the angle is $\Phi_{ij} = \frac{\pi}{3}$. Thus,

$$1 - 2\cos\left(2\Phi_{ij} - \frac{4\pi}{3}\right) = 2, \tag{4.21}$$

$$1 - 2\cos\left(2\Phi_{ij} - \frac{2\pi}{3}\right) = -1, \tag{4.22}$$

$$1 - 2\cos\left(2\Phi_{ij}\right) = 2, \tag{4.23}$$

and the interaction is

$$H_{ij} = -\frac{1}{9\sqrt{3}}[2J_x S_i^x S_j^x - J_y S_i^y S_j^y + 2J_z S_i^z S_j^z]. \tag{4.24}$$

The magnitude of the interaction reduces by $1/(\sqrt{3})^3 = 1/(3\sqrt{3}) \simeq 1/5$ relative to the nearest-neighbor interaction. As shown in Eq. (4.24), interactions of each spin component change its signs and magnitudes depending on positions of interacting sites beyond nearest-neighbor. For this reason, the model appears to be highly frustrated.

4.6 Size Dependence and Finite Size Scaling

Hereafter, we perform PFFRG calculation to obtain the spin susceptibility. We consider the case $J_x = J_y \neq J_z$ in Eq. (4.17) and introduce the anisotropy parameter α ($0 \leq \alpha \leq 3/2$) as

$$\begin{aligned} J_x = J_y &= \pm J\alpha, \\ J_z &= \pm J(3 - 2\alpha), \end{aligned} \tag{4.25}$$

where the upper sign is for ferromagnetic (FM) case, the lower one is for antiferromagnetic (AFM) case. We take J as the energy unit ($J = 1$). In PFFRG calculation, we used 64 positive frequencies with logarithmic mesh between $\omega_{\min} \simeq 10^{-4}$ and $\omega_{\max} = 250$, and 212 Λ-points with $\Lambda_{i+1}/\Lambda_i = 0.95$ and $\Lambda_{\mathrm{UV}} = 500$. We benchmarked our PFFRG codes by reproduction of previous studies about models with Heisenberg-type interaction on square [54] and honeycomb [139] lattice and Kitaev-Heisenberg model on honeycomb lattice [136]. Our codes are designed for openMP+MPI hybrid parallelization and the calculations were performed in Oakbridge-CX in the Information Technology Center, The University of Tokyo, Oakforest-PACS in Center for Computational Sciences, University of Tsukuba and in the Information Technology Center, The University of Tokyo, and MASAMUNE-IMR in Center for Computational Materials Science, Institute for Materials Research, Tohoku University, and sekirei (system B) in the Supercomputer Center, the Institute for Solid State Physics, the University of Tokyo.

For numerical simulation of models with long-range interaction, there is a well-established method called "Ewald sum" [203, 204]. Indeed, Monte Carlo studies of classical Heisenberg dipolar lattice systems [2] on the square, triangular, honeycomb, and Kagome lattices was performed by this trick [205]. However, this trick cannot be implemented in PFFRG formulated in the real space directly [3]. Thus, at first, we conduct calculation while changing the cluster size L to examine the convergence. We consider FM case and set the anisotropy parameter at isotropic point $\alpha = 1$ because we can reduce calculation costs largely for lattice symmetry. We show calculated static spin susceptibility for various system sizes in Fig. 4.2. For the case $\alpha = 1$ the system has the symmetry related simultaneous lattice and spin $3\pi/2$ rotation (along $\boldsymbol{a}_3$-axis for lattice and (1, 1, 1)-direction for spin). It is sufficient to calculate χ^{zz} for

[2] Note that this model

$$\mathcal{H} = \frac{1}{2}\sum_{i,j}^{i\neq j}\left[\frac{\boldsymbol{S}_i \cdot \boldsymbol{S}_j}{r_{ij}^3} - 3\frac{(\boldsymbol{S}_i \cdot \boldsymbol{r}_{ij})(\boldsymbol{S}_j \cdot \boldsymbol{r}_{ij})}{r_{ij}^5}\right], \tag{4.26}$$

is different from the dipolar Heisenberg model described in Eq. (4.13) introduced before in this chapter for the realization of the quantum Heisenberg model in ultracold polar molecules.

[3] In the papers for dipolar Heisenberg model [125, 202], authors do not mention this point

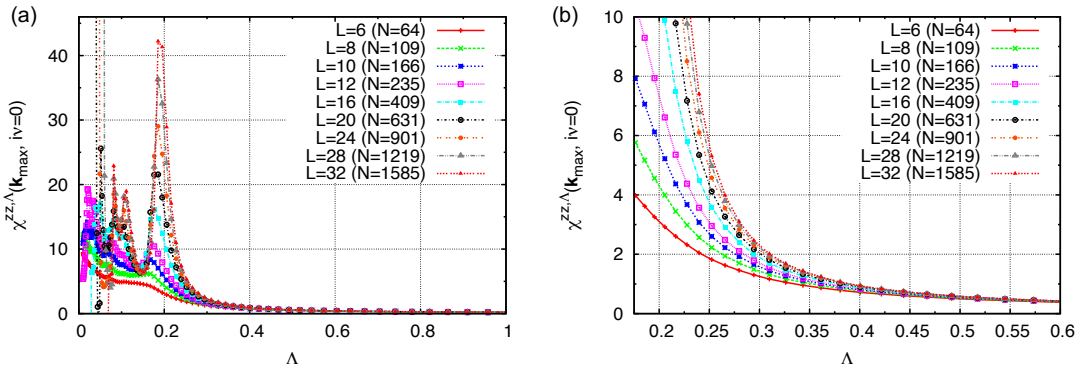

FIGURE 4.2: Calculated static spin susceptibilities (z-component) with different L. (a) $\Lambda = 0$ to 1, and (b) $\Lambda = 0.175$ to 0.6.

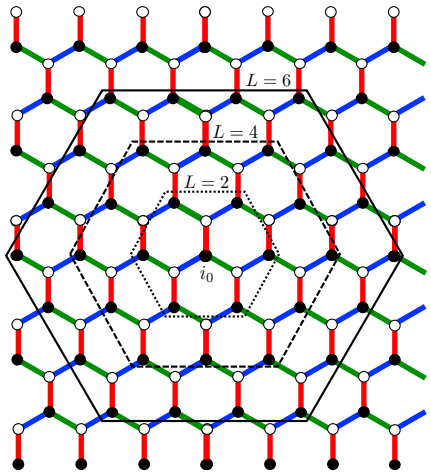

FIGURE 4.3: Schematic figure showing the definition of the cluster with L ($L = 2,\ 4,$ and 6). If we regard site locating center of the figure and labeled i_0 as the reference site, the cluster with $L = 2, 4$, and 6 are sets of sites surrounded by dotted line, dashed line, and thick line, respectively.

this reason. χ^{xx} and χ^{yy} are obtained by $3\pi/2$ and $-3\pi/2$ rotation of χ^{zz} in the momentum space, respectively. The argument $\boldsymbol{k}_{\max}$ is the wave vector at which the susceptibility has maximum value. The behavior of susceptibility shown in Fig. 4.2 indicate that the system undergoes phase transition to magnetic order (see Fig. 3.3) and its ordering wave vector corresponds to $\boldsymbol{k}_{\max}$. As we show later, $\boldsymbol{k}_{\max} = (0, 0)$ and it corresponds FM order. L denotes the distance from the site at the center of the cluster to the farthest site. This distance is defined by the length of the shortest path on the lattice connecting the two sites. Thereby it characterizes system size of the cluster. The clusters with different Ls ($L = 2,\ 4,$ and 6) are shown in Fig. 4.3, for example. N denotes the number of sites in each cluster. As we mention in the footnote in Sec. 4.3, the dipolar interaction $\sim r^{-3}$ is convergent (more precisely absolutely convergent) in two dimensional systems. Thus, as L increases the susceptibility converges, but slowly. To confirm this behavior we show an enlarged section of $\Lambda = 0.175$ to 0.6 in Fig. 4.2 (b).

To obtain ordering scale (critical cutoff) Λ_c of the $L \to \infty$ system, we estimated it

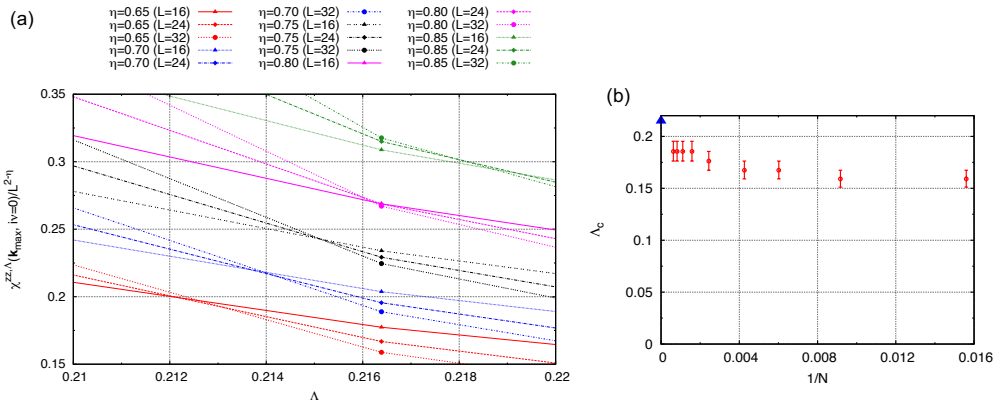

FIGURE 4.4: (a) $\chi^{zz,\Lambda}/L^{2-\eta}$ vs. Λ for $L = 16, 24, 32$ and various values of η for finite size scaling. (b) Ordering scale Λ_c vs. inverse of cluster sites $1/N$. The red circles with error bars indicate calculated breakdown scales and the blue triangle shows its estimated value by finite size scaling with $\eta = 0.75$. The error bars reflect the spacing of the Λ-mesh.

by finite-size scaling. If χ^{Λ} satisfies a scaling relation we know well for the susceptibility at finite temperature,

$$\frac{\chi^{\Lambda}_{L}}{L^{2-\eta}} = f_{\chi}\left(L^{1/\nu}\left|\frac{\Lambda-\Lambda_c}{\Lambda_c}\right|\right), \tag{4.27}$$

where χ^{Λ}_{L} and f_{χ} are susceptibility calculated by PFFRG in size-L cluster and scaling function of susceptibility, respectively. η and ν are critical exponents. As we can see in the above relation, if $\Lambda = \Lambda_c$, $\chi^{\Lambda}_{L}/L^{2-\eta}$ has the same value for any L. We used the data of $L = 16, 24, 32$, and plotted $\chi^{zz}/L^{2-\eta}$ for Λ while changing the value of η. When all the data crossed at one point, that point was determined as the estimated value of Λ_c. The result of the finite size scaling and obtained Λ_c are shown in Fig. 4.4. From finite size scaling as shown in Fig. 4.4 (a), we obtain an estimated ordering scale $\Lambda_c \approx 0.215$ and the exponent $\eta \approx 0.75$. Here, some uncertainty remains at the intersections because we use a coarse Λ-mesh to reduce computation costs. We plot obtained values of Λ_c for $1/N$ in Fig. 4.4 (b). The red circles with error bars represent Λ_c obtained from the flow of the susceptibility shown in Fig. 4.2 and the blue triangle indicates $\Lambda_c \approx 0.215$ obtained by finite size scaling shown in Fig. 4.4 (a). The critical exponent $\eta \approx 0.75$ obtained by finite size scaling is large. Our model Eq. (4.17) has $\mathbb{Z}_6$ symmetry in spin space at $\alpha = 1$. It is known that the exponent is the same with its value of the Ising model $\eta = 0.25$ from studies on 6-state clock model [206–208] [4]. We can consider that this difference in the critical exponent is caused by the difference between Λ and T. It is not strange that finite temperature calculation and zero temperature calculation with cutoff Λ yield different exponents, although both act as infrared cutoffs and they satisfy the relation Eq. (3.150) in high energy/high temperature region. There was no significant change when the finite-size scaling was redone by replacing the definition of L with $L = \sqrt{N}$. From Fig. 4.2

[4] More precisely, there are intermediate BKT (Berezinskii-Kosterlitz-Thouless) phase [209–211] between ordered and disordered phases in 6-state clock model and classical Kitaev-Heisenberg model. The exponent η varies form $1/4$ (at the boundary between disordered and BKT phases) to $1/9$ (at the boundary between BKT and ordered phases).

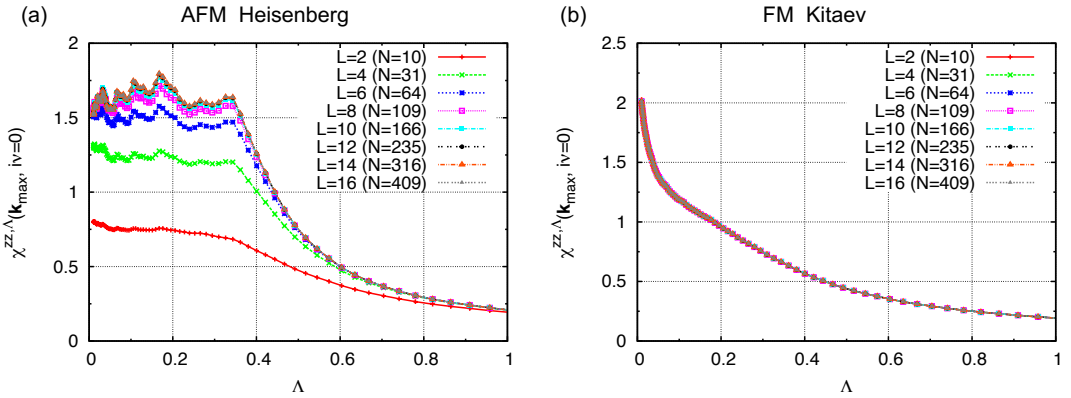

FIGURE 4.5: Calculated static spin susceptibilities (z-component) of (a) the nearest-neighbor AFM Heisenberg model and (b) the Kitaev model with different L.

and Fig. 4.4, we can conclude that $L \geq 10 - 12$ is sufficient to examine whether the system is ordered or not, and that Λ_c deviates only the order of $0.01J$ from the estimate obtained by finite size scaling. We set $L = 20$ for further calculation.

In addition, we show the size dependence of the susceptibility for the nearest-neighbor AFM Heisenberg model on honeycomb lattice and the original Kitaev model in Fig. 4.5, for comparison. The susceptibility of the AFM Heisenberg model (Fig. 4.5 (a)) converges when $L \geq 8$ and indicates the phase transition (to Néel order). Note that spins have full SU(2) symmetry in the Heisenberg model and do not order actually due to Mermin-Wagner theorem [212]. It is an artifact of PFFRG which overestimates ordering tendency [99]. On the other side, The susceptibility of the Kitaev model (Fig. 4.5 (b)) seems to converge even if $L = 2$. This reflects the fact that there are only the nearest-neighbor spin correlations in Kitaev quantum spin liquid state [13, 29]. Comparing the size dependence shown in Fig. 4.2 and Fig. 4.5, we can see that the convergence in the dipolar Kitaev model is very slow.

4.7 Susceptibilities for Various Anisotropy Parameters

In the next step, we calculated the spin susceptibility of the model while changing the anisotropy parameter α and the sign of interaction. In the isotropic case $\alpha = 1$, only the $1/6$ region of the system should be dealt with due to the symmetry, so that the calculation cost can be reduced. However, three times the area in the isotropic case must be calculated if $\alpha \neq 1$. Therefore we set $L = 20$ to reduce computational costs. In this case, we have to solve about 1.65×10^8 coupled integro-differential equations.

At first, we consider FM case i.e. upper sign in Eq. (4.25). Calculated Λ-dependence of the static susceptibilities for some α is shown in Fig. 4.6. If $\alpha \neq 1$, χ^{xx} and χ^{yy} are related by symmetry and we can get one from the other by reversing the sign of k_x, while χ^{xx} and χ^{zz} are not related. Therefore we calculated χ^{zz} and χ^{xx}. At the isotropic point $\alpha = 1$, these two components have the same values as shown in Fig. 4.6 (f). If $0 \leq \alpha < 1$, $\chi^{zz,\Lambda}$ have larger values than $\chi^{xx,\Lambda}$ (Fig. 4.6 (a)-(e)) because the interaction between z-components of spins is dominant. On the other hand, $\chi^{xx,\Lambda}$ is larger than $\chi^{zz,\Lambda}$ for $1 < \alpha \leq 3/2$. We can see that the system undergoes a

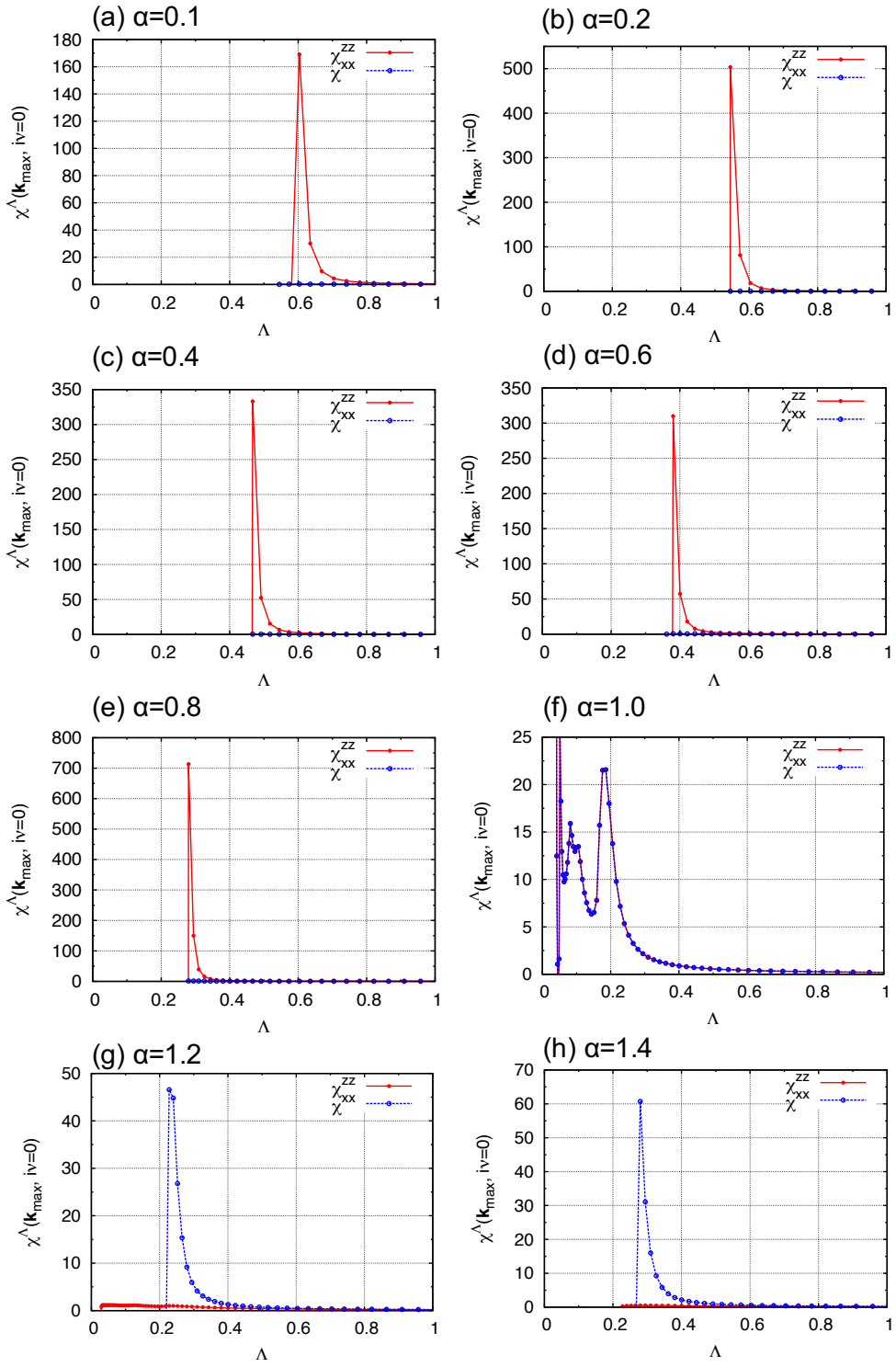

FIGURE 4.6: Calculated static spin susceptibilities $\chi^{zz,\Lambda}$ and $\chi^{xx,\Lambda}$ vs. Λ for some velues of α in the FM case. The results for $\alpha = 0.1$, 0.2, 0.4, 0.6, 0.8, 1.0, 1.2, and 1.4 are shown in (a)-(h), in order.

phase transition to magnetic ordered phase for all α. We show the momentum dependence of the susceptibilities at each critical cutoff Λ_c in Fig. 4.7. In each plot, the inner hexagon and the outer hexagon represent the first and the extended (second) Brillouin zone, respectively. The relationship between the magnetic order and the peak position of the susceptibility is summarized in Fig. 5.14 in the next chapter. We conclude that the ground state of the system is in FM ordered phase for all α.
Next we calculate the homogeneous susceptibility χ^{Λ} obtained as

$$\chi^{\Lambda}(\boldsymbol{k}=0,\mathrm{i}\nu=0)=\sum_{\mu}\chi^{\mu\mu,\Lambda}(\boldsymbol{k}=0,\mathrm{i}\nu=0), \tag{4.28}$$

and calculate Curie-Weiss scale Λ_{CW} by fitting of its inverse. The Curie-Weiss scale is defined [136] as

$$\chi^{\Lambda}(\boldsymbol{k}=0,\mathrm{i}\nu=0)\propto\frac{1}{\Lambda-\Lambda_{\mathrm{CW}}}, \tag{4.29}$$

and it is a counterpart of the Curie-Weiss temperature. We show the Curie-Weiss fitting for some α, ordering scale and Curie-Weiss scale vs. α in Fig. 4.8. At large Λ the susceptibility obeys Curie-Weiss law (Fig. 4.8 (a)), while it deviates from the Curie-Weiss fitting due to quantum effects in low energy region (Fig. 4.8 (b)). We can see that the magnitude relationship between Λ_c and Λ_{CW} is reversed near isotropic point $\alpha=1$ in Fig. 4.8 (c). This means that near $\alpha=1$ the frustration becomes strong. For further understanding the change in the intensity of frustration, we calculated frustration parameter f obtained as

$$f=\frac{|\Lambda_{\mathrm{CW}}|}{\Lambda_c}, \tag{4.30}$$

in Fig. 4.8 (d). This is a phenomenological parameter originally defined by A. P. Ramirez in 1994 [213]. The same definition as Ref. [136] is adopted here for f. The system has strong frustration if $f\geq 5-10$. Now f has its maximum at $\alpha=1$. All three components of the quantum spin interact with the same intensity for isotropic case, so we can see that f is maximum. However, the maximum f is only about 1.4. We can assume that there is no point of strong frustration, even in the case of $J_x\neq J_y\neq J_z$, and therefore the quantum spin liquid state is unlikely to be realized, because f is too small at any α. The system is considered to be FM ordered for all J_x, J_y, and J_z in FM case.

Now let us move on to the AFM case in which we use lower signs in Eq. (4.25). As the above FM case, we calculated the static spin susceptibilities and plot its Λ-dependence in Fig. 4.9, and its momentum dependence at the critical cutoff Λ_c in Fig. 4.10. Even in AFM case, the spin and lattice symmetries are same with those in FM case. Thus we can obtain $\chi^{yy,\Lambda}(\boldsymbol{k},\mathrm{i}\nu)$ from $\chi^{xx,\Lambda}(\boldsymbol{k},\mathrm{i}\nu)$ by $k_x\leftrightarrow -k_x$. As we can see these figures, the zigzag AFM order is realized and the spin liquid state does not appear in all α. The corresponding peak position in extended Brillouin zone and a schematic spin pattern of the zigzag order is shown in Fig. 5.14 and Fig. 5.2 in the next chapter, respectively. Also as in FM case, we performed Curie-Weiss fitting and estimate the Curie-Weiss scale Λ_{CW} through it. Then we calculated the frustration parameter f and show these results in Fig. 4.11. the general trend is the same with FM case altough the Curie-Weiss scale is slightly smaller. Therefore, we can conclude that the ground state is zigzag AFM order for all J_x, J_y, and J_z in AFM case.

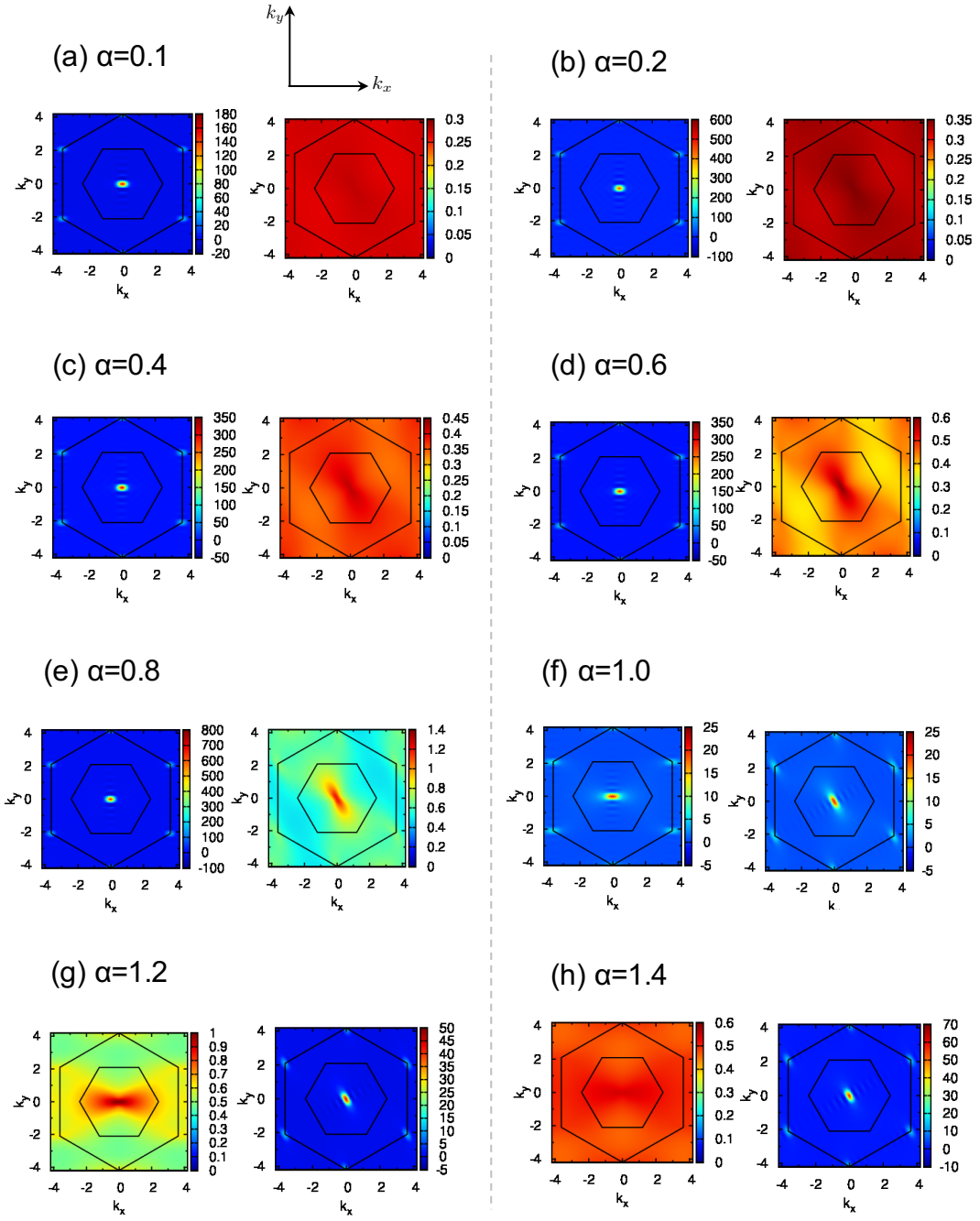

FIGURE 4.7: Momentum dependence of the static susceptibilities $\chi^{zz,\Lambda}$ and $\chi^{xx,\Lambda}$ at the ordering scale $\Lambda = \Lambda_c$. We consider FM case. The results for $\alpha = 0.1$, 0.2, 0.4, 0.6, 0.8, 1.0, 1.2, and 1.4 are shown in (a)-(h), in order. For each α, left panel and right panel show $\chi^{zz,\Lambda_c}(\boldsymbol{k}, i\nu = 0)$ and $\chi^{xx,\Lambda_c}(\boldsymbol{k}, i\nu = 0)$, respectively.

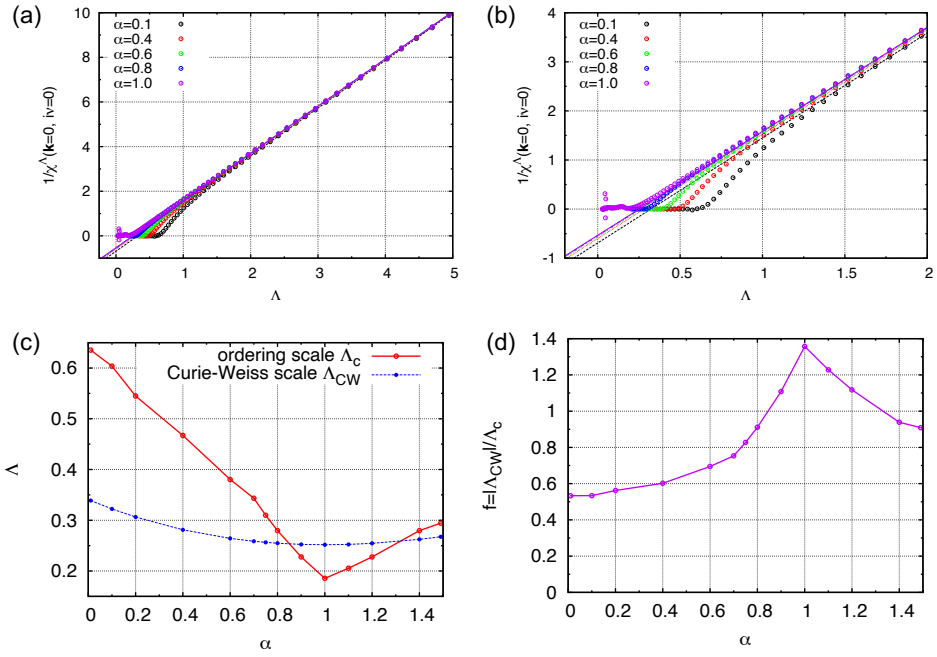

FIGURE 4.8: Λ-dependence of inverse of uniform static spin susceptibility $1/\chi^{\Lambda}(\boldsymbol{k}=0, i\nu=0)$ with Curie-Weiss fitting for some α values in (a) $\Lambda \in [-0.25, 5]$ and (b) $\Lambda \in [-0.2, 2]$. (c) The ordering scale (critical cutoff) Λ_c and Curie-Weiss scale Λ_{CW}, and (d) frustration parameter f vs. anisotropy parameter α. All panels show the results for FM dipolar Kitaev model.

4.8 Collapse of the Kitaev Quantum Spin Liquid

The ground state is FM/zigzag AFM order in dipolar Kitaev model whose interactions are long-ranged, though that in the original Kitaev model with only the nearest-neighbor exchange interactions is quantum spin liquid. Recall that the nearest-neighbor interactions in the dipolar Kitaev model are the same as those in the Kitaev model. So how are these two models connected with each other? What causes the breakdown of the quantum spin liquid state? To find the answers to these questions, we introduce the range of interaction $L_{\rm int}$ as an additional parameter and consider the dipolar Kitaev model with $L_{\rm int}$,

$$\begin{aligned}
\mathcal{H} &= \frac{1}{2}\sum_{i,j}^{1\le\|\boldsymbol{r}_{ij}\|_{\rm b}\le L_{\rm int}} H_{ij}, \\
H_{ij} &= -\frac{J}{3r_{ij}^3}\Big\{[1-2\cos\Big(2\Phi_{ij}-\frac{4\pi}{3}\Big)]S_i^xS_j^x \\
&\qquad + [1-2\cos\Big(2\Phi_{ij}-\frac{2\pi}{3}\Big)]S_i^yS_j^y \\
&\qquad + [1-2\cos\left(2\Phi_{ij}\right)]S_i^zS_j^z\Big\},
\end{aligned} \tag{4.31}$$

where the summation $\sum_{i,j}^{1\le\|\boldsymbol{r}_{ij}\|_{\rm b}\le L_{\rm int}}$ means the summation over all sites for each of i and j with constraint $1 \le \|\boldsymbol{r}_{ij}\|_{\rm b} \le L_{\rm int}$. The norm $\|\boldsymbol{r}_{ij}\|_{\rm b}$ is defined as the shortest

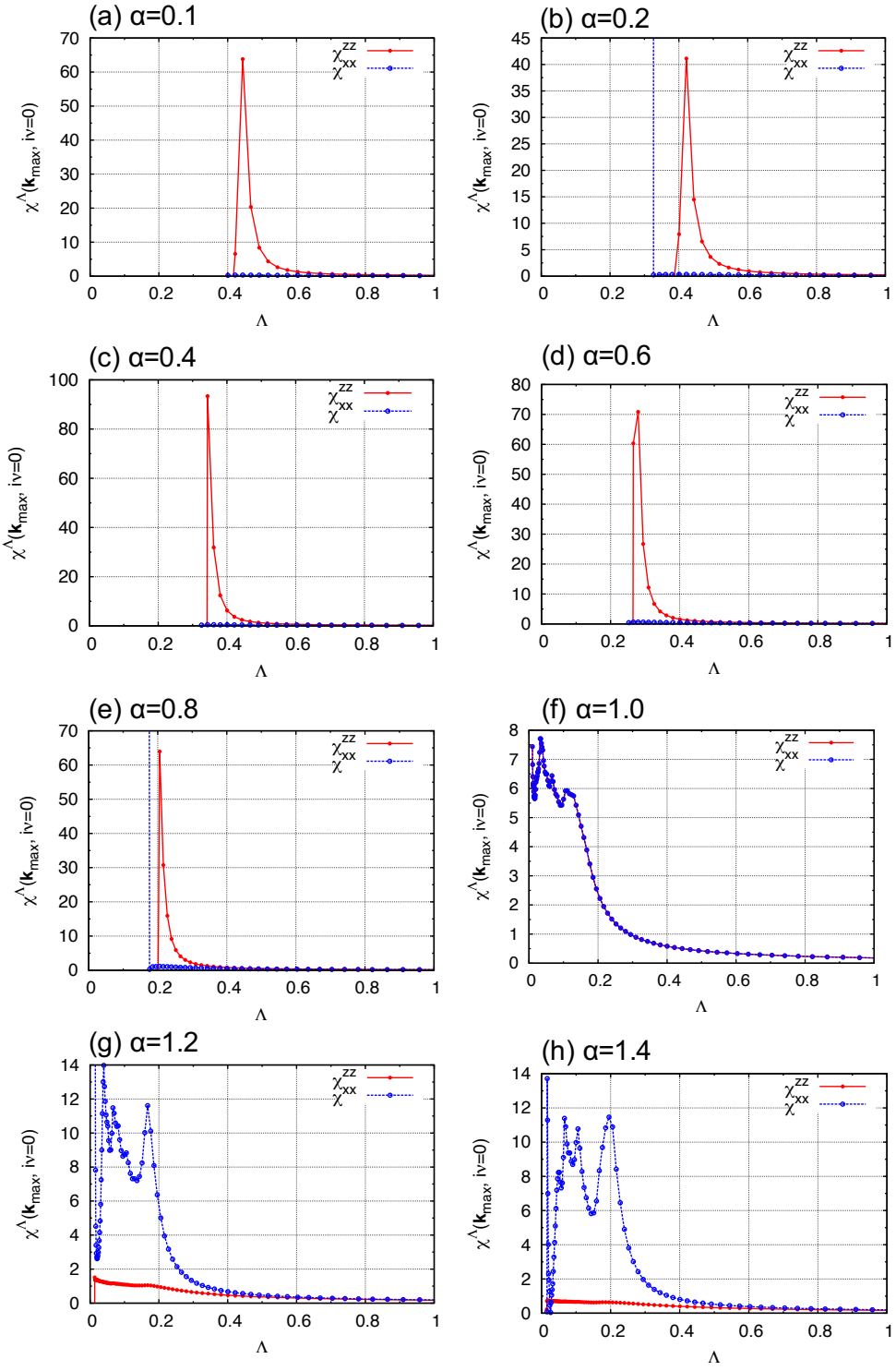

FIGURE 4.9: Calculated static spin susceptibilities $\chi^{zz,\Lambda}$ and $\chi^{xx,\Lambda}$ vs. Λ for some velues of α in the AFM case. The results for $\alpha = 0.1$, 0.2, 0.4, 0.6, 0.8, 1.0, 1.2, and 1.4 are shown in (a)-(h), in order.

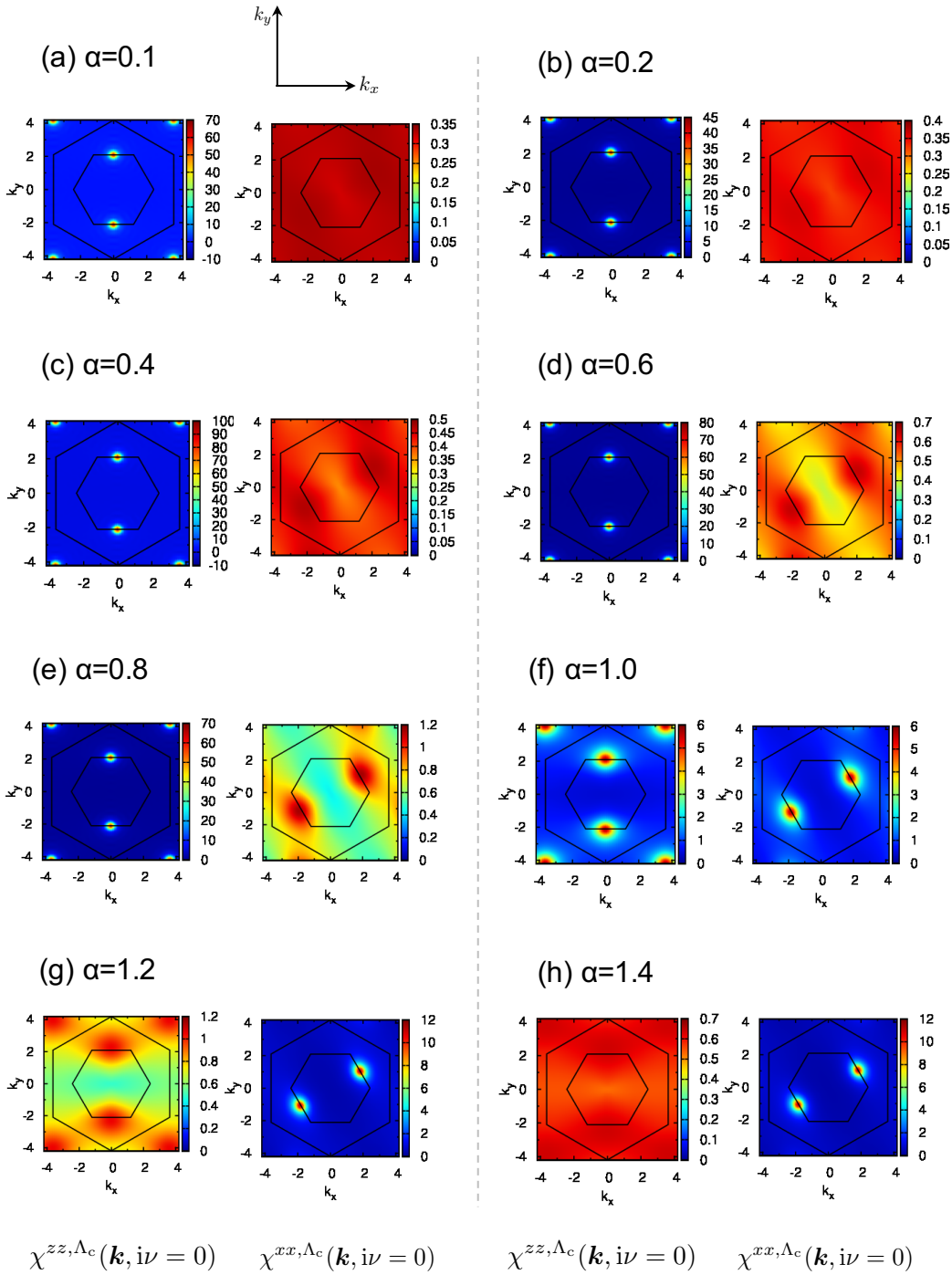

FIGURE 4.10: Momentum dependence of the static susceptibilities $\chi^{zz,\Lambda}$ and $\chi^{xx,\Lambda}$ at the ordering scale $\Lambda = \Lambda_c$. We consider AFM case. The results for $\alpha = 0.1$, 0.2, 0.4, 0.6, 0.8, 1.0, 1.2, and 1.4 are shown in (a)-(h), in order. For each α, left panel and right panel show $\chi^{zz,\Lambda_c}(\boldsymbol{k}, i\nu = 0)$ and $\chi^{xx,\Lambda_c}(\boldsymbol{k}, i\nu = 0)$, respectively.

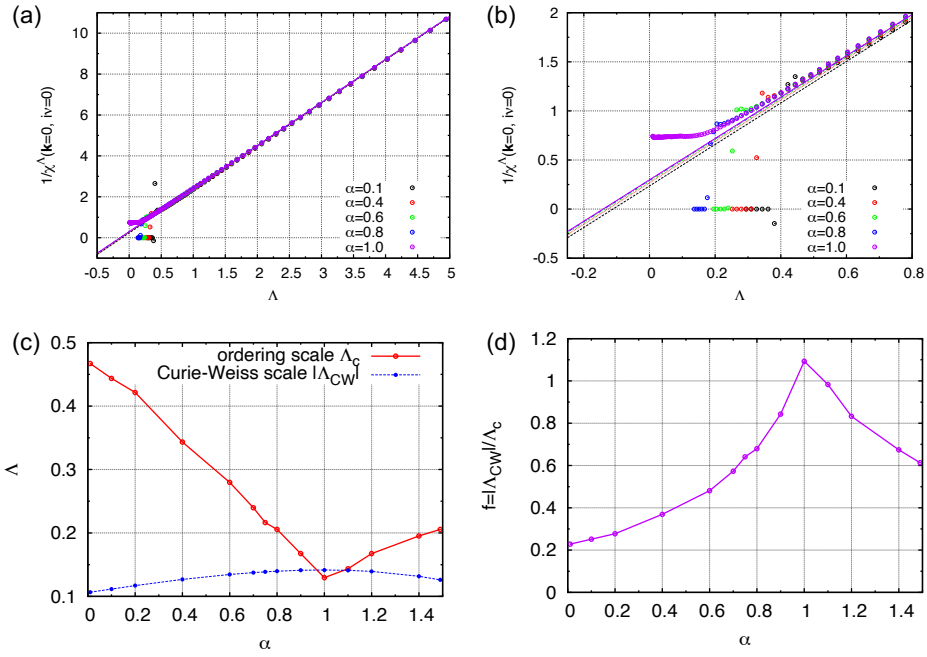

FIGURE 4.11: Λ-dependence of inverse of uniform static spin susceptibility $1/\chi^{\Lambda}(\boldsymbol{k}=0, i\nu=0)$ with Curie-Weiss fitting for some α values in (a) $\Lambda \in [-0.5, 5]$ and (b) $\Lambda \in [-0.25, 0.8]$. (c) The ordering scale (critical cutoff) Λ_c and the absolute value of Curie-Weiss scale Λ_{CW}, and (d) frustration parameter f vs. anisotropy parameter α. All panels show the results for AFM dipolar Kitaev model.

bond connection between sites i and j on the honeycomb lattice. If either sites i or j is the reference site i_0 at the center of the cluster, then L_{int} matches the definition of L (See Fig. 4.3). If $L_{\text{int}} = 1$, this Hamiltonian becomes the Kitaev model Eq. (1.1), and it corresponds to the dipolar Kitaev model Eq. (4.17) if $L_{\text{int}} = L$. Here we consider FM isotropic case and we define $J_x = J_y = J_z = J$. We conducted PFFRG calculation while changing L_{int} from 1 to L, and show the static susceptibility $\chi^{zz,\Lambda}$ at the $\boldsymbol{k}_{\max}$ in Fig. 4.12. We take $L = 20$ cluster for $L_{\text{int}} \geq 2$ though $L = 10$ for L_{int} because there is no significant size dependence in the exact Kitaev model case (see Fig. 4.5 (b)). In Fig. 4.12, we only display the susceptibility for $\Lambda \geq \Lambda_c$ for the model with $L_{\text{int}} \geq 6$ for clarity. It is difficult to conclude from Fig. 4.12 at which L_{int} the system becomes ordered. Thus, we adopt the size dependence of the on-site susceptibility $\chi^{zz,\Lambda}_{ii}(i\nu = 0)$ as a clearer criterion for ordering. Recently, it was pointed out that if the system is ordered, the on-site susceptibility appears to be size-dependent, otherwise it is not [214]. We calculate the on-site susceptibility for different L_{int} as shown in Fig. 4.13. We can see size dependence of the on-site susceptibility of the system with $L_{\text{int}} = 3$ or $L_{\text{int}} = 4$. Hence we can conclude that the system undergoes phase transition to magnetic order for $L_{\text{int}} = 3$ or 4. Further, by fitting we obtained the Curie-Weiss scale and the frustration parameter shown in Fig. 4.14. The plots are connected by lines in the figure for eye guide though L_{int} is a discrete parameter. The system is not ordering for $L_{\text{int}} \leq 2$ and there is no Λ_c in Fig. 4.14 (a), although Curie-Weiss fitting can be performed whether the system is ordered or not. From around $L_{\text{int}} = 5$, both Λ_c and Λ_{CW} begin to asymptotically approach the value of $L_{\text{int}} = L$. This behavior can be seen also in the L_{int}-dependence of the frustration parameter in Fig. 4.14 (b). In the region $L_{\text{int}} \leq 2$, which is grayed out in the figure, f

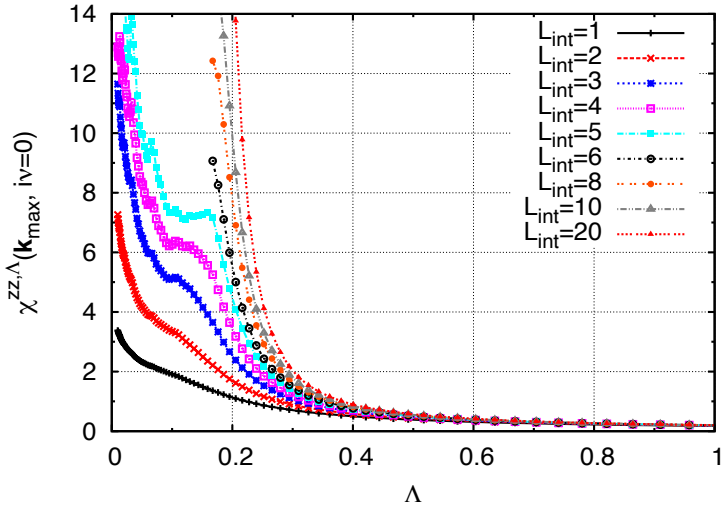

FIGURE 4.12: Λ-dependence of the static susceptibility $\chi^{zz,\Lambda}(\boldsymbol{k}_{\max}, i\nu = 0)$ in the isotropic ($\alpha = 1$) FM dipolar Kitaev systems with several $L_{\rm int}$. For $L_{\rm int} \geq 6$, we show the susceptibility flows $\Lambda \geq \Lambda_c$ for visibility.

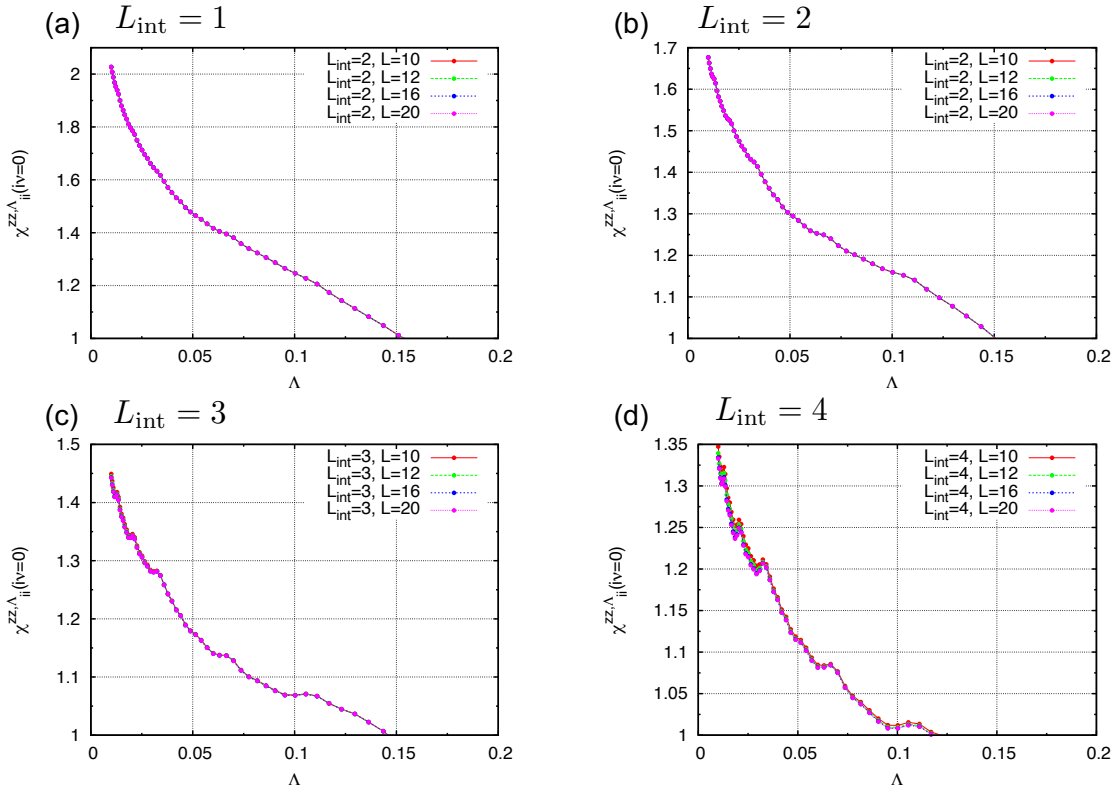

FIGURE 4.13: System size dependence of the on-site susceptibility $\chi^{zz,\Lambda}_{ii}(i\nu = 0)$ for the systems with (a) $L_{\rm int} = 1$, (b) $L_{\rm int} = 2$, (c) $L_{\rm int} = 3$, and (d) $L_{\rm int} = 4$

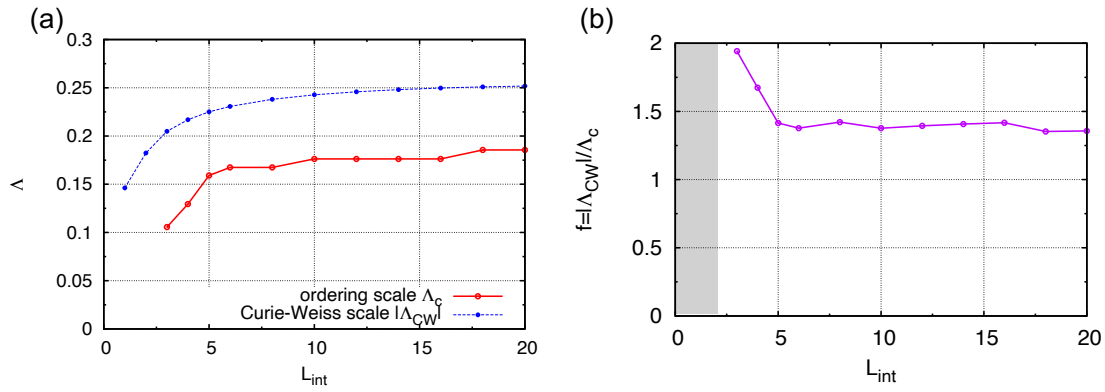

FIGURE 4.14: (a) The ordering scale (critical cutoff) Λ_c and the absolute value of Curie-Weiss scale Λ_{CW}, and (b) frustration parameter f of isotropic FM dipolar Kitaev model vs. L_{int}. L_{int} represents the range of interaction in the model, and the distance between sites is discrete because it is defined in units of bonds, but the plots are connected by lines for eye guide.

is ill-defined because Λ_c does not exist. This region corresponds to $f = \infty$ because the ordering is hindered by strong frustration. In the next step, we investigate the momentum dependence and the spatial dependence of the susceptibilities for each L_{int} shown in Fig. 4.15. In the figures for each parameter, the left panel exhibits the momentum dependence in the extended Brillouin zone, on the other hand the right panel shows the susceptibility in the real space viewed horizontally from the $y < 0$ direction. For $L_{int} \leq 2$, the susceptibilities have no breakdown points, therefore we plot the susceptibilities at $\Lambda = \Lambda_{IR}$. On the other hand, for $L_{int} \geq 3$, we show susceptibilities at $\Lambda = \Lambda_c$. At $L_{int} = 1$, the Hamiltonian Eq. (4.31) is strictly identical to the Kitaev model, and $\chi_{ij}^{zz,\Lambda_{IR}}$ has finite values only if $j = i$ or the case j is the nearest-neighbor of i connected by z-bond, strictly. Thereby the momentum dependence of $\chi^{zz,\Lambda_{IR}}(\boldsymbol{k})$ has a cosine-curve shape in the k_y-direction and the susceptibility $\chi^{zz,\Lambda_{IR}}(\boldsymbol{k})$ has the maximum on the line $k_y = 0$ (see Fig. 4.15 (a)). As L_{int} increases from 1, the figure shows that the region with the maximum susceptibility shrinks rapidly. We can see that the regions eventually shrink at $\boldsymbol{k} = 0$ point, resulting in the peak of the FM order.

These results indicate that the Kitaev spin liquid state collapses with increasing L_{int}. From this, we may consider that the long-range interactions breaks Kitaev quantum spin liquid states. More precisely, there are two-type differences between the dipolar Kitaev model and the Kitaev model:

- The dipolar Kitaev model has (quasi-) long-range interaction.
- In the dipolar Kitaev model, generally complex ($S_i^x S_j^x$, $S_i^y S_j^y$, $S_i^z S_j^z$-mixed) interactions between spins at sites farther apart than the nearest neighbor are observed.

If for the latter reason the spin liquid is destabilized, then designing another interaction by microwave irradiation may realize it. However, according to previous studies of the K_1-K_2 model (Kitaev model + the next-nearest-neighbor Kitaev interactions) [215], the Kitaev spin liquid is fragile to the next-nearest-neighbor interaction,

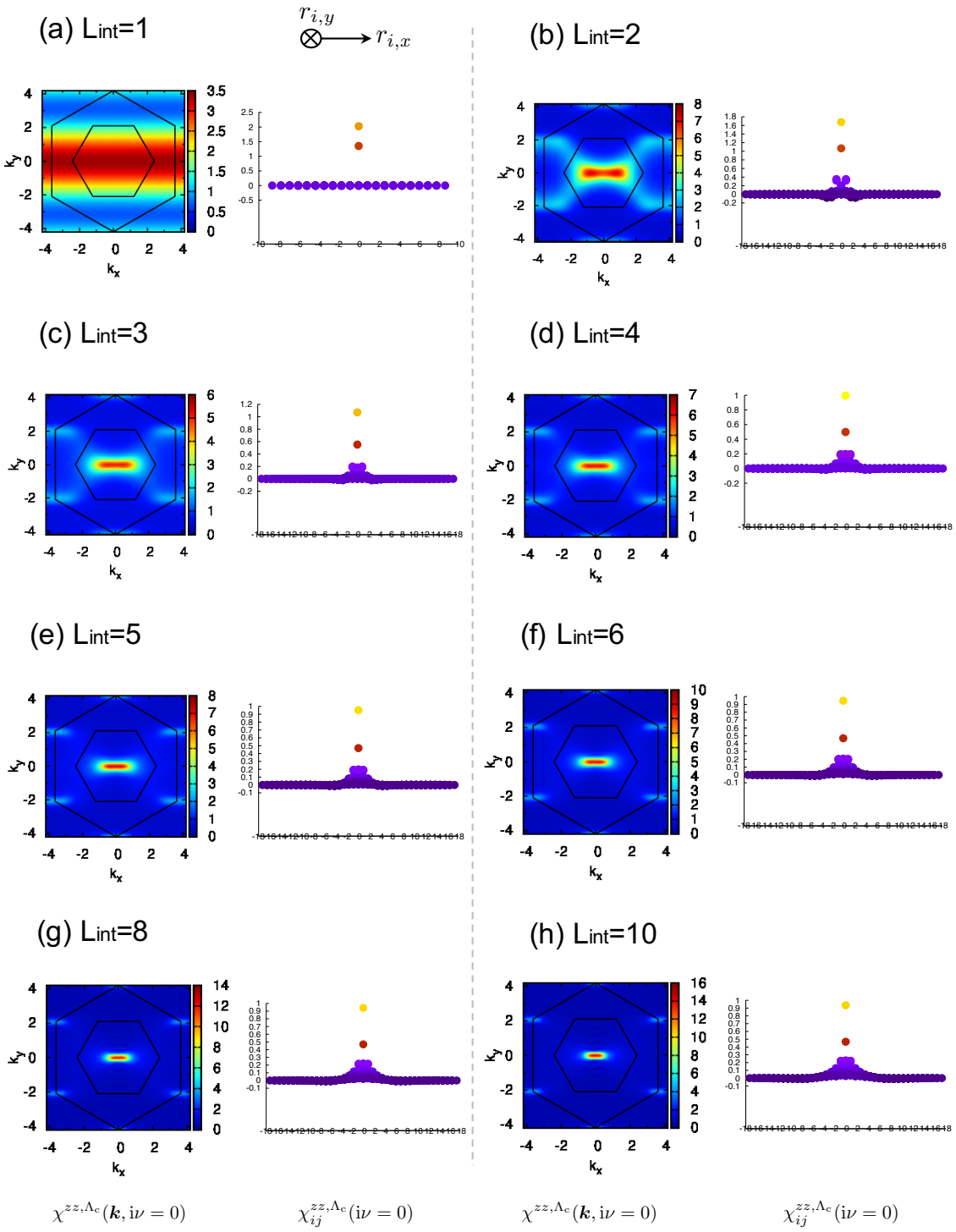

FIGURE 4.15: The momentum dependence of the static susceptibility (left panels) and the susceptibility in real space (right panesl) with several L_{int}: (a)-(h) show the results of the isotropic FM dipolar Kitaev model with $L_{\mathrm{int}} =$ 1-6, 8, and 10, respectively.

even if it is a Kitaev-type interaction. If we set

$$K_2 = \frac{1}{3\sqrt{3}}, \tag{4.32}$$

in K_1-K_2 model ($K_1 = 1$) as the dipolar Kitaev model, this parameter is in ordered phase. In the case of the dipolar Kitaev model, it is not yet ordered at $L_{\text{int}} = 2$, but it is also ordered at $L_{\text{int}} = 3$ (see Fig. 4.12). Therefore, in the dipolar Kitaev model, we conclude that the Kitaev spin liquid is not realized due to the long-range nature of the interaction. This is quite different from the dipolar Heisenberg model. In the dipolar Heisenberg model, the long-range interaction strengthen frustration of the system and the spin liquid states appear as a result [125, 201, 202]. On the other hand, the long-range interaction weaken the frustration and the system is ordered for all anisotropy parameters.

Because the long-range nature of the interaction destroys the Kitaev spin liquid, it is difficult to design another interaction by microwave, as long as it is rooted in the dipole interaction, to realize the Kitaev quantum spin liquid. Since the Kitaev spin liquid is more robust to the next nearest neighbor Heisenberg interaction than to the next nearest neighbor Kitaev type interaction [215], if possible, the Kitaev quantum spin liquid may be realized by designing an interaction such that the long-range interaction is closer to the Heisenberg interaction.

4.9 Summary of This Chapter

In this chapter, we discussed the feasibility of the Kitaev quantum spin liquid in ultracold polar molecular systems trapped in the optical lattice, based on the realization of Kitaev-type interactions proposed in previous studies [34, 35]. First, we introduced the dipolar Heisenberg/XXZ model and its realization in these systems. Then we briefly reviewed the proposals for the realization of Kitaev-type interactions by laser-induced linear coupling of rotational levels in the molecules.

Based on these proposals, we defined the dipolar Kitaev model. The interactions that appear in this model are derived from dipole interactions between molecules, and have long-range nature. The interactions between the nearest-neighboring sites are consistent with the Kitaev-type interaction, but those between sites farther than the next-nearest-neighbor are more complicated.

We have applied PFFRG to this model to investigate the ground state at each anisotropy parameter. The results show that FM order and zigzag AFM order are realized in the FM and AFM dipolar Kitaev model, respectively, for all anisotropy parameters. Next, we investigated the ordering behavior while increasing the range of the interaction from the nearest-neighbor case. As a result, the behavior of the susceptibility shows that the Kitaev quantum spin liquid state quickly collapses and the system undergoes magnetic ordering as the range of the interaction increases.

From these results, we conclude that the Kitaev quantum spin liquid is very fragile against long-range interactions in the proposals. This is difficult to realize Kitaev quantum spin liquid with dipolar-Kitaev interaction and long-range Kitaev interaction. It is necessary to propose another realization of the Kitaev quantum spin liquid in dipole systems.

After the proposal of Kitaev-type interaction in ultracold polar molecular systems by microwave irradiation in 2013, the calculation based on this proposal has

not been performed, and whether Kitaev quantum spin liquid state is actually realized has remained an open question. We addressed this issue with PFFRG and elucidated the above results for the first time.

Chapter 5

Spin-S Kitaev-Heisenberg Model

In this chapter, we now discuss the realization of the Kitaev quantum spin liquid state in solids. In particular, we focus on the Kitaev quantum spin liquid with higher-spin. Recently, the higher-spin Kitaev model has attracted much theoretical attention in terms of conserved quantities and excitations. In addition, the realization of Kitaev interaction in materials with $S = 1$ and $S = 3/2$ spins has been proposed recently. In general, if the spin length S is large, quantum fluctuation is suppressed and magnetic orders is stabilized. Therefore, we would like to evaluate how long S is allowed in candidate materials to realize spin liquid state. Although there are various effects and interactions in real materials, we focus on, in this chapter, the Kitaev-Heisenberg model, which is a minimal model for the candidate compounds. We discuss the above evaluation based on the spin-S PFFRG calculation. The main part of this chapter will be submitted as Ref. [216].

5.1 High-spin Kitaev Model

The Kitaev model is a model for $S = 1/2$ spins originally, and exact solutions for $S > 1/2$ have not been obtained so far. In $S = 1/2$ Kitaev model, the original spin degrees of freedom fractionalize into Majorana fermion and $\mathbb{Z}_2$-flux. It is proved that the $\mathbb{Z}_2$-flux is also a local conserved quantity and the spin-spin correlation is limited in the nearest-neighbor for arbitrary flux distribution [45]. However, other fractionalized degrees of freedom are still unknown. It is clarified that even if $S > 1/2$ the entropy is released in halves as the temperature decreased and the specific heat has a double-peak behavior as that in $S = 1/2$ numerical studies [36–38] This fact means that in low temperature other degrees of freedom contribute to the specific heat in addition to $\mathbb{Z}_2$-flux. Low-energy excitations and magnetic responses are intensively studied, especially for $S = 1$ systems, recently [36, 39–44].

In the toric code limit ($J_z \gg J_x,\ J_y$), there is clear difference between integer spin and half-odd integer spin [217]. The effective model in this limit corresponds to the toric code model [26] if S is half-odd integer, although if S is integer the ground state is topologically trivial. The toric code model is well-understood and what we are really interested in is the isotropic case $J_x = J_y = J_z$ for non-Abelian anyons.

In addition, the mechanisms for higher-spin Kitaev model are proposal recently. Materials with chemical formula $A_3Ni_2XO_6$ (A =Li, Na and X =Bi, Sb) are candidate materials for $S = 1$ Kitaev model [46]. The candidate materials for $S = 3/2$ Kitaev model are CrI_3, $CrBr_3$, $CrSiTe_3$, and $CrGeTe_3$ [47–50]. Experimental and theoretical studies on high-spin Kitaev materials are important not only for material science but also for understanding of high-spin Kitaev quantum spin liquid.

Generally speaking, non-Kitaev interactions cause magnetic ordering and quantum fluctuations in the ordered phases are suppressed for high-spin systems. This

means in higher-spin systems the quantum spin liquid is hard to be stabilised. Therefore, it is important to estimate the upper bound of S for realization of quantum spin liquid in these materials. In this chapter we focus on this estimation by PFFRG and we treat the Kitaev-Heisenberg model, introduced in the next section, as a minimal model for the candidate materials.

5.2 Kitaev-Heisenberg Model ($S = 1/2$)

In the candidate materials, the Kitaev-type interaction is considered to be realized owing to the Jackeli-Khaliullin mechanism [14]. There are, however, other magnetic interactions due to various effects: direct overlap between d-orbitals, deformation of octahedrons, and so on. A minimal model for the candidate materials is the Kitaev-Heisenberg model (J-K model)

$$\mathcal{H} = K\sum_{\mu}\sum_{\langle i,j\rangle_\mu} S_i^\mu S_j^\mu + J\sum_{\langle i,j\rangle} \boldsymbol{S}_i \cdot \boldsymbol{S}_j, \tag{5.1}$$

on the honeycomb lattice. K and J are the coupling constants of Kitaev interaction (we set $J_x = J_y = J_z = K$) and isotropic Heisenberg interaction. The summation $\sum_{\langle i,j\rangle}$ runs over all nearest-neighbor pairs of sites, and the summation $\sum_{\langle i,j\rangle_\mu}$ runs over all pairs of sites on μ-bond (see Fig. 1.1). This model was suggested as a minimal model for iridium oxides A_2IrO_3 (A=Na, Li) originally [51]. In Jackeli-Khaliullin mechanism described in Chap. 1, FM Kitaev interaction ($K < 0$) is obtained via quantum interference between 2 Ir-O-Ir exchange paths. In addition, AFM Heisenberg interaction ($J > 0$) can be finite by direct d-d overlap and onsite Coulomb repulsion in oxigen p-orbitals. Therefore, these interactions are often parametrized as

$$\begin{aligned} K &= -2\alpha, \\ J &= (1-\alpha), \end{aligned} \tag{5.2}$$

by $\alpha \in [0,1]$. At $\alpha = 0$ the Hamiltonian Eq. (5.1) becomes the AFM Heisenberg model, at $\alpha = 1$ the model is the isotropic FM Kitaev model on the other hand. Based on this parametrizeation, several numerical studies clarified that the spin liquid state is stable in the range $\simeq (0.8, 1]$ [51, 136, 218, 219]. In addition to spin liquid phase, there is two magnetic ordered phase: Néel and stripy AFM, and their boundary locate $\alpha \simeq 0.4$. Even so, experimental results suggest zigzag AFM ordered ground state in Na_2IrO_3 [220–224], and incommensurate spiral ordered ground state in Li_2IrO_3 [224–226]. To describe the property of Na_2IrO_3, two types of extensions of Kitaev-Heisenberg model were proposed [1]: (i) inclusion of Heisenberg interaction beyond the nearest-neighbors [229], (ii) considering full parameter region of Eq. (5.1) [52]. In this chapter we concentrate on the latter extension [2]. There are 4 patterns in the latter extension: ($K < 0$, $J > 0$) described in Eq. (5.2), ($K > 0$, $J > 0$), ($K > 0$, $J < 0$), and ($K < 0$, $J < 0$). These signs of couplings are explained by inclusion of t_{2g}-e_g hopping process [52]. Although the incommensurate spiral order in Li_2IrO_3 cannot be explained, the homogeneous susceptibility obtained from this Kitaev-Heisenberg model fits very well with the experimental magnetic susceptibility for both Na_2IrO_3 and Li_2IrO_3. Hence we treat the Kitaev-Heisenberg model as a minimal model for candidate materials in this chapter.

[1] Model obtained by the first principle calculations are in Ref. [227, 228].

[2] For Li_2IrO_3, the extension including the next-nearest FM Heisenberg and AFM Kitaev interactions were proposed to explain the incommensurate order [120].

In addition, the Kitaev-Heisenberg model on other lattices, especially triangular lattice, are also intensively studied and their phase diagrams contain rich physics [230–237] although not covered in this chapter.

Before showing our calculation for $S \geq 1/2$ Kitaev-Heisenberg model, we devote the rest of this section and the next 2 successive sections to review results of previous studies on $S = 1/2, 1$, and ∞ (classical) Kitaev-Heisenberg models.

Phase diagram by ED

J. Chaloupka, G. Jackeli, and G. Khaliullin proposed the original Kitaev-Heisenberg model ($K < 0$, $J > 0$) in 2010 [51] and the full parameter Kitaev-Heisenberg model in 2013 [52]. They calculated the phase diagrams of those models by exact diagonalization (ED) in the same papers. Here we review their resulting phase diagram in Ref. [52]. They introduced the energy scale A and parametrized couplings as

$$\begin{aligned} A &= \sqrt{K^2 + J^2}, \\ K &= A \sin\varphi, \\ J &= A \cos\varphi. \end{aligned} \tag{5.3}$$

The Hamiltonian Eq. (5.1) is rewritten as

$$\mathcal{H} = A \sum_{\mu} \sum_{\langle i,j \rangle_\mu} \left[2 \sin\varphi \, S_i^\mu S_j^\mu + \cos\varphi \, \boldsymbol{S}_i \cdot \boldsymbol{S}_j \right]. \tag{5.4}$$

The range of introduced angle φ is $[0, 2\pi)$, and there are 4 obvious points at which the Hamiltonian becomes exactly solvable models:

- $\varphi = 0$: AFM Heisenberg model
- $\varphi = \pi$: FM Heisenberg model
- $\varphi = \frac{\pi}{2}$: AFM Kitaev model
- $\varphi = \frac{3\pi}{2}$: FM Kitaev model.

The ground states of AFM and FM Heisenberg model are Néel AFM and FM state [3], respectively, and the ground state of both the AFM and FM Kitaev models is quantum spin liquid. In addition, there are 2 more special points:

- $\varphi = \frac{3\pi}{4}$: "hidden" AFM Heisenberg model
- $\varphi = \frac{7\pi}{4}$: "hidden" FM Heisenberg model.

At these points, we can obtain pure AFM/FM Heisenberg model by 4-lattice transformation introduced in Ref. [238]. In this transformation, we divide the system into 4 sublattices 1-4 and consider the sublattice-dependent spin rotation:

1. $\tilde{\boldsymbol{S}}_i = \boldsymbol{S}$
2. $\tilde{\boldsymbol{S}}_i = (S_i^x, -S_i^y, -S_j^z)$
3. $\tilde{\boldsymbol{S}}_i = (-S_i^x, S_i^y, -S_i^z)$
4. $\tilde{\boldsymbol{S}}_i = (-S_i^x, -S_i^y, S_i^z)$,

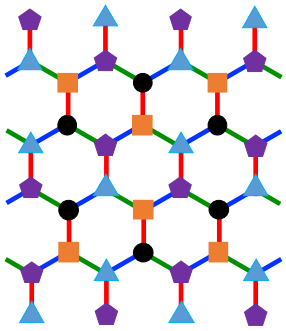

FIGURE 5.1: Sublattices for 4-sublattice transformation. Sites in each sublattice represented by circles, squarse, triangles, and pentagons. Two sites on the diagonal of the honeycomb lattice belong to the same sublattice and each sublattice is a large honeycomb lattice.

simultaneously. These 4 sublattices are shown in Fig. 5.1 Then we obtain

$$\mathcal{H} = \pm\frac{A}{2}\sum_{\mu}\sum_{\langle i,j\rangle_\mu}\tilde{S}_i\cdot\tilde{S}_j, \tag{5.5}$$

at $\varphi = \frac{3\pi}{4}$ $(+)$ and $\frac{7\pi}{4}$ $(-)$. The Hamiltonian can be exactly solved in both cases, and the ground states are Néel AFM at $\varphi = \frac{3\pi}{4}$ and FM state at $\varphi = 7\pi 4$ in rotated spin language. Then we re-rotate spins to the original ones and can obtain the ground states of the original spin representation: zigzag AFM at $\varphi = \frac{3\pi}{4}$ and stripy AFM at $\varphi = \frac{7\pi}{4}$. The schematic spin patterns of these obtained ordered ground states are shown in Fig. 5.2.

Let us move on to the numerical results of 24-site ED calculation in Ref. [52]. The resulting phase diagram is shown in Fig. 5.3. The ground state energy E_{GS} and its second derivative with respect to φ are shown. The phase boundaries are decided by the peak positions in the second derivative. There are 2 spin liquid states near the AFM Kitaev point $\varphi = \frac{\pi}{2}$ and the FM Kitaev point $\varphi = \frac{3\pi}{2}$ (we distinguish the spin liquid realized in the AFM case from that realized in the FM case), and 4 magnetic ordered states mentioned in discussion above. We can see that the FM Kitaev spin liquid is more stable than AFM one although at the exact Kitaev point ($J = 0$ i.e. $K = \pm 1$) the ground states with $K = +1$ and $K = -1$ are connected by unitary transformation and have same E_{GS} [13]. The regions of AFM and FM Kitaev spin liquid are about $[0.49\pi, 0.51\pi]$ and $[1.4\pi, 1.58\pi]$, respectively. These differences are due to the nature of the surrounding ordered states [52]. Néel and zigzag ("hidden" Néel AFM) orders near $\varphi = \frac{\pi}{2}$ are highly quantum, on the other hand FM and stripy AFM ("hidden" FM) orders near $\varphi = \frac{3\pi}{2}$ are rather classical which are less favorable than the Kitaev quantum liquid state energetically.

PFFRG results for the original Kitaev-Heisenberg model

In this section, we refer one more studies on the $S = 1/2$ Kitaev-Heisenberg model. The PFFRG calculation on the original (i.e. $K < 0$ and $J > 0$) Kitaev-Heisenberg model (in 112-site cluster) was performed in Ref. [136]. The result is shown in Fig. 5.4. While the title of the paper is "*Finite-temperature* phase diagram of the

[3]Note that the honeycomb lattice is bipartite and the ground state of the AFM Heisenberg model on it is Néel AFM state.

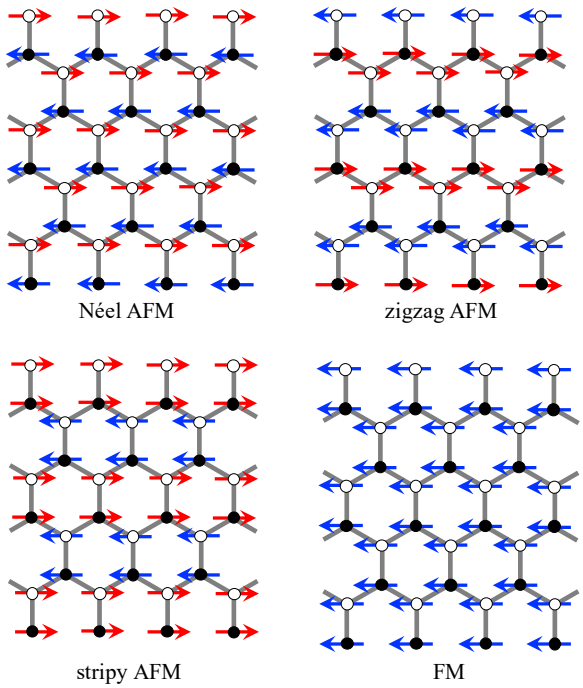

FIGURE 5.2: Schematic figures of the spin patterns of ordered states in Kitaev-Heisenberg model on the honeycomb lattice. 2 sublattices are represented by black and white circles. Spins in the direction of the quantization axis (which is set to the left in the figure) are shown in blue, and spins in the opposite direction are shown in red.

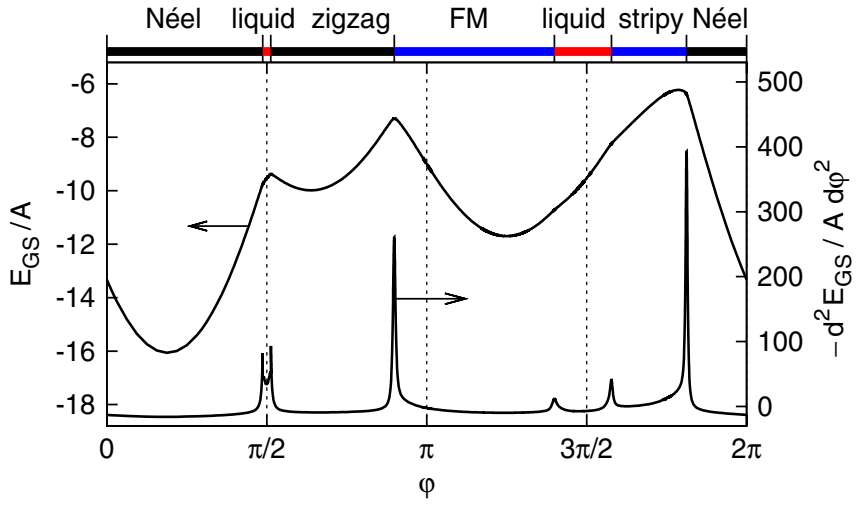

FIGURE 5.3: Ground state phase diagram of the Kitaev-Heisenberg model obtained by 24-site ED calculation with the ground state energy E_{GS} and its second derivative with respect the parameter φ. The phases labeled "liquid" are Kitaev quantum spin liquid phase. Reprinted with permission from Ref. [52] © 2013 by the American Physical Society.

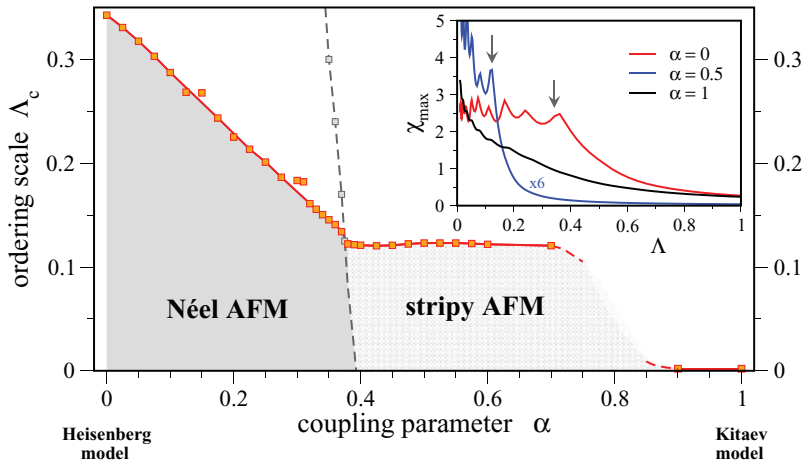

FIGURE 5.4: Λ-α phase diagram of the Kitaev-Heisenberg model with $K < 0$ and $J > 0$ calculated by PFFRG. The definition of α is in Eq. 5.2. Inset shows Λ dependence of the spin susceptibility, $\chi^{zz,\Lambda}(\boldsymbol{k}_{\max}, i\nu = 0)$ in our definition, at $\alpha = 0$, 0.5, and 1. The black arrows in the inset indicate ordering scales. Reprinted with permission from Ref. [136] © 2011 by the American Physical Society.

Heisenberg-Kitaev model", they used the same PFFRG that is introduced in this dissertation. The flow parameter Λ is regarded as the temperature T by the relation Eq. (3.150). By this relation, the finite temperature phase diagram can be discussed by considering Λ roughly as temperature. The definition of α is the same with Eq. 5.2. Note that $\alpha = 0$ and $\alpha = 1$ is identical with $\varphi = 0$ and $\varphi = \frac{3\pi}{2}$ in Eq. (5.4), respectively. The "hidden" FM point at $\varphi = \frac{7\pi}{4}$ corresponds with $\alpha = 0.5$ The phase diagram at $\Lambda = 0$ is consistent to that obtained by ED [51], DMRG [218], and $\varphi = 0$ to $\varphi = \frac{3\pi}{2}$ in Fig. 5.3. Inset shows the flow of the static spin susceptibility $\chi^{zz,\Lambda}(\boldsymbol{k}_{\text{alpha}}, i\nu = 0)$ with the wave vector $\boldsymbol{k}_{\max}$ at which the susceptibility has the maximum value, at $\alpha = 0$, 0.5, 1. At the point $\alpha = 1$, the Hamiltonian is identical with FM Kitaev model and the susceptibility does not diverge up to $\Lambda = \Lambda_{\text{IR}}$, while at $\alpha = 0$ and 0.5, the susceptibility occurs breakdown and it indicates the onset of the phase transition to Néel and stripy AFM ordered phase, respectively. The black arrows in the inset of Fig. 5.4 indicate the ordering scales Λ_c which is regarded as the transition temperature T_c. Actually, the model recovers the complete SU(2) symmetry at $\alpha = 0$ and 0.5 and it should not show a phase transition to ordered phases at finite temperatures according to Mermin-Wagner theorem [212]. If we regard the cutoff Λ as the temperature T, the flows of the susceptibility in the inset contrary to Mermin-Wagner theorem. It is an artifact of PFFRG pointed out in Ref. [99], in which the comparison between the phase diagrams of the XXZ model on the square lattice obtained by the quantum Monte Carlo and PFFRG are performed. These flows ($\alpha = 0$ and 1) coincide with the susceptibility flows in Fig. 4.5 except for constants resulting from different calculation conditions. In addition, note that the boundary between the stripy AFM and the Kitaev spin liquid phases is somewhat ambiguous in Fig. 5.4. This is because it is difficult to judge whether the susceptibilities obtained by PFFRG diverge or not near the phase boundary.

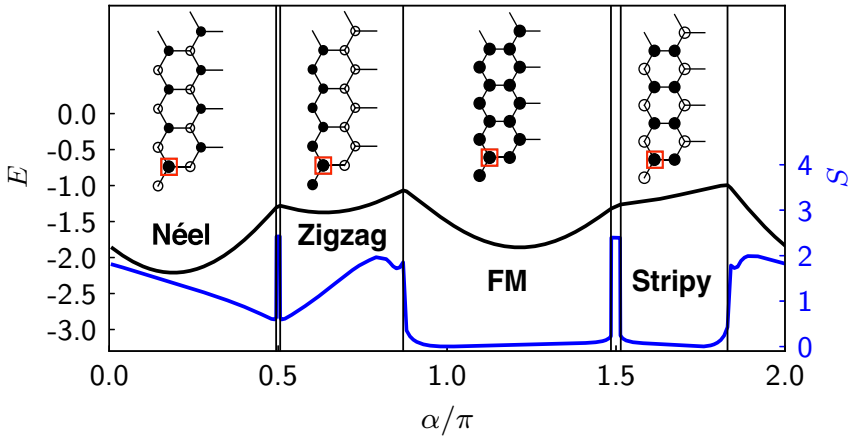

FIGURE 5.5: Ground state phase diagram of the $S = 1$ Kitaev-Heisenberg model by DMRG (iDMRG) calculation. The parameter α coincides with φ in Eq. (5.4). Reprinted with permission from Ref. [40] © 2020 by the American Physical Society.

5.3 $S = 1$ Kitaev-Heisenberg Model

Recently, X-Y Dong and D. N. Sheng calculated the ground state phase diagram of $S = 1$ Kitaev-Heisenberg model by DMRG (infinite DMRG) on an infinite cylinder with circumference 4 unit cells [40]. Their resulting phase diagram is shown in Fig. 5.5. Here, E on the left axis represents energy, and S on the blue axis on the right represents entanglement entropy by cutting the cylinder along a ring [4]. α is identical with φ in Eq. (5.4). There are 4 ordered phases and 2 quantum liquid phases as $S = 1/2$ case. The types of magnetic orders are the same and only the boundaries between them are shifted. The AFM and FM Kitaev quantum spin liquid regions are $[0.494\pi, 0.506\pi]$ and $[1.485\pi, 1.514\pi]$, respectively. The spin liquid phase is narrower than that at S = 1/2 [5]. The entanglement entropy shows a clear difference between the ordered and quantum spin liquid phases. It can also be seen that entanglement entropy is smaller in the "classical" FM and stripy AFM phases than in the AFM and zigzag AFM phases.

5.4 Classical ($S = \infty$) Kitaev-Heisenberg Model

Finally we review the finite temperature phase diagram of the classical Kitaev-Heisenberg model in Ref. [207, 208]. In 2013, the same year that the Kitaev-Heisenberg model was proposed, C. Price and N. B. Perkins published the Monte Carlo study on the classical Kitaev-Heisenberg model and the obtained finite temperature phase diagram is shown in Fig. 5.6. The definition of φ is the same as that in Eq. (5.4) and "N", "Z", "F", and "S" represent Néel AFM, zigzag AFM, FM, and stripy AFM ordered phase, respectively. These 4 magnetic orders in the figure are identical with $S = 1/2$ and $S = 1$ cases. However, the spin liquid phases near $\varphi = \frac{\pi}{2}$ and $\frac{3\pi}{2}$ annihilated. At these Kitaev points, the classical energies of 4 ordered states mentioned above

[4] Entanglement entropy S is confusing with the lengh of spin S. However, the entanglement entropy does not appear in subsequent sections.

[5] According to the previous section, the AFM and FM Kitaev spin liquid regions are respectively $[0.49\pi, 0.511\pi]$ and $[1.4\pi, 1.58\pi]$ at $S = 1/2$.

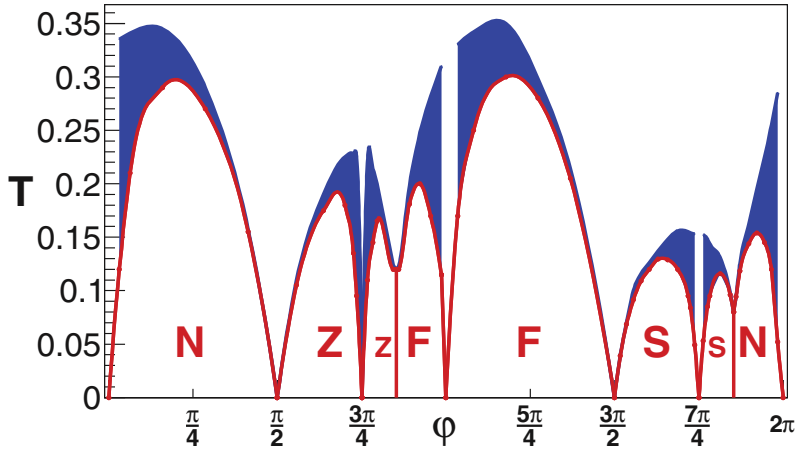

FIGURE 5.6: Finite temperature phase diagram of the classical Kitaev-Heisenberg model calculated by Monte Carlo simulation. "N", "Z", "F", and "S" denote Néel AFM, zigzag AFM, FM, and stripy AFM phases, respectively. Blue shaded regions represent critical phase. Reprinted with permission from Ref. [208] © 2013 by the American Physical Society.

degenerate and spectrum of spin excitations has zero modes [45, 239]. Therefore the order-by-disorder mechanism does not work at these points and no transition to the ordered phase occurs. In addition to these points, there are 4 more special points in the phase diagram as we discussed before: AFM and FM Heisenberg points $\varphi = 0$ and π, and "hidden" AFM and FM Heisenberg points $\varphi = \frac{3\pi}{4}$ and $\frac{7\pi}{4}$, respectively. At these points the Hamiltonian acquires a perfect SU(2) symmetry and magnetic ordering does not occur at finite temperature according to the Mermin-Wagner theorem. The transitions between zigzag AFM and FM phases and stripy AFM and Néel AFM phases are first-order phase transitions and these boundaries are indicated by vertical lines. The shaded blue areas in the figure represent the intermediate phase. This phase is the critical phase and the Berezinskii-Kosterlitz-Thouless (BKT) transition [209–211] occurs at its finite temperature boundaries [207]. This critical phase is identical with the critical phase in 6-state clock model and its critical exponent η is $1/4$ at upper phase boundary ant $1/9$ at lower boundary [206]. In the Fig. 5.6, the upper phase boundary is defined at the location where the critical exponent η reaches $1/4$, and lower one is determined by Binder parameter crossing.

So far, we have explained the nature of the Kitaev-Heisenberg model and reviewed several previous studies on its phase diagram. One of our aims in this chapter is to examine the connection between these quantum and classical phase diagrams of the Kitaev-Heisenberg model. Our calculation results are shown in the next section.

5.5 Spin-S Kitaev Model in PFFRG

Before moving on to the results of the phase diagram of the spin-S Kitaev-Heisenberg model, we present the results for the high-spin Kitaev model by the PFFRG. We apply the spin-S extension described in Sec. 3.7 to the flow equations for the Kitaev-type interaction. Of particular interest to us is the difference between the half-odd

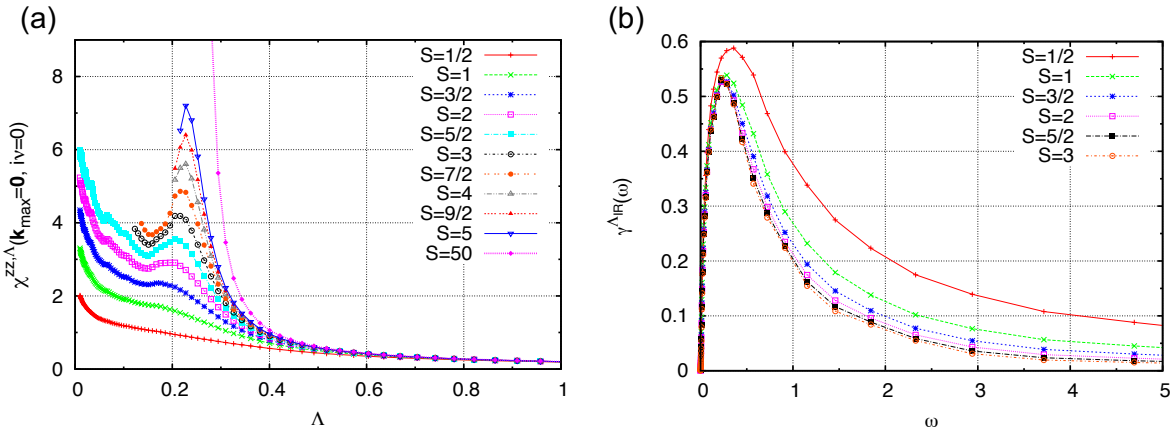

FIGURE 5.7: (a) Flow of the static susceptibility $\chi^{zz,\Lambda}(\boldsymbol{k}_{\max} = 0, i\nu = 0)$ and (b) the Matsubara frequency dependence of the pseudo-fermion damping (≃self-energy) of spin-S Kitaev model.

and integer spins. We extend our PFFRG calculation to spin-S Kitaev model as described in Sec. 3.7 for the Heisenberg model. We introduce flavor index κ, κ' and put $2S$ spins on each site for spin-S model. The Hamiltonian is

$$\mathcal{H} = -|K| \sum_{\langle i,j \rangle_\mu} \left(\sum_{\kappa=1}^{2S} S_{i\kappa}^{\mu} \right) \left(\sum_{\kappa'=1}^{2S} S_{j\kappa'}^{\mu} \right). \tag{5.6}$$

Here we set $K < 0$ and $J = 0$ in Eq. (5.1) to consider (isotropic) FM Kitaev model. Using $|K|$ as a unit of energy, we performed PFFRG calculations with varying S. In PFFRG calculation, we used 64 positive frequencies with logarithmic mesh between $\omega_{\min} \simeq 10^{-4}$ and $\omega_{\max} = 250$, and the internal frequency integration was carried out with a mesh more than twice as dense. We use the cluster with $L = 12$ (235 sites). In addition we take 212 Λ-points with the ratio $\Lambda_{i+1}/\Lambda_i = 0.95$ and $\Lambda_{\mathrm{UV}} = 500$. We benchmarked our spin-S PFFRG codes by reproduction of previous studies on the spin-S Heisenberg model on the honeycomb lattice [139]. Our codes are designed for openMP+MPI hybrid parallelization and the calculations were performed in Reedbush and Oakbridge-CX in the Information Technology Center, The University of Tokyo, Oakforest-PACS in Center for Computational Sciences, University of Tsukuba and in the Information Technology Center, The University of Tokyo, and sekirei (system B) in the Supercomputer Center, the Institute for Solid State Physics, the University of Tokyo.

The flows of the susceptibilities for various S are shown in Fig. 5.7 (a). The susceptibilities after breakdown show non-physical oscillations at low Λ, so they are not displayed below appropriate $\Lambda(< \Lambda_c)$ for readability. The susceptibilities show anomalous behavior. They show breakdown behavior at low Λ for S is more than 3/2 or 2. Especially, that of $S = 50$ system indicates strong divergence. These behaviors coincide with those in magnetic ordered phases. Even if $S = \infty$, there is no ordering at the Kitaev points as we mentioned in the previous section through the review of the earlier studies on the classical Kitaev-Heisenberg model. Therefore, the spin susceptibility should not diverge actually and we can consider that this breakdown behavior is an artifact of spin-S PFFRG extension. So do the susceptibilities obtained by spin-S PFFRG show ordering phenomena for artifacts? If

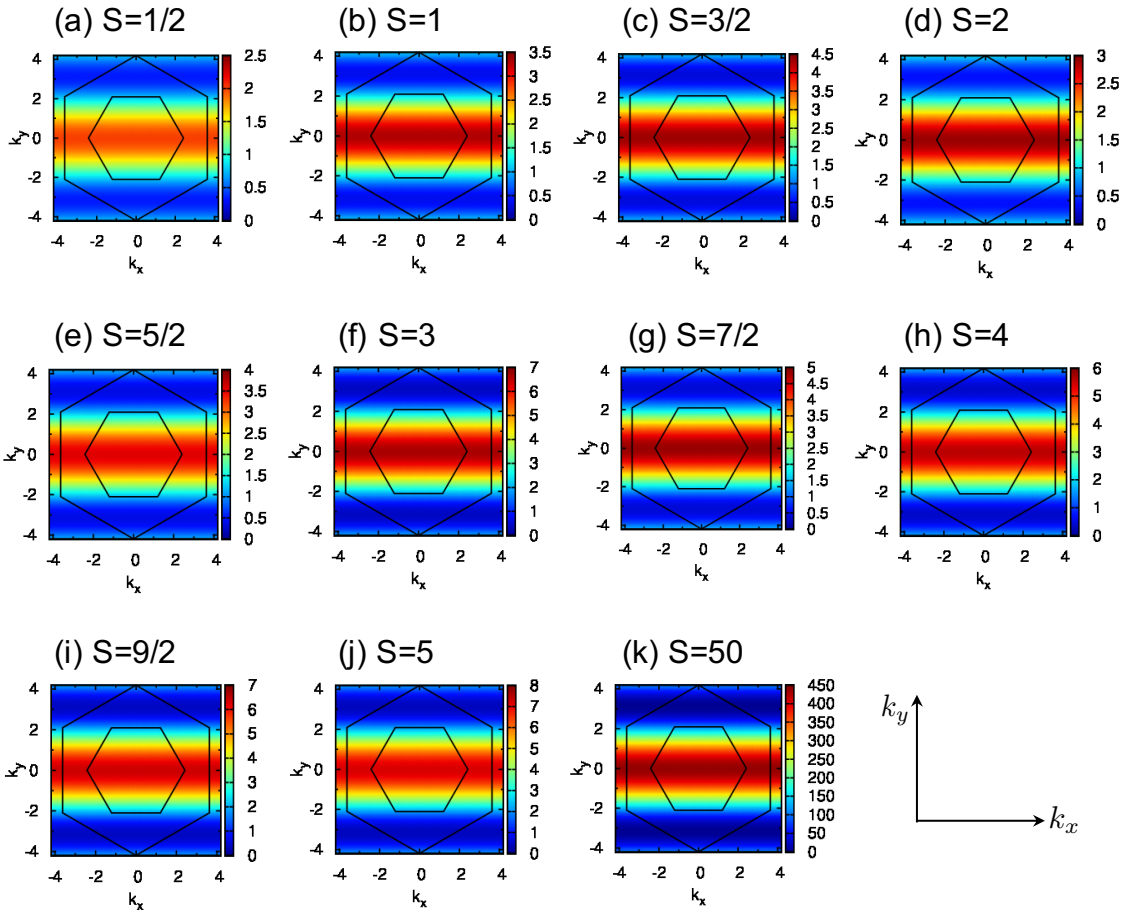

FIGURE 5.8: The momentum dependence of static susceptibility $\chi^{zz,\Lambda}(\boldsymbol{k}, i\nu = 0)$ at $\Lambda = \Lambda_{IR} \sim 0$ in (a)-(c), and at $\Lambda = \Lambda_c$ in (d)-(k). (a)-(k) show the results of spin-S Kitaev model with $S = 1/2$-5, and $S = 50$, respectively. The inner and outer hexagons represent the first and second Brillouin zone.

so, the susceptibilities should have peak at the wave vectors corresponding to the ordering vectors. We show the momentum dependence of the susceptibilities for various S in Fig. 5.8. We plot the susceptibilities $\chi^{zz,\Lambda}(\boldsymbol{k}, i\nu = 0)$ at $\Lambda = \Lambda_{IR} \sim 0$ for $S = 1/2$-$3/2$ systems and at $\Lambda = \Lambda_c$ for $S \geq 2$ because there are the clear breakdown scales Λ_c in the flow for $S \geq 2$ systems. As the same manner with the figures shown in the previous chapter, we show the first and second (extended) Brillouin zones by inner and outer hexagons, respectively. As shown in the figure, the susceptibilities have cosine-shape for all S, and this fact means the spin-spin correlation is finite only between spins on nearest-neighboring sites. This is the very character of the Kitaev quantum spin liquid. Indeed, this nearest-neighbor correlation for general S can be proved exactly [45]. The previous studies on other spin liquid states by spin-S PFFRG [139, 240] show transitions from spin liquids to the ordered phases as S increases. In addition, the ordered states for large-S are predicted by other methods, Luttinger-Tisza method and Monte Carlo simulation, for example. Hence this artifact does not appear. However, for the Kitaev model which does not indicate ordering even with $S = \infty$, the spin-S extension of PFFRG causes artificial breakdowns for large S. In spin-S extension of PFFRG explained in Sec. 3.7, the difference of spin

length results only in the prefactors in the flow equations and all terms in the vertex flow equations except the RPA terms are weakened by the prefactor $\frac{1}{2S}$ in spin-S systems. In the limit $S \to \infty$, only the RPA terms remain in the flow equations. These RPA terms induce ordering tendency and the breakdown of the flow. The cause of this artifact is that the effect of this RPA term cannot be suppressed by other terms for large S. This discussion reveals an important fact. We can speculate that this artifact indicates that the quantum fluctuations are weak in Kitaev quantum spin liquid with $S \geq 2$, and the system is easily ordered by other magnetic interactions.

In the next step, we examine whether there is a difference between the case where S is a half-odd integer and the case where S is an integer. In Fig. 5.7 (b) we show the frequency dependence of the pseudo-fermion damping ($\simeq$ the self-energy) at $\Lambda = \Lambda_{\rm IR}$ for some S. As S increases, it only shows the behavior of converging without depending on the even and odd of $2S$. For more detailed examination, we discuss the S dependence of the vertices. We fix $\Lambda = \Lambda_{\rm IR}$ and only consider vertices $\Gamma^{\rm z}$ and $\Gamma^{\rm d}$ between two nearest-neighbor sites connected by z-bond $\Gamma^{z,\Lambda_{\rm IR}}_{i_0 i_z}(s,t,u)$ and $\Gamma^{{\rm d},\Lambda_{\rm IR}}_{i_0 i_z}(s,t,u)$. Here i_0 represents the reference site (see Fig. 4.3) and i_z represent the site connected to i_0 by z-bond. To plot the frequency dependence, we fix one of the three frequencies s, t, and u. Due to the symmetry between s and u in Eq. (3.71) and Eq. (3.72), we fix $u = \omega_{\rm min}$ and consider only s and t. We show $\Gamma^{z,\Lambda_{\rm IR}}_{i_0 i_z}(s,t,u=\omega_{\rm min})|_{S=1/2} - \Gamma^{z,\Lambda_{\rm IR}}_{i_0 i_z}(s,t,u=\omega_{\rm min})|_{S=1}$, $\Gamma^{z,\Lambda_{\rm IR}}_{i_0 i_z}(s,t,u=\omega_{\rm min})|_{S=1/2} - \Gamma^{z,\Lambda_{\rm IR}}_{i_0 i_z}(s,t,u=\omega_{\rm min})|_{S=3/2}$, $\Gamma^{z,\Lambda_{\rm IR}}_{i_0 i_z}(s,t,u=\omega_{\rm min})|_{S=1/2} - \Gamma^{z,\Lambda_{\rm IR}}_{i_0 i_z}(s,t,u=\omega_{\rm min})|_{S=2}$, and $\Gamma^{z,\Lambda_{\rm IR}}_{i_0 i_z}(s,t,u=\omega_{\rm min})|_{S=1/2} - \Gamma^{z,\Lambda_{\rm IR}}_{i_0 i_z}(s,t,u=\omega_{\rm min})|_{S=5/2}$ in Fig. 5.9 (a), (b), (c), and (d), respectively. In our PFFRG we use the logalithmic meshes for frequencies. Therefore we plot vertices with respect to the integers n_s and n_t which specify the frequencies as $s = \omega(n_s)$ and $t = \omega(n_t)$, where $\omega(\cdot)$ is our frequency mesh. We also show $\Gamma^{{\rm d},\Lambda_{\rm IR}}_{i_0 i_z}(s,t,u=\omega_{\rm min})|_{S=1/2} - \Gamma^{{\rm d},\Lambda_{\rm IR}}_{i_0 i_z}(s,t,u=\omega_{\rm min})|_{S=1}$, $\Gamma^{{\rm d},\Lambda_{\rm IR}}_{i_0 i_z}(s,t,u=\omega_{\rm min})|_{S=1/2} - \Gamma^{{\rm d},\Lambda_{\rm IR}}_{i_0 i_z}(s,t,u=\omega_{\rm min})|_{S=3/2}$, $\Gamma^{{\rm d},\Lambda_{\rm IR}}_{i_0 i_z}(s,t,u=\omega_{\rm min})|_{S=1/2} - \Gamma^{{\rm d},\Lambda_{\rm IR}}_{i_0 i_z}(s,t,u=\omega_{\rm min})|_{S=2}$, and $\Gamma^{{\rm d},\Lambda_{\rm IR}}_{i_0 i_z}(s,t,u=\omega_{\rm min})|_{S=1/2} - \Gamma^{{\rm d},\Lambda_{\rm IR}}_{i_0 i_z}(s,t,u=\omega_{\rm min})|_{S=5/2}$ in Fig. 5.10 (a), (b), (c), and (d), respectively. From these figures, we cannot find the difference between half-odd integers and integers of S. Similar results are obtained for the vertex functions at other frequency points and for the anisotropic Kitaev model, which is close to the toric code limit. As we mentioned in the spin-S extension of PFFRG, the difference of spin length results only in the prefactors in the flow equations. Thereby, it is expected that the topological difference between the Kitaev model with half-odd integer and integer spins is not reflected to the flow in this extension.

From the calculations in this section, we can conclude that (i) while the spin-spin correlation is finite only between nearest-neighbor spins, PFFRG with simple spin-S expansion leads to artificial breakdowns of the susceptibility flow for large S, and (ii) this method cannot describe topological difference between half-odd integer and integer spin Kitaev model. Thus this spin-S PFFRG is not suitable for investigating topological properties of the spin-S Kitaev model. However, we believe it is useful for studying order competitions. In the next section, we discuss the phase diagrams of spin-S Kitaev-Heisenberg model obtained PFFRG.

5.6 Kitaev-Heisenberg Model with General Spin Length S

In this section, we discuss the results obtained by PFFRG calculation for spin-S Kitaev-Heisenberg model, and we elucidate how large S is allowed in order to realize the Kitaev quantum spin liquid in materials.

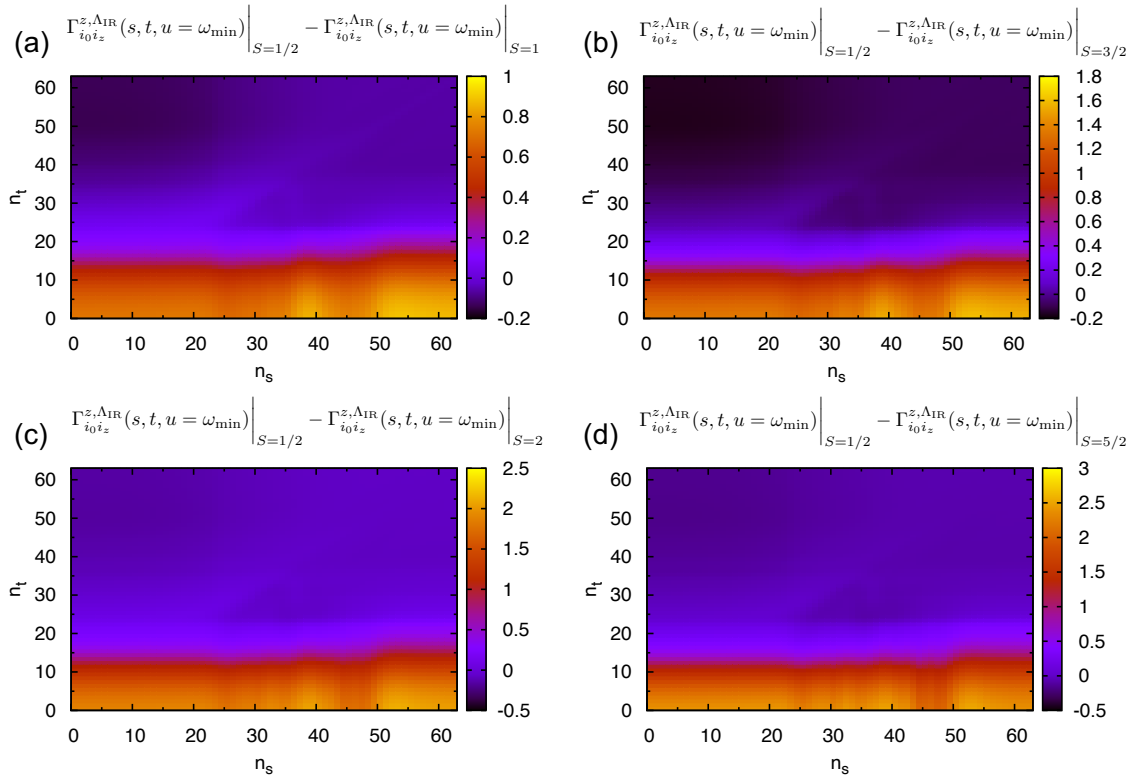

FIGURE 5.9: The differences in spin vertex $\Gamma^{z,\Lambda_{\rm IR}}(s,t,u)$ of the spin-S Kitaev model with different S are shown for frequency. We set $s = \omega(n_s)$, $t = \omega(n_t)$, and $u = \omega_{\rm min}$. (a)-(d) show the difference between $S = 1/2$ and $S = 1$, $S = 1/2$ and $S = 3/2$, $S = 1/2$ and $S = 2$, and $S = 1/2$ and $S = 5/2$ systems, respectively.

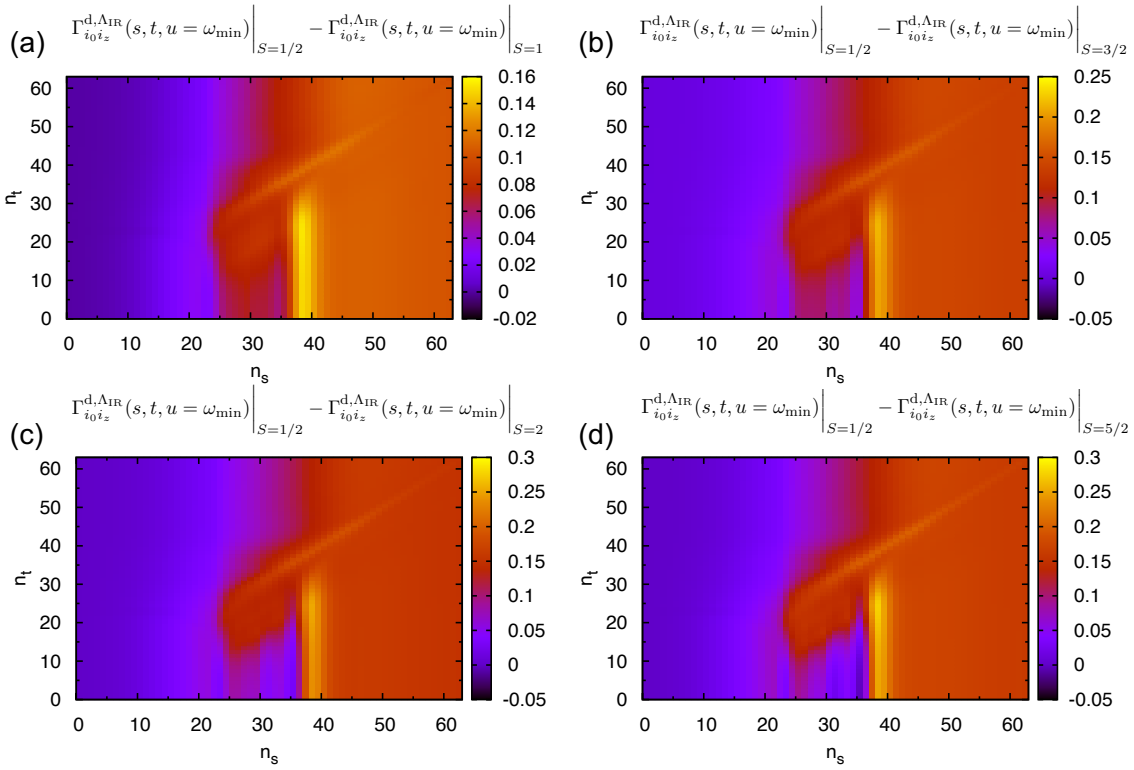

FIGURE 5.10: The differences in density vertex $\Gamma^{\mathrm{d},\Lambda_{\mathrm{IR}}}(s,t,u)$ of the spin-S Kitaev model with different S are shown for frequency. We set $s = \omega(n_s)$, $t = \omega(n_t)$, and $u = \omega_{\mathrm{min}}$. (a)-(d) show the difference between $S = 1/2$ and $S = 1$, $S = 1/2$ and $S = 3/2$, $S = 1/2$ and $S = 2$, and $S = 1/2$ and $S = 5/2$ systems, respectively.

Here we treat the Hamiltonian Eq. (5.4) and introduce a dimensionless parameter $\xi \in [0, 1)$ as

$$\xi = \frac{\varphi}{2\pi}. \tag{5.7}$$

We set A as a unit of energy. For spin-S calculation we introduce the flavor indices in the Kitaev term as in Eq. (5.6) and in the Heisenberg term as in Eq. (3.170). We calculate the susceptibility in the case $S = 1/2$, 1, $3/2$, 2, $5/2$, and 50. $S = 50$ is considered to be large enough to compare with the classical spin result [240]. We solve about 1.45×10^7 coupled integro-differential equations simultaneously for each ξ and S. We used 64 positive frequencies with logarithmic mesh between $\omega_{\min} \simeq 10^{-4}$ and $\omega_{\max} = 250$, and the internal frequency integration was carried out with a mesh more than twice as dense. We use the cluster with $L = 10$ (166 sites). This is smaller than in the previous section to calculate with many parameter values. In addition we take 250 Λ-points with the ratio $\Lambda_{i+1}/\Lambda_i = 0.96$ and $\Lambda_{\mathrm{UV}} = 500$. Here we use a slightly finer mesh than in the previous section for more precise values of Λ_c. Our calculations were performed in Reedbush and Oakbridge-CX in the Information Technology Center, The University of Tokyo, Oakforest-PACS in Center for Computational Sciences, University of Tsukuba and in the Information Technology Center, The University of Tokyo, and sekirei (system B) in the Supercomputer Center, the Institute for Solid State Physics, the University of Tokyo.

At first of the results, we show the behavior of the susceptibility flow for each S at some selected φ values separately in Fig. 5.11 ((a) $\xi = 0.1$, (b) 0.24, (c) 0.25, (d) 0.26, (e) 0.35, and (f) 0.55) and Fig. 5.12 ((a) $\xi = 0.7$, (b) 0.74, (c) 0.75, (d) 0.76, (e) 0.85, and (f) 0.95) for the convenience of the page. For the sake of visibility, the susceptibilities after divergence are truncated with appropriate small Λ. The momentum dependences of the susceptibilities at each ξ are shown in Fig. 5.13. We discuss the behavior of the susceptibility $\chi^{zz,\Lambda}(\boldsymbol{k}_{\max}, i\nu = 0)$ in Fig. 5.11 and Fig. 5.12 from $\xi = 0.1$ shown in Fig. 5.11 (a). The susceptibilities for all S show obvious divergence or breakdown and this indicates phase transition to the Néel AFM order (see Fig. 5.13 (a)). At $\xi = 0.24$ and $\xi = 0.26$ shown in Fig. 5.11 (b) and (d), respectively, the susceptibilities for $S = 1/2$ and $S = 1$ do not indicate phase transitions though those for $S \geq 3/2$ show breakdown. This means that at $\xi = 0.24$ and 0.26 the Kitaev-Heisenberg model with $S = 1/2$ and $S = 1$ in the spin liquid state near AFM Kitaev point $\xi = 0.25$. At exact AFM Kitaev point $\xi = 0.25$ in Fig. 5.11 (c), the susceptibilities for $S = 1/2$-$3/2$ do not show the breakdown while others do. Of course this is an artifact mentioned in the previous section. Actually all susceptibilities should not show the breakdown. At $\xi = 0.35$ and 0.55 all susceptibility flows indicate phase transition shown in Fig. 5.11 (e) and (f), and these correspond to the phase transition to the zigzag and FM orders, respectively. At $\xi = 0.7$, all susceptibilities except $S = 1/2$ show clear divergence in Fig. 5.12 (a). $S = 1/2$ and $S = 1$ susceptibilities at $\xi = 0.74$ show smooth flows although those of $S \geq 3/2$ do not show. At $\xi = 0.75$ (Fig. 5.12 (c)) and 0.76 (Fig. 5.12 (d)), the flows for $S = 1/2$-$3/2$ do not diverge and others show obvious breakdown. Finally, all flows shown in Fig. 5.12 (e) and (f) indicate clearly phase transitions to magnetic orders: stripy ($\xi = 0.85$) and Néel ($\xi = 0.95$) AFM order (see Fig. 5.13 (m) and (p)).

Next we discuss the momentum dependence of the susceptibilities shown in Fig. 5.13. The peak positions corresponding to each magnetic order are shown in Fig. 5.14. The positions of peaks are represented by filled red circles and the relative intensities of the peaks in each order are represented by the size of circles. We show that of $S = 1/2$ systems here because those of $S \geq 1$ are similar to that of $S = 1/2$.

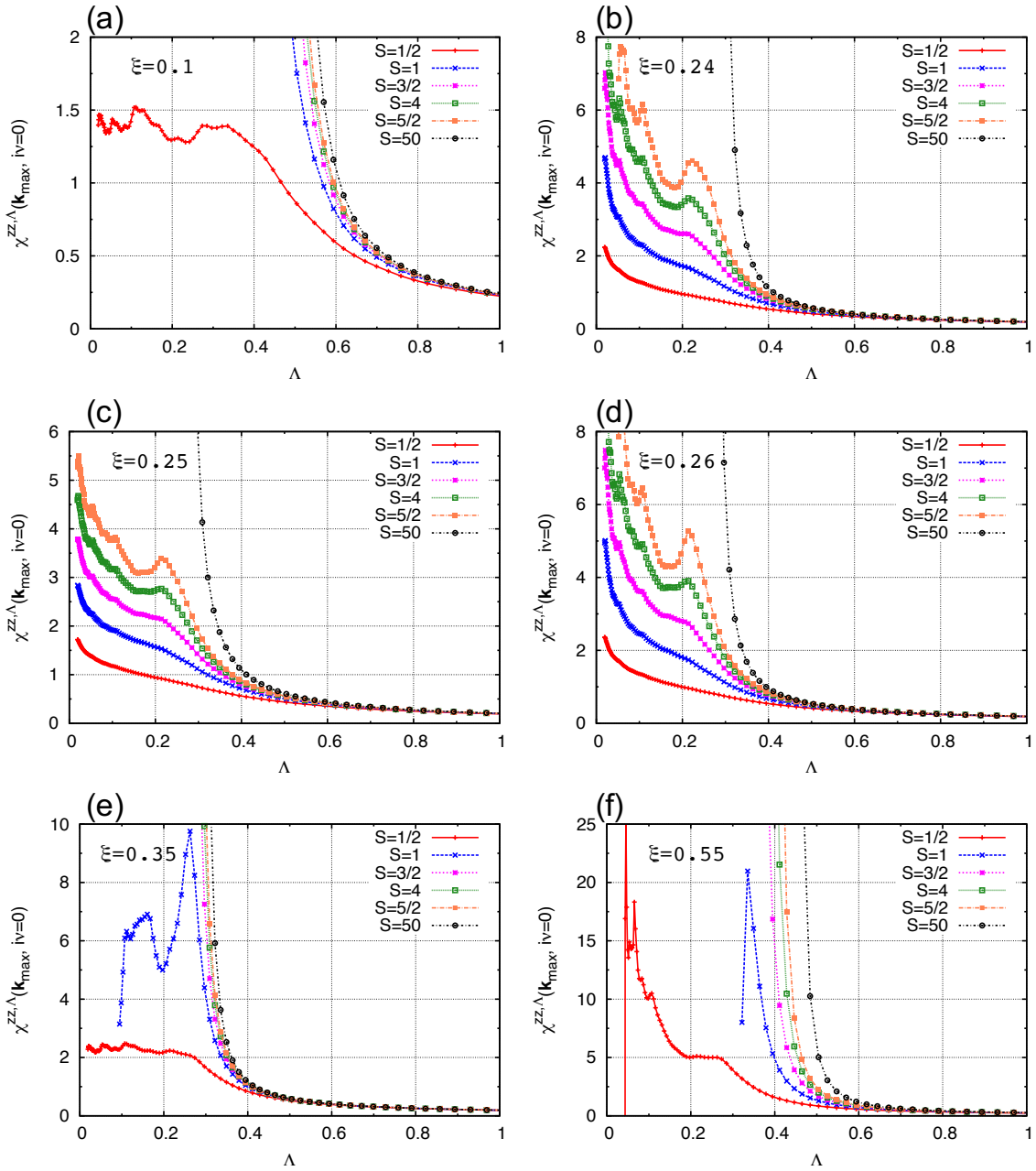

FIGURE 5.11: The susceptibility flows of spin-S Kitaev-Heisenberg model with $S = 1/2$-$5/2$ and $S = 50$. (a)-(f) correspond to the flows at $\xi = 0.1, 0.24, 0.25, 0.26, 0.35$, and 0.55, respectively.

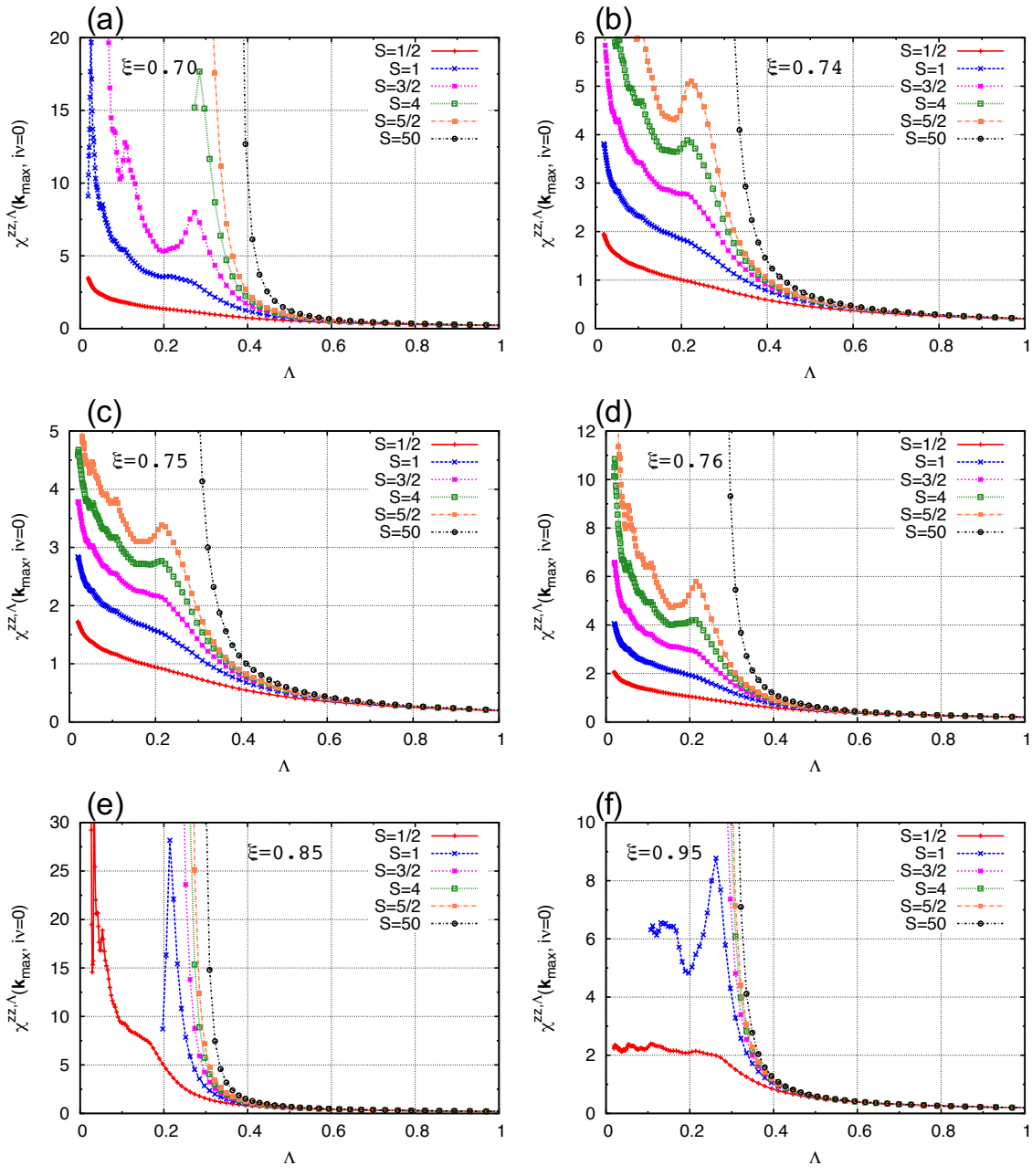

FIGURE 5.12: The susceptibility flows of spin-S Kitaev-Heisenberg model with $S = 1/2$-$5/2$ and $S = 50$. (a)-(f) correspond to the flows at $\xi = 0.7, 0.74, 0.75, 0.76, 0.85$, and 0.95, respectively.

We show the susceptibilities at $\Lambda = \Lambda_c$ in Fig. 5.13 (a), (e)-(h), (m)-(p), and those at $\Lambda = \Lambda_{IR}$ in Fig. 5.13 (b)-(d), (i)-(l) in Fig. 5.13, according to Fig. 5.11 and Fig. 5.12. Let us see from $\xi = 0.1$ in Fig. 5.13 (a). The peaks on each corner of the extended Brillouin zone clearly indicate Néel AFM order. Similarly the momentum dependence at $\xi = 0.95$ shown in Fig. 5.13 (p) shows Néel AFM order.

In addition, the momentum dependence at $\xi = 0.35$ in Fig. 5.13 (e), $\xi = 0.55$ in Fig. 5.13 (h), and $\xi = 0.85$ in Fig. 5.13 (m) indicate clear zigzag AFM, FM, and stripy AFM orders, respectively. Because these points are located deeply in each ordered phase. $\xi = 0.25$ (Fig. 5.13 (c)) and $\xi = 0.75$ (Fig. 5.13 (k)) are AFM and FM Kitaev points and the susceptibilities have cosine-shape momentum dependences. At $\xi = 0.24$ and $\xi = 0.26$, we can see the intermediate momentum dependence between Néel ordered state and AFM Kitaev spin liquid state and AFM spin liquid state and zigzag AFM state, respectively. At $\xi = 0.7$, strong FM peak shown in $\xi = 0.55$ tend to broaden into a cosine form in FM Kitaev spin liquid state. At $\xi = 0.74$ and $\xi = 0.76$ near FM Kitaev point, we can see the intermediate momentum dependence between FM ordered state and FM Kitaev spin liquid state and FM spin liquid state and stripy AFM state, respectively. In addition, the phase boundaries between the zigzag AFM and FM phases, and stripy and Néel AFM phases are located between $\xi = 0.44$ and $\xi = 0.45$, and $\xi = 0.91$ and $\xi = 0.92$, respectively. We can see that the peak positions are switched at these boundaries.

Here we show the full Λ-ξ diagrams for each S in Fig. 5.15. We show the finite Λ phase boundaries of the Néel AFM, zigzag AFM, FM, and stripy AFM by the black, green, blue, and pink lines. Points at which flows do not show breakdown are indicated the filled red circles at $\Lambda = 0$. These regions denote Kitaev quantum spin liquid phases and "QSL" in the figure is an acronym for quantum spin liquid. For $S \geq 2$, there is no points at which the susceptibilities have smooth flows. Actually, there is no magnetic order at $\xi = 0.25$ and 0.75 even in $S = \infty$. Thus we indicate breakdown scales at these points by the red open circles for $S \geq 2$. The phase boundaries between ordered phases in Figs. 5.15 (a), (b), and (f) are in good agreement with those of previous studies shown in Figs. 5.3, 5.5, and 5.6, respectively. In the phase diagram for $S = 1/2$ and $S = 1$, it is found that the region of the spin liquid state is wider than the previous studies (see Figs. 5.3, 5.5). This is because, in addition to the difference in the system size, it is more difficult to distinguish the spin liquid state from the ordered states near the phase boundaries in the PFFRG than in methods of the previous studies. We referred to the behavior of flow shown in Ref. [240] and its supplemental material for the decision of breakdown. If it is still difficult to make a judgment in the phase boundaries, we calculate a dimensionless quantity f defined as [6]

$$f = \left(\frac{A}{2S}\right)^2 \sum_{\Lambda} \left[\chi^{zz,\Lambda+d\Lambda}(\boldsymbol{k}_{\max}, i\nu = 0) - \chi^{zz,\Lambda}(\boldsymbol{k}_{\max}, i\nu = 0)\right]^2, \tag{5.8}$$

in the supplemental material of Ref. [125] and determined that the flow breaks down if $f \geq 0.5$. This evaluation criterion is a value determined from the fitting of figures in the supplemental material of Ref. [125] using WebPlotDigitizer [134] and empirical rules when applied to other systems. Note that here χ and Γ mean $\bar{\chi}$ and $\bar{\Gamma}$ in Eq. (3.167), respectively, for the spins with $S > 1/2$. Thus, they are rescaled using $M = 2S$. f is small when there is no breakdown in the flow, and takes a large value when there is breakdown in the flow because the susceptibility vibrates after breakdown. In addition, in our calculation shown in Fig. 5.15 (f), the susceptibility

[6] Be careful not to confuse them with the frustration parameter in the previous chapter.

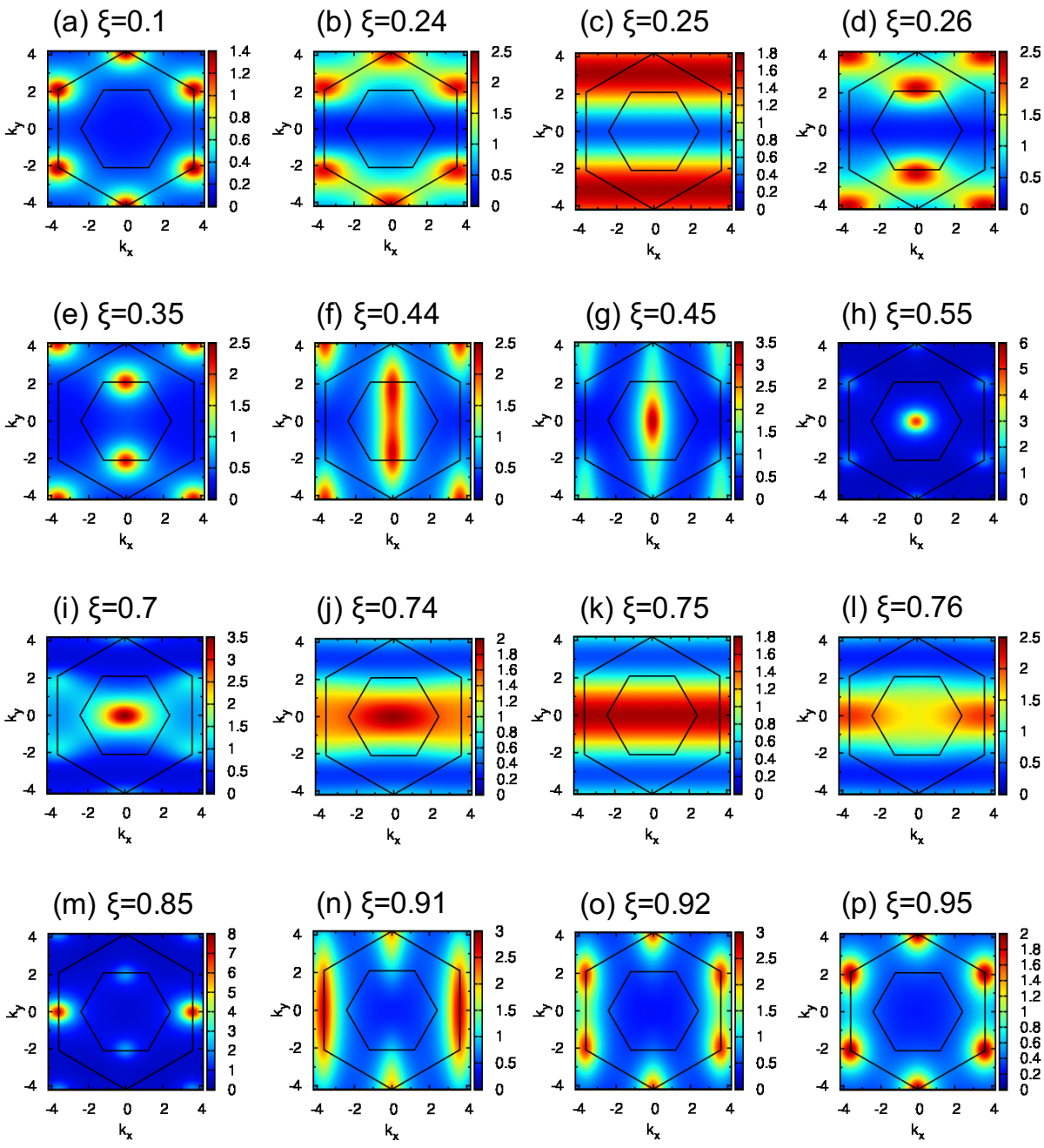

FIGURE 5.13: (a)-(p) Momentum dependence of the spin susceptibility $\chi^{zz,\Lambda}(\boldsymbol{k}, i\nu = 0)$ of the $S = 1/2$ Kitaev-Heisenberg model at $\xi = 0.1$, 0.24, 0.25, 0.26, 0.35, 0.44, 0.45, 0.55, 0.7, 0.74, 0.75, 0.76, 0.85, 0.91, 0.92, and 0.95, respectively. We show the susceptibilities at $\Lambda = \Lambda_c$ in (a), (e)-(h), (m)-(p), and those at $\Lambda = \Lambda_{IR}$ in (b)-(d), (i)-(l). The inner and outer hexagons represent the first and second Brillouin zone.

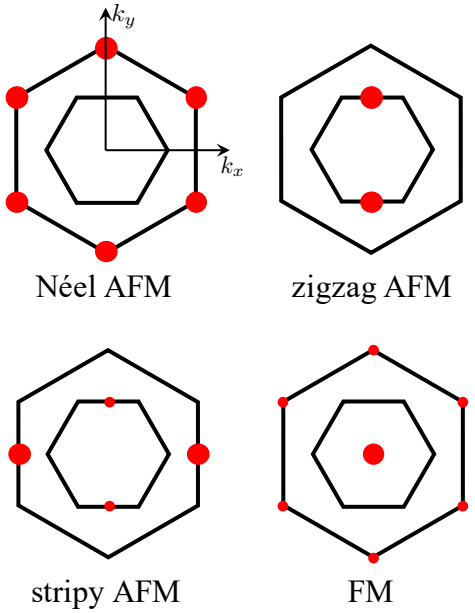

FIGURE 5.14: The positions of the susceptibility peaks in the momentum space corresponding to each magnetic order. The inner and outer hexagons denote the first and the second (extended) Brillouin zones. Filled red circles represent the positions of peaks and the relative intensities of the peaks in each ordered phase are represented by the size of circles.

shows breakdown behavior at six special points $\xi = 0$, 0.25, 0.375, 0.5, 0.75, and 0.875 due to two artifacts: the artifacts appearing in the calculation of the spin-S Kitaev model and the artifacts that violate the Mermin-Wagner theorem introduced in the explanation of Fig. 5.4. However, for the position of the phase boundaries and the shape of the phases, Fig. 5.15 (f) is in good agreement with Fig. 5.6. The range of $\xi = 0.75$ ($\varphi = \frac{3\pi}{2}$) to $\xi = 1$ ($\varphi = 0$) in Fig. 5.15 (a) is roughly consistent with the phase diagram of the previous study by PFFRG shown in Fig. 5.4. However, there is a difference near the boundary between the Néel AFM and stripy AFM phases. It is considered that this is because Λ-mesh (and frequency mesh, possibly) which we use is more sparse. We can see that the quantum spin liquid state survives in $S = 3/2$. This is in contrast to other systems where spin liquids survive only up to $S = 1/2$ or $S = 1$ [139, 240]. It can be attributed to the exactly solvable nature and strong frustration of the Kitaev model.

To show the relationship between the spin length S and the spin liquid state in detail, the S-ξ phase diagram obtained from the above results is shown in Fig. 5.16. The region where the spin liquid state was predicted by PFFRG is shaded in light red. "QSL" in the figure denotes quantum spin liquid. In the case of $S = 1/2$ [52] and $S = 1$ [40], the phase boundary between the spin liquid state and the other orders expected in the previous work is shown by black dashed lines. In addition, the region shaded in dark red is obtained by scaling the region shaded in light red to match the region of the $S = 1/2$ spin liquid state obtained in the earlier study [52]. In this region, the quantum spin liquid state can be expected from both previous research and our calculation. We can conclude that the quantum spin liquid state survives up to $S = 3/2$ at least for $K < 0$. Recently, the realization of AFM Kitaev spin liquid is proposed for $S = 3/2$ two-dimensional candidate materials $CrSiTe_3$

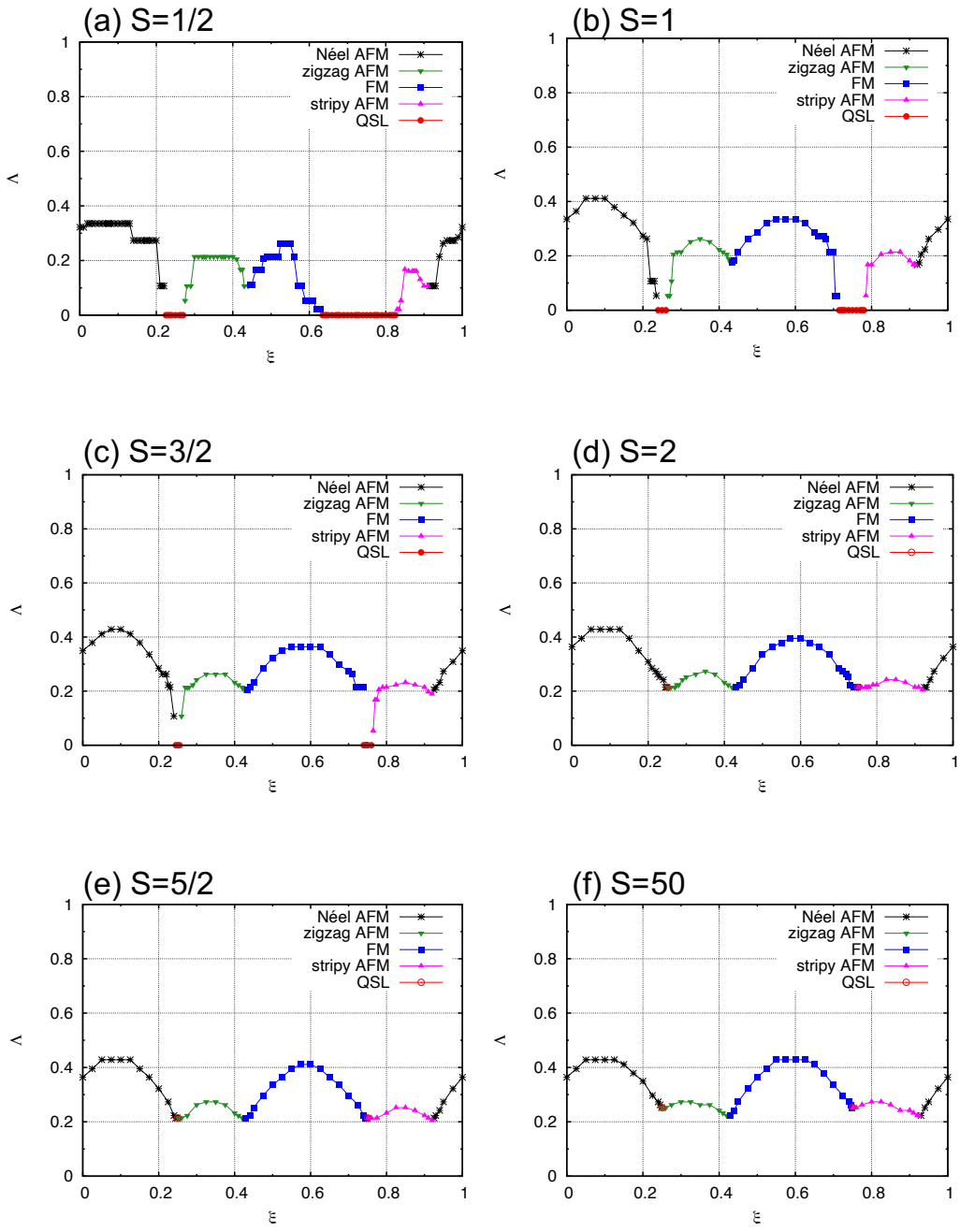

FIGURE 5.15: (a)-(f) Λ-$\tilde{\zeta}$ phase diagrams of the $S = 1/2$-$5/2$ and $S = 50$ Kitaev-Heisenberg model, respectively. QSL means quantum spin liquid.

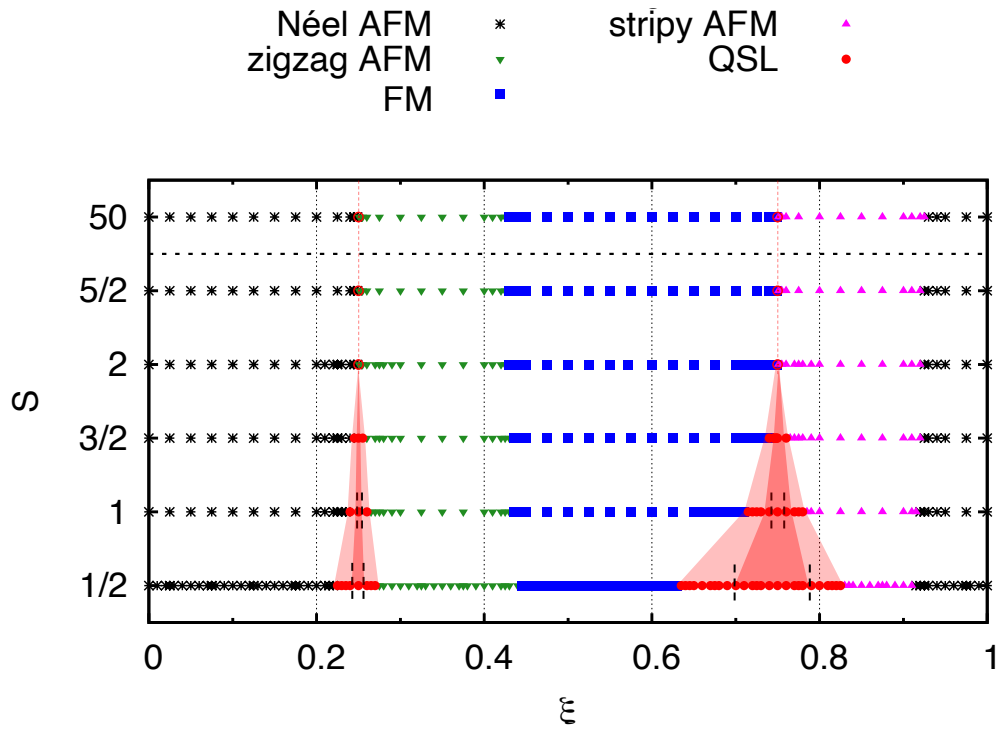

FIGURE 5.16: S-ξ phase diagram of the spin-S Kitaev-Heisenberg model. The region where the spin liquid state was predicted by our PFFRG calculation is shaded in light red. In the region enclosed by the dashed line, the spin liquid state was predicted by previous studies on the $S = 1/2$ and $S = 1$ Kitaev-Heisenberg model. The region shaded in dark red is obtained by scaling the region shaded in light red to match the region of the $S = 1/2$ spin liquid state obtained in the previous study.

and $CrGeTe_3$ under epitaxial strain by ED with parameters obtained by the first-principle calculation [49]. These candidate material includes the off-diagonal spin interactions and anisotropy. These off-diagonal terms does not stabilize the spin liquid states, but rather destabilizes it [241]. Therefore, the Kitaev quantum spin liquid near $\xi = 0.25$ is also expected to survive to S = 3/2 in a narrow range.

5.7 Summary of This Chapter

In this chapter, we have investigated the realization of Kitaev quantum spin liquids in candidate materials with general spin length. We have regarded the Kitaev-Heisenberg model as the minimal model of the Kitaev materials, and calculated phase diagram of the spin-S Kitaev-Heisenberg model by using spin-S extension of PFFRG.

At first, we calculated the susceptibility flow of the spin-S Kitaev model. As a result of our calculation, breakdown behaviors appeared in the flows of the susceptibility of $S \geq 2$ cases, which seemed to suggest phase transition to magnetic order. However, it is known that in the Kitaev model with general S, the spin correlations exist strictly only between the nearest-neighboring sites and the system does not undergo ordering. In fact, the spatial structure of the susceptibility we have calculated is also finite only between the nearest-neighboring sites. Therefore, we can conclude that this breakdown-like behavior is an artifact of spin-S PFFRG. We can speculate that this artifact indicates that the quantum fluctuations are weak in Kitaev quantum spin liquid with $S \geq 2$, and the system is easily ordered by other magnetic interactions. This can be understood from the fact that the spin-S PFFRG reduces the magnitude of the quantum fluctuation terms in the flow equations by a factor of $1/2S$.

In addition, there is no difference in the results of the spin-S PFFRG calculation when S is half-odd-integer and when S is integer. Since the extension of PFFRG to general spin length introduced in Sec. 3.7 produces only monotonic changes in the prefactors of each term in the flow equations, we can conclude that this simple extension does not reflect the differences in topology between half-odd-integer spins and integer spins.

Next, we calculated the phase diagram of the spin-S Kitaev-Heisenberg model with $S = 1/2 - 5/2$ and $S = 50$. The obtained phase diagrams of the Kitaev-Heisenberg model for $S = 1/2$ and $S = 1$ are in general good agreement with the previous studies by other numerical methods. The phase diagram for $S = 50$ is in good agreement with the previous study on the classical Kitaev-Heisenberg model by Monte Carlo simulation, except for six special points: four of the six special points are points where the system recovers continuous symmetry, and the other two are points where the system becomes the Kitaev model. As a result of systematic calculations with different S, for $S \leq 3/2$, both the AFM and FM Kitaev spin liquid regions have a finite extent. For $S \geq 2$, no region showing Kitaev spin liquid state was found. Therefore, we believe that $S = 3/2$ gives an upper bound on the spins possessed by the candidate materials in which Kitaev quantum spin liquid is realized.

The phase diagram calculation of the Kitaev-Heisenberg model with a systematic change of spin S, as we have done here, has not been performed before. This is the first study of the application of spin-S PFFRG to the Kitaev-Heisenberg model. Moreover, the PFFRG calculations for the Kitaev-Heisenberg model with $S = 1/2$

have been performed for all parameter regions in this dissertation, whereas the previous study on the Kitaev-Heisenberg model by PFFRG elucidated the phase diagram for the region $\varphi = \frac{3\pi}{2}$ ($\xi = 0.75$) to $\varphi = 2\pi$ ($\xi = 1$). The results we have obtained here provide a guideline for the recent intensive search for candidate materials of $S \geq 1/2$ Kitaev quantum spin liquid.

Chapter 6

Summary and Perspective

In this doctoral dissertation, we have mainly focused on two studies related to the feasibility of Kitaev quantum spin liquids. In one, we discussed its feasibility in ultracold polar molecular systems trapped in the optical lattice, based on the realization of Kitaev-type interactions proposed in previous studies [34, 35]. In the other, we have investigated the realization of Kitaev quantum spin liquids in candidate materials with general spin length.

We used PFFRG (pseudo-fermion functional renormalization group) as a numerical method to tackle these problems. PFFRG has the advantage of being able to handle relatively large quantum systems even if the system has long-range interactions. Even if the interactions are long-range in nature, the computational cost is not different at all from the case with only nearest-neighbor interactions. In addition, a simple extension to large-S can be implemented using the extension method proposed in 2017 [139], and this results in only the difference of prefactors in the flow equation. Thus, the computational cost is the same as for $S = 1/2$ PFFRG. The PFFRG we used and its extensions are summarized in Chap. 3.

In Chap. 4, we have introduced the dipolar Kitaev model as a realization of Kitaev-type interaction by microwave irradiation in ultracold polar molecular systems. This model has a (quasi-) long-range spin interaction because it originates from the dipole interactions between polar molecules. The Kitaev-type interaction is observed between the nearest-neighboring sites, but between sites farther apart than the nearest-neighboring sites, the interaction is complicated with S^xS^x S^yS^y, and S^zS^z mixing depending on the angle between interacting sites. We calculate the susceptibility using PFFRG with the sign and anisotropy of the spin interaction as parameters, and find that the ferromagnetic order is observed for all anisotropy parameters in the case of ferromagnetic interaction, and the zigzag antiferromagnetic order is observed for all anisotropy parameters in the case of antiferromagnetic interaction.

Furthermore, in order to investigate the reason why the quantum spin liquid state is not realized in the dipolar Kitaev model, we introduced an artificial range of interactions and investigated the susceptibility when approaching the dipolar Kitaev model with long-range interactions from the Kitaev model with only nearest-neighbor interactions. The frustration weakens as the range of interactions is extended, and the spin liquid state realized in the Kitaev model is quickly destroyed. This is in contrast to the dipolar Heisenberg model, which obtains frustration stronger than the nearest-neighbor Heisenberg model due to its long-range nature, and hosts quantum spin liquids.

Considering also the previous study suggesting that the Kitaev quantum spin liquid is fragile against the next-nearest-neighbor Kitaev interaction, it can be concluded that the dipolar Kitaev model does not realize the quantum spin liquid due to its long-range nature of the interaction. Therefore, it is necessary to propose another

realization of the Kitaev quantum spin liquid for ultracold polar molecular systems. After the proposal of Kitaev-type interaction in ultracold polar molecular systems by microwave irradiation in 2013, the calculation based on this proposal has not been performed, and whether Kitaev quantum spin liquid state is actually realized has remained an open question. We addressed this issue with PFFRG and elucidated the above results for the first time.

In Chap. 5, we have performed PFFRG calculations for the spin-S Kitaev model and the spin-S Kitaev-Heisenberg model using an extension of the PFFRG method to large-S. First, we calculated the susceptibility of the original Kitaev model while varying the spin length S. As a result, breakdown-like behaviors of the susceptibility appear for about $S \geq 2$ systems. It has been proved that the $\mathbb{Z}_2$ fluxes are conserved quantities in the Kitaev model with general S, and this means that only the spin correlations between nearest-neighboring sites are finite. It has been also found that the classical Kitaev model corresponding to $S = \infty$ case does not undergo magnetic ordering and there is no order-by-disorder phenomena. Indeed, also in our calculation the susceptibilities for general S are finite only between the nearest-neighboring sites though they indicate breakdown behavior. For these reasons, this behavior is considered to be an artifact of our method. However, we believe that this artifact indicates an important trend. The large-S effect weakens the magnitude of the terms in the flow equations that cause quantum fluctuations by a factor of $1/2S$, without changing the strength of the RPA terms that cause ordering. We can speculate that this artifact indicates that the quantum fluctuations are weak in Kitaev quantum spin liquid with $S \geq 2$, and the system is easily ordered by other magnetic interactions.

Next, we investigated whether the self-energy and interaction vertices in spin-S PFFRG show any difference between half-odd integer spins and integer spins. The results showed that these differences did not appear. In extension of PFFRG for large-S, the difference in S appears only in the monotonic change of the prefactors of each term in the flow equations. Therefore, it is considered that our calculation does not incorporate the topological structure due to the difference in S.

Finally, we have calculated the phase diagram of the spin-S Kitaev-Heisenberg model for $S = 1/2 - 5/2$ and $S = 50$ spins. The obtained phase diagrams for $S = 1/2$ and $S = 1$ cases are in good agreement with previous studies using other methods, except that the regions where the spin liquid state is realized are widely evaluated. This is due to the fact that it is difficult to determine whether the susceptibility flows indicate breakdown or not near boundaries between magnetic ordered phase and quantum paramagnetic phase. In addition, the phase diagram of the Kitaev-Heisenberg model for $S = 50$ spins is in general agreement with the phase diagram of the classical Kitaev-Heisenberg model obtained by the Monte Carlo method, except for a few special points. From the results of these calculations, we have found that the upper limit of the spin length of the candidate material allowed for the realization of Kitaev quantum spin liquid is S=3/2. Of course, there are spin non-diagonal interactions in the candidate materials that are not included in the Kitaev-Heisengerg model, but they generally destabilize the quantum spin liquid state.

The phase diagram calculation of the Kitaev-Heisenberg model with a systematic change of spin S, as we have done here, has not been performed before. PFFRG and its large-S extension have enabled us to do such calculations. Moreover, the PFFRG calculations for the Kitaev-Heisenberg model with $S = 1/2$ have been performed for all parameter regions in this dissertation, whereas the Kitaev term is ferromagnetic and the Heisenberg term is antiferromagnetic in the previous study on this model

using PFFRG. The results we have obtained here provide a guideline for the recent intensive search for candidate materials of $S \geq 1/2$ Kitaev quantum spin liquid.

We close the dissertation with a few perspectives. We concluded that it is difficult to realize Kitaev quantum spin liquid with dipole interaction in ultracold polar molecular systems in Chap. 4. One possible solution is to design the long-range part of the interaction to be Heisenberg-like, since the Kitaev quantum spin liquid is robust against Heisenberg interactions between next-nearest-neighbor sites. Proposals for the realization of Kitaev-type interactions in cooled atomic systems by other mechanisms have been made, and the feasibility of quantum spin liquids in these models should also be investigated in detail. Due to their high controllability, implementations of the high-spin Kitaev model in these systems have also been proposed.

Related to the contents of Chap. 5, our next interest is in effects such as non-diagonal spin interactions and single-ion anisotropy. These effects are important in real materials. The large-S PFFRG used here can also incorporate these effects. As an example, even in the effective models obtained using *ab initio* calculation for $CrSiTe_3$ and $CrGeTe_3$, which have been proposed as $S = 3/2$ Kitaev materials, these terms are present in a non-negligible magnitude [49]. PFFRG has also been used to study frustrated quantum magnets in three dimensions [118, 135] because of its ability to calculate systems with large system sizes, and we are also considering calculations for three-dimensional Kitaev materials.

We also hope to see the development of the PFFRG method used in this dissertation itself. PFFRG is a relatively new method, proposed in 2010, and its extensions are still being actively studied. Just recently, two groups have simultaneously proposed a multi-loop extension of PFFRG. In the context of itinerant electron systems, a quantitative comparison of the results of the multi-loop FRG of the two-dimensional Hubbard model with those of the determinat quantum Monte Carlo method is also presented [72]. The multi-loop extension is expected to improve the accuracy of the PFFRG calculations. Finally, as mentioned at the end of Chap. 3, PFFRG in magnetic fields and at finite temperatures is rarely performed due to the enormous computational cost. We hope to solve this problem by improving the performance of computers and proposing prescriptions. In particular, the calculation of Kitaev quantum spin liquid in magnetic field is very important for the discussion of non-Abelian anyons and spin current generation.

Appendix A

Fourier Transformation

For systematic counting of prefactors, we define Fourier transformation as a non-unitary transformation in this dissertation. Here we only consider frequency dependence of functions for simplicity (other arguments of the functions are not written explicitly) and present the definition of the Fourier transformation use in this dissertation.

The Green's function is defined as

$$G(\tau,\tau') = -\langle\psi(\tau)\overline{\psi}(\tau')\rangle. \tag{A.1}$$

We usually define the Fourier expansion of field variables as

$$\psi(\tau) = \frac{1}{\sqrt{\beta}}\sum_{\omega_n} \mathrm{e}^{-\mathrm{i}\omega_n\tau}\psi(\omega_n), \tag{A.2}$$

$$\overline{\psi}(\tau) = \frac{1}{\sqrt{\beta}}\sum_{\omega_n} \mathrm{e}^{\mathrm{i}\omega_n\tau}\overline{\psi}(\tau). \tag{A.3}$$

For systematic formulation of FRG, we define those as

$$\psi(\tau) = \frac{1}{\beta}\sum_{\omega_n} \mathrm{e}^{-\mathrm{i}\omega_n\tau}\psi(\omega_n), \tag{A.4}$$

$$\overline{\psi}(\tau) = \frac{1}{\beta}\sum_{\omega_n} \mathrm{e}^{\mathrm{i}\omega_n\tau}\overline{\psi}(\tau). \tag{A.5}$$

In the context of the field theory, this definition is often used. We define Fourier expansion in momentum space in similar way (but the signs of exponents are opposite). In this definition, one summation corresponds one prefactor. This fact enables us to construct FRG equations systematically for arbitrary sets of 1-particle state labels and frequencies.
Green's function in frequency space is obtained as

$$\begin{aligned} G(\tau,\tau') &= -\langle\psi(\tau)\overline{\psi}(\tau')\rangle \\ &= \frac{1}{\beta^2}\sum_{\omega_n,\omega_{n'}} \mathrm{e}^{-\mathrm{i}\omega_n\tau+\mathrm{i}\omega_{n'}\tau'}\left\{-\langle\psi(\omega_n)\overline{\psi}(\omega_{n'})\rangle\right\} \\ &= \frac{1}{\beta^2}\sum_{\omega_n,\omega_{n'}} \mathrm{e}^{-\mathrm{i}\omega_n\tau+\mathrm{i}\omega_{n'}\tau'}G(\omega_n,\omega_{n'}). \end{aligned} \tag{A.6}$$

Fourier transformation is performed as

$$\int \mathrm{d}\tau \int \mathrm{d}\tau' \, G(\tau,\tau')\mathrm{e}^{\mathrm{i}\omega_m\tau-\mathrm{i}\omega_{m'}\tau'} \tag{A.7}$$

$$\begin{aligned}
&= \frac{1}{\beta^2}\int \mathrm{d}\tau \int \mathrm{d}\tau' \sum_{\omega_n,\omega_{n'}} \mathrm{e}^{\mathrm{i}\omega_m\tau-\mathrm{i}\omega_{m'}\tau'} G(\omega_n,\omega_{n'})\mathrm{e}^{\mathrm{i}\omega_n\tau-\mathrm{i}\omega_{n'}\tau'} \\
&= \frac{1}{\beta^2}\sum_{\omega_n,\omega_{n'}} \left[\int \mathrm{d}\tau \, \mathrm{e}^{\mathrm{i}(\omega_m-\omega_n)\tau}\right]\left[\int \mathrm{d}\tau' \, \mathrm{e}^{-\mathrm{i}(\omega_{m'}-\omega_{n'})\tau'}\right] G(\omega_n,\omega_{n'}) \\
&= \frac{1}{\beta^2}\sum_{\omega_n,\omega_{n'}} \Big[\beta\delta(\omega_m-\omega_n)\Big]\Big[\beta\delta(\omega_{m'}-\omega_{n'})\Big] G(\omega_n,\omega_{n'}) \\
&= G(\omega_m,\omega_{m'}).
\end{aligned} \tag{A.8}$$

If homogeneous (translational invariant)[1], i.e.

$$G(\tau,\tau') = G(\tau-\tau'), \tag{A.9}$$

we can obtain the relation between $G(\omega_n,\omega_{n'})$ and $G(\omega_n)$:

$$\begin{aligned}
G(\omega_n,\omega_{n'}) &= \int \mathrm{d}\tau \int \mathrm{d}\tau' \, \mathrm{e}^{\mathrm{i}\omega_n\tau-\mathrm{i}\omega_{n'}\tau'} G(\tau-\tau') \\
&\overset{\tau-\tau'=\tau''}{=} \int \mathrm{d}\tau'' \int \mathrm{d}\tau' \, \mathrm{e}^{\mathrm{i}\omega_n(\tau''+\tau')-\mathrm{i}\omega_{n'}\tau'} G(\tau'') \\
&= \left(\int \mathrm{d}\tau' \, \mathrm{e}^{\mathrm{i}(\omega_n-\omega_{n'})\tau'}\right)\left(\int \mathrm{d}\tau'' \, \mathrm{e}^{\mathrm{i}\omega_n\tau''} G(\tau'')\right) \\
&= \beta\delta(\omega_n-\omega_{n'})G(\omega_n).
\end{aligned} \tag{A.10}$$

We can regard this relation as the result of energy conservation.

[1] In Matsubara frequency representation, this condition is always satisfied because we consider thermal equilibrium states.

Appendix B

Other Flow Parameters

Here we review temperature flow and interaction flow schemes although we adopt cutoff flow scheme of FRG in the main text of this dissertation. These two approaches have their own advantages and disadvantages which are different from cutoff flow scheme.

B.1 Temperature Flow

We can choose temperature as a flow parameter of FRG [242]. Local symmetries are not broken in temperature flow. Therefore, the corresponding Ward identities satisfaction is improved at least in the exact flow[1].

In general, bare action is written like

$$\begin{aligned}\mathcal{S}[\overline{\psi},\psi] = -T\sum_{n,x,x'}\overline{\psi}(\mathrm{i}\omega_n,x')Q(\mathrm{i}\omega_n;x',x)\psi(\mathrm{i}\omega_n,x)\\ +\frac{T^3}{4}\sum_{x_1,x_2,x_1',x_2'}\sum_{n_1,n_2,n_1',n_2'}V(\mathrm{i}\omega_{n_1'},x_1',\mathrm{i}\omega_{n_2'},x_2';\mathrm{i}\omega_{n_1},x_1,\mathrm{i}\omega_{n_2},x_2)\\ \times\overline{\psi}(\mathrm{i}\omega_{n_1'},x_1')\overline{\psi}(\mathrm{i}\omega_{n_2'},x_2')\psi(\mathrm{i}\omega_{n_2},x_2)\psi(\mathrm{i}\omega_{n_1},x_1)\\ \times\delta(\omega_{n_1}+\omega_{n_2}-\omega_{n_1'}-\omega_{n_2'}).\end{aligned} \tag{B.1}$$

Here, x is set of the appropriate quantum numbers for single-particle basis, and the summations include appropriate prefactors except temperature. Now we represent temperature explicitly.
We want to shift all temperature dependence of the bare action to the quadratic term i.e. Gaussian integral measure Q.
Rescaling field variables as

$$\overline{\psi}' = T^{3/4}\overline{\psi}, \tag{B.2}$$

$$\psi' = T^{3/4}\psi, \tag{B.3}$$

[1] In general, conserving approximation which satisfies macroscopic conservation lows, does not necessarily satisfy the Ward identities derived from microscopic conservation lows.

we obtain

$$\begin{aligned}\mathcal{S}'^{T}[\overline{\psi}',\psi']\Big(=\mathcal{S}[\overline{\psi},\psi]\Big)&\\ =-T^{-1/2}\sum_{x,x',n}\overline{\psi}'(\mathrm{i}\omega_n,x')Q(\mathrm{i}\omega_n,x',x)\psi'(\mathrm{i}\omega_n,x)&\\ +\frac{1}{4}\sum_{x_1,x_2,x_1',x_2'}\sum_{n_1,n_2,n_1',n_2'}V(\mathrm{i}\omega_{n_1'},x_1',\mathrm{i}\omega_{n_2'},x_2';\mathrm{i}\omega_{n_1},x_1,\mathrm{i}\omega_{n_2},x_2)&\\ \times\overline{\psi}'(\mathrm{i}\omega_{n_1'},x_1')\overline{\psi}'(\mathrm{i}\omega_{n_2'},x_2')\psi'(\mathrm{i}\omega_{n_2},x_2)\psi'(\mathrm{i}\omega_{n_1},x_1).&\end{aligned}\tag{B.4}$$

In this scheme, explicit temperature factor is pushed onto the 1-body term of the action as a flow parameter. Defining a new (inverse) bare propagator as

$$Q'^{T}(\mathrm{i}\omega_n,x',x)=T^{-1/2}Q(\mathrm{i}\omega_n,x',x),\tag{B.5}$$

we can write the action as

$$\begin{aligned}\mathcal{S}'^{T}[\overline{\psi}',\psi']=-\sum_{x,x',n}\overline{\psi}'(\mathrm{i}\omega_n,x')Q'^{T}(\mathrm{i}\omega_n,x',x)\psi'(\mathrm{i}\omega_n,x)&\\ +\frac{1}{4}\sum_{x_1,x_2,x_1',x_2'}\sum_{n_1,n_2,n_1',n_2'}V(\mathrm{i}\omega_{n_1'},x_1',\mathrm{i}\omega_{n_2'},x_2';\mathrm{i}\omega_{n_1},x_1,\mathrm{i}\omega_{n_2},x_2)&\\ \times\overline{\psi}'(\mathrm{i}\omega_{n_1'},x_1')\overline{\psi}'(\mathrm{i}\omega_{n_2'},x_2')\psi'(\mathrm{i}\omega_{n_2},x_2)\psi'(\mathrm{i}\omega_{n_1},x_1).&\end{aligned}\tag{B.6}$$

Prime " ′ " means the function defined by the new fields ψ' and $\overline{\psi}'$, and the suffix T means the function with a flow parameter T. Now temperature dependence of all functions in the bare action is shifted to the new measure Q'^{T}. In the representation using new field $(\overline{\psi}',\ \psi')$, we omit prefactors T with frequency summations.

Before discussion about general m-body propagators and vertices, let us check that temperature T satisfies general properties for flow parameters. For simplicity, we consider single-band systems with translational and spin-rotational symmetry. Due to Fourier transformation we can obtain

$$\left[Q'^{T}(\mathrm{i}\omega_n,\boldsymbol{k})\right]^{-1}=G_0'^{T}(\mathrm{i}\omega_n,\boldsymbol{k})=\frac{T^{1/2}}{\mathrm{i}\omega_n-\xi_{\boldsymbol{k}}}=T^{1/2}G_0(\mathrm{i}\omega_n,\boldsymbol{k}).\tag{B.7}$$

Flow parameters Λ have to satisfy the condition

$$G_0^{\Lambda}=\begin{cases}0 & \Lambda=\Lambda_{\mathrm{UV}}\quad\text{initial condition}\\ \text{singular} & \Lambda=\Lambda_{\mathrm{IR}}\quad\text{final condition.}\end{cases}\tag{B.8}$$

At $\xi_{\boldsymbol{k}}=0$ and $n=0$, the Green's function is

$$G_0'^{T}(\mathrm{i}\pi T,\boldsymbol{k})=\frac{T^{1/2}}{\mathrm{i}\omega_0}=\frac{T^{1/2}}{\mathrm{i}\pi T}=\frac{1}{\mathrm{i}\pi}\cdot\frac{1}{T^{1/2}}.\tag{B.9}$$

This propagator satisfy the condition Eq. (B.8) with initial parameter $T_{\mathrm{UV}}=+\infty$.

Note that the final condition is satisfied only in fermion systems because the smallest absolute value of fermionic Matsubara frequency[2] is πT. In other word, $T^{1/2}$ is regularization function like frequency cutoff function $\theta^T(\omega_n)$.

Now, let us derive the relations between conventional propagators and temperature rescaled propagators. For this purpose, we derive the relations between non-rescaled generating functionals and rescaled generating functionals in the temperature flow. We have to note that

$$\mathcal{S}[\overline{\psi},\psi] = \mathcal{S}'^T[\overline{\psi}',\psi'], \tag{B.10}$$

therefore,

$$\begin{aligned} W[\overline{\eta},\eta] &= \int \mathcal{D}\overline{\psi}\mathcal{D}\psi\, \mathrm{e}^{-\mathcal{S}[\overline{\psi},\psi]+(\overline{\eta},\psi)+(\overline{\psi},\eta)} \\ &= \int \mathcal{D}\overline{\psi}'\mathcal{D}\psi'\, \mathrm{e}^{-\mathcal{S}^T[\overline{\psi}',\psi']+T^{-3/4}(\overline{\eta},\psi')+T^{-3/4}(\overline{\psi},\eta)} \\ &= \int \mathcal{D}\overline{\psi}'\mathcal{D}\psi'\, \mathrm{e}^{-\mathcal{S}'^T[\overline{\psi}',\psi']+(\overline{\eta}',\psi')+(\overline{\psi}',\eta')} \\ &= W'^T[\overline{\eta}',\eta'], \end{aligned} \tag{B.11}$$

where

$$\overline{\eta}' = T^{-3/4}\overline{\eta}, \tag{B.12}$$

$$\eta' = T^{-3/4}\eta. \tag{B.13}$$

From this relation, the generating functional of connected Green's functions satisfies

$$\mathcal{G}[\overline{\eta},\eta] = -\ln W[\overline{\eta},\eta] = -\ln W'^T[\overline{\eta}',\eta'] = \mathcal{G}'^T[\overline{\eta}',\eta']. \tag{B.14}$$

[2]Note that the smallest absolute value of bosonic Matsubara frequency is zero.

Thus,

$$
\begin{aligned}
& T^{2m-1} \sum_{\substack{\omega_{n_1},\cdots,\omega_{n_m} \\ \omega_{n_1'},\cdots,\omega_{n_m'}}} G_{\mathrm{c}}^{(2m)}(x_1,\cdots,x_m;x_1',\cdots,x_m') \\
&= -T^{2m-1} \sum_{\substack{\omega_{n_1},\cdots,\omega_{n_m} \\ \omega_{n_1'},\cdots,\omega_{n_m'}}} \langle \psi(x_1)\cdots\psi(x_m)\overline{\psi}(x_m')\cdots\overline{\psi}(x_1')\rangle_{\mathrm{c}} \\
&= T^{2m-1} \sum_{\substack{\omega_{n_1},\cdots,\omega_{n_m} \\ \omega_{n_1'},\cdots,\omega_{n_m'}}} (-1)^m \frac{\delta^{2m}\mathcal{G}[\overline{\eta},\eta]}{\delta\overline{\eta}(x_1)\cdots\delta\overline{\eta}(x_m)\delta\eta(x_m')\cdots\delta\eta(x_1')}\bigg|_{\eta=\overline{\eta}=0} \\
&= T^{2m-1} \sum_{\substack{\omega_{n_1},\cdots,\omega_{n_m} \\ \omega_{n_1'},\cdots,\omega_{n_m'}}} \frac{(-1)^m}{T^{3m/4}\cdot T^{3m/4}} \frac{\delta^{2m}\mathcal{G}'^{T}[\overline{\eta}',\eta']}{\delta\overline{\eta}'(x_1)\cdots\delta\overline{\eta}'(x_m)\delta\eta'(x_m')\cdots\delta\eta'(x_1')}\bigg|_{\eta'=\overline{\eta}'=0} \\
&= T^{(m-2)/2} \sum_{\substack{\omega_{n_1},\cdots,\omega_{n_m} \\ \omega_{n_1'},\cdots,\omega_{n_m'}}} (-1)^m \frac{\delta^{2m}\mathcal{G}'^{T}[\overline{\eta}',\eta']}{\delta\overline{\eta}'(x_1)\cdots\delta\overline{\eta}'(x_m)\delta\eta'(x_m')\cdots\delta\eta'(x_1')}\bigg|_{\eta'=\overline{\eta}'=0} \\
&= -T^{(m-2)/2} \sum_{\substack{\omega_{n_1},\cdots,\omega_{n_m} \\ \omega_{n_1'},\cdots,\omega_{n_m'}}} \langle \psi'(x_1)\cdots\psi'(x_m)\overline{\psi}'(x_m')\cdots\overline{\psi}'(x_1')\rangle_{\mathrm{c}} \\
&= \sum_{\substack{\omega_{n_1},\cdots,\omega_{n_m} \\ \omega_{n_1'},\cdots,\omega_{n_m'}}} T^{(m-2)/2} G_{\mathrm{c}}'^{(2m)T}.
\end{aligned} \tag{B.15}
$$

This is the relationship between the conventional Green's functions and the Green's functions in new field representation regularized temperature factor [243].
Set $m = 1$,

$$G^{(2)} = T^{-1/2} G'^{(2)T}. \tag{B.16}$$

This is consistent with Eq. (B.7). Now let us consider the generating functional of 1PI vertex functionals in the temperature flow. As the same manner above, performing Legendre transformation

$$
\begin{aligned}
\Gamma'^{T}[\overline{\psi}',\psi'] &= \mathcal{G}'^{T}[\overline{\eta}',\eta'] + (\overline{\eta}',\psi') + (\overline{\psi}',\eta') \\
&= \mathcal{G}[\overline{\eta},\eta] + (T^{-3/4}\overline{\eta}, T^{3/4}\psi) + (T^{3/4}\overline{\psi}, T^{-3/4}\eta) \\
&= \Gamma[\overline{\psi},\psi],
\end{aligned} \tag{B.17}
$$

we can conclude

$$\Gamma[\overline{\psi},\psi] = \Gamma'^{T}[\overline{\psi}',\psi']. \tag{B.18}$$

From the definition of the vertex functions by Taylor expansion,

$$\begin{aligned}
\Gamma[\overline{\psi},\psi] &= -\ln\mathcal{Z} + \sum_{m=1}^{\infty} T^{2m-1} \sum_{\substack{\omega_{n_1},\cdots,\omega_{n_m} \\ \omega_{n'_1},\cdots,\omega_{n'_m}}} \Gamma^{(2m)} \underbrace{\overline{\psi},\cdots,\overline{\psi}}_{m \text{ pieces}} \underbrace{\psi,\cdots,\psi}_{m \text{ pieces}} \\
&= -\ln\mathcal{Z} + \sum_{m=1}^{\infty} T^{2m-1} \sum_{\substack{\omega_{n_1},\cdots,\omega_{n_m} \\ \omega_{n'_1},\cdots,\omega_{n'_m}}} \Gamma^{(2m)} \underbrace{\overline{\psi}',\cdots,\overline{\psi}'}_{m \text{ pieces}} \underbrace{\psi',\cdots,\psi'}_{m \text{ pieces}} \times T^{-3m/2} \\
&= -\ln\mathcal{Z} + \sum_{m=1}^{\infty} \sum_{\substack{\omega_{n_1},\cdots,\omega_{nm} \\ \omega_{n'_1},\cdots,\omega_{n'_m}}} T^{(m-2)/2}\Gamma^{(2m)} \underbrace{\overline{\psi}',\cdots,\overline{\psi}'}_{m \text{ pieces}} \underbrace{\psi',\cdots,\psi'}_{m \text{ pieces}} \\
&= -\ln\mathcal{Z} + \sum_{m=1}^{\infty} \sum_{\substack{\omega_{n_1},\cdots,\omega_{nm} \\ \omega_{n'_1},\cdots,\omega_{n'_m}}} \Gamma'^{(2m)T} \underbrace{\overline{\psi}',\cdots,\overline{\psi}'}_{m \text{ pieces}} \underbrace{\psi',\cdots,\psi'}_{m \text{ pieces}}.
\end{aligned} \tag{B.19}$$

Therefore,

$$\Gamma^{(2m)} = T^{-(m-2)/2}\Gamma'^{(2m)T}. \tag{B.20}$$

Set $m = 1$, this relation is consistent with Dyson equation:

$$\Gamma^{(2)}G^{(2)} = 1 \quad \rightarrow \quad \Gamma'^{(2)T}G'^{(2)T} = \Gamma^{(2)}T^{-1/2} \times T^{1/2}G^{(2)} = \Gamma^{(2)}G^{(2)} = 1. \tag{B.21}$$

From the relation

$$\Gamma^{(2)} = [G_0^{(2)}]^{-1} - \Sigma, \tag{B.22}$$

we can obtain the relation for self-energy:

$$\begin{aligned}
\Gamma^{(2)} = [G_0^{(2)}]^{-1} - \Sigma \quad \rightarrow \quad T^{1/2}\Gamma'^{(2)T} &= [T^{-1/2}G_0'^{(2)T}]^{-1} - \Sigma \\
&= T^{1/2}[G_0'^{(2)T}]^{-1} - \Sigma \\
&= T^{1/2}[G_0'^{(2)T}]^{-1} - T^{1/2}[T^{-1/2}\Sigma] \\
&= T^{1/2}[G_0'^{(2)T}]^{-1} - T^{1/2}\Sigma'^{T}.
\end{aligned} \tag{B.23}$$

Thus

$$\Gamma'^{(2)T} = [G_0'^{(2)T}]^{-1} - \Sigma'^{T}, \tag{B.24}$$

and

$$\Sigma = T^{1/2}\Sigma'^{T}. \tag{B.25}$$

From these relations, we can write full propagator:

$$\begin{aligned}
\left[G'^{(2)T}\right]^{-1}(\mathrm{i}\omega_n,\boldsymbol{k}) &= \Gamma'^{(2)T}(\mathrm{i}\omega_n,\boldsymbol{k}) \\
&= [G_0'^{(2)T}]^{-1}(\mathrm{i}\omega_n,\boldsymbol{k}) - \Sigma'^{T}(\mathrm{i}\omega_n,\boldsymbol{k}) \\
&= T^{-1/2}(\mathrm{i}\omega_n - \xi_{\boldsymbol{k}}) - \Sigma'^{T}(\mathrm{i}\omega_n,\boldsymbol{k}) \\
&= T^{-1/2}\left[\mathrm{i}\omega_n - \xi_{\boldsymbol{k}} - T^{1/2}\Sigma'^{T}(\mathrm{i}\omega_n,\boldsymbol{k})\right], \\
&\downarrow \\
G'^{(2)T}(\mathrm{i}\omega_n,\boldsymbol{k}) &= \frac{T^{1/2}}{\mathrm{i}\omega_n - \xi_{\boldsymbol{k}} - T^{1/2}\Sigma'^{T}(\mathrm{i}\omega_n,\boldsymbol{k})}.
\end{aligned} \tag{B.26}$$

At last, we derive the single-scale propagator:

$$\begin{aligned}\frac{\mathrm{d}}{\mathrm{d}T}Q'^{T}(\mathrm{i}\omega_n,\boldsymbol{k}) &= \frac{\mathrm{d}}{\mathrm{d}T}T^{-1/2}(\mathrm{i}\omega_n-\xi_{\boldsymbol{k}})\\ &= -\frac{1}{2T^{3/2}}(\mathrm{i}\omega_n-\xi_{\boldsymbol{k}})+T^{-1/2}\frac{\mathrm{i}\omega_n}{T}\\ &= \frac{1}{2T^{3/2}}(-\mathrm{i}\omega_n+\xi_{\boldsymbol{k}}+2\mathrm{i}\omega_n)\\ &= \frac{\mathrm{i}\omega_n+\xi_{\boldsymbol{k}}}{2T^{3/2}},\end{aligned} \tag{B.27}$$

thus

$$\begin{aligned}S'^{T}(\mathrm{i}\omega_n,\boldsymbol{k}) &= -G'^{(2)T}(\mathrm{i}\omega_n,\boldsymbol{k})\left(\frac{\mathrm{d}}{\mathrm{d}T}Q'^{T}(\mathrm{i}\omega_n,\boldsymbol{k})\right)G'^{(2)T}(\mathrm{i}\omega_n,\boldsymbol{k})\\ &= -\frac{T^{1/2}}{\mathrm{i}\omega_n-\xi_{\boldsymbol{k}}-T^{1/2}\Sigma'^{T}(\mathrm{i}\omega_n,\boldsymbol{k})}\cdot\frac{\mathrm{i}\omega_n+\xi_{\boldsymbol{k}}}{2T^{3/2}}\frac{T^{1/2}}{\mathrm{i}\omega_n-\xi_{\boldsymbol{k}}-T^{1/2}\Sigma'^{T}(\mathrm{i}\omega_n,\boldsymbol{k})}\\ &= -\frac{1}{2}\frac{T^{-1/2}(\mathrm{i}\omega_n+\xi_{\boldsymbol{k}})}{\left[\mathrm{i}\omega_n-\xi_{\boldsymbol{k}}-T^{1/2}\Sigma'^{T}(\mathrm{i}\omega_n,\boldsymbol{k})\right]^2}.\end{aligned} \tag{B.28}$$

B.2 Interaction Flow

In this section we review interaction flow scheme which is a FRG scheme choosing magnitude of interaction as a flow parameter [244].

In general, bare action is written like

$$\mathcal{S}=-\sum\overline{\psi}[G_0]^{-1}\psi+\frac{1}{4}\sum V\overline{\psi}\overline{\psi}\psi\psi. \tag{B.29}$$

Here, we do not write arguments of field operator for simplicity.
We introduce uniform scaling factor of the Grassmann variables:

$$\overline{\psi}'=\lambda^{-1/2}\overline{\psi}, \tag{B.30}$$

$$\psi'=\lambda^{-1/2}\psi. \tag{B.31}$$

This factor λ acts as a flow parameter in the interaction flow.
As a result, the full action is transformed as

$$\begin{aligned}\mathcal{S}^{\lambda} &= -\sum\overline{\psi}'\lambda^{-1}[G_0]^{-1}\psi'+\frac{1}{4}\sum\lambda^2V\overline{\psi}'\overline{\psi}'\psi'\psi'\\ &= -\sum\overline{\psi}'[G_0^{\lambda}]^{-1}\psi'+\frac{1}{4}\sum\lambda^2V\overline{\psi}'\overline{\psi}'\psi'\psi'.\end{aligned} \tag{B.32}$$

Here, we define the bare propagator in the interaction flow as

$$G_0^{\lambda}=\lambda G_0. \tag{B.33}$$

Note that interaction is transformed as

$$V\to\lambda^2V. \tag{B.34}$$

In the interaction flow scheme, we set $\lambda = 0$ initially and calculate toward $\lambda = 1$. At the initial condition $\lambda = 0$, interaction is not taken into account. At the end of flow $\lambda = 1$, on the other hand, G_0^λ is corresponds G_0 and the interaction fully contributes to action.
In the same manner as the case of temperature flow, we can derive the relation between non-rescaled functions and scaled functions in the interaction flow:

$$G^{(2m)} = \lambda^{-m} G^{(2m)\lambda}, \tag{B.35}$$

$$\Gamma^{(2m)} = \lambda^{m} \Gamma^{(2m)\lambda}. \tag{B.36}$$

The full and single-scale propagators are given as

$$G^\lambda(\mathrm{i}\omega_n, \boldsymbol{k}) = \frac{\lambda}{\mathrm{i}\omega_n - \xi_{\boldsymbol{k}} - \lambda\Sigma^\lambda(\mathrm{i}\omega_n, \boldsymbol{k})}, \tag{B.37}$$

$$S^\lambda(\mathrm{i}\omega_n, \boldsymbol{k}) = \frac{\mathrm{i}\omega_n - \xi_{\boldsymbol{k}}}{[\mathrm{i}k_0 - \xi_{\boldsymbol{k}} - \lambda\Sigma^\lambda(\mathrm{i}\omega_n, \boldsymbol{k})]^2}. \tag{B.38}$$

Interaction flow has great advantage. If we neglect self-energy correction, the propagators has the same form at each step in the flow and each one-loop integral needs to be done only once. This property reduce computational costs. However, this λ cannot regularize infrared divergence of the propagators. Nevertheless, if problems are suitable to this scheme, we can obtain results similar to cutoff scheme with less computation.

Appendix C

Approximate Relation $T \simeq \frac{\pi}{2}\Lambda$

Here we prove that the relation $T \simeq \frac{\pi}{2}\Lambda$ is valid not only in mean-field theory but also in the leading order of high-temperature expansion.

We consider the mean-field theory of Heisenberg model under external field $\boldsymbol{H}$. The Hamiltonian is

$$\mathcal{H} = \sum_{\langle i,j \rangle} J_{ij} \boldsymbol{S}_i \cdot \boldsymbol{S}_j - \sum_i \boldsymbol{H} \cdot \boldsymbol{S}_i. \tag{C.1}$$

To perform mean-field approximation, we define the mean-field on the site i

$$\boldsymbol{H}_i^{\mathrm{MF}} = -\sum_j J_{ij} \langle \boldsymbol{S}_j \rangle + \boldsymbol{H}, \tag{C.2}$$

and the effective Hamiltonian on the site i

$$\mathcal{H}_i^{\mathrm{MF}} = -\boldsymbol{H}_i^{\mathrm{MF}} \cdot \boldsymbol{S}_i. \tag{C.3}$$

Now we can calculate the magnetization on the site i as

$$M_i = |\langle \boldsymbol{S}_i \rangle| = \frac{\sum_{m=-S}^{S} m\, \mathrm{e}^{\frac{H_i^{\mathrm{MF}} m}{T}}}{\mathrm{Tr}[\mathrm{e}^{-\mathcal{H}_i^{\mathrm{MF}}/T}]} = \frac{\sum_{m=-S}^{S} m\, \mathrm{e}^{\frac{1}{T} H_i^{\mathrm{MF}} m}}{\sum_{m=-S}^{S} \mathrm{e}^{\frac{1}{T} H_i^{\mathrm{MF}} m}} = S \cdot B_S\left(\frac{H_i^{\mathrm{MF}} S}{T}\right) \tag{C.4}$$

with $H_i^{\mathrm{MF}} = |\boldsymbol{H}_i^{\mathrm{MF}}|$. Here, $B_S(x)$ is the Brillouin function and it has the asymptotic forms

$$B_S(x) \approx \begin{cases} \frac{S+1}{3S} x - \frac{(2S^2+2S+1)(S+1)}{90S^3} x^3 & (x \to 0) \\ 1 & (x \to +\infty) \end{cases}. \tag{C.5}$$

Considering ferromagnetic case ($M_i = M$) [1], the mean-field is homogeneous (site-independent) and we can write it as

$$H^{\mathrm{MF}} = H_i^{\mathrm{MF}} = -\sum_j J_{ij} M + H \tag{C.6}$$

$$= -J(\boldsymbol{0}) M + H. \tag{C.7}$$

Here, we define the Fourier transformation of the magnetic interaction as

$$J(\boldsymbol{k}) = \sum_j \mathrm{e}^{-\mathrm{i}\boldsymbol{k} \cdot (\boldsymbol{r}_i - \boldsymbol{r}_j)} J_{ij}. \tag{C.8}$$

[1] It is for simplisity.

Therefore, FM magnetization is given by the self-consistent equation

$$M = S \cdot B_S\left(\frac{S(H - J(\mathbf{0})M)}{T}\right). \tag{C.9}$$

Now we consider high temperature regime where the argument of the Brillouin function B_S is sufficiently small. We adopt the asymptotic behavior of the Brillouin function and iterative expansion to the 2nd order of T^{-1}

$$\begin{aligned} M &= S \cdot \frac{S+1}{3S} \cdot \frac{SH}{T} - S \cdot \frac{S+1}{3S} \cdot \frac{SMJ(\mathbf{0})}{T} - S \cdot \frac{(2S^2+2S+1)(S+1)}{90S^3}\left(\frac{S(H-J(\mathbf{0})}{T}\right)^3 \\ &= \frac{S(S+1)}{3T}H - \frac{S(S+1)J(\mathbf{0})}{3T}M + \mathcal{O}(T^{-3}) \\ &= \frac{S(S+1)}{3T}H - \frac{[S(S+1)]^2 J(\mathbf{0})}{9T^2}H + \mathcal{O}(T^{-3}). \end{aligned} \tag{C.10}$$

The first term gives Curie's law. The second term is correction term from high temperature expansion. Defining homogeneous FM susceptibility by $M = \chi H$, the explicit form of the susceptibility in high temperature regime is given by

$$\chi \simeq \frac{S(S+1)}{3T} - \frac{[S(S+1)]^2 J(\mathbf{0})}{9T^2}. \tag{C.11}$$

In order to clarify the relation between temperature T and RG cutoff scale Λ, we consider high energy regime in PFFRG. To compare mean-field theory, we adopt static approximation and consider only RPA term in direct particle-hole channel. The reduced flow equations are shown in Eqs. (3.137) and (3.138). Here we consider the Heisenberg-type interaction which is isotropic in spin space, so we define $\Gamma_{ij}^{\mathrm{s},\Lambda}$ as (see Eq. (3.75))

$$\Gamma_{ij}^{\mathrm{s},\Lambda} = \Gamma_{ij}^{x,\Lambda} = \Gamma_{ij}^{y,\Lambda} = \Gamma_{ij}^{z,\Lambda}. \tag{C.12}$$

We rewrite Eqs. (3.137) and (3.138) by $\Gamma_{ij}^{\mathrm{s},\Lambda}$:

$$\frac{\mathrm{d}}{\mathrm{d}\Lambda}\Gamma_{ij}^{\mathrm{s},\Lambda} \simeq \frac{2}{\pi\Lambda^2}\sum_l \Gamma_{il}^{\mathrm{s},\Lambda}\Gamma_{lj}^{\mathrm{s},\Lambda}, \tag{C.13}$$

and

$$\chi_{ij}^{\Lambda} \simeq \frac{1}{2\pi\Lambda}\delta_{ij} - \frac{1}{\pi^2\Lambda^2}\Gamma_{ij}^{\mathrm{s},\Lambda}, \tag{C.14}$$

respectively. Here we omit the spin component indices of the susceptibility because $\chi = \chi^{xx} = \chi^{yy} = \chi^{zz}$. Defining Fourier transformation of the spin vertex by

$$\Gamma^{\mathrm{s},\Lambda}(\boldsymbol{k}) = \sum_j \mathrm{e}^{-\mathrm{i}\boldsymbol{k}\cdot(\boldsymbol{r}_i - \boldsymbol{r}_j)}\Gamma_{ij}^{\mathrm{s},\Lambda}, \tag{C.15}$$

the homogeneous susceptibility ($\boldsymbol{k} = \mathbf{0}$) is given by

$$\chi^{\Lambda} = \frac{1}{2\pi\Lambda} - \frac{1}{\pi^2\Lambda^2}\Gamma^{\mathrm{s},\Lambda}(\mathbf{0}). \tag{C.16}$$

In high energy regime, we can assume that $\Gamma_{ij}^{s,\Lambda}$ does not change a lot from initial condition i.e. bare interaction

$$\Gamma_{ij}^{s,\Lambda} \approx \Gamma_{ij}^{s,\Lambda_{UV}} = \frac{1}{4}J_{ij} \quad (\text{if } \Lambda \gg J_{ij}). \tag{C.17}$$

Therefore, we can obtain an approximate form of the susceptibility in high energy regime

$$\chi^{\Lambda} \approx \frac{1}{2\pi\Lambda} - \frac{1}{4\pi^2\Lambda^2}J(\mathbf{0}). \tag{C.18}$$

Now we compare it with mean-field result eq. (C.11) with $S = 1/2$

$$\begin{aligned}\chi &\simeq \frac{3}{4}\cdot\frac{1}{3T} - \frac{9}{16}\cdot\frac{1}{9T^2}J(\mathbf{0}) \\ &= \frac{1}{4T} - \frac{1}{16T^2}J(\mathbf{0}).\end{aligned} \tag{C.19}$$

Surprisingly, above 2 equation have the same form if we set

$$T = \frac{\pi}{2}\Lambda. \tag{C.20}$$

We obtain the scaling factor connecting T and Λ. Of course, this relation is valid only in high temperature/high energy region. Therefore we represent $T \simeq \frac{\pi}{2}\Lambda$ in this dissertation.

Bibliography

[1] X.-G. Wen, *Quantum Field Theory of Many-Body Systems* (Oxford University Press, Oxford, 2007).

[2] L. Balents, "Spin liquids in frustrated magnets", Nature **464**, 199–208 (2010).

[3] C. Lacroix, P. Mendels, and F. Mila, eds., *Introduction to Frustrated Magnetism*, Vol. 164, Springer Series in Solid-State Sciences (Springer Berlin Heidelberg, Berlin, Heidelberg, 2011).

[4] H. T. Diep, *Frustrated Spin Systems* (World Scientific, 2013).

[5] L. Savary and L. Balents, "Quantum spin liquids: a review", Rep. Prog. Phys. **80**, 016502 (2017).

[6] Y. Zhou, K. Kanoda, and T.-K. Ng, "Quantum spin liquid states", Rev. Mod. Phys. **89**, 025003 (2017).

[7] J. Knolle and R. Moessner, "A Field Guide to Spin Liquids", Annu. Rev. Condens. Matter Phys. **10**, 451–472 (2019).

[8] V. R. Shaginyan, V. A. Stephanovich, A. Z. Msezane, G. S. Japaridze, J. W. Clark, M. Y. Amusia, and E. V. Kirichenko, "Theoretical and experimental developments in quantum spin liquid in geometrically frustrated magnets: a review", J. Mater. Sci. **55**, 2257–2290 (2020).

[9] C. Broholm, R. J. Cava, S. A. Kivelson, D. G. Nocera, M. R. Norman, and T. Senthil, "Quantum spin liquids", Science (80-.). **367**, eaay0668 (2020).

[10] P. Anderson, "Resonating valence bonds: A new kind of insulator?", Mater. Res. Bull. **8**, 153–160 (1973).

[11] P. Fazekas and P. W. Anderson, "On the ground state properties of the anisotropic triangular antiferromagnet", Philos. Mag. **30**, 423–440 (1974).

[12] Y. Motome and J. Nasu, "Hunting Majorana Fermions in Kitaev Magnets", J. Phys. Soc. Jpn **89**, 012002 (2020).

[13] A. Kitaev, "Anyons in an exactly solved model and beyond", Ann. Phys. (N. Y). **321**, 2–111 (2006).

[14] G. Jackeli and G. Khaliullin, "Mott insulators in the strong spin-orbit coupling Limit: From Heisenberg to a Quantum Compass and Kitaev Models", Phys. Rev. Lett. **102**, 2–5 (2009).

[15] Y. Kasahara, K. Sugii, T. Ohnishi, M. Shimozawa, M. Yamashita, N. Kurita, H. Tanaka, J. Nasu, Y. Motome, T. Shibauchi, and Y. Matsuda, "Unusual Thermal Hall Effect in a Kitaev Spin Liquid Candidate α-RuCl3", Phys. Rev. Lett. **120**, 217205 (2018).

[16] Y. Kasahara, T. Ohnishi, Y. Mizukami, O. Tanaka, S. Ma, K. Sugii, N. Kurita, H. Tanaka, J. Nasu, Y. Motome, T. Shibauchi, and Y. Matsuda, "Majorana quantization and half-integer thermal quantum Hall effect in a Kitaev spin liquid", Nature **559**, 227–231 (2018).

[17]Z. Nussinov and J. van den Brink, "Compass and Kitaev models – Theory and Physical Motivations", arXiv:1303.5922 (2013).

[18]J. G. Rau, E. K.-H. Lee, and H.-Y. Kee, "Spin-Orbit Physics Giving Rise to Novel Phases in Correlated Systems: Iridates and Related Materials", Annu. Rev. Condens. Matter Phys. **7**, 195–221 (2016).

[19]S. Trebst, "Kitaev Materials", arXiv:1701.07056 (2017).

[20]S. M. Winter, A. A. Tsirlin, M. Daghofer, J. van den Brink, Y. Singh, P. Gegenwart, and R. Valentí, "Models and materials for generalized Kitaev magnetism", J. Phys. Condens. Matter **29**, 493002 (2017).

[21]M. Hermanns, I. Kimchi, and J. Knolle, "Physics of the Kitaev Model: Fractionalization, Dynamic Correlations, and Material Connections", Annu. Rev. Condens. Matter Phys. **9**, 17–33 (2018).

[22]H. Takagi, T. Takayama, G. Jackeli, G. Khaliullin, and S. E. Nagler, "Concept and realization of Kitaev quantum spin liquids", Nat. Rev. Phys. **1**, 264–280 (2019).

[23]Y. Motome, R. Sano, S. Jang, Y. Sugita, and Y. Kato, "Materials design of Kitaev spin liquids beyond the Jackeli-Khaliullin mechanism", J. Phys. Condens. Matter **32**, 10.1088/1361-648X/ab8525 (2020).

[24]Z. Nussinov and J. van den Brink, "Compass models: Theory and physical motivations", Rev. Mod. Phys. **87**, 1–59 (2015).

[25]A. Y. Kitaev, "Unpaired Majorana fermions in quantum wires", Physics-Uspekhi **44**, 131–136 (2001).

[26]A. Kitaev, "Fault-tolerant quantum computation by anyons", Ann. Phys. (N. Y). **303**, 2–30 (2003).

[27]E. Majorana, "Teoria simmetrica dell'elettrone e del positrone", Nuovo Cim. **14**, 171–184 (1937).

[28]E. H. Lieb, "Flux Phase of the Half-Filled Band", Phys. Rev. Lett. **73**, 2158–2161 (1994).

[29]G. Baskaran, S. Mandal, and R. Shankar, "Exact Results for Spin Dynamics and Fractionalization in the Kitaev Model", Phys. Rev. Lett. **98**, 247201 (2007).

[30]T. Takayama, A. Kato, R. Dinnebier, J. Nuss, H. Kono, L. S. I. Veiga, G. Fabbris, D. Haskel, and H. Takagi, "Hyperhoneycomb Iridate βLi2IrO3 as a Platform for Kitaev Magnetism", Phys. Rev. Lett. **114**, 077202 (2015).

[31]K. A. Modic, T. E. Smidt, I. Kimchi, N. P. Breznay, A. Biffin, S. Choi, R. D. Johnson, R. Coldea, P. Watkins-Curry, G. T. McCandless, J. Y. Chan, F. Gandara, Z. Islam, A. Vishwanath, A. Shekhter, R. D. McDonald, and J. G. Analytis, "Realization of a three-dimensional spin–anisotropic harmonic honeycomb iridate", Nat. Commun. **5**, 4203 (2014).

[32]A. Shitade, H. Katsura, J. Kuneš, X.-L. Qi, S.-C. Zhang, and N. Nagaosa, "Quantum Spin Hall Effect in a Transition Metal Oxide Na2IrO3", Phys. Rev. Lett. **102**, 256403 (2009).

[33]K. Kitagawa, T. Takayama, Y. Matsumoto, A. Kato, R. Takano, Y. Kishimoto, S. Bette, R. Dinnebier, G. Jackeli, and H. Takagi, "A spin–orbital-entangled quantum liquid on a honeycomb lattice", Nature **554**, 341–345 (2018).

[34]S. R. Manmana, E. M. Stoudenmire, K. R. A. Hazzard, A. M. Rey, and A. V. Gorshkov, "Topological phases in ultracold polar-molecule quantum magnets", Phys. Rev. B **87**, 081106 (2013).

[35]A. V. Gorshkov, K. R. Hazzard, and A. M. Rey, "Kitaev honeycomb and other exotic spin models with polar molecules", Mol. Phys. **111**, 1908–1916 (2013).

[36]T. Suzuki and Y. Yamaji, "Thermal properties of spin-S Kitaev-Heisenberg model on a honeycomb lattice", Phys. B Condens. Matter **536**, 637–639 (2018).

[37]A. Koga, H. Tomishige, and J. Nasu, "Ground-state and Thermodynamic Properties of an S = 1 Kitaev Model", J. Phys. Soc. Jpn **87**, 063703 (2018).

[38]J. Oitmaa, A. Koga, and R. R. P. Singh, "Incipient and well-developed entropy plateaus in spin-S Kitaev models", Phys. Rev. B **98**, 214404 (2018).

[39]H.-Y. Lee, N. Kawashima, and Y. B. Kim, "Tensor network wave function of S=1 Kitaev spin liquids", Phys. Rev. Res. **2**, 033318 (2020).

[40]X.-Y. Dong and D. N. Sheng, "Spin-1 Kitaev-Heisenberg model on a honeycomb lattice", Phys. Rev. B **102**, 121102 (2020).

[41]I. Khait, P. P. Stavropoulos, H.-Y. Kee, and Y. B. Kim, "Characterizing spin-one Kitaev quantum spin liquids", arXiv:2001.06000 (2020).

[42]C. Hickey, C. Berke, P. P. Stavropoulos, H.-Y. Kee, and S. Trebst, "Field-driven gapless spin liquid in the spin-1 Kitaev honeycomb model", Phys. Rev. Res. **2**, 023361 (2020).

[43]Z. Zhu, Z.-Y. Weng, and D. N. Sheng, "Magnetic field induced spin liquids in S=1 Kitaev honeycomb model", Phys. Rev. Res. **2**, 022047 (2020).

[44]A. Koga, T. Minakawa, Y. Murakami, and J. Nasu, "Spin Transport in the Quantum Spin Liquid State in the S = 1 Kitaev Model: Role of the Fractionalized Quasiparticles", J. Phys. Soc. Jpn **89**, 033701 (2020).

[45]G. Baskaran, D. Sen, and R. Shankar, "Spin-S Kitaev model: Classical ground states, order from disorder, and exact correlation functions", Phys. Rev. B **78**, 115116 (2008).

[46]P. P. Stavropoulos, D. Pereira, and H.-Y. Kee, "Microscopic Mechanism for a Higher-Spin Kitaev Model", Phys. Rev. Lett. **123**, 037203 (2019).

[47]C. Xu, J. Feng, H. Xiang, and L. Bellaiche, "Interplay between Kitaev interaction and single ion anisotropy in ferromagnetic CrI3 and CrGeTe3 monolayers", npj Comput. Mater. **4**, 57 (2018).

[48]M. Kim, P. Kumaravadivel, J. Birkbeck, W. Kuang, S. G. Xu, D. G. Hopkinson, J. Knolle, P. A. McClarty, A. I. Berdyugin, M. Ben Shalom, R. V. Gorbachev, S. J. Haigh, S. Liu, J. H. Edgar, K. S. Novoselov, I. V. Grigorieva, and A. K. Geim, "Micromagnetometry of two-dimensional ferromagnets", Nat. Electron. **2**, 457–463 (2019).

[49]C. Xu, J. Feng, M. Kawamura, Y. Yamaji, Y. Nahas, S. Prokhorenko, Y. Qi, H. Xiang, and L. Bellaiche, "Possible Kitaev Quantum Spin Liquid State in 2D Materials with S=3/2", Phys. Rev. Lett. **124**, 087205 (2020).

[50]I. Lee, F. G. Utermohlen, D. Weber, K. Hwang, C. Zhang, J. van Tol, J. E. Goldberger, N. Trivedi, and P. C. Hammel, "Fundamental Spin Interactions Underlying the Magnetic Anisotropy in the Kitaev Ferromagnet CrI3", Phys. Rev. Lett. **124**, 017201 (2020).

[51]J. Chaloupka, G. Jackeli, and G. Khaliullin, "Kitaev-Heisenberg Model on a Honeycomb Lattice: Possible Exotic Phases in Iridium Oxides A2IrO3", Phys. Rev. Lett. **105**, 027204 (2010).

[52]J. Chaloupka, G. Jackeli, and G. Khaliullin, "Zigzag Magnetic Order in the Iridium Oxide Na2IrO3", Phys. Rev. Lett. **110**, 097204 (2013).

[53]J. Reuther and P. Wölfle, "A diagrammatic theory of the antiferromagnetic frustrated 2d Heisenberg model", J. Phys. Conf. Ser. **200**, 022051 (2010).

[54]J. Reuther and P. Wölfle, "J1-J2 frustrated two-dimensional Heisenberg model: Random phase approximation and functional renormalization group", Phys. Rev. B **81**, 144410 (2010).

[55]W. Metzner, M. Salmhofer, C. Honerkamp, V. Meden, and K. Schönhammer, "Functional renormalization group approach to correlated fermion systems", Rev. Mod. Phys. **84**, 299–352 (2012).

[56]P. Kopietz, L. Bartosch, and F. Schütz, *Introduction to the Functional Renormalization Group*, Vol. 798, Lecture Notes in Physics (Springer Berlin Heidelberg, Berlin, Heidelberg, 2010).

[57]M. Salmhofer, *Renormalization* (Springer Berlin Heidelberg, Berlin, Heidelberg, 1999).

[58]M. Salmhofer, "Continuous Renormalization for Fermions and Fermi Liquid Theory", Commun. Math. Phys. **194**, 249–295 (1998).

[59]M. Salmhofer and C. Honerkamp, "Fermionic Renormalization Group Flows: Technique and Theory", Prog. Theor. Phys. **105**, 1–35 (2001).

[60]J. Berges, N. Tetradis, and C. Wetterich, "Non-perturbative renormalization flow in quantum field theory and statistical physics", Phys. Rep. **363**, 223–386 (2002).

[61]M. Salmhofer, C. Honerkamp, W. Metzner, and O. Lauscher, "Renormalization Group Flows into Phases with Broken Symmetry", Prog. Theor. Phys. **112**, 943–970 (2004).

[62]R. Hedden, V. Meden, T. Pruschke, and K. Schönhammer, "A functional renormalization group approach to zero-dimensional interacting systems", J. Phys. Condens. Matter **16**, 5279–5296 (2004).

[63]I. Boettcher, J. M. Pawlowski, and S. Diehl, "Ultracold atoms and the Functional Renormalization Group", Nucl. Phys. B - Proc. Suppl. **228**, 63–135 (2012).

[64]A. Schwenk and J. Polonyi, eds., *Renormalization Group and Effective Field Theory Approaches to Many-Body Systems*, Vol. 852, Lecture Notes in Physics (Springer Berlin Heidelberg, Berlin, Heidelberg, 2012).

[65]C. Platt, W. Hanke, and R. Thomale, "Functional renormalization group for multi-orbital Fermi surface instabilities", Adv. Phys. **62**, 453–562 (2013).

[66]N Dupuis, L Canet, A Eichhorn, W Metzner, J. M. Pawlowski, M Tissier, and N Wschebor, "The nonperturbative functional renormalization group and its applications", 1–135 (2020).

[67]R. Shankar, "Renormalization-group approach to interacting fermions", Rev. Mod. Phys. **66**, 129–192 (1994).

[68]A. A. Abrikosov, L. P. Gorkov, and I. E. Dzyaloshinski, *Methods of Quantum Field Theory in Statistical Physics* (Prentice-Hall, Englewood Cliffs, New Jersey, 1963).

[69]F. J. Wegner and A. Houghton, "Renormalization Group Equation for Critical Phenomena", Phys. Rev. A **8**, 401–412 (1973).

[70]J. Polchinski, "Renormalization and effective lagrangians", Nucl. Phys. B **231**, 269–295 (1984).

[71]C. Wetterich, "Exact evolution equation for the effective potential", Phys. Lett. B **301**, 90–94 (1993).

[72]C. Hille, F. B. Kugler, C. J. Eckhardt, Y.-Y. He, A. Kauch, C. Honerkamp, A. Toschi, and S. Andergassen, "Quantitative functional renormalization group description of the two-dimensional Hubbard model", Phys. Rev. Res. **2**, 033372 (2020).

[73]J. W. Negele and H. Orland, *Quantum Many-Particle Systems* (CRC Press, 2018).

[74]A. Altland and B. D. Simons, *Condensed Matter Field Theory*, 2nd ed. (Cambridge University Press, Cambridge, 2010).

[75]M. C. M. Wright, "Green function or green's function?", Nat. Phys. **2**, 646–646 (2006).

[76]K. Held, "Dynamical Vertex Approximation", Autumn School on Correlated Electrons. DMFT at 25: Infinite Dimensions, edited by E. PaVarini, E. Koch, D. Vollhardt, and A. Lichtenstein (2014).

[77]J. M. Luttinger and J. C. Ward, "Ground-State Energy of a Many-Fermion System. II", Phys. Rev. **118**, 1417–1427 (1960).

[78]G. Baym, "Self-Consistent Approximations in Many-Body Systems", Phys. Rev. **127**, 1391–1401 (1962).

[79]J. M. Cornwall, R. Jackiw, and E. Tomboulis, "Effective action for composite operators", Phys. Rev. D **10**, 2428–2445 (1974).

[80]T. R. Morris, "The Exact Renormalization Group and Approximate Solutions", Int. J. Mod. Phys. A **09**, 2411–2449 (1994).

[81]A. A. Katanin, "Fulfillment of Ward identities in the functional renormalization group approach", Phys. Rev. B **70**, 115109 (2004).

[82]C. De Dominicis and P. C. Martin, "Stationary Entropy Principle and Renormalization in Normal and Superfluid Systems. I. Algebraic Formulation", J. Math. Phys. **5**, 14–30 (1964).

[83]B. Roulet, J. Gavoret, and P. Noziéres, "Singularities in the X-Ray Absorption and Emission of Metals. I. First-Order Parquet Calculation", Phys. Rev. **178**, 1072–1083 (1969).

[84]N. E. Bickers, "Self-Consistent Many-Body Theory for Condensed Matter Systems", in *Theoretical methods for strongly correlated electrons*, edited by D. Sénéchal, A.-M. Trembly, and C. Bourbonnais (Springer-Verlag, New York, 2004), pp. 237–296.

[85]F. B. Kugler and J. von Delft, "Multiloop functional renormalization group for general models", Phys. Rev. B **97**, 035162 (2018).

[86]F. B. Kugler and J. von Delft, "Multiloop Functional Renormalization Group That Sums Up All Parquet Diagrams", Phys. Rev. Lett. **120**, 057403 (2018).

[87]F. B. Kugler and J. von Delft, "Derivation of exact flow equations from the self-consistent parquet relations", New J. Phys. **20**, 123029 (2018).

[88]J. Diekmann and S. G. Jakobs, "Parquet approximation and one-loop renormalization group: equivalence on the leading-logarithmic level", arXiv:2009.04761 (2020).

[89]C. J. Halboth and W. Metzner, "Renormalization-group analysis of the two-dimensional Hubbard model", Phys. Rev. B **61**, 7364–7377 (2000).

[90]P. Wölfle and P. Schmitteckert, "Quantum phase transitions in frustrated magnetic systems", Eur. Phys. J. Spec. Top. **224**, 1087–1103 (2015).

[91]J. Reuther, "Frustrated Quantum Heisenberg Antiferromagnets: Functional Renormalization-Group Approach in Auxiliary-Fermion Representation", PhD thesis (Karlsruhe Instituts für Technologie, 2011).

[92]A. Rançon, "Nonperturbative renormalization group approach to quantum XY spin models", Phys. Rev. B **89**, 214418 (2014).

[93]A. Rançon and N. Dupuis, "Kosterlitz-Thouless signatures in the low-temperature phase of layered three-dimensional systems", Phys. Rev. B **96**, 214512 (2017).

[94]J. Krieg, D. Strassel, S. Streib, S. Eggert, and P. Kopietz, "Thermodynamics and renormalized quasiparticles in the vicinity of the dilute Bose gas quantum critical point in two dimensions", Phys. Rev. B **95**, 024414 (2017).

[95]J. Brinckmann and P. Wölfle, "Auxiliary-fermion approach to critical fluctuations in the two-dimensional quantum antiferromagnetic Heisenberg model", Phys. Rev. B **70**, 174445 (2004).

[96]J. Brinckmann and P. Wölfle, "Description of magnetic short-range order in the 2D Heisenberg model: Auxiliary fermions with reduced self-consistency", Phys. B Condens. Matter **359-361**, 798–800 (2005).

[97]J. Brinckmann and P. Wölfle, "Diagrammatic approximations for the 2d quantum antiferromagnet: exact projection of auxiliary fermions", arXiv:0803.3312 (2008).

[98]A. A. Abrikosov, "Electron scattering on magnetic impurities in metals and anomalous resistivity effects", Phys. Phys. Fiz. **2**, 5–20 (1965).

[99]S. Göttel, S. Andergassen, C. Honerkamp, D. Schuricht, and S. Wessel, "Critical scales in anisotropic spin systems from functional renormalization", Phys. Rev. B **85**, 214406 (2012).

[100]S. Göttel, "Renormalization Group Approaches to Low-Dimensional Systems", PhD thesis (RWTH Aachen University, 2015).

[101]D. Tarasevych, J. Krieg, and P. Kopietz, "A rich man's derivation of scaling laws for the Kondo model", Phys. Rev. B **98**, 235133 (2018).

[102]J. Krieg and P. Kopietz, "Exact renormalization group for quantum spin systems", Phys. Rev. B **99**, 060403 (2019).

[103]R. Goll, D. Tarasevych, J. Krieg, and P. Kopietz, "Spin functional renormalization group for quantum Heisenberg ferromagnets: Magnetization and magnon damping in two dimensions", Phys. Rev. B **100**, 174424 (2019).

[104]R. Goll, A. Rückriegel, and P. Kopietz, "Zero-magnon sound in quantum Heisenberg ferromagnets", arXiv:2010.08425 (2020).

[105]N. Niggemann, B. Sbierski, and J. Reuther, "Frustrated Quantum Spins at finite Temperature: Pseudo-Majorana functional RG approach", arXiv:2012.14836 (2020).

[106]Y. A. Izyumov and Y. N. Skryabin, *Statistical Mechanics of Magnetically Ordered Systems* (Consultants Bureau, New York, 1988).

[107]A. M. Tsvelik, *Quantum Field Theory in Condensed Matter Physics* (Cambridge University Press, 2003).

[108]R. P. Feynman, "The Behavior of Hadron Collisions at Extreme Energies", in *Special relativity and quantum theory*, edited by M. E. Noz and Y. Kim (Springer, Dordrecht, 1988), pp. 289–304.

[109] A. A. Abrikosov and A. A. Migdal, "On the theory of the Kondo effect", J. Low Temp. Phys. **3**, 519–536 (1970).

[110] P. Coleman, "New approach to the mixed-valence problem", Phys. Rev. B **29**, 3035–3044 (1984).

[111] V. Popov and S. Fedotov, "The functional integration method and diagram technique for spin systems", Sov. Phys. JETP **67**, 535–541 (1988).

[112] M. N. Kiselev and R. Oppermann, "Spin-glass transition in a Kondo lattice with quenched disorder", J. Exp. Theor. Phys. Lett. **71**, 250–254 (2000).

[113] R. Dillenschneider and J. Richert, "Site-occupation constraints in mean-field approaches to quantum spin systems at finite temperature", Phys. Rev. B **73**, 024409 (2006).

[114] S. Andergassen, T. Enss, V. Meden, W. Metzner, U. Schollwöck, and K. Schönhammer, "Functional renormalization group for Luttinger liquids with impurities", Phys. Rev. B **70**, 075102 (2004).

[115] T. Enss, V. Meden, S. Andergassen, X. Barnabé-Thériault, W. Metzner, and K. Schönhammer, "Impurity and correlation effects on transport in one-dimensional quantum wires", Phys. Rev. B **71**, 155401 (2005).

[116] F. Bauer, J. Heyder, E. Schubert, D. Borowsky, D. Taubert, B. Bruognolo, D. Schuh, W. Wegscheider, J. von Delft, and S. Ludwig, "Microscopic origin of the '0.7-anomaly' in quantum point contacts", Nature **501**, 73–78 (2013).

[117] F. Bauer, J. Heyder, and J. von Delft, "Functional renormalization group approach for inhomogeneous interacting Fermi systems", Phys. Rev. B **89**, 045128 (2014).

[118] F. L. Buessen, "A Functional Renormalization Group Perspective on Quantum Spin Liquids in Three-Dimensional Frustrated Magnets", PhD thesis (Universität zu Köln, 2019).

[119] F. L. Buessen, V. Noculak, S. Trebst, and J. Reuther, "Functional renormalization group for frustrated magnets with nondiagonal spin interactions", Phys. Rev. B **100**, 125164 (2019).

[120] J. Reuther, R. Thomale, and S. Rachel, "Spiral order in the honeycomb iridate Li2IrO3", Phys. Rev. B **90**, 100405 (2014).

[121] M. U. Ubbens and P. A. Lee, "Flux phases in the t - J model", Phys. Rev. B **46**, 8434–8439 (1992).

[122] I. Affleck and J. B. Marston, "Large- n limit of the Heisenberg-Hubbard model: Implications for high- T c superconductors", Phys. Rev. B **37**, 3774–3777 (1988).

[123] M. E. Peskin and D. V. Schroeder, *An Introduction To Quantum Field Theory* (Westview Press, Boulder, CO, 1995).

[124] M. Hering, J. Sonnenschein, Y. Iqbal, and J. Reuther, "Characterization of quantum spin liquids and their spinon band structures via functional renormalization", Phys. Rev. B **99**, 100405 (2019).

[125] A. Keleş and E. Zhao, "Absence of Long-Range Order in a Triangular Spin System with Dipolar Interactions", Phys. Rev. Lett. **120**, 187202 (2018).

[126] R. R. P. Singh, Z. Weihong, C. J. Hamer, and J. Oitmaa, "Dimer order with striped correlations in the J1-J2 Heisenberg model", Phys. Rev. B **60**, 7278–7283 (1999).

[127] L. Capriotti, F. Becca, A. Parola, and S. Sorella, "Resonating Valence Bond Wave Functions for Strongly Frustrated Spin Systems", Phys. Rev. Lett. **87**, 097201 (2001).

[128]M. Mambrini, A. Läuchli, D. Poilblanc, and F. Mila, "Plaquette valence-bond crystal in the frustrated Heisenberg quantum antiferromagnet on the square lattice", Phys. Rev. B **74**, 144422 (2006).

[129]J. Sirker, Z. Weihong, O. P. Sushkov, and J. Oitmaa, "J1-J2 model: First-order phase transition versus deconfinement of spinons", Phys. Rev. B **73**, 184420 (2006).

[130]R. Darradi, O. Derzhko, R. Zinke, J. Schulenburg, S. E. Krüger, and J. Richter, "Ground state phases of the spin-1/2 J1-J2 Heisenberg antiferromagnet on the square lattice: A high-order coupled cluster treatment", Phys. Rev. B **78**, 214415 (2008).

[131]H.-C. Jiang, H. Yao, and L. Balents, "Spin liquid ground state of the spin-1/2 J1-J2 Heisenberg model", Phys. Rev. B **86**, 024424 (2012).

[132]F. L. Buessen and S. Trebst, "Competing magnetic orders and spin liquids in two- and three-dimensional kagome systems: Pseudofermion functional renormalization group perspective", Phys. Rev. B **94**, 235138 (2016).

[133]J. Yoshitake, J. Nasu, and Y. Motome, "Temperature evolution of spin dynamics in two- and three-dimensional Kitaev models: Influence of fluctuating <math> <msub> <mi>Z</mi> <mn>2</mn> </msub> </math> flux", Phys. Rev. B **96**, 064433 (2017).

[134]A. Rohatgi, "WebPlotDigitizer: ver. 4.4", https://automeris.io/WebPlotDigitizer (2020).

[135]Y. Iqbal, R. Thomale, F. Parisen Toldin, S. Rachel, and J. Reuther, "Functional renormalization group for three-dimensional quantum magnetism", Phys. Rev. B **94**, 140408 (2016).

[136]J. Reuther, R. Thomale, and S. Trebst, "Finite-temperature phase diagram of the Heisenberg-Kitaev model", Phys. Rev. B **84**, 100406 (2011).

[137]F. L. Buessen, D. Roscher, S. Diehl, and S. Trebst, "Functional renormalization group approach to SU(N) Heisenberg models: Real-space renormalization group at arbitrary N", Phys. Rev. B **97**, 064415 (2018).

[138]Z.-X. Liu, Y. Zhou, and T.-K. Ng, "Fermionic theory for quantum antiferromagnets with spin S > 1 / 2", Phys. Rev. B **82**, 144422 (2010).

[139]M. L. Baez and J. Reuther, "Numerical treatment of spin systems with unrestricted spin length S : A functional renormalization group study", Phys. Rev. B **96**, 045144 (2017).

[140]N. V. Prokof'ev and B. V. Svistunov, "From the Popov-Fedotov case to universal fermionization", Phys. Rev. B **84**, 073102 (2011).

[141]J. M. Luttinger and L. Tisza, "Theory of Dipole Interaction in Crystals", Phys. Rev. **70**, 954–964 (1946).

[142]J. M. Luttinger, "A Note on the Ground State in Antiferromagnetics", Phys. Rev. **81**, 1015–1018 (1951).

[143]M. L. Baez, "Numerical methods for frustrated magnetism: From quantum to classical spin systems", PhD thesis (Freien Universitat Berlin, 2018).

[144]M. Hering and J. Reuther, "Functional renormalization group analysis of Dzyaloshinsky-Moriya and Heisenberg spin interactions on the kagome lattice", Phys. Rev. B **95**, 054418 (2017).

[145]M. Hering, "New States of Matter in Strongly Frustrated Quantum Magnets", PhD thesis (Freien Universitat Berlin, 2018).

[146]J. Reuther and R. Thomale, "Cluster functional renormalization group", Phys. Rev. B **89**, 024412 (2014).

[147]D. Roscher, N. Gneist, M. M. Scherer, S. Trebst, and S. Diehl, "Cluster functional renormalization group and absence of a bilinear spin liquid in the J1-J2 Heisenberg model", Phys. Rev. B **100**, 125130 (2019).

[148]D. Roscher, F. L. Buessen, M. M. Scherer, S. Trebst, and S. Diehl, "Functional renormalization group approach to SU(N) Heisenberg models: Momentum-space renormalization group for the large-N limit", Phys. Rev. B **97**, 064416 (2018).

[149]J. Reuther, D. A. Abanin, and R. Thomale, "Magnetic order and paramagnetic phases in the quantum J1-J2-J3 honeycomb model", Phys. Rev. B **84**, 014417 (2011).

[150]R. Suttner, C. Platt, J. Reuther, and R. Thomale, "Renormalization group analysis of competing quantum phases in the J1-J2 Heisenberg model on the kagome lattice", Phys. Rev. B **89**, 020408 (2014).

[151]Y. Iqbal, H. O. Jeschke, J. Reuther, R. Valentí, I. I. Mazin, M. Greiter, and R. Thomale, "Paramagnetism in the kagome compounds (Zn,Mg,Cd)Cu3(OH)6Cl2", Phys. Rev. B **92**, 220404 (2015).

[152]Y. Iqbal, P. Ghosh, R. Narayanan, B. Kumar, J. Reuther, and R. Thomale, "Intertwined nematic orders in a frustrated ferromagnet", Phys. Rev. B **94**, 224403 (2016).

[153]Y. Iqbal, T. Müller, P. Ghosh, M. J. Gingras, H. O. Jeschke, S. Rachel, J. Reuther, and R. Thomale, "Quantum and Classical Phases of the Pyrochlore Heisenberg Model with Competing Interactions", Phys. Rev. X **9**, 011005 (2019).

[154]M. Rück and J. Reuther, "Effects of two-loop contributions in the pseudofermion functional renormalization group method for quantum spin systems", Phys. Rev. B **97**, 144404 (2018).

[155]J. Thoenniss, M. K. Ritter, F. B. Kugler, J. von Delft, and M. Punk, "Multiloop pseudofermion functional renormalization for quantum spin systems: Application to the spin-1/2 kagome Heisenberg model", arXiv:2011.01268 (2020).

[156]D. Kiese, T. Mueller, Y. Iqbal, R. Thomale, and S. Trebst, "Multiloop functional renormalization group approach to quantum spin systems", arXiv:2011.01269 (2020).

[157]K. Fukui, Y. Kato, J. Nasu, and Y. Motome, "Absence of quantum spin liquid in dipolar Kitaev model for ultracold polar molecules", Prep. (2021).

[158]J. Doyle, B. Friedrich, R. V. Krems, and F. Masnou-Seeuws, "Editorial: Quo vadis, cold molecules?", Eur. Phys. J. D **31**, 149–164 (2004).

[159]D. S. Jin and J. Ye, "Polar molecules in the quantum regime", Phys. Today **64**, 27–31 (2011).

[160]A. J. Daley, "Rotating molecules as quantum magnets", Nature **501**, 497–498 (2013).

[161]B. Gadway and B. Yan, "Strongly interacting ultracold polar molecules", J. Phys. B At. Mol. Opt. Phys. **49**, 152002 (2016).

[162]K.-K. Ni, S. Ospelkaus, M. H. G. de Miranda, A. Pe'er, B. Neyenhuis, J. J. Zirbel, S. Kotochigova, P. S. Julienne, D. S. Jin, and J. Ye, "A High Phase-Space-Density Gas of Polar Molecules", Science (80-.). **322**, 231–235 (2008).

[163]J. G. Danzl, E. Haller, M. Gustavsson, M. J. Mark, R. Hart, N. Bouloufa, O. Dulieu, H. Ritsch, and H.-C. Nagerl, "Quantum Gas of Deeply Bound Ground State Molecules", Science (80-.). **321**, 1062–1066 (2008).

[164]F. Lang, K. Winkler, C. Strauss, R. Grimm, and J. H. Denschlag, "Ultracold Triplet Molecules in the Rovibrational Ground State", Phys. Rev. Lett. **101**, 133005 (2008).

[165]J. Deiglmayr, A. Grochola, M. Repp, K. Mörtlbauer, C. Glück, J. Lange, O. Dulieu, R. Wester, and M. Weidemüller, "Formation of Ultracold Polar Molecules in the Rovibrational Ground State", Phys. Rev. Lett. **101**, 133004 (2008).

[166]J. Deiglmayr, M. Repp, A. Grochola, K. Mörtlbauer, C. Glück, O. Dulieu, J. Lange, R. Wester, and M. Weidemüller, "Formation of ultracold dipolar molecules in the lowest vibrational levels by photoassociation", Faraday Discuss. **142**, 335 (2009).

[167]J. G. Danzl, M. J. Mark, E. Haller, M. Gustavsson, N. Bouloufa, O. Dulieu, H. Ritsch, R. Hart, and H.-C. Nägerl, "Precision molecular spectroscopy for ground state transfer of molecular quantum gases", Faraday Discuss. **142**, 283 (2009).

[168]S. Ospelkaus, K.-K. Ni, M. H. G. de Miranda, B. Neyenhuis, D. Wang, S. Kotochigova, P. S. Julienne, D. S. Jin, and J. Ye, "Ultracold polar molecules near quantum degeneracy", Faraday Discuss. **142**, 351 (2009).

[169]J. G. Danzl, M. J. Mark, E. Haller, M. Gustavsson, R. Hart, J. Aldegunde, J. M. Hutson, and H.-C. Nägerl, "An ultracold high-density sample of rovibronic ground-state molecules in an optical lattice", Nat. Phys. **6**, 265–270 (2010).

[170]S. Ospelkaus, K.-K. Ni, G. Quéméner, B. Neyenhuis, D. Wang, M. H. G. de Miranda, J. L. Bohn, J. Ye, and D. S. Jin, "Controlling the Hyperfine State of Rovibronic Ground-State Polar Molecules", Phys. Rev. Lett. **104**, 030402 (2010).

[171]K. Aikawa, D. Akamatsu, M. Hayashi, K. Oasa, J. Kobayashi, P. Naidon, T. Kishimoto, M. Ueda, and S. Inouye, "Coherent Transfer of Photoassociated Molecules into the Rovibrational Ground State", Phys. Rev. Lett. **105**, 203001 (2010).

[172]M. H. G. de Miranda, A. Chotia, B. Neyenhuis, D. Wang, G. Quéméner, S. Ospelkaus, J. L. Bohn, J. Ye, and D. S. Jin, "Controlling the quantum stereodynamics of ultracold bimolecular reactions", Nat. Phys. **7**, 502–507 (2011).

[173]A. Chotia, B. Neyenhuis, S. A. Moses, B. Yan, J. P. Covey, M. Foss-Feig, A. M. Rey, D. S. Jin, and J. Ye, "Long-Lived Dipolar Molecules and Feshbach Molecules in a 3D Optical Lattice", Phys. Rev. Lett. **108**, 080405 (2012).

[174]P. K. Molony, P. D. Gregory, Z. Ji, B. Lu, M. P. Köppinger, C. R. Le Sueur, C. L. Blackley, J. M. Hutson, and S. L. Cornish, "Creation of Ultracold 87Rb133Cs Molecules in the Rovibrational Ground State", Phys. Rev. Lett. **113**, 255301 (2014).

[175]T. Takekoshi, L. Reichsöllner, A. Schindewolf, J. M. Hutson, C. R. Le Sueur, O. Dulieu, F. Ferlaino, R. Grimm, and H.-C. Nägerl, "Ultracold Dense Samples of Dipolar RbCs Molecules in the Rovibrational and Hyperfine Ground State", Phys. Rev. Lett. **113**, 205301 (2014).

[176]J. W. Park, S. A. Will, and M. W. Zwierlein, "Ultracold Dipolar Gas of Fermionic 23Na40K Molecules in Their Absolute Ground State", Phys. Rev. Lett. **114**, 205302 (2015).

[177]M. Guo, B. Zhu, B. Lu, X. Ye, F. Wang, R. Vexiau, N. Bouloufa-Maafa, G. Quéméner, O. Dulieu, and D. Wang, "Creation of an Ultracold Gas of Ground-State Dipolar 23Na87Rb Molecules", Phys. Rev. Lett. **116**, 205303 (2016).

[178]T. M. Rvachov, H. Son, A. T. Sommer, S. Ebadi, J. J. Park, M. W. Zwierlein, W. Ketterle, and A. O. Jamison, "Long-Lived Ultracold Molecules with Electric and Magnetic Dipole Moments", Phys. Rev. Lett. **119**, 143001 (2017).

[179]F. Seeßelberg, N. Buchheim, Z.-K. Lu, T. Schneider, X.-Y. Luo, E. Tiemann, I. Bloch, and C. Gohle, "Modeling the adiabatic creation of ultracold polar 23Na40K molecules", Phys. Rev. A **97**, 013405 (2018).

[180]H. Yang, D.-C. Zhang, L. Liu, Y.-X. Liu, J. Nan, B. Zhao, and J.-W. Pan, "Observation of magnetically tunable Feshbach resonances in ultracold 23 Na 40 K + 40 K collisions", Science (80-.). **363**, 261–264 (2019).

[181]J. A. Blackmore, R. Sawant, P. D. Gregory, S. L. Bromley, J. Aldegunde, J. M. Hutson, and S. L. Cornish, "Controlling the ac Stark effect of RbCs with dc electric and magnetic fields", Phys. Rev. A **102**, 053316 (2020).

[182]R. Barnett, D. Petrov, M. Lukin, and E. Demler, "Quantum Magnetism with Multicomponent Dipolar Molecules in an Optical Lattice", Phys. Rev. Lett. **96**, 190401 (2006).

[183]A. Micheli, G. K. Brennen, and P. Zoller, "A toolbox for lattice-spin models with polar molecules", Nat. Phys. **2**, 341–347 (2006).

[184]H. P. Büchler, E. Demler, M. Lukin, A. Micheli, N. Prokof'ev, G. Pupillo, and P. Zoller, "Strongly Correlated 2D Quantum Phases with Cold Polar Molecules: Controlling the Shape of the Interaction Potential", Phys. Rev. Lett. **98**, 060404 (2007).

[185]A. V. Gorshkov, S. R. Manmana, G. Chen, E. Demler, M. D. Lukin, and A. M. Rey, "Quantum magnetism with polar alkali-metal dimers", Phys. Rev. A **84**, 033619 (2011).

[186]A. V. Gorshkov, S. R. Manmana, G. Chen, J. Ye, E. Demler, M. D. Lukin, and A. M. Rey, "Tunable Superfluidity and Quantum Magnetism with Ultracold Polar Molecules", Phys. Rev. Lett. **107**, 115301 (2011).

[187]L. He and W. Hofstetter, "Supersolid phase of cold fermionic polar molecules in two-dimensional optical lattices", Phys. Rev. A **83**, 053629 (2011).

[188]N. Y. Yao, C. R. Laumann, A. V. Gorshkov, S. D. Bennett, E. Demler, P. Zoller, and M. D. Lukin, "Topological Flat Bands from Dipolar Spin Systems", Phys. Rev. Lett. **109**, 266804 (2012).

[189]A. Macia, D. Hufnagl, F. Mazzanti, J. Boronat, and R. E. Zillich, "Excitations and Stripe Phase Formation in a Two-Dimensional Dipolar Bose Gas with Tilted Polarization", Phys. Rev. Lett. **109**, 235307 (2012).

[190]N. Y. Yao, A. V. Gorshkov, C. R. Laumann, A. M. Läuchli, J. Ye, and M. D. Lukin, "Realizing Fractional Chern Insulators in Dipolar Spin Systems", Phys. Rev. Lett. **110**, 185302 (2013).

[191]N. Y. Yao, M. P. Zaletel, D. M. Stamper-Kurn, and A. Vishwanath, "A quantum dipolar spin liquid", Nat. Phys. **14**, 405–410 (2018).

[192]R. P. Feynman, "Simulating physics with computers", Int. J. Theor. Phys. **21**, 467–488 (1982).

[193]D. DeMille, "Quantum Computation with Trapped Polar Molecules", Phys. Rev. Lett. **88**, 067901 (2002).

[194]S. F. Yelin, K. Kirby, and R. Côté, "Schemes for robust quantum computation with polar molecules", Phys. Rev. A **74**, 050301 (2006).

[195]J. Zhu, S. Kais, Q. Wei, D. Herschbach, and B. Friedrich, "Implementation of quantum logic gates using polar molecules in pendular states", J. Chem. Phys. **138**, 024104 (2013).

[196]F. Herrera, Y. Cao, S. Kais, and K. B. Whaley, "Infrared-dressed entanglement of cold open-shell polar molecules for universal matchgate quantum computing", New J. Phys. **16**, 075001 (2014).

[197]K.-K. Ni, T. Rosenband, and D. D. Grimes, "Dipolar exchange quantum logic gate with polar molecules", Chem. Sci. **9**, 6830–6838 (2018).

[198]M. Hughes, M. D. Frye, R. Sawant, G. Bhole, J. A. Jones, S. L. Cornish, M. R. Tarbutt, J. M. Hutson, D. Jaksch, and J. Mur-Petit, "Robust entangling gate for polar molecules using magnetic and microwave fields", Phys. Rev. A **101**, 062308 (2020).

[199]R. Sawant, J. A. Blackmore, P. D. Gregory, J. Mur-Petit, D. Jaksch, J. Aldegunde, J. M. Hutson, M. R. Tarbutt, and S. L. Cornish, "Ultracold polar molecules as qudits", New J. Phys. **22**, 013027 (2020).

[200]K. A. Kuns, A. M. Rey, and A. V. Gorshkov, "D-wave superfluidity in optical lattices of ultracold polar molecules", Phys. Rev. A **84**, 063639 (2011).

[201]H. Zou, E. Zhao, and W. V. Liu, "Frustrated Magnetism of Dipolar Molecules on a Square Optical Lattice: Prediction of a Quantum Paramagnetic Ground State", Phys. Rev. Lett. **119**, 050401 (2017).

[202]A. Keleş and E. Zhao, "Renormalization group analysis of dipolar Heisenberg model on square lattice", Phys. Rev. B **97**, 245105 (2018).

[203]J.-J. Weis, "Simulation of quasi-two-dimensional dipolar systems", J. Phys. Condens. Matter **15**, S1471–S1495 (2003).

[204]M. P. Allen and D. J. Tildesley, *Computer Simulation of Liquids*, 2nd ed. (Oxford University Press, Oxford, 2017).

[205]Y. Tomita, "Monte Carlo Study of Two-Dimensional Heisenberg Dipolar Lattices", J. Phys. Soc. Jpn **78**, 114004 (2009).

[206]J. V. José, L. P. Kadanoff, S. Kirkpatrick, and D. R. Nelson, "Renormalization, vortices, and symmetry-breaking perturbations in the two-dimensional planar model", Phys. Rev. B **16**, 1217–1241 (1977).

[207]C. C. Price and N. B. Perkins, "Critical Properties of the Kitaev-Heisenberg Model", Phys. Rev. Lett. **109**, 187201 (2012).

[208]C. Price and N. B. Perkins, "Finite-temperature phase diagram of the classical Kitaev-Heisenberg model", Phys. Rev. B **88**, 024410 (2013).

[209]V. L. Berezinskii, "Destruction of Long-range Order in One-dimensional and Two-dimensional Systems having a Continuous Symmetry Group I. Classical Systems", Sov. J. Exp. Theor. Phys. **32**, 493–500 (1971).

[210]V. L. Berezinskii, "Destruction of Long-range Order in One-dimensional and Two-dimensional Systems Possessing a Continuous Symmetry Group. II. Quantum Systems", Sov. J. Exp. Theor. Phys. **34**, 610 (1972).

[211]J. M. Kosterlitz and D. J. Thouless, "Ordering, metastability and phase transitions in two-dimensional systems", J. Phys. C Solid State Phys. **6**, 1181–1203 (1973).

[212]N. D. Mermin and H. Wagner, "Absence of Ferromagnetism or Antiferromagnetism in One- or Two-Dimensional Isotropic Heisenberg Models", Phys. Rev. Lett. **17**, 1133–1136 (1966).

[213]A. P. Ramirez, "Strongly Geometrically Frustrated Magnets", Annu. Rev. Mater. Sci. **24**, 453–480 (1994).

[214]D. Kiese, F. L. Buessen, C. Hickey, S. Trebst, and M. M. Scherer, "Emergence and stability of spin-valley entangled quantum liquids in moiré heterostructures", Phys. Rev. Res. **2**, 013370 (2020).

[215]I. Rousochatzakis, J. Reuther, R. Thomale, S. Rachel, and N. B. Perkins, "Phase Diagram and Quantum Order by Disorder in the Kitaev K1-K2 Honeycomb Magnet", Phys. Rev. X **5**, 041035 (2015).

[216]K. Fukui, Y. Kato, J. Nasu, and Y. Motome, "Spin-S Kitaev-Heisenberg model: spin liquid survival up to spins with S<2", Prep. (2021).

[217]T. Minakawa, J. Nasu, and A. Koga, "Quantum and classical behavior of spin-S Kitaev models in the anisotropic limit", Phys. Rev. B **99**, 104408 (2019).

[218]H.-c. Jiang, Z.-c. Gu, X.-l. Qi, and S. Trebst, "Possible proximity of the Mott insulating iridate Na2IrO3 to a topological phase: Phase diagram of the Heisenberg-Kitaev model in a magnetic field", Phys. Rev. B **83**, 245104 (2011).

[219]F. Trousselet, G. Khaliullin, and P. Horsch, "Effects of spin vacancies on magnetic properties of the Kitaev-Heisenberg model", Phys. Rev. B **84**, 054409 (2011).

[220]Y. Singh and P. Gegenwart, "Antiferromagnetic Mott insulating state in single crystals of the honeycomb lattice material Na2IrO3", Phys. Rev. B **82**, 064412 (2010).

[221]X. Liu, T. Berlijn, W.-G. Yin, W. Ku, A. Tsvelik, Y.-J. Kim, H. Gretarsson, Y. Singh, P. Gegenwart, and J. P. Hill, "Long-range magnetic ordering in Na2IrO3", Phys. Rev. B **83**, 220403 (2011).

[222]S. K. Choi, R. Coldea, A. N. Kolmogorov, T. Lancaster, I. I. Mazin, S. J. Blundell, P. G. Radaelli, Y. Singh, P. Gegenwart, K. R. Choi, S.-W. Cheong, P. J. Baker, C. Stock, and J. Taylor, "Spin Waves and Revised Crystal Structure of Honeycomb Iridate Na2IrO3", Phys. Rev. Lett. **108**, 127204 (2012).

[223]F. Ye, S. Chi, H. Cao, B. C. Chakoumakos, J. A. Fernandez-Baca, R. Custelcean, T. F. Qi, O. B. Korneta, and G. Cao, "Direct evidence of a zigzag spin-chain structure in the honeycomb lattice: A neutron and x-ray diffraction investigation of single-crystal Na2IrO3", Phys. Rev. B **85**, 180403 (2012).

[224]Y. Singh, S. Manni, J. Reuther, T. Berlijn, R. Thomale, W. Ku, S. Trebst, and P. Gegenwart, "Relevance of the Heisenberg-Kitaev Model for the Honeycomb Lattice Iridates A2IrO3", Phys. Rev. Lett. **108**, 127203 (2012).

[225]S. Manni, S. Choi, I. I. Mazin, R. Coldea, M. Altmeyer, H. O. Jeschke, R. Valentí, and P. Gegenwart, "Effect of isoelectronic doping on the honeycomb-lattice iridate A2IrO3", Phys. Rev. B **89**, 245113 (2014).

[226]S. C. Williams, R. D. Johnson, F. Freund, S. Choi, A. Jesche, I. Kimchi, S. Manni, A. Bombardi, P. Manuel, P. Gegenwart, and R. Coldea, "Incommensurate counterrotating magnetic order stabilized by Kitaev interactions in the layered honeycomb α-Li2IrO3", Phys. Rev. B **93**, 195158 (2016).

[227]V. M. Katukuri, S. Nishimoto, V. Yushankhai, A. Stoyanova, H. Kandpal, S. Choi, R. Coldea, I. Rousochatzakis, L. Hozoi, and J. V. D. Brink, "Kitaev interactions between j = 1/2 moments in honeycomb Na 2 IrO 3 are large and ferromagnetic: insights from ab initio quantum chemistry calculations", New J. Phys. **16**, 013056 (2014).

[228]Y. Yamaji, Y. Nomura, M. Kurita, R. Arita, and M. Imada, "First-Principles Study of the Honeycomb-Lattice Iridates Na2IrO3 in the Presence of Strong Spin-Orbit Interaction and Electron Correlations", Phys. Rev. Lett. **113**, 107201 (2014).

[229]I. Kimchi and Y.-Z. You, "Kitaev-Heisenberg-J2-J3 model for the iridates A2IrO3", Phys. Rev. B **84**, 180407 (2011).

[230]I. Kimchi and A. Vishwanath, "Kitaev-Heisenberg models for iridates on the triangular, hyperkagome, kagome, fcc, and pyrochlore lattices", Phys. Rev. B **89**, 014414 (2014).

[231]G. Jackeli and A. Avella, "Quantum order by disorder in the Kitaev model on a triangular lattice", Phys. Rev. B **92**, 184416 (2015).

[232]M. Becker, M. Hermanns, B. Bauer, M. Garst, and S. Trebst, "Spin-orbit physics of j=1/2 Mott insulators on the triangular lattice", Phys. Rev. B **91**, 155135 (2015).

[233]K. Li, S.-L. Yu, and J.-X. Li, "Global phase diagram, possible chiral spin liquid, and topological superconductivity in the triangular Kitaev–Heisenberg model", New J. Phys. **17**, 043032 (2015).

[234]I. Rousochatzakis, U. K. Rössler, J. van den Brink, and M. Daghofer, "Kitaev anisotropy induces mesoscopic Z2 vortex crystals in frustrated hexagonal antiferromagnets", Phys. Rev. B **93**, 104417 (2016).

[235]K. Shinjo, S. Sota, S. Yunoki, K. Totsuka, and T. Tohyama, "Density-Matrix Renormalization Group Study of Kitaev–Heisenberg Model on a Triangular Lattice", J. Phys. Soc. Jpn **85**, 114710 (2016).

[236]K. Morita, M. Kishimoto, and T. Tohyama, "Ground-state phase diagram of the Kitaev-Heisenberg model on a kagome lattice", Phys. Rev. B **98**, 134437 (2018).

[237]M. Kishimoto, K. Morita, Y. Matsubayashi, S. Sota, S. Yunoki, and T. Tohyama, "Ground state phase diagram of the Kitaev-Heisenberg model on a honeycomb-triangular lattice", Phys. Rev. B **98**, 054411 (2018).

[238]G. Khaliullin, "Orbital Order and Fluctuations in Mott Insulators", Prog. Theor. Phys. Suppl. **160**, 155–202 (2005).

[239]S. Chandra, K. Ramola, and D. Dhar, "Classical Heisenberg spins on a hexagonal lattice with Kitaev couplings", Phys. Rev. E **82**, 031113 (2010).

[240]F. L. Buessen, M. Hering, J. Reuther, and S. Trebst, "Quantum Spin Liquids in Frustrated Spin-1 Diamond Antiferromagnets", Phys. Rev. Lett. **120**, 057201 (2018).

[241]J. G. Rau, E. K.-H. Lee, and H.-Y. Kee, "Generic Spin Model for the Honeycomb Iridates beyond the Kitaev Limit", Phys. Rev. Lett. **112**, 077204 (2014).

[242]C. Honerkamp and M. Salmhofer, "Temperature-flow renormalization group and the competition between superconductivity and ferromagnetism", Phys. Rev. B **64**, 184516 (2001).

[243]T. Enss, "Renormalization, Conservation Laws and Transport in Correlated Electron Systems", PhD thesis (Universitat Stuttgart, 2005).

[244]C. Honerkamp, D. Rohe, S. Andergassen, and T. Enss, "Interaction flow method for many-fermion systems", Phys. Rev. B **70**, 235115 (2004).